

Synthesis and Characterization of Eco-friendly Inorganic Yellow Pigments for Coloring Applications

Thesis submitted to
COCHIN UNIVERSITY OF SCIENCE AND TECHNOLOGY

in partial fulfillment of the requirements for the degree of
DOCTOR OF PHILOSOPHY IN CHEMISTRY

UNDER THE FACULTY OF SCIENCE

By
SAMEERA S.

Under the guidance of
Dr. P. PRABHAKAR RAO



Materials Science and Technology Division
**CSIR-NATIONAL INSTITUTE FOR INTERDISCIPLINARY
SCIENCE AND TECHNOLOGY (CSIR-NIIST)**
Thiruvananthapuram, 695 019, Kerala, India
October 2015

Dedicated to my parents....

DECLARATION

I hereby declare that the thesis entitled “**Synthesis and characterization of eco-friendly inorganic yellow pigments for coloring applications**” embodies the results of investigations carried out by me at Materials Science and Technology Division of Council of Scientific and Industrial Research - National Institute for Interdisciplinary Science and Technology (CSIR-NIIST), Thiruvananthapuram as a full time research scholar under the supervision of **Dr. P. Prabhakar Rao** and the same has not been submitted elsewhere for any other degree.

In keeping with the general practice of reporting scientific observations, due acknowledgement has been made wherever the work described is based on the findings of other investigators.

SAMEERA S.

Thiruvananthapuram
October, 2015

COUNCIL OF SCIENTIFIC & INDUSTRIAL RESEARCH
NATIONAL INSTITUTE FOR INTERDISCIPLINARY SCIENCE
AND TECHNOLOGY



GOVERNMENT OF INDIA
Thiruvananthapuram-695 019, Kerala,
India

Telephone: 91-471-2515311
Fax: 91-471-2491712

Dr. P. Prabhakar Rao
Chief Scientist
Materials Science and Technology Division

CERTIFICATE

This is to certify that the work embodied in the thesis entitled “**Synthesis and characterization of eco-friendly inorganic yellow pigments for coloring applications**” has been carried out by **Ms. Sameera S.** under my supervision and guidance at the Materials Science and Technology Division of National Institute for Interdisciplinary Science and Technology (CSIR-NIIST), Thiruvananthapuram and the same has not been submitted elsewhere for any other degree. All the relevant corrections, modifications and recommendations suggested by the audience and the doctoral committee members during the pre-synopsis seminar of **Ms. Sameera S.** have been incorporated in the thesis.

P. Prabhakar Rao
(Thesis supervisor)

Thiruvananthapuram
October, 2015

e-mail: padala_rao@yahoo.com

ACKNOWLEDGEMENTS

I would like to express my sincere gratitude to my research supervisor, Dr. P. Prabhakar Rao for his support, inspiration, encouragement and thoughtful guidance throughout my research. He has always been there when things looked dark and far from colorful. It is an honour to work with him and I am sure that the training I received under him will be helpful in all my future scientific endeavours.

I am grateful to Dr. A. Ajayaghosh, Director, CSIR-NIIST and former Directors Dr. P. Gangan Pratap, Dr. Suresh Das, Dr. B. C. Pai for kindly providing the necessary facilities and infrastructure to carry out research work.

I thank all the former and present members of Energy Materials group for their kind advice and assistance.

I would like to thank Mr. M. R Chandran for SEM imaging.

I wish to thank scientists and technical staff of NIIST for the help rendered during the course of this work.

I sincerely thank Mr. K. Harikrishna Bhat for extending the research facilities of BSMR lab towards us.

I express my sincere gratitude to Prof. S. Sugunan, Dept of Chemistry, CUSAT for his support as an external expert in Doctoral Committee.

I acknowledge CSIR, New Delhi for the award of Senior Research Fellowship and ICDD, USA for the financial assistance towards a project during the early stages of my research. This work has also been benefitted from DRDO and CSIR Network Project SURE.

All my friends, with whom I shared good times, will always be remembered, and those times will be cherished. In particular, I thank Athira, Sreena and Soumya for their wholehearted help, exhilaration and support through the crucial stages of the writing process; Vineetha for the warm friendship while working in the area of pigments.

I am always indebted to my parents Abdul Naseer and Saithathul Fathimah, who raised me, supported me in all my pursuits and for their love, care and prayers. I thank my sister Sameeha who has been a good critic and Farha, my little niece for her giggles that relaxed me. My dear son Adil has shown unimaginable patience during my work and whose smile has always lifted me up. I thank my husband Aneez Fayaz, who has always been there to encourage and listen to me.

Above all, I humbly bow before Almighty for all the blessings showered upon me.

Sameera S.

CONTENTS

Declaration		i
Certificate		ii
Acknowledgements		iii
Abbreviations		ix
Preface		x
Chapter 1	INTRODUCTION	1-38
1.1	Inorganic pigments	3
1.2	The need for pigments	4
1.3	A brief history of inorganic pigments	4
1.4	Classification of inorganic pigments	6
1.5	Color	7
1.5.1	Origin of Color	7
1.5.2	Describing color	8
1.5.3	Color properties	9
1.6	Research efforts in yellow pigments	18
1.7	IR reflecting pigments	26
1.8	Motivation and objective of the work	30
1.9	References	32
Chapter 2A	YELLOW PIGMENTS IN $\text{BiVO}_4\text{-CaWO}_4$ SYSTEM	39-50
2A.1	Introduction	41
2A.2	Experimental Section	43
2A.2.1	Materials and Methods	43
2A.2.2	Characterizations	43
2A.3	Results and Discussion	44
2A.3.1	X-ray Diffraction Analysis	44
2A.3.2	Morphological and Micro chemical Studies	45
2A.3.3	UV Visible Studies	46
2A.3.4	Color Analysis	48

2A.3.5	Color Performance	50
2A.4	Conclusions	50
Chapter 2B	YELLOW PIGMENTS IN BiVO₄-CaMoO₄ SYSTEM	51-66
2B.1	Introduction	53
2B.2	Experimental Section	54
2B.2.1	Materials and Methods	54
2B.2.2	Characterizations	54
2B.3	Results and Discussion	55
2B.3.1	X-ray Diffraction Analysis	55
2B.3.2	Morphological and Micro chemical Studies	56
2B.3.3	UV Visible Studies	59
2B.3.4	Color Analysis	60
2B.3.5	IR Reflectance Studies	61
2B.3.6	Color Performance	62
2B.4	Conclusions	63
2.5	References	64
Chapter 3	YELLOW PIGMENTS IN BiVO₄- (LiLa)_{1/2}MoO₄/(LiCaLa)_{1/3}MoO₄ SYSTEM	67-92
3.1	Introduction	69
3.2	Experimental Section	70
3.2.1	Materials and Methods	70
3.2.2	Characterizations	71
3.3	Results and Discussion	72
3.3.1	X-ray Diffraction Analysis	72
3.3.2	Morphological and Micro chemical Studies	77
3.3.3	Particle Size Analysis	81
3.3.4	UV Visible Studies	81

3.3.5	Color Analysis	84
3.3.6	IR Reflectance Studies	86
3.4	Conclusions	89
3.5	References	90
Chapter 4	YELLOW PIGMENTS IN BiVO₄- (LiRE)_{1/2}MoO₄ SYSTEM	93-110
4.1	Introduction	95
4.2	Experimental Section	96
4.2.1	Materials and Methods	96
4.2.2	Characterizations	97
4.3	Results and Discussion	97
4.3.1	X-ray Diffraction Analysis	97
4.3.2	Morphological and Micro chemical Studies	100
4.3.3	UV Visible Studies	102
4.3.4	Band Gap Analysis	103
4.3.5	Color Analysis	104
4.3.6	IR Reflectance Studies	107
4.4	Conclusions	107
4.5	References	108
Chapter 5A	YELLOW PIGMENTS IN BiVO₄- YNbO₄ SYSTEM	111-122
5A.1	Introduction	113
5A.2	Experimental Section	114
5A.2.1	Materials and Methods	114
5A.2.2	Characterizations	114
5A.3	Results and Discussion	115
5A.3.1	X-ray Diffraction Analysis	115
5A.3.2	Morphological and Micro chemical Studies	117
5A.3.3	UV Visible Studies	118

5A.3.4	Color Analysis	119
5A.3.5	IR Reflectance Studies	121
5A.4	Conclusions	122
Chapter 5B	YELLOW PIGMENT IN BiVO₄- YNbO₄ SYSTEM BY CITRATE GEL METHOD	123-132
5B.1	Introduction	125
5B.2	Experimental Section	126
5B.2.1	Materials and Methods	126
5B.2.2	Characterizations	126
5B.3	Results and Discussion	127
5B.3.1	X-ray Diffraction Analysis	127
5B.3.2	Morphological and Micro chemical Studies	128
5B.3.3	UV Visible Studies	129
5B.3.4	Color Analysis	131
5B.3.5	IR Reflectance Studies	131
5B.4	Conclusions	132
Chapter 5C	YELLOW PIGMENTS IN BiV_{1-x}Nb_xO₄ SYSTEM BY CITRATE GEL METHOD	133-162
5C.1	Introduction	135
5C.2	Experimental Section	136
5C.2.1	Materials and Methods	136
5C.2.2	Characterizations	137
5C.3	Results and Discussion	138
5C.3.1	X-ray Diffraction Analysis	138
5C.3.2	Raman Spectra Analysis	142
5C.3.3	Morphological and Micro chemical Studies	144
5C.3.4	UV Visible Studies	147
5C.3.5	Color Analysis	149
5C.3.6	IR Reflectance Studies	149

5C.3.7	Photocatalytic Studies	151
5C.4	Conclusions	155
5.5	References	156
Chapter 6	APPLICATION STUDY OF POTENTIAL YELLOW PIGMENTS	163-184
6.1	Introduction	165
6.2	Methods	167
6.3	Application study of $\text{Li}_{0.15}\text{RE}_{0.15}\text{Bi}_{0.7}\text{Mo}_{0.3}\text{V}_{0.7}\text{O}_4$ pigment (RE = La, Gd)	169
6.3.1	Coloration of plastics	169
6.3.2	IR reflectance study on an asbestos cement roofing sheet	170
6.3.3	IR reflectance study on concrete cement	173
6.3.4	IR reflectance study on aluminium metal panel	176
6.4	Chemical resistance tests of $\text{Li}_{0.15}\text{RE}_{0.15}\text{Bi}_{0.7}\text{Mo}_{0.3}\text{V}_{0.7}\text{O}_4$ pigment (RE = La, Gd)	178
6.5	Application study of $(\text{BiV})_{0.975}\text{Nb}_{0.025}\text{O}_4$ pigment over concrete cement	179
6.6	Chemical resistance tests of $(\text{BiV})_{0.975}\text{Nb}_{0.025}\text{O}_4$ pigment	182
6.7	Conclusions	183
6.8	References	184
Chapter 7	CONCLUSIONS AND FUTURE SCOPE OF THE WORK	185-190
7.1	Conclusions	187
7.2	Future scope	190
	List of publications	191
	Papers presented at conferences (oral/poster)	194

Abbreviations

ISO	International Organization for Standardisation
DIN	Deutsches Institute fur Normung (German Standards Organisation)
CIE	Commission Internationale de l'Eclairage
UV	Ultraviolet
vis	Visible
NIR	Near Infrared
XRD	X-Ray Diffraction
PDF	Powder Diffraction File
SEM	Scanning Electron Microscope
EDS	Energy Dispersive Spectrometer
TEM	Transmission Electron Microscope
PTFE	Poly-tetrafluoroethylene
PMMA	poly(methyl methacrylate)
ASTM	American Society for Testing and Materials
SSR	Solid State Route
CG	Citrate Gel
RE	Rare Earth
VB	Valence Band
CB	Conduction Band
MB	Methylene Blue

PREFACE

Research in the fields of ceramic pigments is oriented towards the enlargement of the chromatic set of colors together with a replacement for more expensive and less stable organic pigments. Novel non-toxic inorganic pigments have been required to answer environmental laws to remove elements like lead, chromium, cobalt entering in the composition of usual pigments widely used in paints and plastics. Yellow is particularly an important color in the pigment industry and consumption of yellow exceeds that of any other colored pigments. Apart from this, high infrared reflective pigments are now in great demand for usage in coatings, cement pavements, automotives and camouflage applications. They not only impart color to an object, but also reflect the invisible heat from the object to minimize heat build-up, when exposed to solar radiation. With this in view, the present work aims at developing new functional yellow pigments for these applications. A series of IR reflecting yellow pigments have been synthesized and analyzed for their crystalline structure, morphological, composition and optical characteristics, coloring and energy saving applications.

The introductory chapter of the thesis portrays the importance of IR reflecting non toxic pigments particularly yellow. Main objectives of the present work are highlighted and the motivation and importance of choosing BiVO_4 based pigments is emphasized.

The scheelite structured BiVO_4 with the typical formula ABO_4 provides flexibility for cation substitution on both A and B sites. A crucial way to improve the properties of materials is through compositional design in the form of solid solutions. Solid solutions between BiVO_4 and CaWO_4 as well as CaMoO_4 leading to fine tuning of optical band gap are described in second chapter. Yellow hues were significantly improved in $(\text{BiV})_x(\text{CaW/Mo})_{1-x}\text{O}_4$ pigments over those of BiVO_4 .

Chapter three comprises of efforts to give a range of toxic-metal free yellow colorants in $\text{BiVO}_4(\text{LiLa})_{1/2}\text{MoO}_4$ as well as $\text{BiVO}_4(\text{LiCaLa})_{1/3}\text{MoO}_4$ solid solutions prepared by a solid state route. These pigments crystallize in tetragonal scheelite form. Various shades of yellow pigments ranging from reddish to greenish tint are obtained. Optimization of coloristic properties has been successfully employed using

various mineralizers. The color characteristics are comparable to commercial BiVO_4 pigment. The high IR reflectance of the pigments indicates their potential to be used as cool colorants.

Rare earth substitution allows further tuning of band gap of the material. Chapter four deals with an attempt to substitute different rare earths in the selected composition to produce various colorants in $\text{Li}_{0.10}\text{RE}_{0.10}\text{Bi}_{0.8}\text{Mo}_{0.2}\text{V}_{0.8}\text{O}_4$; RE = La, Pr, Sm, Gd, Tb, Dy, Y, Yb and Lu system. These solid solutions allow the manipulation of valence and conduction band edges leading to desirable yellow hues. La substitution exhibits intense yellow color characterized by the highest b^* (color) value among the developed pigments. High IR reflectance is obtained by incorporation of La, Gd, Tb, Y and Lu.

Isovalent dopants namely Y^{3+} and Nb^{5+} on BiVO_4 yielded brilliant yellow inorganic pigments in $(\text{BiV})_{1-x}(\text{YNb})_x\text{O}_4$ system with significant enhancement of NIR reflectance to 91 % when compared to undoped BiVO_4 . The enhancement of the optical properties of BiVO_4 is mainly ascribed to the reduction in particle size and structural distortion in the lattice. In an attempt to modify pigmentary characteristics typical compositions BiVO_4 , $(\text{BiV})_{0.94}(\text{YNb})_{0.06}\text{O}_4$ and $\text{BiV}_{1-x}\text{Nb}_x\text{O}_4$ are synthesized by the citrate gel method followed by calcination at various temperatures leading to fine particles. Chapter five details these results.

Chapter six presents the application study of selected pigments to evaluate their coloring performance. Typical $\text{Li}_{0.10}\text{La}/\text{Gd}_{0.10}\text{Bi}_{0.8}\text{Mo}_{0.2}\text{V}_{0.8}\text{O}_4$ pigments impart their color as well as IR reflectance to various substrates like PMMA, asbestos cement, concrete slab and metal panel. Nb^{5+} doped BiVO_4 pigments exhibit better good coloristic properties and impressive IR reflectance than BiVO_4 over concrete cement. The results imply the usage of these pigments for energy saving coatings for buildings and automotives.

Chapter seven summarizes the major findings and conclusions drawn from the work and gives the scope for further studies. The relevant references cited in this work have been given towards the end of each chapter.

CHAPTER 1

INTRODUCTION

Overview

The color of objects in our world has significant importance. The quest for colored materials continues, driven by both functional and aesthetic purposes. This chapter gives a general introduction regarding inorganic pigments, color and also the recent developments in this field.



1.1 Inorganic pigments

Since prehistoric times, pigments derived from various natural minerals have been used as colorants by man. The word ‘pigment’ is derived from the Latin word pigmentum — pingere, which means ‘to paint’. An internationally accepted definition¹ has been provided by the Color Pigments Manufacturers Association of America (CPMA): Pigments are colored black, white, or fluorescent particulate; organic or inorganic solids; which are insoluble in, and essentially physically and chemically unaffected by the vehicle or substrate in which they are incorporated. They alter appearance by selective absorption and/or scattering of light. Pigments are usually dispersed in vehicles or substrates for application, as for instance in the manufacture of ink, paints, plastics, or other polymeric materials. Pigments retain a crystal or particulate structure throughout the coloration process. Today, modern pigments are advanced masterpieces of chemical engineering. Pigments provide two types of main benefits to any coating: aesthetics and functionality. Pigments have a very important aspect which is more than just color; they can increase the overall performance by enhancing durability and increasing the protection of the substrate.

Pigments and dyes are included in the general term ‘coloring materials’, which denotes materials used for their coloring properties. The property that distinguishes pigments from soluble organic dyes is their low solubility in solvents and binders. One of the reasons for their popularity is their high temperature stability, which means that they can be coated on ceramics that are prepared by firing at high temperature. They score over organic pigments in this regard. Inorganic pigments are typically larger, easier to disperse, and more color stable in different applications than organic pigments.

In general, inorganic pigments are capable of offering excellent resistance to heat, light, weathering, solvents and chemicals, and in those respects they can offer technical advantage over most organic pigments. Inorganic pigments are, in general, high refractive index materials which are capable of giving high opacity while organic pigments are of low refractive index and consequently are transparent.² Inorganic pigments have been linked to high opacity and durability so that they have been mostly used in outdoor applications. In the case of anticorrosive pigments, they aid in corrosion-prevention of metal substrates.

1.2 The need for pigments

Inorganic pigments contribute to the beauty and functionality of the objects around us. The color pigments have found a wide variety of applications in various fields such as paints, varnishes, plastics, artists' colors, printing inks for paper and textiles, leather decoration, building materials (cement, renderings, concrete bricks and tiles, mostly based on iron oxide and chromium oxide pigments), imitation leather, floor coverings, rubber, paper, cosmetics, ceramic glazes, and enamels.³

Inorganic pigments are now highly engineered particles those impart color or functionality to the objects in which they are used. While inorganic pigments are still used in conventional applications, their resistance to the effects of radiation, temperature, and chemical attack has also led to use in high-technology applications, such as fibers, engineering plastics, and highly durable coatings applied to roofing panels and even space equipment.⁴

1.3 A brief history of inorganic pigments

The development of inorganic pigments has been one of the major pursuits of man from ages. Over 60,000 years ago, natural ocher ($\text{Fe}_2\text{O}_3 \cdot \text{H}_2\text{O}$) was used in the 'Ice Age' as a coloring material. Prehistoric cave paintings, give evidence of the use of ocher, hematite, brown iron ore, and other mineral based pigments more than 30,000 years ago. Pigments were made by grinding naturally colored materials into minute particles and then mixing them into a binder material. Cinnabar (HgS), azurite ($2\text{CuCO}_3 \cdot \text{Cu}(\text{OH})_2$), malachite ($\text{CuCO}_3 \cdot \text{Cu}(\text{OH})_2$), and lapis lazuli have been traced back to the third millennium BC in China and Egypt. About 2000 BC, natural ocher was burnt, sometimes in mixtures with manganese ores, to produce red, violet, and black pigments for pottery. Ultramarine (lapis lazuli) and artificial lapis lazuli (Egyptian blue and cobalt aluminum spinel) were the first blue pigments. Terra verte, malachite, and a synthetically prepared copper hydroxychloride were the first green pigments. Calcite, some phases of calcium sulfate, and kaolinite were the white pigments used at that time. Antimony sulfide and galena (PbS) were commonly used as black pigments, cinnabar as a red pigment, and ground cobalt glass and cobalt aluminum oxide as blue pigments. The Greeks' contribution to painting was the manufacture of white lead pigment (basic lead carbonate ($2\text{Pb}(\text{CO}_3) \cdot 2\text{Pb}(\text{OH})_2$))⁵ which remained the most used white pigment available to artists until the 19th century.

The pigment industry started in the 18th century with products such as Berlin blue; $\text{Fe}[\text{Fe}_2(\text{CN})_6]_3$ in 1704, cobalt blue (CoAl_2O_4); in 1777, Scheele's green; $\text{Cu}(\text{AsO}_2)_2$, $\text{Cu}(\text{OH})_2$, and chrome yellow; PbCrO_4 in 1778. In the 19th century, ultramarine $\text{Na}_8[\text{Al}_6\text{Si}_6\text{O}_{24}]\text{S}_n$; Guignet's green (hydrated Cr_2O_3), cobalt pigments, iron oxide pigments, and cadmium pigments were developed in quick succession. In the 20th century, pigments increasingly became the subject of scientific investigation. In the past few decades, the synthetic colored pigments cadmium red, manganese blue, molybdenum red, and mixed oxides with bismuth came onto the market. Titanium dioxide with anatase or rutile structures, and acicular zinc oxide were introduced as new synthetic white pigments and extenders respectively. Luster pigments (metal effect, pearl/luster, and interference pigments) have assumed increasing importance.³

As far as yellow pigments are concerned, the oldest yellow pigment is yellow ochre, which was amongst the first pigments used by humans (Fig. 1.1). Egyptians and the ancient world made wide use of the mineral orpiment for a more brilliant yellow than yellow ochre. Arsenic sulfide (As_2S_3) and Naples yellow ($\text{Pb}_2\text{Sb}_2\text{O}_7$) were the first clear yellow pigments. In the Middle Ages, Europeans manufactured lead tin yellow (two types of which type I is tetragonal Pb_2SnO_4 and type II is cubic pyrochlore $\text{Pb}(\text{Sn},\text{Si})\text{O}_3$). They later rediscovered the method for the production of Naples yellow, which was used by the Egyptians. Ever increasing expertise and technology led to the creation of many other yellows, including chrome yellow, cadmium yellow (CdS), lemon yellow, and cobalt yellow ($\text{Na}_3\text{Co}(\text{NO}_2)_6$).⁶



Fig. 1.1 Image of a horse colored with [yellow ochre](#) (17,300 BC) from [Lascaux](#) cave, France.

1.4 Classification of inorganic pigments

Inorganic pigments can be classified from various points of view such as color, natural or synthetic and by chemical types. The classification given in Table 1.1 follows a system recommended by ISO and DIN; it is based on coloristic and chemical considerations.³

Table 1.1 Classification of inorganic pigments

Term	Definition
White pigments	the optical effect is caused by nonselective light scattering (examples: titanium dioxide and zinc sulfide pigments, lithopone, zinc white)
Colored pigments	the optical effect is caused by selective light absorption and also to a large extent by selective light scattering (examples: iron oxide red and yellow, cadmium pigments)
Black pigments	the optical effect is caused by nonselective light absorption (examples: carbon black pigment, iron oxide black)
Effect pigments	the optical effect is caused by regular reflection or interference
Metal effect pigments	regular reflection takes place on mainly flat and parallel metallic pigment particles (example: aluminum flakes)
Pearl luster pigments	regular reflection takes place on highly refractive parallel pigment platelets (example: titanium dioxide on mica)
Interference pigments	the optical effect of colored luster pigments is caused wholly or mainly by the phenomenon of interference (example: iron oxide on mica)
Luminescent pigments	the optical effect is caused by the capacity to absorb radiation and to emit it as light of a longer wavelength
Fluorescent pigments	the light of longer wavelength is emitted after excitation without a delay (example: silver-doped zinc sulfide)
Phosphorescent pigments	the light of longer wavelength is emitted within several hours after excitation (example: copper-doped zinc sulfide)

Pigments appear the colors they are because they selectively reflect and absorb certain wavelengths of visible light. Before looking at the research efforts in pigments, the various aspects of color are described in detail.

1.5 Color

Color is everywhere around us and forms an important part of our everyday life. Color influences our moods and emotions and generally enhances the way in which we enjoy our surroundings.² Colors have meaning, which vary from culture to culture and continent to continent. For instance, yellow is often considered as an auspicious color. The word yellow comes from the Old English 'geolu'. Yellow is associated with sunshine, knowledge, and the flourishing of living creatures, but also with autumn and maturity.

1.5.1 Origin of color

Color is a perception, not a physical property of a material. The beginning of every color experience is a physiological response to a stimulus of light. Human beings can perceive specific wavelengths as colors. The color of an object is a sensory impression received by the individual and triggered by a color stimulus. The color stimulus consists of light from the object incident on the eye, 'light' denoting electromagnetic radiation in the range of wavelengths between about 400 nm and about 700 nm. In terms of the color stimulus, the color impression depends on the distribution of radiant energy over the wavelengths of the visible spectrum. The effect of illumination is due to differences in the distribution of light energy within the visible part of the spectrum.

Colors are experienced in two very different ways. The illuminant mode of vision has two variables: a light source and a viewer. Colors seen in the illuminant mode of vision are seen as direct light and are called additive colors. The object mode of vision has three variables: the light source, the viewer, and the light modifying characteristics of an object. With respect to the object, it is important which fraction of the light incident on it reaches the observer's eye (object mode of vision). This fraction is generally a function of the wavelength, and the nature of this wavelength dependence determines the color. Both the fraction and its wavelength dependence can be controlled through the type of pigment and the level of pigmentation. Colors in

the object mode of vision are seen as light reflected from a surface material and are called subtractive colors.⁷

1.5.2 Describing color

The basic qualities of colors are hue, value, and saturation/chroma. Hue means the name of the color. Hue describes the color of an object using words such as ‘red’, ‘yellow’, ‘green’ and ‘blue’. It is possible to assign the value of hue in terms of the number of degrees around the circle as a gradual progression through the different colors from 0 to 360 degrees. Hues are the most prominent aspects of a chromatic color experience. Value (lightness) describes how light or dark a color is. The third conventional attribute of color is chroma, a specific case of the general attribute saturation. Chroma is the perceived difference in color between the chromatic center and the immediate surround of comparable lightness. Saturation is the perceived difference in color between the chromatic center and the white background. While hue represents the qualitative aspect of a chromatic color, chroma represents a quantitative aspect. This usage of the term chroma was introduced by Munsell and has become widely accepted.⁸ A pictorial representation of hue, value, and saturation/chroma is shown in Fig. 1.2.

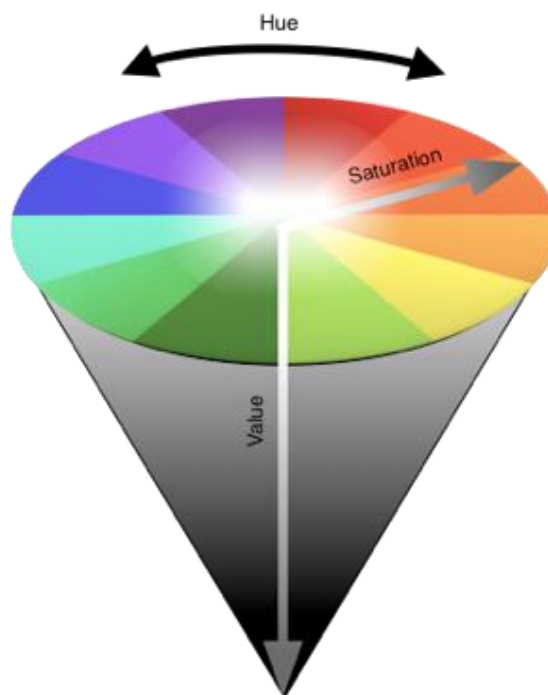


Fig. 1.2 Representation of hue, saturation and lightness.

1.5.3 Color properties

Pigments and coatings are characterized by their spectral reflectance curves $\rho(\lambda)$ or spectral reflectance factor curves $R(\lambda)$.

CIE system of colorimetry

Colorimetry relates the perceived color quality to the color stimulus, which in turn is based on the reflectance spectrum $\rho(\lambda)$. The CIE, or Commission Internationale de l'Eclairage (translated as the International Commission on Illumination), is the body responsible for international recommendations for photometry and colorimetry. In 1931 the CIE standardized color order systems by specifying the light source (or illuminants), the observer and the methodology used to derive values for describing color.

The CIE Color Systems utilize three coordinates to locate a color in a color space. These color spaces include: CIE XYZ , CIE $L^*a^*b^*$, CIE $L^*C^*h^\circ$. The basic CIE color space is CIE XYZ . It is based on the visual capabilities of a Standard Observer, a hypothetical viewer derived from the CIE's extensive research of human vision. A hypothetical observer having the tristimulus color-mixture data was recommended in 1931 by the CIE for a 2° viewing angle. A supplementary observer for a larger angle of 10° was adopted in 1964. If not specified, the 2° Standard Observer should be assumed. If the field of view is larger than 4° , the 10° Standard Observer should be used.

Color matching functions are the tristimulus values of the equal-energy spectrum as a function of wavelength. The coordinates X , Y , and Z were assigned to the three primaries – red, green and blue - that must be present in order for the average human visual system to perceive all the colors of the visible spectrum. Separate sets of three color-matching functions are specified for the 2° Standard Observer and 10° Standard Supplementary Observer. The color matching for the 2° Standard Observer and 10° Standard Supplementary Observer is shown in Fig.1.3.

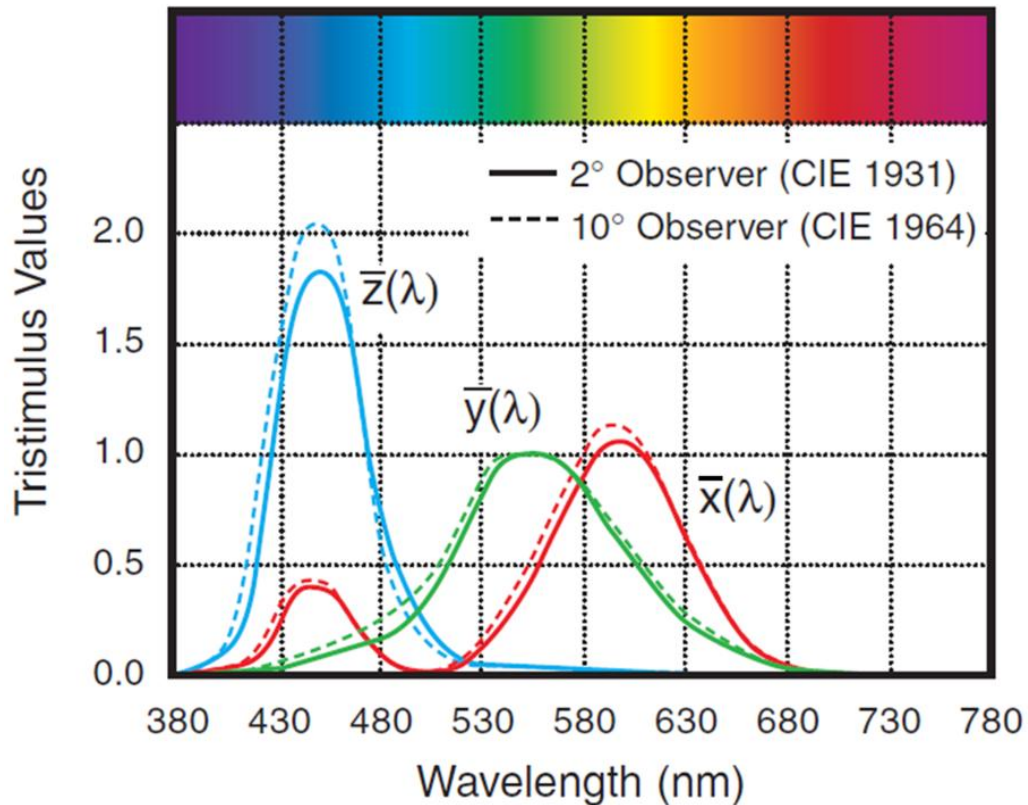


Fig. 1.3 CIE 2° and 10° Standard Observers (courtesy: www.x-rite.com)

The illuminant is a graphical representation of the light source under which the samples are viewed. Defining the properties of the illuminant is an important part of describing color in many applications. The CIE's standards provide a universal system of pre-defined spectral data for several commonly-used illuminant types. Standard illuminant sources which serve as illuminants are classified into four types shown in Table 1.2.

The D65 illuminant represents a standard daylight typical of average daylight. D55 represents a yellower daylight such as may be provided by sun-light with sky-light and that labelled D75 represents a bluer daylight such as may be provided by a north sky. The spectral power distribution of D65 is shown in Fig. 1.4.

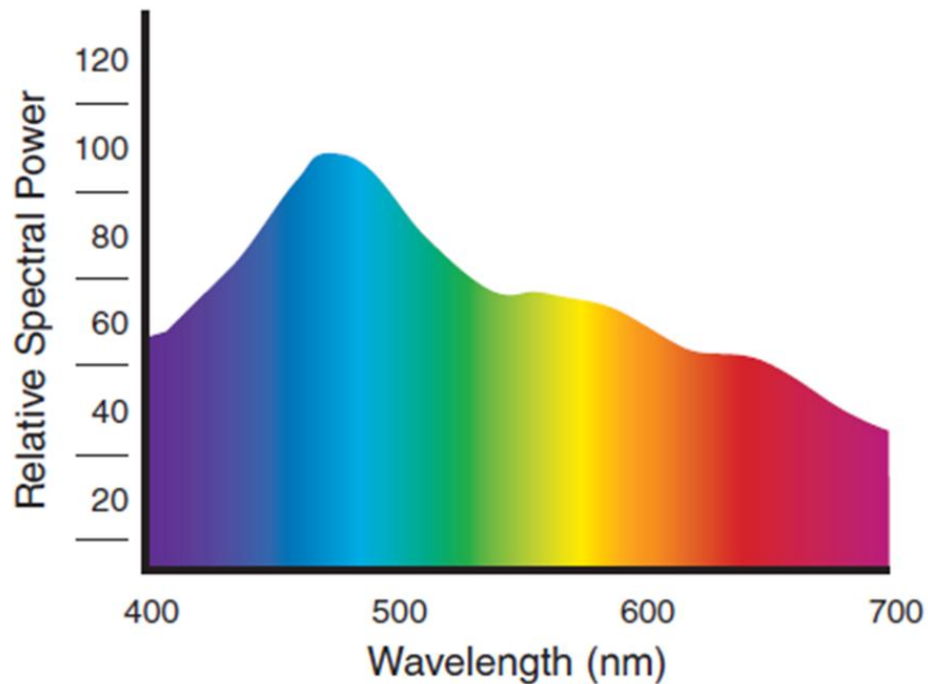


Fig. 1.4 Daylight - Standard Illuminant D65/10° (courtesy: www.x-rite.com)

Table 1.2 Standard Illuminants

Illuminant	Characteristics
A	CIE Standard Illuminants for incandescent illumination, yellow-orange in color, with a correlated color temperature of 2856 K
B	represents direct sunlight at about 4874 K
C	CIE Standard Illuminants for tungsten illumination that simulates average daylight (ultraviolet region not included), bluish in color, with a correlated color temperature of 6774 K
D	CIE Standard Illuminants for daylight, based on actual spectral measurements of daylight. D65 with a correlated color temperature of 6504 K is most commonly used. Others include D50, D55, and D75
F	CIE Standard Illuminant for fluorescent illumination. F2 represents a cool white fluorescent lamp (4200 K), F7 represents a broad-band daylight fluorescent lamp (6500 K), and F11 represents a narrow-band white fluorescent lamp (4000 K)

As said earlier, to obtain X , Y , Z values, we must understand how they are calculated. The instrument perceives the reflected light wavelengths as numeric values. These values are recorded as points across the visible spectrum and are called spectral data which is the most precise description of the color of an object.

Spectral data is represented as a spectral curve which is the color's fingerprint (Fig.1.5). The color's reflectance curve is taken and multiplied the data by a CIE standard illuminant. The result of this calculation is multiplied by the CIE standard observer. Once these values are calculated, the data is converted into the tristimulus values of X, Y, Z . Thus tristimulus value of the object color (X, Y, Z) = Spectral distribution of the illuminants x spectral reflectance of the measurement object x color matching functions.

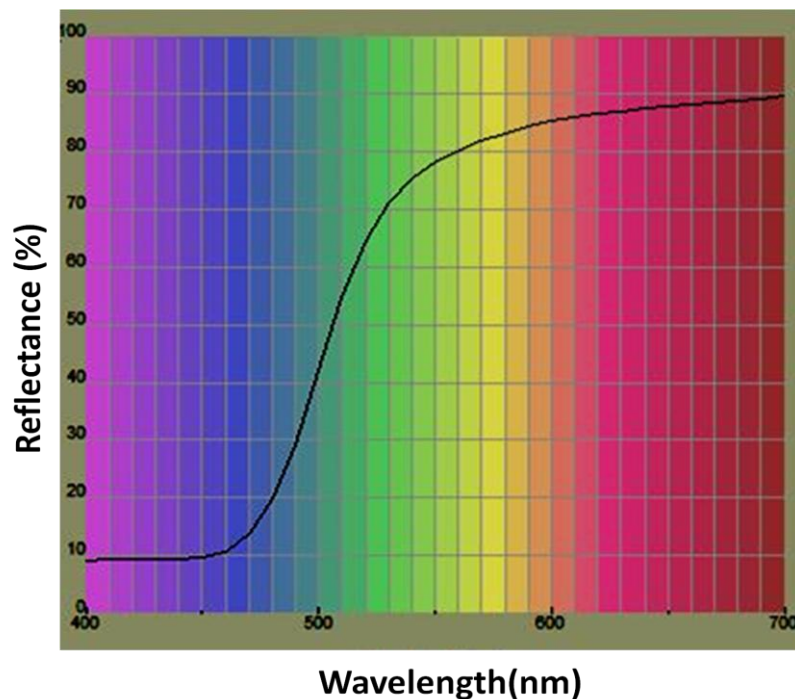


Fig. 1.5 Spectral curve from a measured sample.

Chromaticity Values

By using the color matching functions, light stimuli having any spectral power distribution can be specified for color by three values:

$$X = \int_{400}^{700} \bar{x}(\lambda) \rho(\lambda) S(\lambda) d(\lambda) \quad (1.1)$$

$$Y = \int_{400}^{700} \bar{y}(\lambda) \rho(\lambda) S(\lambda) d(\lambda) \quad (1.2)$$

$$Z = \int_{400}^{700} \bar{z}(\lambda) \rho(\lambda) S(\lambda) d(\lambda) \quad (1.3)$$

where $\bar{x}(\lambda)$, $\bar{y}(\lambda)$, and $\bar{z}(\lambda)$ are the CIE tristimulus values of the spectral colors and are called the CIE spectral tristimulus values (color matching function). The CIE chromaticity coordinates (x , y , and z) are given by

$$x = \frac{X}{X + Y + Z} \quad (1.4)$$

$$y = \frac{Y}{X + Y + Z} \quad (1.5)$$

$$z = 1 - x - y \quad (1.6)$$

They are represented as coordinates in a color plane. The chromaticity coordinates x and y are used to specify the saturation and hue of any color in the CIE chromaticity diagram. A third color variable is specified in addition to x and y , namely the CIE tristimulus value Y , which is a measure of lightness. One drawback of the 1931 chromaticity diagram is the fact that equal distances on the chart do not represent equally perceived color differences because of the non linear nature of the human eye. The 1976 uniform chromaticity CIE chart (Fig.1.6) was developed to provide a perceptually more uniform color spacing for colors at approximately the same luminance. The coordinates used here are denoted (u' , v') and can be computed from the 1931 x , y coordinates by the following transformation:

$$u' = \frac{4x}{(-2x + 12y + 3)} \quad (1.7)$$

$$v' = \frac{9y}{(-2x + 12y + 3)} \quad (1.8)$$

This system allows exact measurement of color with worldwide agreement. For pigment testing, however, this is not sufficient because small color differences usually have to be determined and evaluated. Using the CIE system, it is certainly possible to say which spectral distributions are visually identical, but this is not suitable for determining color differences. To establish color differences an “absolute color space” must be used. Here, colors are arranged three-dimensionally such that the distance between two colors in any direction in space corresponds to the perceived

difference. Such a type of color space can be based on the color qualities: lightness, hue, and saturation. Several such systems exist. The most widespread color system is probably the Munsell system, which is available in the form of an atlas.

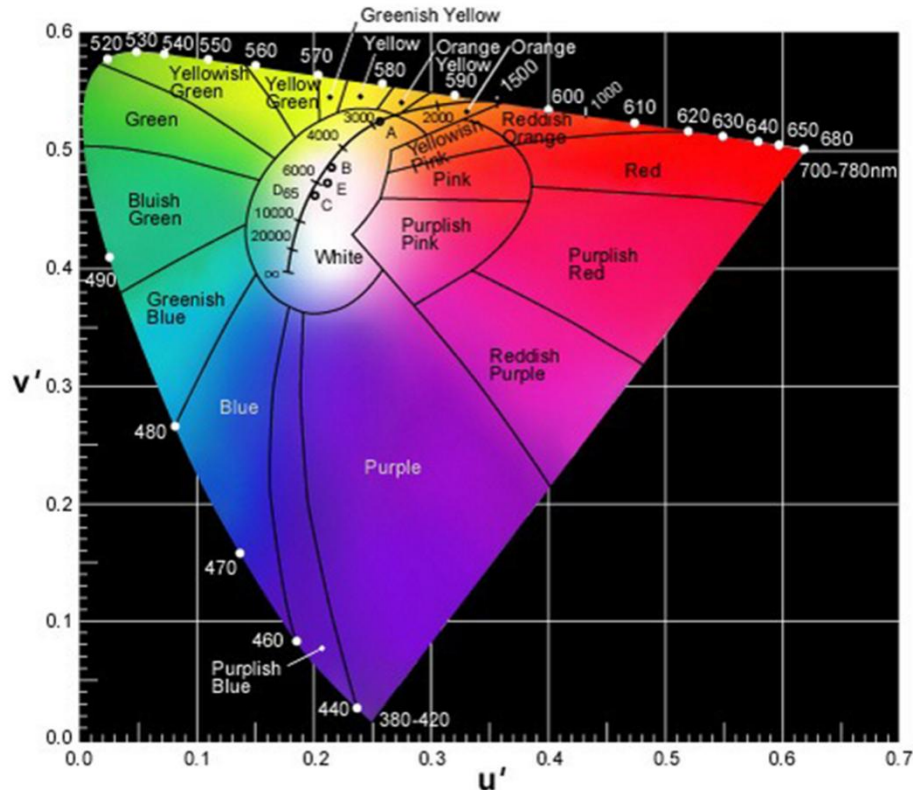


Fig. 1.6 The 1976 CIE chromaticity diagram.

For the quantitative determination of color differences, the transformation relationships between the CIE system and the physiologically equidistant color system must be established. Color differences can then be calculated in the latter system. To overcome the limitations of chromaticity diagrams, the CIE recommended a uniform color scale: CIE 1976 ($L^*a^*b^*$) utilizing an Adams-Nickerson cube root formula, adopted by the CIE in 1976 for use in the measurement of small color differences. When a color is expressed in CIELAB, L^* defines lightness, a^* denotes the red/green value and b^* the yellow/blue value (Fig.1.7). CIELAB uses Cartesian coordinates to calculate a color in a color space.³

To calculate the CIE $L^*a^*b^*$ coordinates, X , Y , and Z are first converted into the functions X^* , Y^* , and Z^* by using a relationship that approximately takes account of the physiologically equidistant lightness steps.

$$X^* = \sqrt[3]{\frac{X}{X_n}}; Y^* = \sqrt[3]{\frac{Y}{Y_n}}; Z^* = \sqrt[3]{\frac{Z}{Z_n}} \quad (1.9)$$

where X_n , Y_n and Z_n are the CIE tristimulus values of a perfect reflecting diffuser ($R(\lambda)=1$). For radicands ≤ 0.008856 , these equations become

$$X^* = 7.787 \frac{X}{X_n} + 0.138 \quad (1.10)$$

$$Y^* = 7.787 \frac{Y}{Y_n} + 0.138 \quad (1.11)$$

$$Z^* = 7.787 \frac{Z}{Z_n} + 0.138 \quad (1.12)$$

The L^* , a^* and b^* values are then calculated as:

$$L^* = 116 Y^* - 16 \quad (1.13)$$

$$a^* = 500 (X^* - Y^*) \quad (1.14)$$

$$b^* = 200 (Y^* - Z^*) \quad (1.15)$$

The components of the color difference are obtained as differences between the test sample (T) and the reference pigment (R).

$$\Delta E_{ab}^* = \sqrt{(\Delta L^*)^2 + (\Delta a^*)^2 + (\Delta b^*)^2} \quad (1.16)$$

$$\Delta L^* = L_T^* - L_R^* \quad (1.17)$$

$$\Delta a^* = a_T^* - a_R^* \quad (1.18)$$

$$\Delta b^* = b_T^* - b_R^* \quad (1.19)$$

A significant advantage of the CIE system is that the color difference can be broken down into components in another way: into brightness, chroma and hue, corresponding to the arrangement in the color space.^{3,9}

The lightness, chroma and hue difference are given by the following equations,

$$\Delta L^* = L_T^* - L_R^* \quad (1.20)$$

$$\Delta C_{ab}^* = C_{ab(T)}^* - C_{ab(R)}^* = \left(\sqrt{(a_T^*)^2 + (b_T^*)^2} - \sqrt{(a_R^*)^2 + (b_R^*)^2} \right) \quad (1.21)$$

$$\Delta H_{ab}^* = \sqrt{(\Delta E_{ab}^*)^2 - (\Delta L^*)^2 - (\Delta C_{ab}^*)^2} \quad (1.22)$$

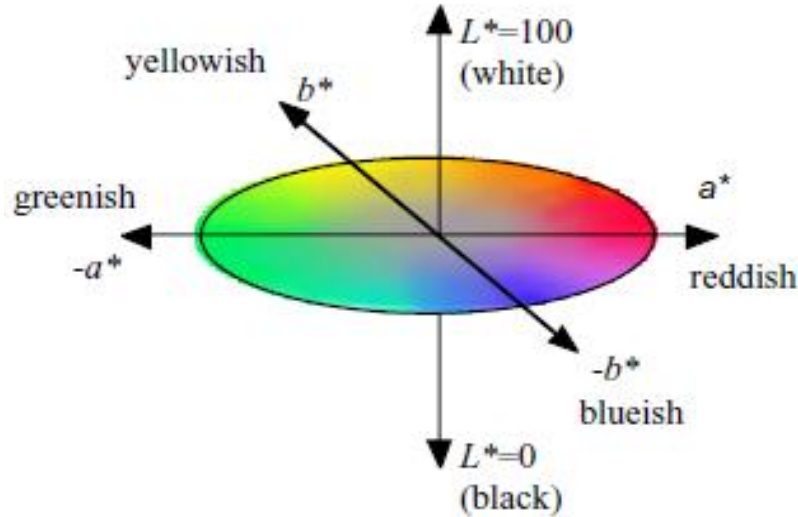


Fig. 1.7 Representation of the CIE *Lab* system.

Kubelka–Munk theory

The Kubelka–Munk theory relates $\rho(\lambda)$ to scattering coefficient S , absorption coefficient K , film thickness h . The Kubelka–Munk theory is based on the fact that the optical properties of a film which absorbs and scatters light may be described by two constants: the absorption coefficient K and the scattering coefficient S . In a simplification, the flux of the diffuse incident light is represented by a single beam L^+ , and the flux of the light scattered in the opposite direction by a beam L^- . Each beam is attenuated by absorption and scattering losses, but is reinforced by the scattering losses of the respectively opposite beam. The absorption and scattering losses are determined quantitatively by the two coefficients K and S . A simple system of two linked differential equations can be written. These can be integrated for the valid boundary conditions at the incident light side, and at the opposite side. Solutions for the transmittance τ and the reflectance ρ are obtained from these integrals as a function of K , S , h , and in special cases of the reflectance ρ_0 of a given substrate. The most important and widely used quantity derived from the Kubelka–Munk theory is the reflectance of an opaque (infinitely thick) film that is described by a very simple equation:

$$\frac{K}{S} = \frac{(1 - \rho_{\infty})^2}{2\rho_{\infty}} \quad (1.23)$$

From this expression (Kubelka–Munk function) it follows that, within the range of validity of the theory, ρ_{∞} depends only on the ratio of the absorption coefficient to the scattering coefficient, and not on their individual values.¹⁰ This theory is widely accepted for explaining the optical properties of complex systems such as powders.

Multiple scattering

The theory of multiple scattering relates the scattering coefficient to the pigment volume concentration and to the scattering cross section of the individual particle. The absorption coefficient is directly proportional to the absorption cross section and to the pigment volume concentration. However the relationship between the scattering coefficient S and the concentration gives rise to problems. The distance between the pigment particles decreases with increasing concentration; consequently there is interaction and hindrance between the light scattered by individual particles, and their scattering power usually falls. The scattering coefficient is therefore linearly related to concentration only at low concentrations (the Beer's law region), at higher concentrations it remains below the linear value.¹⁰

Mie's theory

Mie's theory finally relates scattering and absorption cross section to the particle size, the wavelength, and the optical constants of the material namely refractive index and optical index.

Fig.1.8 represents a schematic diagram showing the relationship between optical properties of pigments and their theoretical fundamentals.

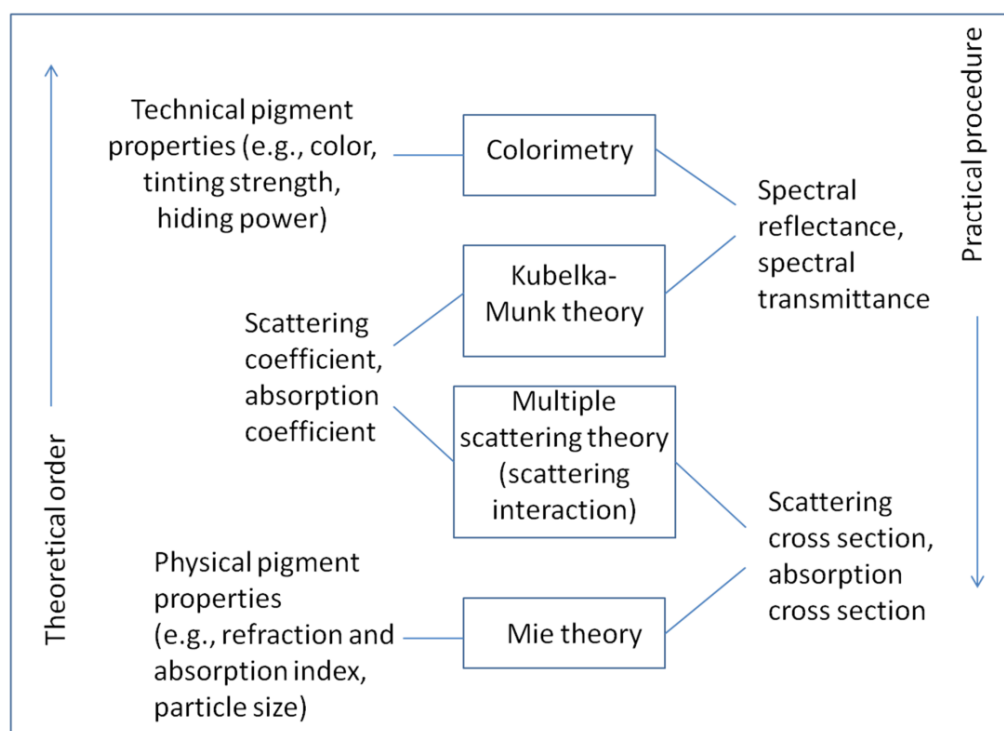


Fig. 1.8 Relationship between the optical properties of pigments and their theoretical basis.³

1.6 Research efforts in yellow pigments

The most known yellow inorganic pigments are praseodymium-zircon yellow, vanadium-zirconia yellow, tin-vanadium yellow, chromates of alkaline earth metal ions, lead and zinc, lead antimonate, cadmium yellow, iron oxide yellow (α and γ -FeOOH), and nickel-antimony doped rutile phase TiO₂. Among these inorganic yellow pigments, the application of iron oxide yellow gets constrained due to thermal stability only up to 220°C,¹¹ while the toxicity¹² of Cr(VI), cadmium and lead based yellow pigments restricts their commercial usage. A wide class of materials has been investigated for their pigmentary properties. Some important families of yellow inorganic pigments are given in the preceding section.

Praseodymium zircon yellow

Praseodymium yellow (ZrSiO₄:Pr)¹³ has been known as one of the environment-friendly inorganic yellow pigments for ceramics. The cations are generally assumed to form a solid solution with the zircon lattice. In general, Pr ions are considered to be located at the triangular dodecahedral positions of Zr⁴⁺, however it is also suggested that Pr⁴⁺ may substitute for both Zr⁴⁺ and Si⁴⁺ of the zircon

lattice.¹⁴ Studies suggest that temperature, particle size and reactivity of the zirconia, and mineralizer content are important variables. Various formulations in the literature indicate that, to obtain an intense yellow, the praseodymium oxide content should be in the range of 3–8 wt%.¹⁵ Lesser contents are too weak to produce a homogeneous, bright color. In high percentages, praseodymium oxide imparts a greenish-yellow color, because the coloring component is not fully incorporated into the zircon lattice.¹⁶ The difference in color properties between samples of Pr yellow prepared in the absence or in the presence of NaF has been reported. The main role of NaF in the preparation of Pr-Zircon pigments is to decrease the temperature of zircon formation to the range in which the chromophore responsible for the bright yellow color, i.e. the Pr (IV) – zircon solid solution, is stable.¹⁷ The color produced in Pr-Zircon pigment is due to the f electrons moving across the energy gap created by the crystal field splitting of the f orbitals of the coloring ion Pr³⁺. The magnitude of the splitting depends on the interactions of f electrons of the Pr³⁺ ion with the surrounding electrons and also determines the intensity of the color. But this pigment has to be synthesized at elevated temperatures (above 1273 K), which tends to induce particle growth of the pigments. Accordingly, it is difficult to apply the praseodymium yellow to paints and inks in which fine dispersion of the pigments is essential.¹⁸ Various shades of yellow (different from the Pr-Zircon yellow) were observed when terbium oxide was incorporated into the zircon host lattice. The variation in shade is considered due to the presence of different types and amounts of mineralizer, calcined at various temperatures.¹⁹

Rutile yellow

Ni doped-TiO₂ with rutile structure has been traditionally used in ceramic pigments for its intense optical properties. Due to their high thermal stability these pigments have gained considerable industrial interest in recent years as potential alternatives to praseodymium zircon yellow pigment, essentially for bulk coloration of porcelain stoneware tiles.²⁰ Sorly *et al.* reported the structure and color of nickel doped rutile phase yellow pigment Ni_xA_{1-3x}B_{2x}O₂ [A = Ti(IV), Sn(IV); B = Sb(V), Nb(V)] prepared by conventional ceramic method.²¹ The role of counterions (Mo, Nb, Sb, W) in doped rutile ceramic pigments with compositions Ni_xA_{1-3x}B_{2x}O₂ and Ni_xA_{1-2x}B_xO₂ [A = Ti(IV), Sn(IV); B = W(VI), Mo(VI)] has been investigated and tungsten is found to be the most suitable counterion for best titanate pigments formulation in

glaze applications.²² Nanosized rutile structured $\text{Ni}_{0.1}\text{W}_{0.1}\text{Ti}_{0.8}\text{O}_2$ prepared by pyrolysis of precursor solution exhibited yellow coloration with reddish shades.²⁰

Ni-containing rutile crystals appear more or less bright yellow shade depending on the Ni content in the solid solution but also on the nature of the co-doping ion. This yellow color is mainly caused by absorption in the blue and red regions of the spectrum of Ni^{2+} ions in an octahedral coordination. The comparison of classical ceramic synthesis of $\text{Ti}_{1-2x}\text{Nb}_x\text{Ni}_x\text{O}_{2-x/2}$ system with the sol-gel methodology, which allows a reduction of the anatase-rutile transformation temperature has been reported. Ni^{2+} was the main specie responsible for the yellow coloration.²³ The composition was optimized in order to obtain a unique rutile phase with the minimum amount of pollutant Ni (II) and enhanced chromatic coordinates.

Yellow oxynitrides

Ternary metal oxynitrides have attracted considerable attention because of their bright coloring, while oxide perovskites are usually colorless. As a function of progressive nitrogen enrichment, oxynitride solid solutions constitute a promising alternative as colored pigments.²⁴ The optical properties of the oxynitride solid solution $\text{GaN}:\text{ZnO}$ were investigated by Maeda *et al.*²⁵ They found that these materials have yellowish color. The $(\text{Ga}_{1-x}\text{Zn}_x)(\text{N}_{1-x}\text{O}_x)$ compounds have smaller band gap values than the pure end members GaN and ZnO. The samples have their absorption edges shifted to longer wavelengths when x (Zn content) increases.

The system $\text{Ta}_{(3-x)}\text{Zr}_x\text{N}_{(5-x)}\text{O}_x$ ($0 \leq x \leq 0.6$) was studied by Guenther and Jansen.²⁶ Pure Ta_3N_5 is dark red and with the introduction of $\text{Zr}^{4+}/\text{O}^{2-}$ in the crystal lattice, the compounds start presenting orange and yellow colors. By substituting the “softer” nitrogen atoms for the “harder” oxygen atoms, the band gap increases and the color is shifted from red to yellow.

Solid solutions of the perovskites CaTaO_2N and LaTaON_2 are proposed as promising candidates for cadmium based pigment. The band gap widening is brought about by increasing the difference of electronegativities between the respective cationic and anionic elements, and vice versa. Their color can be tuned through the desired range, from yellow through orange to deep red, by simple composition adjustments. Although these pigments are non-toxic and show excellent color hue, it is necessary to heat the starting materials in a flow of toxic and inflammable ammonia gas for a long time (20–60 h) to synthesize them.²⁷

New oxynitride compositions with a defect fluorite-type structure have been synthesized by a thermal ammonolysis of rare earth tungstates. Starting from the tungstates $\text{Re}_{14}\text{W}_4\text{O}_{33}$ and $\text{Re}_6\text{WO}_{12}$ (where Re = Rare earth ions) a progressive substitution of nitrogen for oxygen within the anionic network is shown to be possible with the formation of two oxynitride solid solution domains. The color of the powders changes continuously from white to yellow with the nitrogen enrichment as a function of the nitridation temperature and time. Among these oxynitride compositions, the samarium based phase $\text{Sm}_{14}\text{W}_4\text{O}_{23.4}\text{N}_{6.4}$ is particularly attractive by its spectral characteristics. The coloring mechanism is explained by a decrease in the energy band gap, as nitrogen gives with cationic elements more covalent bonds than oxygen. Thus, progressive $\text{N}^{3-}/\text{O}^{2-}$ anionic substitution gives access to a new class of pigments with, in addition, the possibility to tune the absorption edge position to a precise value.²⁸

Pyrochlore based yellows

The basic representative of pyrochlore pigments is the Naples yellow $\text{Pb}_2\text{Sb}_2\text{O}_7$ which represents sulphur-yellow up to orange-yellow tint depending on the mass ratio of lead and antimony. Since development of harmless inorganic pigments has been required in order to replace the toxic pigments by environmentally friendly or less toxic ones new pyrochlore based pigments have been investigated. The $\text{Ln}_2\text{Zr}_{1.5}\text{V}_{0.5}\text{O}_7$ compounds, where Ln = Dy, Ho, Er, Tm, Yb and Lu, were studied as pigments. The richest hues were obtained by using holmium and thulium. All pigments give the yellow color in ceramic glazes, but those containing Ho and Er provide orange hues.²⁹

Pyrochlore type $\text{Y}_{2-x}\text{Ca}_x\text{Ti}_{2-x}\text{V}_x\text{O}_7$ pigments with x varying between 0.02 and 0.3 were reported by Pailhe *et al.*³⁰ Moreover, various synthesis temperatures were performed and the influence of a post-mechanical grinding of the sample was studied. Pigments with various colorations from yellow to deep orange can be obtained depending on the synthesis parameters linked to a slight modification of the vanadium coordination environment. For a same composition, the pigment coloration depends on the creation of Frenkel pairs inside the structure corresponding to a displacement of an oxygen atom toward one interstitial empty site.

Ceria based yellows

Different lanthanides-based yellow inorganic pigments have been studied by researchers as alternative to the existing toxic pigments. Pigments based on CeO_2 have been extensively studied for their coloring properties. The coloring mechanism is essentially based on the charge transfer band from O_{2p} – Ce_{4f} in the semiconducting CeO_2 . In the development of new pigments using cerium, rare-earth-containing pyrochlore system $\text{Ce}_2\text{Ti}_2\text{O}_7$ has been reported. The coloration of titanates was ascribed to charge-transfer transitions in which an electron is transferred from the metal ion to the empty 3d orbitals of the Ti^{4+} ion. In contrast, the presence of Ce^{4+} can generate charge-transfer bands that are also related to the color mechanism, which, in this case, a yellow coloration. Calcination in air or with the use of soft reducing agents leads to CeO_2 – TiO_2 compositions (including solid solutions) with yellow to green colorations. In contrast, with the use of an aggressive reducing agent such as H_2 , the pyrochlore structure is obtained, and the color changes to brownish shades.

In amorphous $\text{Ce}_{1-x}\text{Zr}_x\text{W}_2\text{O}_8$ ³¹ ($\text{M} = \text{Zr}$ or Ti , $0 \leq x \leq 0.6$) based pigments, the coloring mechanism is based on $\text{O } 2p$ – $\text{Ce } 4f$ and $\text{O } 2p$ – $\text{W } 5d$ double charge–transfer transitions. The optical absorption edge of these pigments depends on the Zr or Ti content. CeO_2 – ZrO_2 – Bi_2O_3 solid solutions synthesized by a citrate complex route have been reported as potential environment-friendly pigments by Masui *et al.* The yellow hue of the pigment was significantly enhanced by the introduction of zirconium and bismuth into the CeO_2 lattice, which produces intrinsic strain and a hybrid orbital of Bi 6s and O 2p. The most attractive yellow color was obtained for $\text{Ce}_{0.43}\text{Zr}_{0.37}\text{Bi}_{0.20}\text{O}_{1.9}$. Similarly, pigments with the formula $\text{Ce}_{1-x-y}\text{Si}_x\text{Bi}_y\text{O}_{2-y/2}$ were prepared by a sol-gel method. Among the samples, $\text{Ce}_{0.36}\text{Si}_{0.31}\text{Bi}_{0.33}\text{O}_{1.835}$, demonstrated comparable color properties over that of zircon yellow. Here, the origin of color is due to synergetic modification of the band structure by the hybrid orbital formed from the Bi 6s and O 2p orbitals, as well as the formation of intermediate energy levels due to Si^{4+} doping.³² The variation of hue obtained by substituting Bi^{3+} in Ce^{3+} sites in $\text{LiCeMo}_2\text{O}_8$, $\text{NaCeMo}_2\text{O}_8$, $\text{Ca}_{0.5}\text{CeMo}_2\text{O}_8$ and $\text{Ca}_{0.5}\text{CeMo}_2\text{O}_8$ was studied by Odaki *et al.* In addition, the change of hue of the compounds when Mo^{6+} is replaced by W^{6+} was also investigated. The results indicate that changes in the chemical bonding nature of the crystal have a great impact on the color development of Ce^{3+} ion.³³

The Ce-S-Si system has been explored in search of new, yellow nontoxic pigments. As yellow pigments to substitute for CdS, PbCrO₄, and PbMoO₄, sulfides of Ce³⁺ are also appropriate if their Ce³⁺ 4f¹-5d⁰ transition starts at 2.5 eV. This might be achieved by increasing the ionicity of the Ce-S bonds. According to the inductive effect, the ionicity of a Ce-S bond can be increased by forming a Ce-S-M bond linkage with a third element M that makes a strong covalent bond with S. In a Ce-S-M compound, one might expect that this energy-lowering effect is larger for the 4f than for the 5d orbitals of Ce, thereby increasing the Ce 4f¹-5d⁰ gap, because the Ce 4f orbitals are much more localized on the Ce atom than are the Ce 5d orbitals. Ce₆Si₄S₁₇ and Ce₄Si₃S₁₂ exhibit chromatic properties that are comparable to those of the industrial pigments.³⁴

Tantalum doping into zirconia matrix of Ce_{0.8}Zr_{0.2}O₂ leads to the formation of Ce_{1-(x+y)}Zr_xTa_yO_{2+δ} (*x* ranges from 0.15 to 0.20 and *y* ranges from 0 to 0.05) displaying colors ranging from white to yellow. The coloring mechanism is based on the strong absorptions of the pigments in the visible region under 500 nm, which could originate from the additional energy level between O 2p valence band and the Ce 4f conduction band by forming a hybrid orbital of Ta 5d and O 2p. The designed yellow pigments were also found to be suitable candidates for the coloration of plastics.³⁵ Yellow pigments based on solid solutions of mixed oxides with the general formula Sm_{6-x}W_{1-y}Zr_xMo_yO_{12+δ} was prepared by solid-state route. The systematic substitution of Mo⁶⁺ for W⁶⁺ in Sm₆WO₁₂ gently shifted the absorption edge from 374 to 460 nm and consequently the designed compounds exhibited colors ranging from white to yellow.³⁶

Tungstate and molybdate yellows

There are a relatively few number of tungstates used as pigments. Tungstate pigments of the formula MNdW₂O₈ where M = Ni, Zn and Mn were synthesized by solid state method. MnNd₂W₂O₁₀ was obtained as really monophasic sample with ochre yellow color.³⁷

New tungstate based ceramic pigments, displaying Zn_xNi_{1-x}WO₄ stoichiometry, were obtained at low temperature using a polymeric precursor method. The absorption spectra of the Zn_xNi_{1-x}WO₄ pigments separated into discrete absorption Gaussian bands, showing absorption bands centered in the range of 2.71-2.78 eV, due to [NiO₆] transitions. The maximum absorption of such band takes place

in the blue region, from 458 to 446 nm, and the pigment color perceived corresponds to yellow, the complementary color of blue.³⁸

A new chromium doped powellite (Cr-CaMoO_4) yellow ceramic pigment alternative to yellow of praseodymium-zircon has been obtained based on $\text{Cr}_x\text{CaMo}_{1-x}\text{O}_4$ solid solution of Cr^{6+} substituting Mo^{6+} in the powellite lattice. Using an ammonia coprecipitation method and firing at 950°C , a yellow ceramic pigment is obtained which show a yellow color similar to the commercial praseodymium-zircon yellow pigment. However the release and possible mobilization of the Cr (VI) should be controlled in order to get its industrial implementation.³⁹

Bismuth based yellows

Pigments on the base of Bi_2O_3 belong to pigments of oxide types and seem to be interesting, because they provide interesting color hues from yellow to orange. The high temperature phase of $\delta\text{-Bi}_2\text{O}_3$ may be stabilized below room temperature by partial cationic substitution for Bi^{3+} . Thus, the use of Ln^{3+} cations has been appeared effective though a variety of crystal phases have been observed depending on the kind and amount of the rare earth cation used and the synthesis conditions employed.⁴⁰

In $(\text{Bi}_2\text{O}_3)_{1-x}(\text{RE}_2\text{O}_3)_x$ where $\text{RE} = \text{Y}$ and Ce , results show that Y doped pigments exhibit better properties like phase purity and coloration.⁴¹ Y-doped Bi_2MoO_6 pigments have been synthesized and it is observed that the substitution of yttrium for bismuth red shifted the absorption edge of the colorants leading to yellow color. These pigments absorb the visible and the ultraviolet light under 500 nm efficiently, which is originated in the transition from the valence band consisting of the O 2p orbitals to the conduction band derived from the primary Mo 4d orbitals in MoO_6 octahedra and the secondary Bi 6p orbitals. The effective yellow hue was observed for BiYMoO_6 , which imparted good coloration to plastics.⁴²

A zinc oxide pigment with an admixture of bismuth oxide has been prepared as a new yellow pigment for coloring plastics and paints. The effect of the Bi_2O_3 content in the starting mixture on the color hue of the pigment and the temperature conditions for the pigment synthesis have been evaluated.⁴³

Pigments of the $\text{Bi}_{2(1-x)}\text{RE}_{2x}\text{O}_3$ type, where $x = 0.5$ and $\text{RE} = \text{Er}$, Ho , La , Nd , Lu , Dy and Y , were studied. The color of these compounds is orange (with Er), yellow–orange (Ho, Y, Lu, Dy and Nd) and light yellow (for La).⁴⁴ Intense yellow-

orange colors in $\text{Bi}_{2-x}\text{Er}_{x/2}\text{Zr}_{3x/8}\text{O}_3$ pigments are based on the incorporation of doped Er^{3+} and Zr^{4+} ions into the host lattice of Bi_2O_3 .

BiVO₄ based yellows

Bismuth vanadates (BiVO_4) belong to a relatively new class of pigments. The status of knowledge in the area of BiVO_4 based colorants has been reviewed from literatures.

U.S Patent No. 4,115,142 describes the processes for the preparation of this pigment by reacting bismuth nitrate with an alkali vanadate under controlled conditions to obtain a bismuth vanadate gel followed by aqueous digestion or calcination to produce pigmentary, bright primrose yellow monoclinic bismuth vanadate.⁴⁵ U.S Patent No. 4,455,174 proposes bismuth vanadate/molybdate derivatives and bismuth vanadate/ tungstate derivatives as yellow pigments. These are multi-phase products consisting of a bismuth vanadate phase and also a bismuth molybdate and/or bismuth tungstate phase.⁴⁶ U.S Patent No. 4,272,296 discloses BiVO_4 based yellow pigments diluted with 10-90 % by weight of orthorhombic BaSO_4 .⁴⁷ U.S Patent No. 4,026,722 describes the preparation of pigments with composition $\text{BiVO}_4 \cdot x\text{Al}_2\text{O}_3 \cdot y\text{SiO}_2$ where x is 0.25-2.0, y is 0.1-3.5, and $x + y$ is ≥ 1 . Compared with cadmium sulphide the resulting pigments possess low color purity and low hiding power. U.S Patent No. 4,230,500 discloses a new greenish-yellow, yellow and orange-yellow pigments which consist substantially of bismuth vanadate of monoclinic structure, bismuth phosphate of monoclinic structure and aluminum phosphate of orthorhombic structure and which, in the case of the yellow and orange-yellow pigments, also comprise a compound based on Bi_2O_3 and V_2O_5 .⁴⁸ U.S Patent No. 4,251,283 discloses greenish-yellow pigments based on BiVO_4 are disclosed which based on BiVO_4 obtained by the calcination, in the presence of air, of a mixture of BiPO_4 , V_2O_5 and an oxide of Ca, Ba, Mg or Zn.⁴⁹

Bright yellow coloration and enhanced NIR reflectance of monoclinic bismuth vanadate are obtained by the substitution of Ta/P into the vanadium sites of BiVO_4 . Pentavalent metal ion substitution in BiVO_4 blue shifted the absorption edge leading to bright yellow coloration and the color properties are comparable to that of commercially praseodymium yellow.⁵⁰

Transparent, yellow bismuth vanadate nanoparticles were made by flame spray pyrolysis. Depending on the particle collection temperature, either pale,

amorphous materials or brilliant yellow-green, crystalline BiVO_4 with particle size of about 50 nm were formed by direct calcination above 300°C . The addition of Si during flame synthesis of BiVO_4 resulted in smaller such crystals of about 20 nm that were embedded in silica. This prevented sintering of the BiVO_4 particles during calcination at 400°C and resulted in thermally stable, highly transparent, yellow particles.⁵¹

$\text{Bi}_{1-x}\text{La}_x\text{VO}_4$ ($0 \leq x \leq 0.15$)⁵² and $\text{Bi}_{1-x-y}\text{Ca}_x\text{Zn}_y\text{VO}_{4-(x+y)/2}$ ($0 \leq x \leq 0.10$; $0 \leq y \leq 0.10$)⁵³ solid solutions as novel inorganic yellow pigments with brilliant yellow colors were prepared by hydrothermal and evaporative drying method respectively. Thus, the color of BiVO_4 can be tuned by introducing other elements into the BiVO_4 lattice to control the lattice size. The extent of the orbital hybridization in the valence band should depend on the interionic distance between Bi^{3+} and O^{2-} . Novel inorganic yellow pigments, $\text{Bi}_{1-x-y-z}\text{Ca}_x\text{Zn}_y\text{La}_z\text{VO}_{4-(x+y)/2}$ ($0.04 \leq x \leq 0.12$; $0.01 \leq y \leq 0.05$; $0.01 \leq z \leq 0.10$) were synthesized as environmentally friendly inorganic materials, using an evaporative drying method. The color of the pigments depended on the amount of Ca^{2+} , Zn^{2+} and La^{3+} , and the most vivid yellowness was obtained for $\text{Bi}_{0.85}\text{Ca}_{0.08}\text{Zn}_{0.02}\text{La}_{0.05}\text{VO}_{3.950}$.⁵⁴

1.7 IR reflecting pigments

Visible light (0.4–0.7 μm) contains 43% of the power in the air-mass 1.5 global solar irradiance spectrum (0.3–2.5 μm); the remainder arrives as near-infrared (NIR) radiation (0.7–2.5 μm , 52%) or ultraviolet (UV) radiation (0.3–0.4 μm , 5%).⁵⁵ Heat is a direct consequence of infrared radiation incident on an object. These radiations on absorption as well as conduction result in heating up of the surface of materials. Absorption of solar energy by concrete and paved structures raises their surface temperature several degrees over that of the ambient air, which also then increases. Consequently, urban heat island effect, a phenomena caused by the lower albedo (reflective power) of urban surfaces and the replacement of vegetation by buildings is increasing.⁵⁶ This effect is becoming more intense in urban areas, changing their microclimate. Summer urban heat islands with daytime average air temperatures 5.6°C higher than the surrounding rural areas are present in many cities around the world.⁵⁷ The heat island effect has been documented in hundreds of cities worldwide. Apart from causing thermal discomfort, the greater consumption of

cooling energy drive up energy demand and costs,⁵⁸ and accelerate the formation of harmful smog.⁵⁹

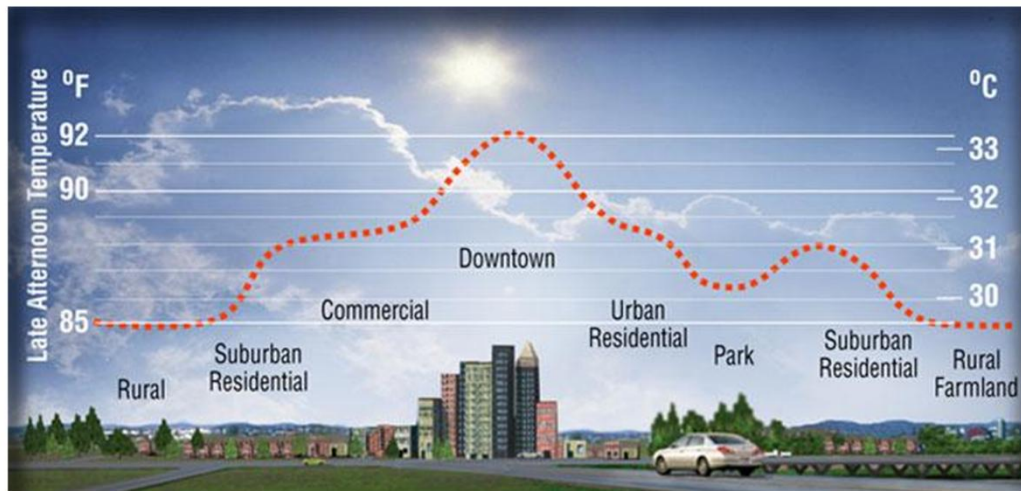


Fig. 1.9 Urban heat island effect ⁶⁰

Urban heat island effect is schematically represented in Fig.1.9. To reduce the increasing demand for energy consumption for air conditioning, there is a need for cooler roofs. Reflecting the sun's radiation minimizes the amount of energy absorbed by the building. Mitigating the urban heat island phenomenon requires cool materials that are characterized by high solar reflectance and IR emittance values.⁶¹ A roof with high solar reflectance stays cool in the sun, reducing demand for cooling power in conditioned buildings and increasing occupant comfort in unconditioned buildings.⁶² These techniques also work by lowering the temperature of the ambient air, because the cooler the surface, the lower the heat convection intensity. The need to save energy, which comes as a result of the depletion of natural resources and increasing prices, has pronounced relevance in a developing country like India. The influence of solar reflection on roofs of surrounding buildings is estimated by a coupled simulation of radiation and convection around buildings, and the results show that reflective solar radiation from high-reflectance roofs to the walls of neighbouring buildings is considerably less than direct radiation from the sun and sky.

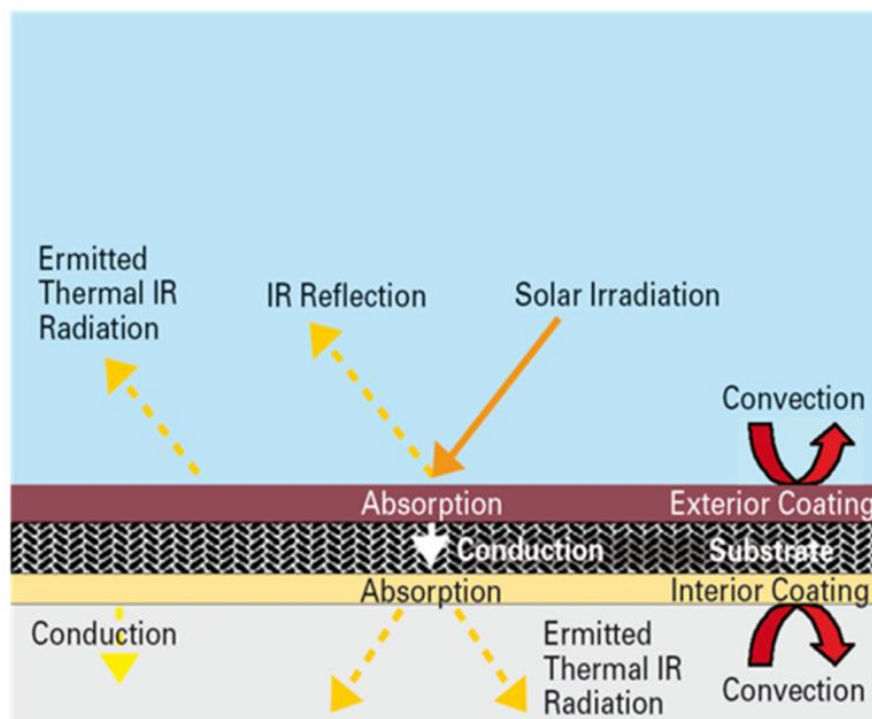


Fig. 1.10 Energy transfer in buildings (courtesy: www.ferro.com)

Recently, infrared reflective inorganic pigments have been attracting more and more interest which not only impart color to an object, but also reflect the invisible heat from the object to minimize heat build-up, when exposed to solar radiation (Fig.1.10). Inorganic class of IR reflectors are mainly metal oxides and are primarily useful in two major applications: (i) visual camouflage and (ii) reducing heat build-up on the surface of building roofing materials.⁶³

In recent decades, the application of solar reflective pigments on buildings and urban infrastructures has been studied by many researchers. Advanced cool colored materials have been developed by including IR reflective pigments in the basic formulation of traditional paints.⁶⁴ A comprehensive analysis has been conducted by Levinson *et al.*⁶⁵ who have published a detailed survey of 87 organic and inorganic pigments with high IR reflecting properties. Most of them have found application in roof products such as clay and concrete tiles, metal roofs and asphalt shingles leading to an increase of solar reflectance up to 20% for most absorbing materials. A number of cool materials are currently available commercially for buildings and other surfaces of the urban environment. In a study from Greece, the increasing heat island effect in urban areas was investigated.⁶⁴ The heat island effect caused discomfort, heavy energy demand and the smog formation. Infrared reflecting pigments were found to

lower the surface as well as near surface air temperatures. The surface temperature was up to 10°C lower, and the air temperature up to 1.6°C lower.

Pigment color is closely related to the effect of heat reflection. White materials have the best performance in heat reflection. For instance, white coating made from titanium dioxide pigment can reach a reflectance as high as 87%.⁶⁵ However, white coating has some disadvantages such as

- Cool/white top coated roofs can reflect adversely toward overlooking or uphill neighbours,
- Airline pilots can be negatively impacted by such reflections for the same reason at particular angles to the sun.
- Many white topcoat products discolor with dirt and cannot be cleaned.

So, white pigments are unsatisfactory for people with demands for coating function and color. Nevertheless, non white pigments are preferred considering artistic beauty. IR reflective pigments are increasingly used for roof and building coatings because of their excellent weatherability, which indicate their vast potential application. However many of these pigments encompass toxic metals such as chromium green, cobalt blue, cadmium stannate, lead chromate, cadmium yellow and chrome titanate yellow, and hence their consumption is being limited.

In view of this many IR reflective pigments have been proposed as alternatives to traditional toxic IR pigments. The U.S Patent No. 6,541,112 describes a process for the synthesis of a series of rare earth manganese oxides, $(RE_xMn)O_y$ (RE = Y, La, Ce, Pr, Nd, and Sm) with good IR reflectivity.⁶⁶ Manganese vanadium oxide pigments of the formula $Mn_2V_2O_7$ with improved infrared reflectivity suitable for reducing IR-induced heat buildup has been described in U.S Patent No. 6,485,557.⁶⁷

Some recently proposed IR reflective inorganic pigments include yellow $Sr_2Ce_{1-x}Tb_xO_4$,⁶⁸ nano yellow $NiTiO_3$,⁶⁹ yellow Fe^{3+} doped $La_2Mo_2O_7$,⁷⁰ blue Fe^{3+} doped $YMnO_3$,⁷¹ nano brown Mg^{2+} doped $ZnFe_2O_4$,⁷² nano yellow Nd^{3+} doped Y_6MoO_{12} ,⁷³ Fe^{3+} doped $KZnPO_4$ ⁷⁴ and brown pigments based on a Fe_2O_3 - Sb_2O_3 - SiO_2 - Al_2O_3 - TiO_2 composition.⁷⁵ However, the color characteristics are not high compared to IR reflectance in these pigments.

Thus the use of IR reflective coatings with high solar reflectance could be the solutions for ever demanding energy savings.

1.8 Motivation and objective of the work

Yellow is an important color in pigment industry. Road markings, signs and safety markings are often bright yellow. The agricultural, construction and engineering markets often use bright yellow for visibility and identity. Heavy metals such as lead, chromium (VI), cadmium, zinc are major components of several inorganic pigments that historically played a major role in the high performance of decorative and industrial coatings. To insure that their benefits far outweigh their liabilities, research efforts are directed toward the development of environmentally acceptable pigments that do not release any toxic materials into the environment during their production, use or disposal. There exist a large number of yellow inorganic pigments. However, their color properties are not satisfactory as compared to the existing industrially used toxic pigments. In addition, the demand for infrared reflective pigments that can be used in the coating formulation to reduce the heat build-up of the buildings, roofs, cars etc. is increasing. So developing less toxic inorganic pigments that have a greater infrared reflectivity versus traditional toxic pigments for high performance coatings is highly essential while maintaining the appropriate light absorption in the visible spectrum to impart color.

BiVO_4 belongs to a new class of inorganic pigments that has steadily gained importance over the past few years. But it has been difficult to control the pigmentary properties of BiVO_4 . Color intensity depends on many factors including phase composition, stoichiometry, particle size and morphology. Also, the photophysical properties of BiVO_4 are strongly influenced by the way of preparation and its crystal structure (Fig.1.11).⁷⁶



Fig.1.11 BiVO_4 powders synthesized by different methods⁷⁶

However, bismuth pigments are relatively expensive materials, lowering the commercial competitiveness. Therefore, there is interest in developing new materials containing the BiVO_4 phase, which might enable a more competitive use of this pigment. Also, the IR reflecting property of BiVO_4 based pigments have not been explored well. So the present work focuses on developing new eco-friendly yellow inorganic pigments for various coloring applications by improving the coloristic as well as IR reflecting properties of BiVO_4 by forming solid solutions with transition metals as well as rare earths.

The objectives of this thesis are as follows:

- Synthesize less-toxic yellow pigments in these systems as viable alternatives to the traditional pigment formulations.
 - ▶ $(\text{CaW/Mo})\text{O}_4 - \text{BiVO}_4$
 - ▶ $(\text{LiLa})_{1/2}\text{MoO}_4 / (\text{LiCaLa})_{1/3}\text{MoO}_4 - \text{BiVO}_4$
 - ▶ $(\text{LiRE})_{1/2}\text{MoO}_4 - \text{BiVO}_4$
 - ▶ $(\text{Y/Nb})\text{O}_4 - \text{BiVO}_4$
- Study the structural and optical properties of pigments and explore their coloring mechanism and band gap tuning.
- To modify synthesized pigments using various mineralizers and synthesis methods.
- Application study of the developed pigments for their color as well as IR reflective property on various substrates

1.9 References

1. In *Amer Inkmaker*, DCMA: **1989**.
2. Christie, R. M.; *Colour chemistry*. The Royal Society of Chemistry: UK, **2001**.
3. Buxbaum, G.; Pfaff, G., Eds.; Introduction. In *Industrial Inorganic Pigments*. WILEY-VCH Verlag GmbH & Co KGaA, Weinheim, **2005**.
4. Novotny, M.; Solc, Z.; Trojan, M., Pigments, Inorganic. In *Kirk-Othmer Encyclopedia of Chem. Technol. J.*, John Wiley & Sons, Inc.: **2000**.
5. Barnett, J. R.; Miller, S.; Pearce, E., Colour and art: A brief history of pigments. *Opt. Laser Technol.* **2006**, 38 (4–6), 445–453.
6. <http://www.webexhibits.org/pigments/intro/yellows.html> (accessed 20 June 2015).
7. (a) Herbst, W.; Hunger, K.; Wilker, G.; Ohleier, H.; Winter, R., General. In *Industrial Organic Pigments*, Wiley-VCH Verlag GmbH & Co. KGaA: **2005**;
(b) Holtzschue, L., *Understanding color : an introduction for designers*. John Wiley & Sons, Inc., Hoboken, New Jersey: **2011**.
8. Shevell, S. K., Color Appearance. In *The Science of Color (Second Edition)*, Shevell, S. K., Ed. Elsevier Science Ltd: Amsterdam, **2003**.
9. Volz, H. G., *Industrial color testing: Fundamentals and techniques*. Wiley–VCH, Weinheim: **2002**.
10. Buxbaum, G., Introduction to Inorganic High Performance Pigments. In *High Performance Pigments*, Wiley-VCH Verlag GmbH & Co. KGaA: **2003**.
11. Cornell, R. M.; Schwertmann, U., *The iron oxides; structure, properties, reactions, occurrence and uses*. Wiley–VCH, Weinheim,: **1996**.
12. Badenes, J. A.; Llusar, M.; Tena, M. A.; Calbo, J.; Monros, G., Praseodymium–doped cubic Ca–ZrO₂ ceramic stain. *J. Eur. Ceram. Soc.* **2002**, 22, 1981–1990.
13. Kato, E., Synthesis of yellow Pr-ZrSiO₄ pigments. *Keram. Zeit* **1961**, 13, 617–622.
14. Shoyama, M.; Nasu, H.; Kamiya, K., Preparation of rare earth–zircon pigments by the sol–gel method *J. Ceram. Soc. Jpn. Int. Ed.* **1998**, 106, 279–284.

15. (a) Linke, E. A. E.; Zwart, C. H.; Smout, A. D., Doped zirconium mixed silicate pigment, method for the preparation thereof and products containing such pigment or a thus prepared pigment. U.S. Patent No. 5,275,649, **1994**; (b) Murdock, S. H.; Wise, T. D.; Eppler, R. A., Measurement and interpretation of color in glazes. *Ceram. Eng. Sci. Proc.* **1990**, *11* (3–4), 270–77.
16. Hill, K.; Lehman, R.; Swiler, D., Effects of selected processing variables on color formation in praseodymium-doped zircon pigments. *J. Am. Ceram. Soc.* **2000**, *83* (9), 2177–82.
17. Ocana, M.; Caballero, A.; Gonzalez–Elipse, A. R.; Tartaj, P.; Serna, C. J.; Merino, R. I., The effects of the NaF flux on the oxidation state and localisation of praseodymium in Pr-doped zircon pigments. *J.Eur.Ceram.Soc.* **1999**, *19*, 641–648.
18. Furukawa, S.; Masui, T.; Imanaka, N., New environment-friendly yellow pigments based on CeO₂–ZrO₂ solid solutions. *J. Alloys Compd.* **2008**, *451*, 640–643.
19. Kar, J. K.; Stevens, R.; Bowen, C. R., Novel terbium-zircon yellow pigment. *J. Mater.Sci* **2004**, *39*, 5755 – 5763.
20. Biswas, S. K.; Dhak, D.; Pathak, A.; Pramanik, P., Chemical synthesis of environment– friendly nanosized yellow titanate pigments. *Mater. Res. Bull.* **2008**, *43*, 665–675.
21. Sorly, S.; Tena, M. A.; Badenes, J. A.; Calbo, J.; Llusar, M.; Monros, G., Structure and color of Ni_xA_{1–3x}B_{2x}O₂ (A = Ti, Sn; B = Sb, Nb) solid solutions. *J. Eur. Ceram. Soc.* **2004**, *24*, 2425–2432.
22. (a) Matteucci, F.; Cruciani, G.; Dondi, M.; Raimondo, M., The role of counterions (Mo, Nb, Sb, W) in Cr-, Mn-, Ni- and V-doped rutile ceramic pigments: Part 1. Crystal structure and phase transformations. *Ceram. Int.* **2006**, *32* (4), 385–392; (b) Dondi, M.; Cruciani, G.; Guarini, G.; Matteucci, F.; Raimondo, M., The role of counterions (Mo, Nb, Sb, W) in Cr-, Mn-, Ni- and V-doped rutile ceramic pigments: Part 11. Colour and technological properties. *Ceram. Int.* **2006**, *32* (4), 393–405.
23. Martos, M.; Julián, B.; Dehouli, H.; Gourier, D.; Cordoncillo, E.; Escribano, P., Synthesis and characterization of Ti_{1–2x}Nb_xNi_xO_{2–x/2} solid solutions. *J.Solid State Chem.* **2007**, *180* (2), 679–687.

24. Aguiar, R.; Logvinovich, D.; Weidenkaff, A.; Rachel, A.; Reller, A.; Ebbinghaus, S. G., The vast colour spectrum of ternary metal oxynitride pigments. *Dyes Pigm.* **2008**, *76* (1), 70-75.
25. Maeda, K.; Takata, T.; Hara, M.; Saito, N.; Inoue, Y.; Kobayashi, H.; Domen, K., GaN:ZnO solid solution as a photocatalyst for visible-light-driven overall water splitting. *J. Am. Chem. Soc.* **2005**, *127* (23), 8286-8287.
26. Guenther, E.; Jansen, M., Optical properties of $\text{Ta}_{(3-x)}\text{Zr}_x\text{N}_{(5-x)}\text{O}_x$ semiconductor pigments. *Mater. Res. Bull.* **2001**, *36* (7-8), 1399-1405.
27. Jansen, M.; Letschert, H. P., Inorganic yellow-red pigments without toxic metals. *Nature* **2000**, *404* (6781), 980-982.
28. Diot, N.; Larcher, O.; Marchand, R.; Kempf, J. Y.; Macaudiere, P., Rare-earth and tungsten oxynitrides with a defect fluorite-type structure as new pigments. *J. Alloys Compd.* **2001**, *323-324*, 45-48.
29. Bukovska, L.; Šulcova, P.; Vondrasek, M., The effect of lanthanides on color properties of the $\text{Ln}_2\text{Zr}_{1.5}\text{V}_{0.5}\text{O}_7$ pigments. *Ceram. Mater.* **2011**, *63* (2), 244-247.
30. Pailhé, N.; Gaudon, M.; Demourgues, A., $(\text{Ca}^{2+}, \text{V}^{5+})$ co-doped $\text{Y}_2\text{Ti}_2\text{O}_7$ yellow pigment. *Mater. Res. Bull.* **2009**, *44* (8), 1771-1777.
31. Masui, T.; Furukawa, S.; Imanaka, N., Preparation and characterization of amorphous $\text{Ce}_{1-x}\text{Zr}_x\text{W}_2\text{O}_8$ fine particles for environmental-friendly yellow pigments. *Chem. Lett.* **2005**, *34* (10), 1322-1323.
32. Imanaka, N.; Masui, T.; Furukawa, S., Novel nontoxic and environment-friendly inorganic yellow pigments. *Chem. Lett.* **2008**, *37* (1), 104-105.
33. Odaki, T.; Hashimoto, K.; Toda, Y., The color shift of cerium molybdenum scheelite by substituting Bi^{3+} or W^{6+} ion. *J. Jpn. Soc. Colour Mater.*, **2008**, *81* (3), 73-79.
34. Gauthier, G.; S. Jobic, S.; M. Evain, M.; Koo, H.-J.; Whangbo, M.-H.; Fouassier, C.; Brec, R., Syntheses, structures, and optical properties of yellow Ce_2SiS_5 , $\text{Ce}_6\text{Si}_4\text{S}_{17}$, and $\text{Ce}_4\text{Si}_3\text{S}_{12}$ materials. *Chem. Mater.* **2003**, *15*, 828-837.
35. Vishnu, V. S.; George, G.; Divya, V.; Reddy, M. L. P., Synthesis and characterization of new environmentally benign tantalum-doped $\text{Ce}_{0.8}\text{Zr}_{0.2}\text{O}_2$ yellow pigments: Applications in coloring of plastics. *Dyes Pigm.* **2009**, *82* (1), 53-57.

36. Vishnu, V. S.; Jose, S.; Reddy, M. L., Novel environmentally benign yellow inorganic pigments based on solid solutions of samarium–transition metal mixed oxides. *J. Am. Ceram. Soc.* **2011**, *94* (4), 997-1001.
37. Blovska, V.; Belina, P.; Sulcova, P., Synthesis of tungstate pigments of the formula $MNd_2W_2O_{10}$ (M = Ni, Zn, Mn). *J. Therm. Anal. Calorim.* **2013**, *113*, 83–89.
38. de Oliveira, A. L. M.; Ferreira, J. M.; Silva, M. R. S.; Braga, G. S.; Soledade, L. E. B.; Maria Aldeiza, M. A. M.; Paskocimas, C. A.; Lima, S. J. G.; Longo, E.; Gouveia de Souza, A.; Garcia dos Santos, I. M., Yellow $Zn_xNi_{1-x}WO_4$ pigments obtained using a polymeric precursor method. *Dyes Pigm.* **2008**, *77* (1), 210-216.
39. Galindo, R.; Gargori, C.; Fas, N.; Llusar, M.; Monrós, G., New chromium doped powellite ($Cr-CaMoO_4$) yellow ceramic pigment. *Ceram. Int.* **2015**, *41* (5, Part A), 6364-6372.
40. (a) Takahashi, T.; Iwahara, H., Oxide ion conductors based on bismuth sesquioxide. *Mater. Res. Bull.* **1978**, *13*, 1447–53; (b) Gonzalvo, B.; Romero, J.; Fernandez, F.; Torralvo, M. J., $(Bi,R)_2O_3$ (R: Nd, Sm and Dy) oxides as potential pigments. *J. Alloys Compd.* **2001**, *323-324*, 372–375.
41. Prabhakar Rao, P.; Reddy, M. L. P., Synthesis and characterisation of $(BiRE)_2O_3$ (RE: Y, Ce) pigments. *Dyes Pigm.* **2004**, *63* (2), 169-174.
42. Kumari, L. S.; Gayathri, T. H.; Sameera, S.; Rao, P. P., Y-doped Bi_2MoO_6 yellow pigments for the coloration of plastics. *J. Am. Ceram. Soc.* **2011**, *94* (2), 320-323.
43. Šulcová, P.; Trojan, M., New yellow pigments: $ZnO-Bi_2O_3$. *Dyes Pigm.* **1998**, *36* (4), 287-293.
44. Šulcová, P., Thermal stability and colour properties of new pigments based on $BiREO_3$. *J. Therm. Anal. Calorim.* **2012**, *109* (2), 639-642.
45. Hess, R. W. Pigmentary bright primrose yellow monoclinic bismuth vanadate and processes for the preparation thereof. US Patent No. 4,115,142, **1978**.
46. Wienand Yellow pigment containing bismuth vanadate and having the composition $BiVO_4 \cdot xBi_2MoO_6 \cdot yBi_2WO_6$. U.S Patent No.4,455,174, **1984**.
47. Balducci, L.; Rustioni, M. New inorganic pigments and process for their preparation. U.S Patent No.4,272,296, **1981**.

48. Balducci, L.; Rustioni, M. Inorganic pigments and method for preparing same. U.S Patent No.4,230,500, **1980**.
49. Balducci, L.; Rustioni, M. Bismuth vanadate pigments and process for preparing same. U.S Patent No.4,251,283, **1981**.
50. Sandhya Kumari, L.; Prabhakar Rao, P.; Narayana Pillai Radhakrishnan, A.; James, V.; Sameera, S.; Koshy, P., Brilliant yellow color and enhanced NIR reflectance of monoclinic BiVO₄ through distortion in VO₄³⁻ tetrahedra. *Sol. Energy Mater. Sol. Cells* **2013**, *112*, 134-143.
51. Strobel, R.; Metz, H. J.; Pratsinis, S. E., Brilliant yellow, transparent pure, and SiO₂-coated BiVO₄ nanoparticles made in flames. *Chem. Mater.* **2008**, *20* (20), 6346-6351.
52. Wendusu; Ikawa, K.-i.; Masui, T.; Imanaka, N., Novel environment-friendly yellow pigments based on (Bi, La)VO₄. *Chem. Lett.* **2011**, *40* (8), 792-794.
53. Masui, T.; Honda, T.; Wendusu; Imanaka, N., Novel and environmentally friendly (Bi,Ca,Zn)VO₄ yellow pigments. *Dyes Pigm.* **2013**, *99* (3), 636-641.
54. Wendusu; Honda, T.; Masui, T.; Imanaka, N., Novel environmentally friendly (Bi, Ca, Zn, La)VO₄ inorganic yellow pigments. *RSC Adv.* **2013**, *3* (47), 24941-24945.
55. ASTM G 173-03: Standard tables for reference solar spectral irradiances: Direct normal and hemispherical on 37° tilted surface. ASTM International: West Conshohocken,PA, **2012**.
56. Taha, H., Urban climates and heat islands: albedo, evapotranspiration, and anthropogenic heat. *Energy Build.* **1997**, *25* (2), 99-103.
57. (a) Bendiganavale, A. K.; Malshe, V. C., Infrared Reflective Inorganic Pigments. *Recent Patents on Chemical Engineering* **2008**, *1*, 67-69; (b) Synnefa, A.; Santamouris, M.; Livada, I., A study of the thermal performance of reflective coatings for the urban environment. *Sol. Energy* **2006**, *80* (8), 968-981.
58. (a) Akbari, H.; Berdahl, P.; Levinson, R.; Wiel, S.; Miller, W.; Desjarlais, A. *Cool-Color Roofing Material. California Energy Commission, PIER Building End-Use Energy Efficiency Program; CEC-500-2006-067; 2006; (b) Santamouris, M., *Energy and Climate in the Urban Built Environment*. James and James, London: **2001**; (c) Santamouris, M.; Papanikolaou, N.; Livada, I.; Koronakis, I.; Georgakis, C.; Argiriou, A.; Assimakopoulos, D. N., On the*

- impact of urban climate on the energy consumption of buildings. *Sol. Energy* **2001**, *70* (3), 201-216.
59. Akbari, H.; Pomerantz, M.; Taha, H., Cool surfaces and shade trees to reduce energy use and improve air quality in urban areas. *Sol. Energy* **2001**, *70* (3), 295-310.
60. <https://heatland.lbl.gov/> (accessed 04 August 2015).
61. Bretz, S.; Akbari, H.; Rosenfeld, A., Practical issues for using solar-reflective materials to mitigate urban heat islands. *Atmos. Environ.* **1997**, *32*, 95–101.
62. Doulos, L.; Santamouris, M.; Livada, I., Passive cooling of outdoor urban spaces. The role of materials. *Sol. Energy* **2004**, *77* (2), 231-249.
63. Jeevanandam, P.; Mulukutla, R. S.; Phillips, M.; Chaudhuri, S.; Erickson, L. E.; Klabunde, K. J., Near infrared reflectance properties of metal oxide nanoparticles. *J. Phys. Chem. C* **2007**, *111* (5), 1912-1918.
64. Synnefa, M.; Santamouris, M.; Apostolakis, K., On the development, optical properties and thermal performance of cool colored coatings for the urban environment. *Sol. Energy* **2007**, *81*, 488–497.
65. Levinson, R.; Berdahl, P.; Akbari, H., Solar spectral optical properties of pigments—Part II: survey of common colorants. *Sol. Energy Mater. Sol. Cells* **2005**, *89* (4), 351-389.
66. Swiler, R. D.; Axtell, E. A. Rare earth manganese oxide pigments. U.S. Patent No. 6,541,112, **2003**.
67. Swiler, R. D. Manganese vanadium oxide pigments. U.S. Patent No. 6,485,557, **2002**.
68. Raj, A. K. V.; Rao, P. P.; Sameera, S.; James, V.; Divya, S., Synthesis of novel nontoxic yellow pigments: $\text{Sr}_2\text{Ce}_{1-x}\text{Tb}_x\text{O}_4$. *Chem. Lett.* **2014**, *43* (7), 985-987.
69. Wang, J.-L.; Li, Y.-Q.; Byon, Y.-J.; Mei, S.-G.; Zhang, G.-L., Synthesis and characterization of NiTiO_3 yellow nano pigment with high solar radiation reflection efficiency. *Powder Technol.* **2013**, *235*, 303-306.
70. Han, A.; Ye, M.; Liu, L.; Feng, W.; Zhao, M., Estimating thermal performance of cool coatings colored with high near-infrared reflective inorganic pigments: Iron doped $\text{La}_2\text{Mo}_2\text{O}_7$ compounds. *Energy Build.* **2014**, *84*, 698-703.

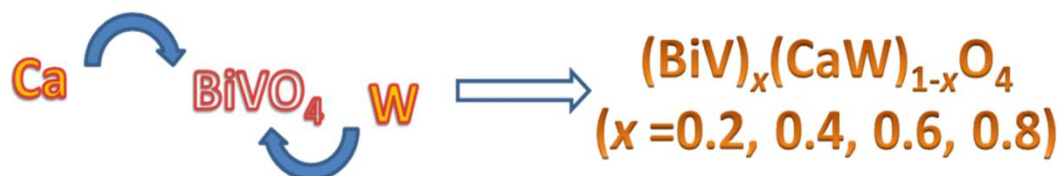
71. Han, A.; Ye, M.; Zhao, M.; Liao, J.; Wu, T., Crystal structure, chromatic and near-infrared reflective properties of iron doped YMnO_3 compounds as colored cool pigments. *Dyes Pigm.* **2013**, *99* (3), 527-530.
72. Liu, L.; Han, A.; Ye, M.; Feng, W., The evaluation of thermal performance of cool coatings colored with high near-infrared reflective nano-brown inorganic pigments: Magnesium doped ZnFe_2O_4 compounds. *Sol. Energy* **2015**, *113*, 48-56.
73. Zhao, X.; Zhang, Y.; Huang, Y.; Gong, H.; Zhao, J., Synthesis and characterization of neodymium doped yttrium molybdate high NIR reflective nano pigments. *Dyes Pigm* **2015**, *116*, 119-123.
74. Wang, D.; Su, D.; Zhong, M., Chromatic and near-infrared reflective properties of Fe^{3+} doped KZnPO_4 . *Sol. Energy* **2014**, *110*, 1-6.
75. Thongkanluang, T.; Chirakanphaisarn, N.; Limsuwan, P., Preparation of NIR reflective brown pigment. *Procedia Engineering* **2012**, *32*, 895-901.
76. Gotić, M.; Musić, S.; Ivanda, M.; Šoufek, M.; Popović, S., Synthesis and characterisation of bismuth(III) vanadate. *J. Mol. Struc.* **2005**, *744–747*, 535-540.

CHAPTER 2A

YELLOW PIGMENTS IN BiVO₄ - CaWO₄ SYSTEM

Overview

New yellow pigments based on scheelite solid solutions, (BiV)_x(CaW)_{1-x}O₄ ($x = 0.2, 0.4, 0.6, 0.8$) exhibit color parameters L^* , a^* , b^* significantly than that of BiVO₄ and are also comparable to praseodymium yellow. CaWO₄ tailored with BiVO₄ allows fine tuning of the band gap resulting in various shades of yellow.



- Modification of the band structure
 - Artificial control of the band gap width
 - New ecological inorganic pigments with various hues

2A.1 Introduction

The scheelite structure is adopted by a large family of compounds with a composition ABO₄. Here A cations with oxidation states +1, +2, +3, +4 and B cation with oxidation states +7, +6, +5, and +4 can be easily accommodated. Some examples, which demonstrate the ability of the scheelite structure to host the cations with variable oxidation state, are: KReO₄ and AgIO₄ (A⁺ and B⁷⁺); CdMoO₄ and CaWO₄ (A²⁺ and B⁶⁺); BiVO₄ and YNbO₄ (A³⁺ and B⁵⁺); ZrGeO₄ (A⁴⁺ and B⁴⁺).¹ The scheelite is the mineral CaWO₄ and the general name of the compounds crystallizing in the tetragonal I41/a phase.² CaWO₄ with a scheelite structure is an important optical material, which has attracted particular interest because of luminescent, scintillators and laser host applications.³ The scheelite-type ABO₄ structure is made up of AO₈ polyhedra and BO₄ tetrahedra connected via common vertices. AO₈ polyhedra connect via the edges and form a three dimensional framework (Fig.2A.1). A number of crystal structures in ABX₄ compounds, consist of BX₄ tetrahedra and AX₈ eight-coordinated polyhedral, which can be seen as two interpenetrating tetrahedra, known as bidisphenoids or dodecahedra.^{2, 4} The crystal structure can be related well with the fluorite type structure where the cations get rearranged due to difference in ionic radii.⁵

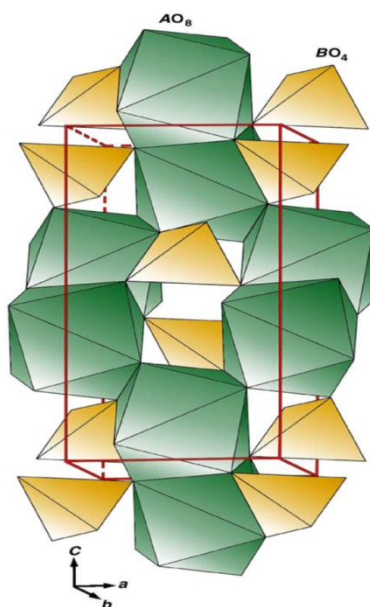


Fig. 2A.1 Polyhedral view of the scheelite-type structure.¹

Currently, there is a strong incentive to design new colorants based on inorganic materials to substitute for industrial pigments that are based on heavy elements. These

pigments are hazardous to health and the environment. For decades PbCrO₄ was one of the most widely used yellow pigments, but concerns about the toxicity of both lead and chromate have significantly reduced its use.⁶ Chrome yellows, oranges and molybdate oranges are used in a large number of different paint systems, which are restricted mostly to maintenance and industrial finishes, because of their toxicity and potential carcinogenic nature. Traditional use of these pigments has been decreasing as a result of environmental regulations. Thus serious need arises to search for environmentally friendly and economically viable materials for the replacement of toxic inorganic yellow pigments.

Less toxic, inorganic metal-oxide yellow pigments, such as titanium-nickel yellow, bismuth vanadate and their combinations with organic pigments, are being used increasingly as a replacement for lead chromate pigments.⁷ Recent investigations reveal that the toxic yellow pigments can be replaced by solid solutions of CeO₂-SiO₂-Bi₂O₃⁸ and CeO₂-ZrO₂-Bi₂O₃.⁹ Among transition metals, vanadium, and more particularly in the pentavalent state, is well known for its coloring properties. For example, vanadium pentoxide V₂O₅, whose color is due to the charge transfer band from O_{2p}²⁻ to V_{3d}⁵⁺, is commonly used as classic yellow pigment in glazes field.¹⁰ The charge transfer energy of the colorless VO₄³⁻ ion is larger than that of the yellow CrO₄²⁻ ion. Consequently, many vanadate salts are white. Among the numerous A_xV_yO_z colored ternary oxides, BiVO₄ is particularly notable. BiVO₄ with scheelite structure, especially a tetragonal system of a high-temperature is found to exhibit murky yellow than monoclinic scheelite BiVO₄ which shows vivid yellow.¹¹

Bismuth vanadate (BiVO₄) is a yellow pigment widely used in ceramics and polymeric systems. However, it has been proven difficult to control the pigmentary colors of BiVO₄.¹² The extension of the color pallet of BiVO₄ is a factor that will increase the commercial competitiveness of this pigment. CaWO₄ is a white powder which absorbs below 400 nm with a wide band gap. Band structure engineering by making solid solutions between two compounds with different band gap can be regarded as one of the efficient methods for producing various shades of the colorants. Since BiVO₄ and CaWO₄ crystallize in similar structures, solid solutions between these two may lead to yellow scheelite based colorants.

In the present chapter, new yellow pigments having the formula (BiV)_x(CaW)_{1-x}O₄ ($x = 0.2, 0.4, 0.6, 0.8$) have been synthesized by solid state method and characterized for their structural and optical properties.

2A.2 Experimental Section

2A.2.1 Materials and Methods

Compositions based on (BiV)_x(CaW)_{1-x}O₄ ($x = 0.2, 0.4, 0.6, 0.8$) were prepared from the corresponding oxides: CaCO₃, Bi₂O₃, V₂O₅ and WO₃ (99.9% purity Acros Organics). Stoichiometric proportions of the chemicals were weighed and were thoroughly wet mixed in agate mortar with acetone as the wetting medium for 1 h and dried in an air oven. This process of mixing and drying was repeated three times to obtain homogeneous mixture. The dried powders were then calcined at 900°C in air for 6 h in a platinum crucible. The pigment compositions thus obtained were ground in an agate mortar in order to refine and homogenize the particle size.

2A.2.2 Characterizations

The phase purity of the samples were investigated by powder X-ray diffraction analysis (XRD) with Ni filtered CuK α radiation ($\lambda = 1.54056 \text{ \AA}$) using PANalytical X'pert Pro diffractometer. Data were collected from 10 to 90° 2 θ range with a step size of 0.016°. Optical reflectance of the powders was measured with UV–vis spectrophotometer (Shimadzu, UV-2401) using barium sulphate as a reference. The measurement conditions were as follows: an illuminant D65, 10° complementary observer and measuring geometry d/8°. The band gap values were calculated from the corresponding absorbance spectra by straight forward extrapolation method using the formula $E_g(\text{eV}) = hc/\lambda$ (where λ represents the wavelength in nm). The color of the pigments was evaluated according to The Commission Internationale del' Eclairage (CIE) through $L^*a^*b^*$ 1976 color scales (CIE-LAB 1976 color scales). In this system L^* is the color lightness (L^* is zero for black and L^* is 100 for white), a^* is the green (-)/ red (+) axis, and b^* is the blue (-)/yellow (+) axis. The parameter C^* (chroma) represents saturation of the color and h° represents the hue angle. The chroma is defined as

$$C^* = \sqrt{(a^*)^2 + (b^*)^2} \quad (2.1)$$

The hue angle, h° is expressed in degrees and ranges from 0 to 360° and is calculated using the formula

$$h^\circ = \tan^{-1} \left(\frac{b^*}{a^*} \right) \quad (2.2)$$

Particle morphological analysis of the powders was performed by means of a scanning electron microscope with a JEOL JSM-5600 LV SEM with an acceleration voltage of 15 kV. The quantitative microanalysis of the samples was carried out by energy dispersive spectrometer (EDAX, USA).

2A.3 Results and Discussion

2A.3.1 X-Ray Diffraction Analysis

The X-ray diffraction patterns of the pigments are given in Fig. 2A.2. The intense and sharp peaks found in the diffraction patterns reveal the crystalline nature of the powders. All compounds crystallize with the tetragonal scheelite structure (space group I4_{1/a}) and the X-ray diffraction patterns are in good agreement with the powder X-ray diffraction file: PDF No.77- 2233. The formation of tetragonal scheelite type structure is confirmed by the absence of characteristic scheelite monoclinic peak at 15°. ¹¹ The crystallite size was calculated from Debye Scherrer formula, $D = 0.9\lambda/\beta\cos\theta$, where D is the crystallite size, λ is the wave length of X – ray used, β and θ are the half width of X – ray diffraction lines and half diffraction angle of 2 θ . The crystallite size is found to decrease with decrease in concentration of bismuth and vanadium in the range from 140-53 nm.

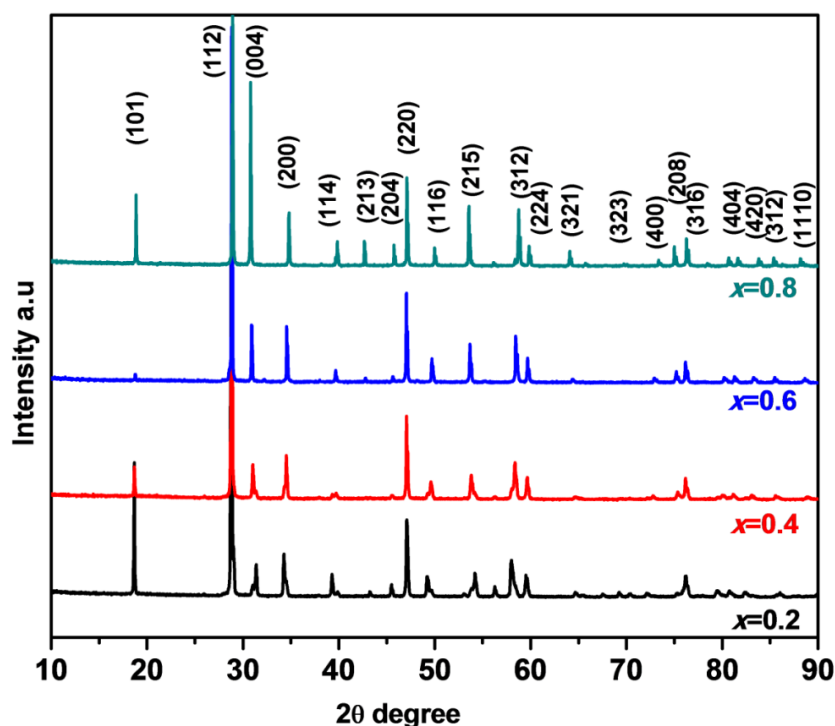


Fig. 2A.2 Powder XRD patterns of (BiV)_x(CaW)_{1-x}O₄ ($x = 0.2, 0.4, 0.6, 0.8$).

2A.3.2 Morphological and Micro chemical Studies

The SEM micrographs of the pigments are shown in Fig. 2A.3. The particles are agglomerated to some extent. SEM analysis shows that the morphology is irregular and average size of sample increases as concentration of BiVO_4 increases. The particle sizes of these pigments vary from 1-8 μm .

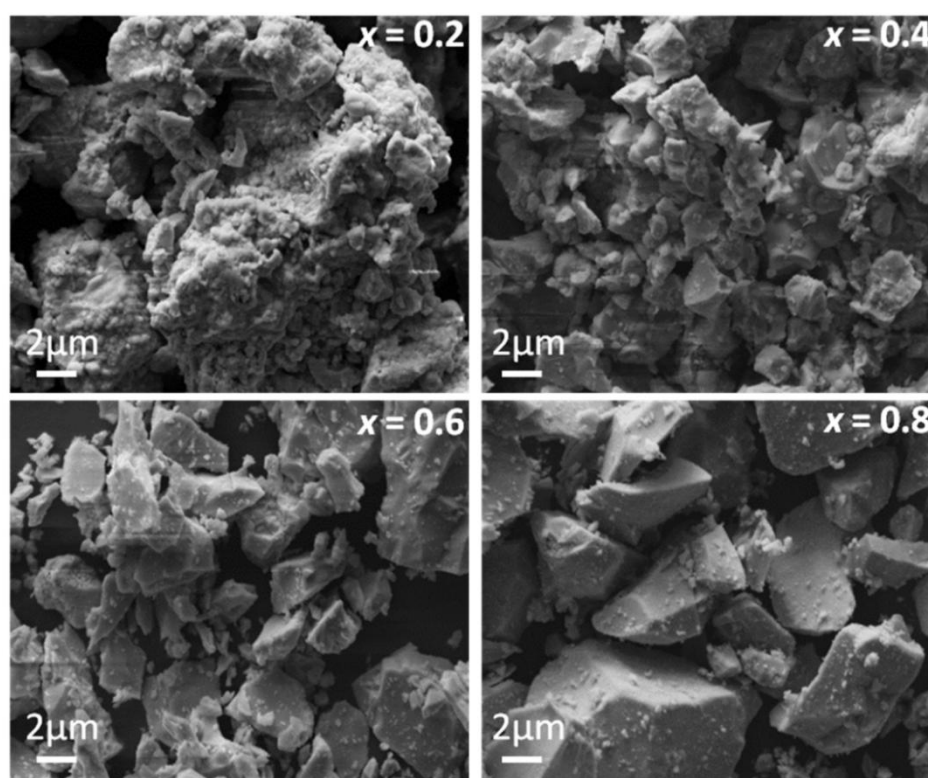


Fig. 2A.3 SEM photographs of $(\text{BiV})_x(\text{CaW})_{1-x}\text{O}_4$ ($x = 0.2, 0.4, 0.6, 0.8$).

Energy dispersive spectra analysis was used to further determine the chemical composition of the as-obtained pigments. The elemental analysis of two typical solid solutions ($x = 0.2$ and 0.8) was performed by EDAX attached to scanning electron microscope. It is found that the obtained stoichiometric composition is very close to the theoretical composition in the analyzed regions (Fig. 2A.4). There was no loss of bismuth and vanadium. This is probably due to the presence of calcium and tungsten whose melting point is relatively very high.

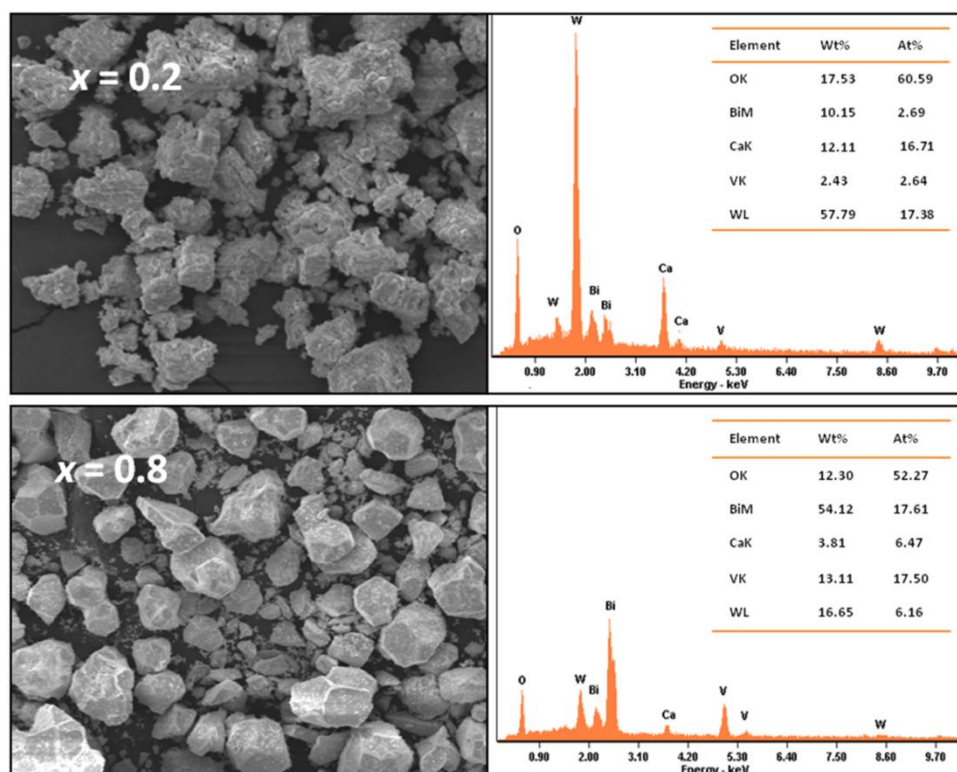


Fig. 2A.4 EDS analysis of $(\text{BiV})_x(\text{CaW})_{1-x}\text{O}_4$ ($x = 0.2, 0.8$).

2A.3.3 UV Visible Studies

Fig. 2A.5 shows the diffuse reflectance spectra of the pigment samples. The diffuse reflectance spectra of both BiVO₄ and CaWO₄ show a shape of two overlapping absorption bands (inset Fig. 2A.5). This feature is weakened in the quaternary solid solutions and a steep absorption can be observed. In the diffuse reflectance spectra it is seen that with increase in concentration of bismuth and vanadium a red shift is observed and consequently the band gap is also seen to be decreasing.

The apparent band gap energies are also listed in Table 2A.1. The steep absorption at higher energies is attributable to the fine tuning of the band gap. The band gap energy strongly depend on the composition and varies with x from 2.79 - 2.50 eV. The band gap of BiVO₄ and CaWO₄ were detected as 2.34 and 3.8 eV, respectively.¹³ The band gap of $\text{Ca}_{1-x}\text{Bi}_x\text{V}_x\text{W}_{1-x}\text{O}_4$ compounds which is intermediate between either end member clearly indicates the possibility of tuning the band gap by mixing two solid solutions with different band gaps to produce pigments with different shades.

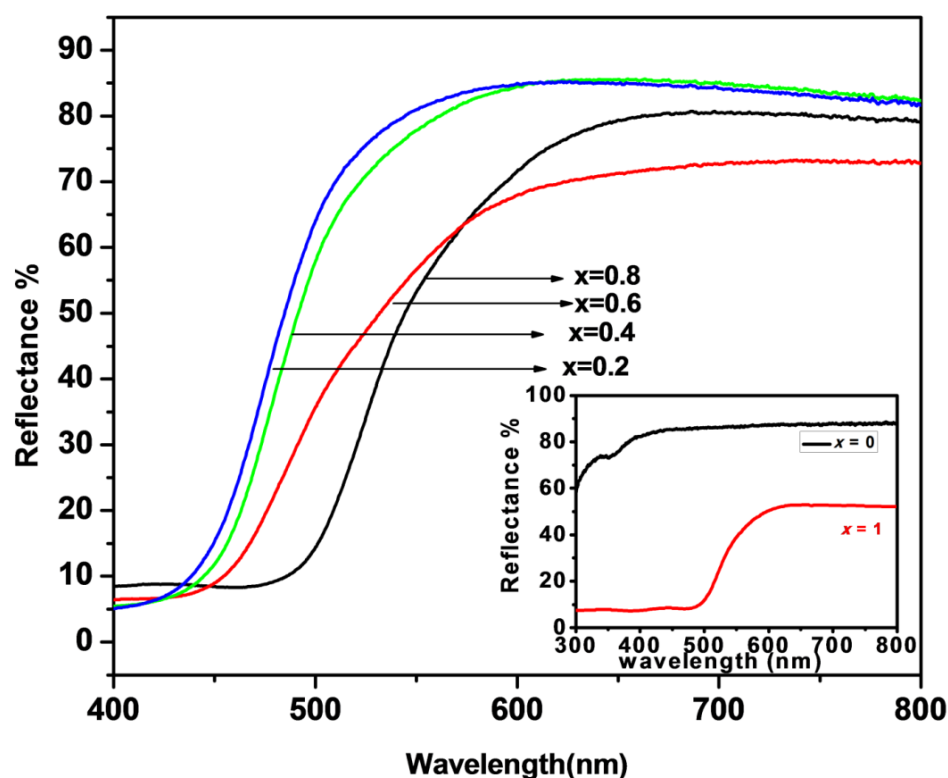


Fig. 2A.5 Reflectance spectra of $(\text{BiV})_x(\text{CaW})_{1-x}\text{O}_4$ ($x = 0 - 1$).

CaWO₄ have large, nearly identical band gap that falls in the UV region. Aron *et al.*¹⁴ reports that BiVO₄ is found to be a direct band gap semiconductor and direct gap is maintained via coupling among V 3d, O 2p, and Bi 6p, which lowers the conduction band minimum. Ca_{1-x}Bi_xV_xW_{1-x}O₄ pigments absorb in the visible blue region which arises due to three main charge transfer transitions, O_{2p} – V_{3d}, O_{2p} – W_{5d} and the O_{2p} – Bi_{6p} (Fig. 2A.6). Doping of Bi³⁺ and V⁵⁺ into CaWO₄ lattice results in enhancement of visible blue light absorption due to the transition from a new hybrid band made up of hybrid orbitals of Bi 6s, V 3d and O 2p into the W 5d conduction band. When Ca²⁺ is replaced by Bi³⁺, the filled Bi 6s orbitals raise the top of the valence band while the Bi 6p orbitals lower the bottom of the conduction band, resulting in a reduction in the band gap with $\Delta E = 1.01$ and 1.30 for the typical compositions with $x = 0.2$ and 0.8 respectively. Thus, these solid solutions allow fine band gap tuning resulting in various shades of yellow.

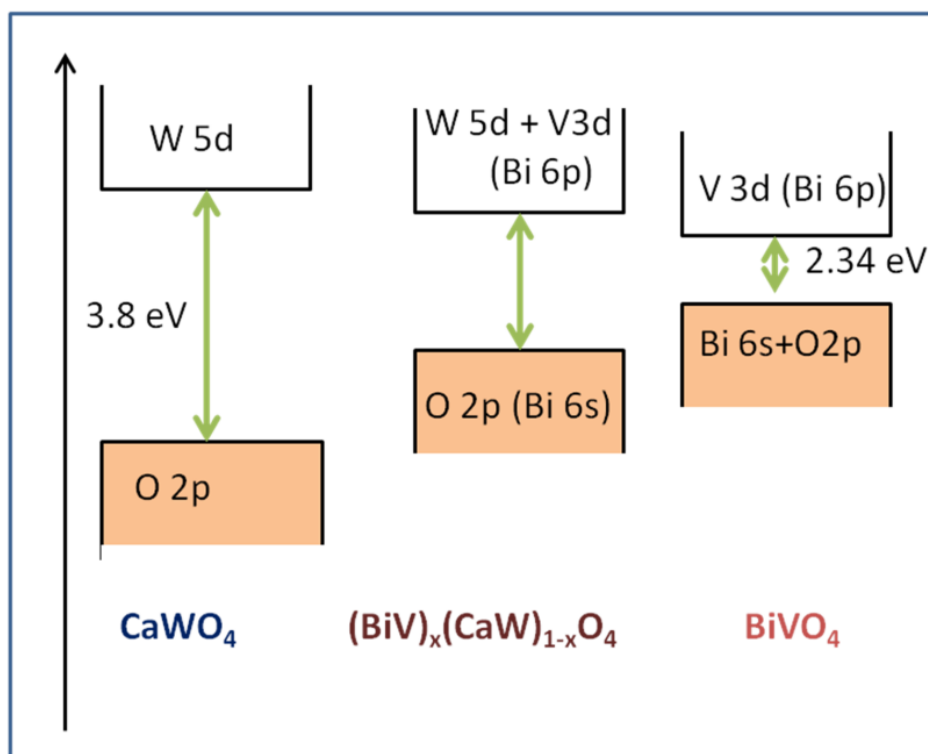



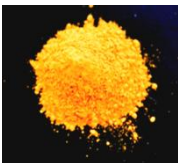
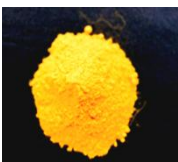
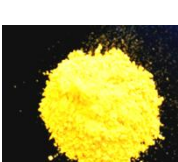


Fig. 2A.6 Band structure of $(\text{BiV})_x(\text{CaW})_{1-x}\text{O}_4$ ($x = 0 - 1$).

2A.3.4 Color Analysis

Color co-ordinates of the synthesized pigments are listed in Table 2A.1. The pigments show lightness value L^* ranging from 76 - 90, color coordinates with low a^* and high b^* (+ve) values. Compared to BiVO_4 , the L^* , a^* , and b^* values of the synthesized pigments were improved significantly in the solid solutions of $(\text{BiV})_x(\text{CaW})_{1-x}\text{O}_4$ and are also comparable to praseodymium yellow (Table 2A.1). This may be due to the high refractive index (1.97) and opacity of CaWO_4 .¹⁵

An ideal yellow color is characterized by high lightness $L^* > 60$, yellowness $b^* > 50$, high purity C_{ab}^* (0-100) and hue angle $\sim 90^\circ$. The pigment composition with $x = 0.6$, exhibits high lightness, purity (C_{ab}) and hue angle, h_{ab} close to 90° . By introducing bismuth and vanadium into CaWO_4 , various shades of bright yellow pigments with greenness ($-a^*$) and redness ($+a^*$) can be produced along with high purity yellow pigment ($x = 0.6$).

Table 2A.1 Color coordinates and band gap of (BiV)_x(CaW)_{1-x}O₄ (x = 0.2 - 1)

Composition	<i>L</i> *	<i>a</i> *	<i>b</i> *	<i>C</i> *	<i>h</i> °	Eg(eV)
 BiVO ₄ ¹⁶	68.00	16.50	42.30	54.57	74.78	2.34
 (BiV) _{0.8} (CaW) _{0.2} O ₄	76.78	13.23	68.92	70.12	79.17	2.51
 (BiV) _{0.6} (CaW) _{0.4} O ₄	79.35	-1.29	61.79	61.84	88.89	2.74
 (BiV) _{0.4} (CaW) _{0.6} O ₄	89.40	-10.52	65.00	65.87	80.82	2.76
 (BiV) _{0.2} (CaW) _{0.8} O ₄	90.69	-13.64	59.96	61.43	77.18	2.79
 Praseodymium yellow ¹⁷	83.5	-3.28	70.3	----	----	2.42

2A.3.5 Color performance

To evaluate the yellow hue consistency of the synthesized pigments for various applications such as in coloration of plastics, the typical (BiV)_{0.6}(CaW)_{0.4}O₄ pigment with greenish yellow hue was selected for the studies. 10 wt % of the pigment was incorporated in poly(methyl methacrylate) PMMA to obtain cylindrical disc (image is shown in Fig. 2A.7). The color coordinates of the polymer discs were analyzed at different locations on the surface and the values obtained were more or less the same, revealing the uniform distribution of the pigment particles in the polymer substrate.

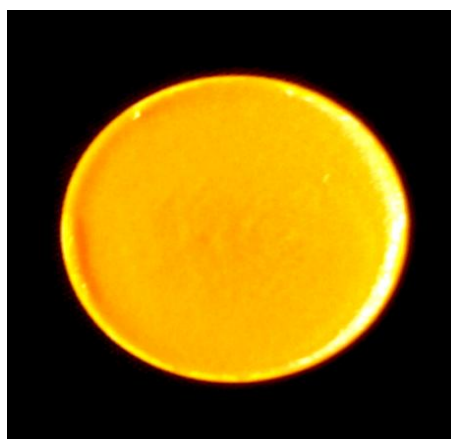


Fig. 2A.7 Photographs of 10 wt% (BiV)_{0.6}(CaW)_{0.4}O₄ + PMMA.

Table 2A.2 Color coordinates of 10 wt% (BiV)_{0.6}(CaW)_{0.4}O₄ pigment in PMMA

Composition	<i>L</i> *	<i>a</i> *	<i>b</i> *	<i>C</i> *	<i>h</i> ⁰
(BiV) _{0.6} (CaW) _{0.4} O ₄	79.35	-1.29	61.79	61.84	88.89
PMMA+10% (BiV) _{0.6} (CaW) _{0.4} O ₄	68.17	-2.81	65.63	76.89	87.55

2A.4 Conclusions

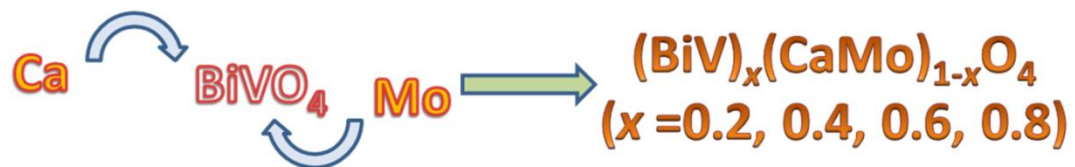
New inorganic yellow pigments: (BiV)_{*x*}(CaW)_{1-*x*}O₄ (*x* = 0.2, 0.4, 0.6, 0.8) have been synthesized using the conventional solid state method. The color of the pigments varies as BiVO₄ is introduced into CaWO₄. The developed pigments are found to be suitable for the coloration of plastics. The characteristics of the pigments suggest that these have immense potential to be used as environmental-secure yellow pigments as interesting alternatives to the existing toxic yellow pigments.

CHAPTER 2B

YELLOW PIGMENTS IN BiVO₄ - CaMoO₄ SYSTEM

Overview

New yellow pigments based on powellite solid solutions, (BiV)_x(CaMo)_{1-x}O₄ ($x = 0.2, 0.4, 0.6, 0.8$) exhibit color parameters L^* , a^* , b^* significantly higher than that of BiVO₄ and (BiV)_x(CaW)_{1-x}O₄. High IR reflectance displayed by the developed pigments make them good candidates in the formulation of cool pigments.



- Solid solution formation between BiVO₄ and CaMoO₄
 - Improve and tune color of BiVO₄
 - IR reflective pigments for cool roof applications
-

2B.1 Introduction

As a fascinating group of inorganic-functional materials, optical properties of molybdates have attracted special attention because of their use as luminescent materials and pigments.¹⁸ Scheelite-type molybdates and tungstate of the divalent metal are easily soluble over the entire compositional range, which results in a rich family of solid-solution compounds. CaMoO₄ belongs to scheelite type molybdates family crystallizing in scheelite type structure with a space group I4_{1/a}, No.88, particularly the crystal structure of CaMoO₄ is known as powellite and that of CaWO₄ as scheelite. Here, the central Ca²⁺ ion is coordinated by eight singly-bound molybdate MoO₄²⁻ tetrahedra groups. The structure is ideally suited for the formation of solid solutions, as it exhibits significant compositional flexibility. When trivalent ions are substituted for the divalent Ca²⁺ ion charge compensation has been found to proceed via coupled substitution with monovalent cations e.g. alkali metal ions. This mechanism has been identified for other solid solutions as well. In other Ln³⁺-molybdates defect structures have been identified where two trivalent cations substitute for three divalent calcium ions. The observation of a homogeneous composition throughout the full series range suggests an ideal solid solution behaviour.¹⁹

In an attempt to modify the properties of BiVO₄ for formulating less toxic pigments for various applications, the effect of various cations doping on the crystal structure of scheelite BiVO₄ need to be examined. Oxides in the Bi-Mo-V-O family have been examined extensively before. A narrow stability region for the solid solution series Bi_{1-x/3}Mo_xV_{1-x}O₄, where (0 ≤ x ≤ 0.55) was reported with the partial absence of Bi at the A site of the ABO₄ type oxides.²⁰ Hoffart *et al.* pointed out that higher-valent cations doping at B sites can stabilize the BO₄ tetrahedra, whereas higher-valent cations doping at A sites may destabilize the rigid BO₄ coordination and reduce the strength of the B-O bonds.²¹ Recently, Ramanan *et al.* attempted to incorporate Na and Mo into the A and B sites of BiVO₄, respectively, and finally observed the formation of a continuous solid solution for the series Na_{x/2}Bi_{1-x/2}Mo_xV_{1-x}O₄ (0 ≤ x ≤ 1).²² BiVO₄ - CaMoO₄ based solid solutions have been explored for their photocatalytical properties by Yao *et al.*¹³ They found that CaMoO₄ and BiVO₄ can fully form solid solution in the compositional range of Ca_{1-x}Bi_xMo_{1-x}V_xO₄ (0 ≤ x ≤ 1).

Inorganic pigments with high IR reflectance are in great demand for exterior coloring applications on roofs and walls as energy saving products. Solar heat reflective coatings have been industrialized and applied extensively to structures such as building rooftops, offshore drilling platforms and oil storage tanks.²³ In a quest for exploring less toxic yellow pigments for various applications, the color as well as IR reflecting properties of $(\text{BiV})_x(\text{CaMo})_{1-x}\text{O}_4$ ($x = 0.2, 0.4, 0.6, 0.8$) based solid solutions have been explored in this section of the chapter.

2B.2 Experimental Section

2B.2.1 Materials and Methods

Compositions based on $(\text{BiV})_x(\text{CaMo})_{1-x}\text{O}_4$ ($x = 0.2, 0.4, 0.6, 0.8$) were prepared from the corresponding oxides: CaCO_3 , V_2O_5 (99.9% purity Acros Organics), Bi_2O_3 and MoO_3 (99.9% purity Aldrich). Stoichiometric proportions of the chemicals were weighed and were thoroughly wet mixed in agate mortar with acetone as the wetting medium for 1 h and dried in an air oven. This process of mixing and drying was repeated three times to obtain homogeneous mixture. The dried powders were then calcined at 800°C in air for 6 h in a platinum crucible. The pigment compositions thus obtained were ground in an agate mortar in order to refine and homogenize the particle size.

2B.2.2 Characterizations

The phase purity of the samples were investigated by powder X-ray diffraction analysis (XRD) with Ni filtered $\text{CuK}\alpha$ radiation using PANalytical X'pert Pro diffractometer. Data were collected from 10 to 90° 2θ range with a step size of 0.016° . Optical reflectance of the powders was measured with UV-vis-NIR spectrophotometer (Shimadzu, UV-3600) using barium sulphate as a reference. The measurement conditions were as follows: an illuminant D65, 10° complementary observer and measuring geometry $d/8^\circ$. The band gap values were calculated from the corresponding absorbance spectra by straight forward extrapolation method using the formula $E_g(\text{eV}) = hc/\lambda$ (where λ represents the wavelength in nm). Color coordinates were determined using CIE-LAB 1976 color scales as described in the previous part of this chapter. Particle morphological analysis of the powders was performed by means of a scanning electron microscope with a Carl Zeiss EVO SEM with an

acceleration voltage of 15 kV. The quantitative microanalysis and elemental mapping of the samples was carried out by silicon drift detector X-MaxN attached with a Carl Zeiss EVO SEM apparatus. The near infrared reflectance of the samples was measured with a UV-vis-NIR spectrophotometer (Shimadzu, UV-3600) using polytetrafluoroethylene (PTFE) as a reference. Optical measurements were performed in the 700 to 2500 nm range.

2B.3 Results and Discussion

2B.3.1 X-Ray Diffraction Analysis

The X-ray diffraction patterns of the pigments are given in Fig. 2B.1. The intense and sharp peaks found in the diffraction patterns reveal the crystalline nature of the powders. All compounds crystallize with the tetragonal scheelite structure (space group $I4_{1/a}$) and the XRD patterns are in good agreement with the powder X-ray diffraction file: PDF No.77- 2233. The formation of tetragonal scheelite type structure is confirmed by the absence of characteristic scheelite monoclinic peak at 15° as seen earlier in the first part of this chapter.

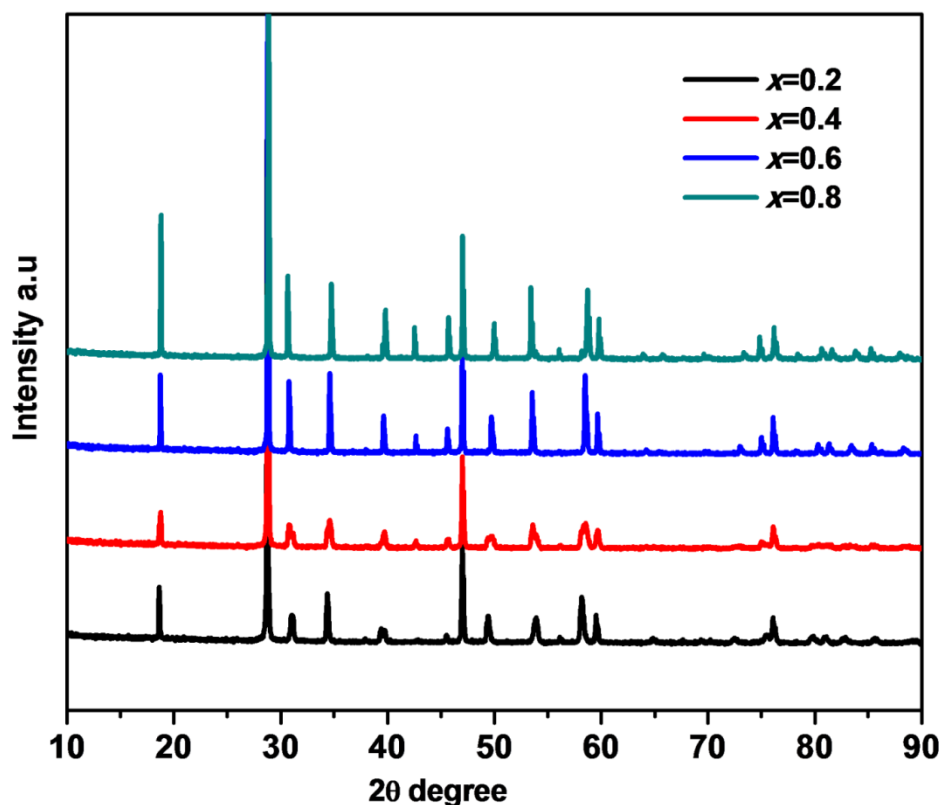


Fig. 2B.1 Powder XRD patterns of $(\text{BiV})_x(\text{CaMo})_{1-x}\text{O}_4$ ($x = 0.2, 0.4, 0.6, 0.8$).

The crystallite size was calculated from Debye Scherrer formula, $D = 0.9\lambda/\beta\cos\theta$, where D is the crystallite size, λ is the wave length of X – ray used, β and θ are the half width of X – ray diffraction lines and half diffraction angle of 2θ . The crystallite size is found to decrease with decrease in concentration of bismuth and vanadium in the range from 122-84 nm.

2B.3.2 Morphological and Micro chemical Studies

The SEM micrographs obtained are shown in Fig.2B.2. The particles are slightly agglomerated. SEM analysis shows that the morphology is almost spherical and average size of sample increases as concentration of BiVO_4 increases. The particle sizes vary from 1-3 μm .

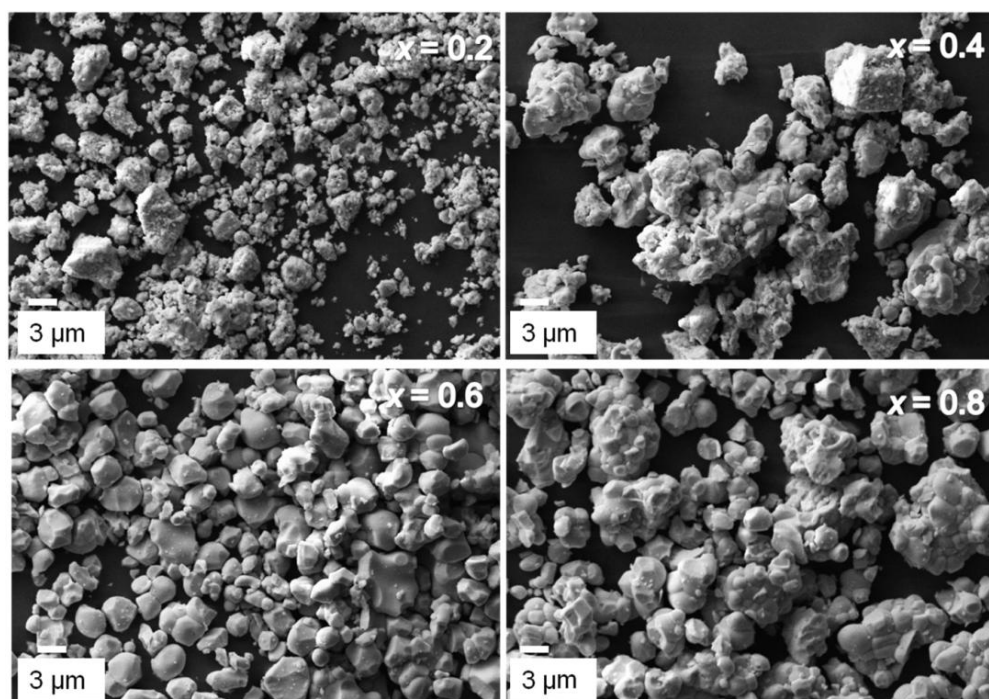


Fig. 2B.2 SEM photographs of $(\text{BiV})_x(\text{CaMo})_{1-x}\text{O}_4$ ($x = 0.2, 0.4, 0.6, 0.8$).

Energy dispersive spectra analysis (EDS) was used to further determinate the chemical composition of the as-obtained pigments. The elemental analysis of two typical solid solutions ($x = 0.2$ and 0.8) revealed that the obtained stoichiometric composition is very close to the theoretical composition in the analyzed regions (Fig.2B.3). X-ray dot mapping analysis revealed that the elements are uniformly distributed within the matrix as seen in Fig. 2B.4.

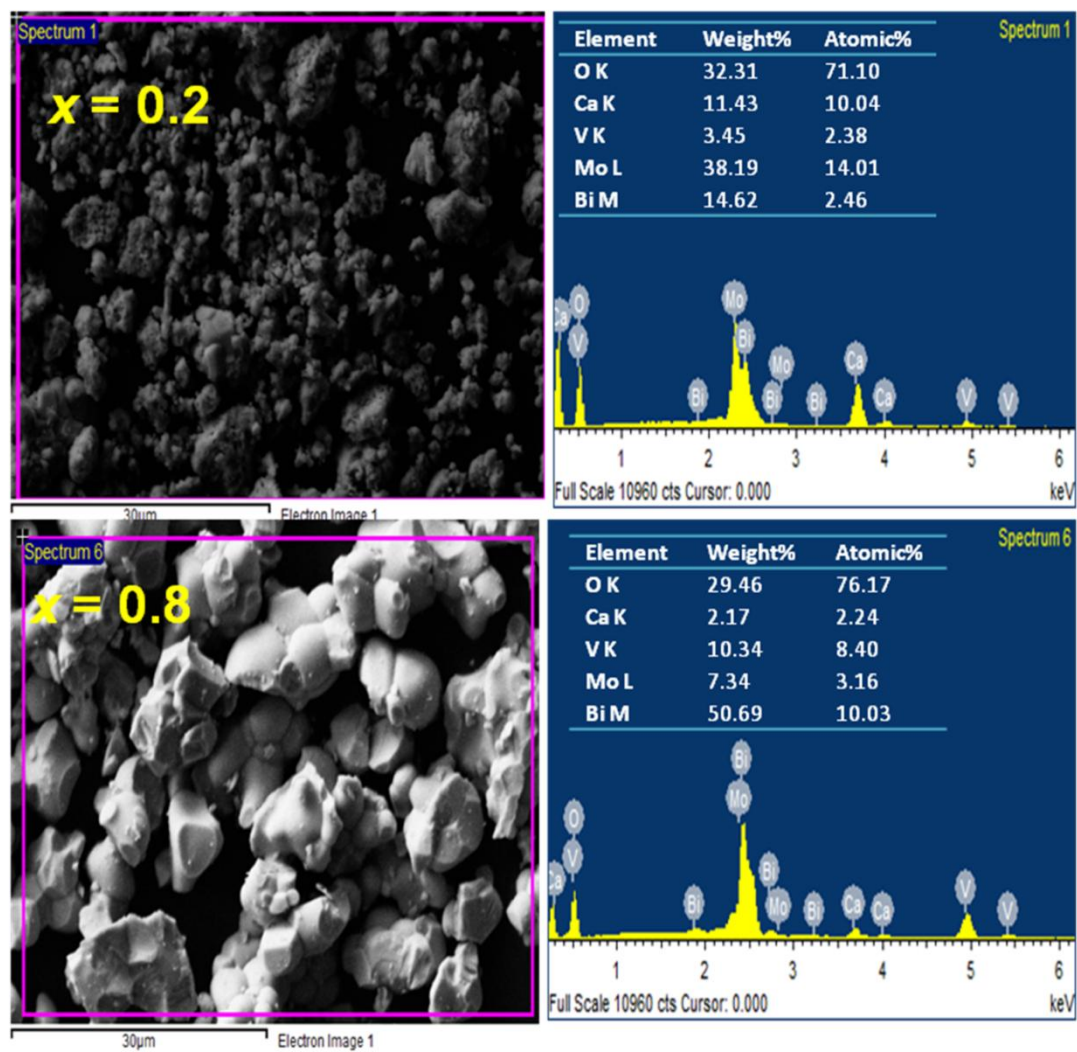


Fig. 2B.3 EDS analysis of $(\text{BiV})_x(\text{CaMo})_{1-x}\text{O}_4$ ($x = 0.2, 0.8$).

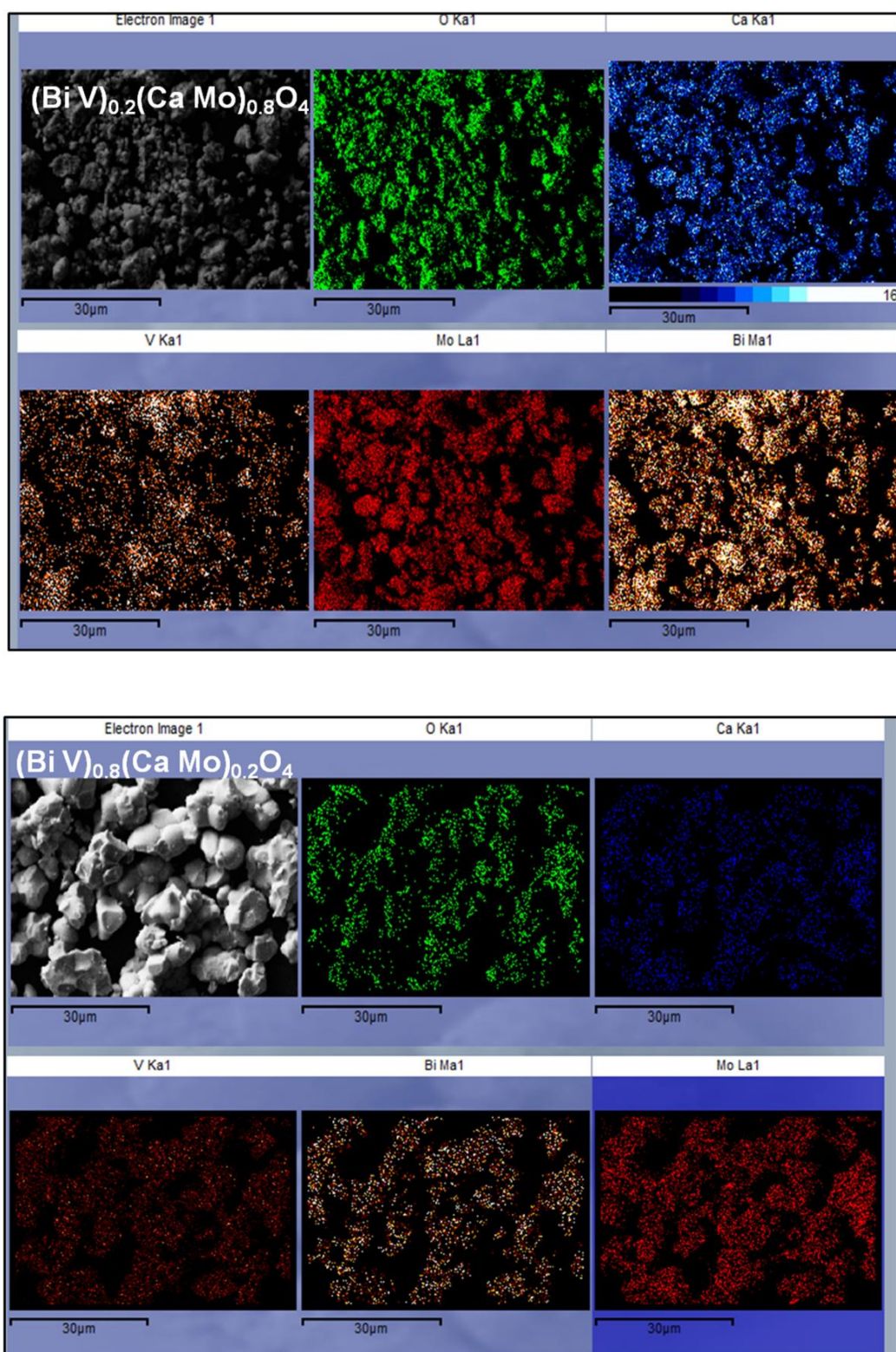


Fig. 2B.4 X-ray dot mapping of $(\text{BiV})_x(\text{CaW})_{1-x}\text{O}_4$ ($x = 0.2, 0.8$).

2B.3.3 UV Visible studies

The reflectance spectra of (BiV)_x(CaMo)_{1-x}O₄ pigments is displayed in Fig. 2B.5 with the reflectance spectra of BiVO₄ and CaMoO₄ shown inset. It is seen that the reflectance spectra red-shifts monotonically as the value of x increased indicating solid solutions of BiVO₄ and CaMoO₄. The absorption edges of the (BiV)_x(CaMo)_{1-x}O₄ solid solutions were notably located in a position between those of CaMoO₄ and BiVO₄. The band gaps of these pigments were estimated to be 2.39-2.81 eV as shown in Table 2B.1.

Doping of Bi³⁺ and V⁵⁺ into CaMoO₄ lattice results in enhancement of visible blue light absorption due to the transition from a new hybrid band made up of hybrid orbitals of Bi 6s, V 3d and O 2p into the Mo 4d conduction band. When Ca²⁺ is replaced by Bi³⁺, the filled Bi 6s orbitals raise the top of the valence band while the Bi 6p orbitals lower the bottom of the conduction band. Compared to (BiV)_x(CaW)_{1-x}O₄ solid solutions, the band gaps obtained here are low. This may be due the fact that the band gap of CaWO₄ is larger than that of CaMO₄.²⁴ Thus, these solid solutions allow fine band gap tuning resulting in various shades of yellow.

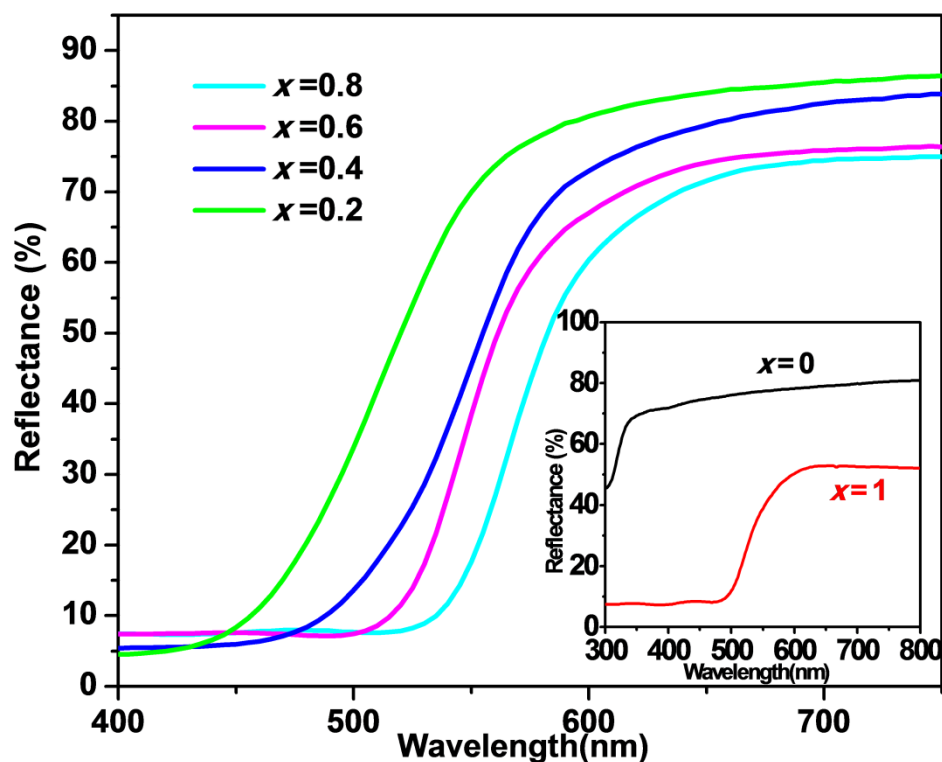


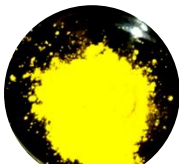
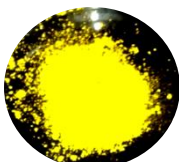
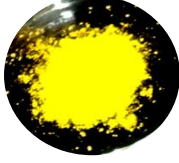



Fig. 2B.5 Reflectance spectra of (BiV)_x(CaMo)_{1-x}O₄ ($x = 0 - 1$).

2B.3.4 Color Analysis

Table 2B.1 displays the CIE 1976 color coordinates of the (BiV)_x(CaMo)_{1-x}O₄ pigments. Incorporation of CaMoO₄ into BiVO₄ gently increases the *b** component up to 74.17 which is significantly higher than BiVO₄ reported elsewhere.¹⁶ The lightness (*L**) and chroma (*C**) values are also enhanced which implies that the obtained pigments are of significant interest. The color coordinates are comparable to commercial praseodymium yellow also.

Table 2B.1 Color coordinates and band gap of (BiV)_x(CaMo)_{1-x}O₄ (*x* = 0.2 - 1)

	Composition	<i>L</i> *	<i>a</i> *	<i>b</i> *	<i>C</i> *	<i>h</i> ⁰	E _g (eV)
	BiVO ₄ ¹⁶	68.00	16.50	42.30	54.57	74.78	2.34
	(BiV) _{0.8} (CaMo) _{0.2} O ₄	77.06	13.28	74.17	75.35	79.84	2.39
	(BiV) _{0.6} (CaMo) _{0.4} O ₄	81.82	1.09	75.77	75.77	89.16	2.47
	(BiV) _{0.4} (CaMo) _{0.6} O ₄	85.40	-1.53	64.69	65.01	91.36	2.55
	(BiV) _{0.2} (CaMo) _{0.8} O ₄	91.69	-6.59	41.15	41.68	99.10	2.81
	Pr yellow ¹⁷	83.5	-3.28	70.3	----	----	2.42

2B.3.5 IR Reflectance studies

The UV-vis-NIR reflectance spectra of selected pigments are displayed in Fig. 2B.6. NIR reflectance follows the order $91 > 89 > 87 > 81$ in the 1100 nm range for $x = 0.2, 0.4, 0.6, 0.8$ respectively. According to the Kubelka Munk theory in general, the reflectance of a material increases as the particle size decreases. The IR reflectance depends on the mean particle size coupled with smaller crystallite size. It is the mean particle size that is important in deciding the reflectance of a particular sample, and usually reflectance increases with a decrease in mean particle size.²⁵ In $(\text{BiV})_x(\text{CaMo})_{1-x}\text{O}_4$, $x = 0.2$ has the smallest particle size around 1 μm range. Increase in reflectance can be correlated to decrease in crystallite size also. Highest NIR reflectance of 91 % was observed for $x = 0.2$ with crystallite size of 82 nm. With decrease in crystallite size, the number of reflections at the grain boundaries increases. Thus, these pigments are favorable for use as IR reflecting pigments.

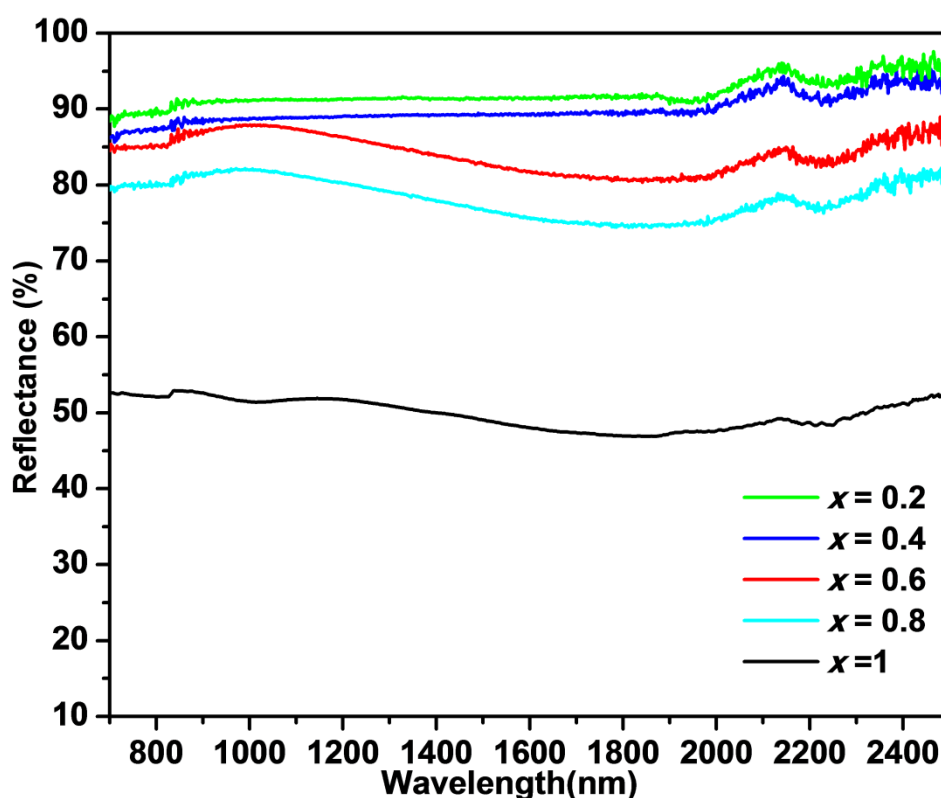


Fig. 2B.6 IR Reflectance spectra of $(\text{BiV})_x(\text{CaMo})_{1-x}\text{O}_4$ ($x = 0.2 - 1$).

2B.3.6 Color performance

To evaluate the yellow hue consistency of the synthesized pigments for various applications such as cool paint formulations, the typical (BiV)_{0.4}(CaMo)_{0.6}O₄ pigment with greenish yellow hue was selected for the studies. A small piece of concrete was pre-coated with TiO₂, an inexpensive white pigment possessing high NIR reflectance. In the second step, the designed typical pigment was applied to the pre-coated substrate material. The pigment samples were ground and was ultrasonicated (Vibronics, 250W, India) for 10 min to ensure the complete dispersion of the pigment particles in acrylic acid using polyurethane as a binder. The resulted viscous solution was coated on the concrete surface and was allowed to dry in an oven at 150°C.

NIR reflectance enhances up to 94% when applied over a TiO₂ base coat with 150 µm thickness over concrete cement shown in Fig. 2B.7. The color coordinates of the resulting coating are ($L^* = 86.14$, $a^* = -1.3$, $b^* = 76.88$, $C^* = 76.89$, $h^0 = 90.98$).

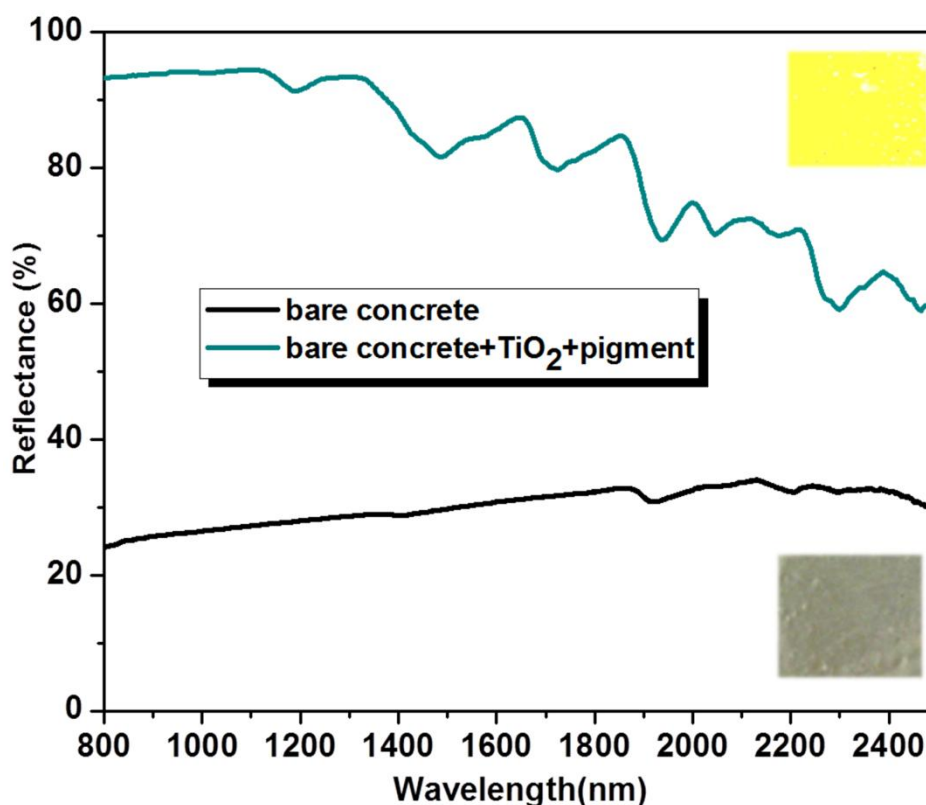


Fig. 2B.7 IR reflectance spectra of (BiV)_{0.4}(CaMo)_{0.6}O₄ coated over concrete surface.

2B.4 Conclusions

New inorganic yellow-pigments: $(\text{BiV})_x(\text{CaMo})_{1-x}\text{O}_4$ ($x = 0.2, 0.4, 0.6, 0.8$) have been synthesized using the conventional solid state method. The color of the pigments varies as BiVO_4 is introduced into CaMoO_4 . The characteristics of the pigments suggest that these have potential to be used as environmental-secure IR reflecting yellow pigments as interesting alternatives to existing toxic yellow pigments.

2.5 References

1. Morozov, V. A.; Mironov, A. V.; Lazoryak, B. I.; Khaikina, E. G.; Basovich, O. M.; Rossell, M. D.; Van Tendeloo, G., Ag_{1/8}Pr_{5/8}MoO₄: An incommensurately modulated scheelite -type structure. *J. Solid State Chem.* **2006**, *179* (4), 1183-1191.
2. Hazen, R. M.; Finger, L. W.; Mariathasan, J. E. E., High-pressure crystal chemistry of scheelite-type tungstates and molybdates. *J. Phys.Chem.Solids* **1985**, *46* (2), 253–263.
3. (a) Oishi, S.; Hirao, M., Growth of CaWO₄ whiskers from KCl flux. *J.Mater. Sci. Lett.* **1989**, *8* (12), 1397–1398; (b) Treadaway, M. J.; Powell, R. C., Energy transfer in samarium-doped calcium tungstate crystals. *Phys. Rev.B.* **1975**, *11* (2), 862–874; (c)Scharmann, A.; Schwarz, G., Luminescence decay and delayed spectra of CaWO₄ single crystals. *Phys. Status Solidi B* **1970**, *42* (2), 781-785.
4. Manjón, F. J.; Errandonea, D., Pressure-induced structural phase transitions in materials and earth sciences. *Phys. Status Solidi B* **2009**, *246* (1), 9-31.
5. Achary, S. N.; Patwe, S. J.; Mathews, M. D.; Tyagi, A. K., High temperature crystal chemistry and thermal expansion of synthetic powellite (CaMoO₄): A high temperature X-ray diffraction (HT-XRD) study. *J. Phy. Chem. Solids* **2006**, *67* (4), 774-781.
6. Buxbaum, G., Introduction to Inorganic High Performance Pigments. In *High Performance Pigments*, Smith, H. M., Ed. Wiley-VCH Verlag GmbH & Co. KGaA: **2003**.
7. Novotny, M.; Solc, Z.; Trojan, M., Pigments, Inorganic. In *Kirk-Othmer Encyclopedia of Chem. Technol. J.*, John Wiley & Sons, Inc.: **1996**.
8. Imanaka, N.; Masui, T.; Furukawa, S., Novel nontoxic and environment friendly inorganic yellow pigments. *Chem. Lett.* **2008**, *37* (1), 104-105.
9. N. Imanaka, N.; T. Masui, T.; Furukawa, S., Synthesis and Characterization of CeO₂-ZrO₂-Bi₂O₃ Solid Solutions for Environment-friendly Yellow Pigments. *Chem. Lett.* **2006**, *9* (35), 1032-1034.
10. http://www.claymaker.com/ceramic_central/info/glazes.htm. (accessed 20-07 2009).

11. Saimi, T.; Hideki, K.; Akihiko, K., Selective preparation of monoclinic and tetragonal BiVO₄ with scheelite structure and their photocatalytic properties. *Chem. Mater.* **2001**, *13*, 4624-4628.
12. Gotić, M.; Musić, S.; Ivanda, M.; Šoufek, M.; Popović, S., Synthesis and characterisation of bismuth(III) vanadate. *J. Mol. Struct.* **2005**, *744–747*, 535-540.
13. Yao, W.; Ye, J., Photocatalytic properties of CaBiVMO₈ (where M = W and Mo) compounds. *Catal. Today* **2006**, *116* (1), 18-21.
14. Walsh, A.; Yan, Y.; Huda, M. N.; Al-Jassim, M. M.; Wei, S.-H., Band edge electronic structure of BiVO₄: Elucidating the role of the Bi s and V d orbitals. *Chem. Mater.* **2009**, *21* (3), 547-551.
15. Wahl, D.; Mikhailik, V. B.; Kraus, H., The Monte-Carlo refractive index matching technique for determining the input parameters for simulation of the light collection in scintillating crystals. *Nucl. Instrum. Methods Phys. Res., Sect. A* **2007**, *570* (3), 529-535.
16. Neves, M. C.; Lehocky, M.; Soares, R.; Lapick Jr., L.; Trindade, T., Chemical bath deposition of cerium doped BiVO₄. *Dyes Pigm.* **2003**, *59* (2), 181-184.
17. Furukawa, S.; Masui, T.; Imanaka, N., New environment-friendly yellow pigments based on CeO₂-ZrO₂ solid solutions. *J. Alloys Compd.* **2008**, *451*, 640-643.
18. (a) Spassky, D.; Ivanov, S.; Kitaeva, I.; Kolobanov, V.; Mikhailin, V.; Ivleva, L.; Voronina, I., Optical and luminescent properties of a series of molybdate single crystals of scheelite crystal structure. *Phys. Status Solidi C* **2005**, *2* (1), 65-68; (b) George, G.; George, G.; Prabhakar Rao, P.; Reddy, M. L. P., Synthesis and characterization of environmentally benign nontoxic pigments: RE₂Mo₂O₉ (RE = La or Pr). *Chem. Lett.* **2005**, *34* (12), 1702-1703; (c) Thomas, M.; Prabhakar Rao, P.; Deepa, M.; Chandran, M. R.; Koshy, P., Novel powellite-based red-emitting phosphors:CaLa_{1-x}NbMoO₈:xEu³⁺ for white light emitting diodes. *J. Solid State Chem.* **2009**, *182*, 203–207.
19. Schmidt, M.; Heck, S.; Bosbach, D.; Ganschow, S.; Walther, C.; Stumpf, T., Characterization of powellite-based solid solutions by site-selective time resolved laser fluorescence spectroscopy. *Dalton Trans.* **2013**, *42* (23), 8387-8393.

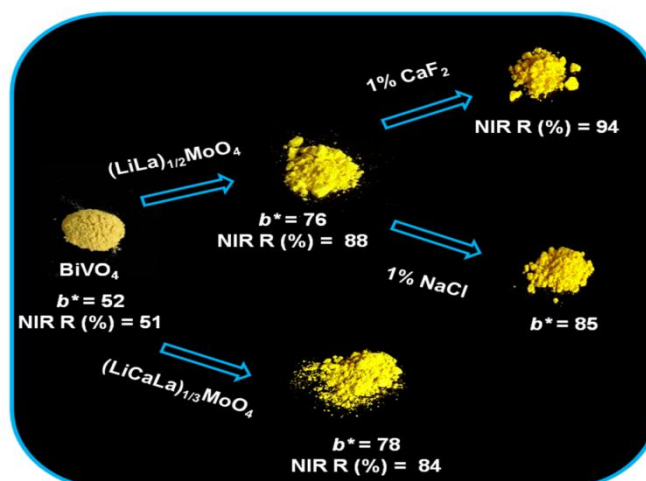
20. (a) Cesari, M.; Perego, G.; Zazzetta, A.; Manara, G.; Notari, B., The crystal structures of the bismuth molybdovanadates and of the α -phase bismuth molybdate. *J. Inorg. Nucl. Chem.* **1971**, *33* (10), 3595-3597; (b) Guo, W.; Ward, T. L.; Porter, C.; Datye, A. K., Phase content and particle morphology of Bi–Mo–V–O powders produced by aerosol pyrolysis. *Mater. Res. Bull.* **2005**, *40* (8), 1371-1387.
21. Hoffart, L.; Heider, U.; Jörissen, L.; Huggins, R. A.; Witschel, W., Transport properties of materials with the scheelite structure. *Solid State Ionics* **1994**, *72*, Part 2, 195-198.
22. Duraisamy, T.; Ramanan, A., Na_{x/2}Bi_{1-x/2}Mo_xV_{1-x}O₄ and Bi_{1-x/3}Mo_xV_{1-x}O₄: New scheelite-related phases. *Solid State Ion.* **1999**, *120* (1–4), 233-237.
23. Song, Z.; Zhang, W.; Shi, Y.; Song, J.; Qu, J.; Qin, J.; Zhang, T.; Li, Y.; Zhang, H.; Zhang, R., Optical properties across the solar spectrum and indoor thermal performance of cool white coatings for building energy efficiency. *Energy and Build.* **2013**, *63*, 49-58.
24. Y. Zhang, N.; Holzwarth, N. A. W.; Williams, R. T., Electronic band structures of the scheelite materials CaMoO₄, CaWO₄, PbMoO₄, and PbWO₄. *Phys. Rev.B* **1998**, *57* (20), 12738-12750.
25. Jeevanandam, P.; Mulukutla, R. S.; Phillips, M.; Chaudhuri, S.; Erickson, L. E.; Klabunde, K. J., Near infrared reflectance properties of metal oxide nanoparticles. *J. Phys. Chem. C* **2007**, *111* (5), 1912-1918.

CHAPTER 3

YELLOW PIGMENTS IN $\text{BiVO}_4\text{-(LiLa)}_{1/2}\text{MoO}_4 / \text{(LiCaLa)}_{1/3}\text{MoO}_4$ SYSTEM

Overview

Various shades of toxic metal free yellow pigments having the formula $[(\text{Li}_{0.5}\text{La}_{0.5})_x \text{Bi}_{1-x}][\text{Mo}_x\text{V}_{1-x}]\text{O}_4$ ($x = 0, 0.1, 0.2, 0.3, 0.4, 0.5$) as well as $[(\text{Li}_{0.33}\text{Ca}_{0.33}\text{La}_{0.33})_x\text{Bi}_{1-x}][\text{Mo}_x\text{V}_{1-x}]\text{O}_4$ ($x = 0.05, 0.10, 0.15, 0.2$) were prepared via a solid state method. Addition of various mineralizers significantly enhanced the yellow hue making it better than a commercially available BiVO_4 pigment. The IR reflectance of BiVO_4 is enhanced with substitution and addition of a mineralizer.



3.1 Introduction

Inorganic pigments are found in a variety number of applications including paints, inks, plastics, rubbers, ceramics, enamels and glasses.¹ Particular interest may be given to yellow pigments which find enormous applicability in automotive, industrial and decorative paints and plastics. A worldwide consensus against the use of toxic products has led to the expulsion of $\text{Pb}_2\text{Sb}_2\text{O}_7$, PbCrO_4 and CdS yellow pigments from the market. Recently, many rare-earth based inorganic pigments have been proposed by several researchers including our group to replace these toxic pigments. Cerium sulfide and its analogues, such as the doped cerium sulfide, have been reported as safe replacements for cadmium sulphide pigments.² Lanthanum-tantalum oxy-nitrides have interesting color shades in the red to yellow range but the development into industrially available pigments has yet to be proven.³ (Ca^{2+} , V^{5+}) co-doped $\text{Y}_2\text{Ti}_2\text{O}_7$,⁴ Y-doped Bi_2MoO_6 ,⁵ perovskite structure based $\text{BaSn}_{1-x}\text{Tb}_x\text{O}_3$,⁶ solid solutions based on $\text{CeO}_2\text{-ZrO}_2\text{-Bi}_2\text{O}_3$ ⁷ are some possible ecologically improved yellow inorganic pigments. Also, the recent advance in usage of inorganic pigments for coating applications that reduces heat build-up in buildings are in great demand to save energy. Currently developed yellow pigments are not well explored for their NIR reflecting properties. The selection of appropriate cool roofing materials with higher reflectance in the infra red region will be a good alternative solution to prevent solar gain thus rendering indoor temperatures more comfortable and reduce the increasing demand in air conditioning energy by the building sector.

The scheelite structure with the typical formula ABO_4 provides flexibility for cation substitution on both A and B sites.⁸ Among the scheelite structured ABO_4 compounds, BiVO_4 has received attention for a wide variety of applications, such as pigments, photocatalytic materials, electronic conductor materials and photochromic materials.⁹⁻¹⁴ BiVO_4 exists in three phases, tetragonal zircon, monoclinic scheelite, and tetragonal scheelite.¹⁰ The tetragonal zircon BiVO_4 can be synthesized by the co-precipitation method.¹⁵ When heated above 670–770 K, the tetragonal zircon BiVO_4 irreversibly transforms into the monoclinic scheelite phase. The monoclinic scheelite BiVO_4 can reversibly transition to the tetragonal scheelite phase by high temperature and applied external pressure¹⁶ via a second order ferroelastic phase transition.

Disordered tetragonal (scheelite-like) alkali rare earth double molybdates, belonging to the family $\text{ARE}(\text{MoO}_4)_2$ (where A = Li, Na, K and RE = La–Lu), are

eligible host materials for developing tuneable solid state lasers.¹⁷ A crucial way to improve the properties of materials is through compositional design in the form of solid solutions. In this work, the Li^+ and La^{3+} ions are chosen to substitute for the Bi^{3+} on the A site and Mo^{6+} to substitute V^{5+} on the B site to study the solid solution possibility between $(\text{LiLa})_{1/2}\text{MoO}_4$ and BiVO_4 . Another batch of pigments were prepared by substituting Li^+ , Ca^{2+} and La^{3+} ions for the Bi^{3+} on the A site and Mo^{6+} to substitute V^{5+} on the B site.

BiVO_4 belongs to a new class of yellow ceramic pigment and it is often used as a replacement for cadmium-based yellows. Since color and color intensity depend on many factors including phase composition, structure, particle size and morphology, it has proven difficult to control the pigmentary colors of BiVO_4 .¹⁸ Several researches have been done to improve the color properties of BiVO_4 by doping^{19, 20} as well as nanosheet formation.²¹ Here an attempt has been made to improve and tune the color characteristics of BiVO_4 through solid solution formation with $(\text{LiLa})_{1/2}\text{MoO}_4$ as well as $(\text{LiCaLa})_{1/3}\text{MoO}_4$.

Mineralizers have significant effect on the crystal lattice as well as on the color of pigments. They act as fluxing agents and facilitate the formation of the desired phase by providing a molten medium, where ionic diffusion becomes significantly fast, even in a moderate temperature range. So the effect of various mineralizers on the calcination temperature as well as the optical properties of selected pigment has also been evaluated.

3.2 Experimental Section

3.2.1 Materials and Methods

The pigments of the formula $[(\text{Li}_{0.5}\text{La}_{0.5})_x \text{Bi}_{1-x}][\text{Mo}_x\text{V}_{1-x}]\text{O}_4$ ($x = 0, 0.1, 0.2, 0.3, 0.4, 0.5$) and $[(\text{Li}_{0.33}\text{Ca}_{0.33}\text{La}_{0.33})_x \text{Bi}_{1-x}][\text{Mo}_x\text{V}_{1-x}]\text{O}_4$ ($x = 0.05, 0.10, 0.15, 0.20$) were prepared by a conventional solid state reaction route. Li_2CO_3 (99.9 % purity, Acros Organics), CaCO_3 (99.9 % purity, Acros Organics) La_2O_3 (99.9 % purity, Acros Organics), Bi_2O_3 (99.999 % purity, Sigma-Aldrich), MoO_3 (99.99 % purity, Acros Organics) and V_2O_5 (99.9 % purity, Acros Organics) were weighed in the required stoichiometric amount and then were wet mixed thoroughly in an agate mortar using acetone as the medium. The mixed product was dried in an air oven at 100°C for 1 h. The process of mixing and drying was repeated three times to get a homogeneous

mixture. The dried mixture was then calcined in a platinum crucible in an electrical furnace. The heating of the furnace was programmed increasing the temperature initially at 10°C per minute up to the temperature (400-500°C) and afterward, the heating rate was decreased to 5°C per minute up to the final required temperature (500-800°C). The samples were maintained at the final temperature of 800°C for about 6 h. The calcined samples were ground thoroughly in an agate mortar into a fine powder. Typical pigment composition $[(Li_{0.5}La_{0.5})_x Bi_{1-x}][Mo_xV_{1-x}]O_4$ with $x = 0.3$ was also prepared in the presence of different mineralizers like NaCl, CaF₂, H₃BO₃ and MgF₂ with the aim of evaluating their influence on their optical properties. The mineralizer was used at 1 wt. % level on the total weight of the precursors. The resultant stoichiometric mixtures of samples were calcined at an optimized temperature (700°C) for 6 h. The pigment compositions thus obtained were ground in an agate mortar in order to refine and homogenize the particle size.

3.2.2 Characterizations

The crystalline structure of the calcined powders were characterized by means of X-ray powder diffraction (XRD) using a Ni-filtered Cu-K α radiation ($\lambda = 1.54056$ Å) with a PANalytical X'pert Pro diffractometer operated at 40kV and 30mA. Data were collected from 10 to 90° 2 θ range with a step size of 0.016°. The structural refinement of all the XRD patterns was performed by the Rietveld analysis using the X'pert plus program. Particle morphological analysis of the powder was performed by means of a scanning electron microscope with a JEOL JSM-5600 LV SEM with an acceleration voltage of 15 kV. The quantitative microanalysis and elemental mapping of the samples was carried out by silicon drift detector X-MaxN attached with a Carl Zeiss EVO SEM apparatus. The UV visible spectra of the samples was measured with a UV-vis-NIR spectrophotometer (Shimadzu, UV-3600) using BaSO₄ as a reference. The measurement conditions were as follows: an illuminant D65, 10° complementary observer and measuring geometry d/8°. The color coordinates were determined by coupling analytical software (UVPC Color Analysis Personal Spectroscopy Software V3, Shimadzu) to the UV-3600 spectrophotometer. The color of the pigments was evaluated described in previous sections. The particle size distribution of the typical pigment sample was investigated in an aqueous medium with calgon as the dispersing agent using the laser scattering particle size distribution analyzer (CILAS 930 Liquid). The samples were ultrasonically homogenized for 180 s during measurement and the

signal was evaluated on the basis of Fraunhofer bending. The near-infrared reflectance of the powdered pigment samples was measured with a UV-vis-NIR spectrophotometer (Shimadzu, UV-3600 with an integrating sphere attachment) using poly-tetrafluoroethylene (PTFE) as a reference in the 700 to 2500 nm range. The NIR solar reflectance spectra were determined from ASTM Standard G173-03.²²

3.3 Results and Discussion

3.3.1 X-Ray Diffraction Analysis

The powder X-ray diffraction patterns of the samples $[(\text{Li}_{0.5}\text{La}_{0.5})_x\text{Bi}_{1-x}][\text{Mo}_x\text{V}_{1-x}]\text{O}_4$ ($x = 0, 0.1, 0.2, 0.3, 0.4, 0.5$) calcined at 800°C are shown in Fig.3.1. The solid solutions were successfully formed within this compositional range as indicated by the XRD patterns. The BiVO_4 and $(\text{LiLa})_{1/2}\text{MoO}_4$ compounds are isostructural with the scheelite crystal system. Thus the formation of a solid-solution between BiVO_4 and $(\text{LiLa})_{1/2}\text{MoO}_4$ can be understood. The peaks can be well indexed to the powder diffraction file 01-074-4892 of BiVO_4 with tetragonal scheelite phase (t-s). But $x = 0$ crystallize in the monoclinic scheelite phase (m-s). The basis of distinguishing between the BiVO_4 (m-s) and BiVO_4 (t-s) is by the splitting of peaks at 18°, 35° and 46° of 2θ in the XRD patterns.¹⁰ Thus addition of $(\text{LiLa})_{1/2}\text{MoO}_4$ causes structural transformation in BiVO_4 from monoclinic scheelite to tetragonal scheelite form. The sharp and intense peaks confirm the crystalline nature of the phases formed. In $[(\text{Li}_{0.5}\text{La}_{0.5})_x\text{Bi}_{1-x}][\text{Mo}_x\text{V}_{1-x}]\text{O}_4$, the A-site is 8 coordinated with Bi^{3+} , Li^+ and La^{3+} having an ionic radii of 1.17, 0.92 and 1.16 Å and the B-site is 4 coordinated with V^{5+} and Mo^{6+} having an ionic radii of 0.355 and 0.41 Å according to Shannon radii.²³ From $x = 0.3$ onwards a slight segregation into BiVO_4 and $(\text{LiLa})_{1/2}\text{MoO}_4$ phases are seen (shown in inset of Fig.3.1). The composition with $x = 0.3$ was chosen for further studies and various mineralizers such as NaCl, CaF_2 , H_3BO_3 and MgF_2 were added and XRD patterns of those samples indicated a highly crystalline product with sharp intensity peaks (Fig.3.2). This indicates the role of mineralizers acting as fluxing agents and aiding in the formation of the host lattice structure at a lower calcination temperature.

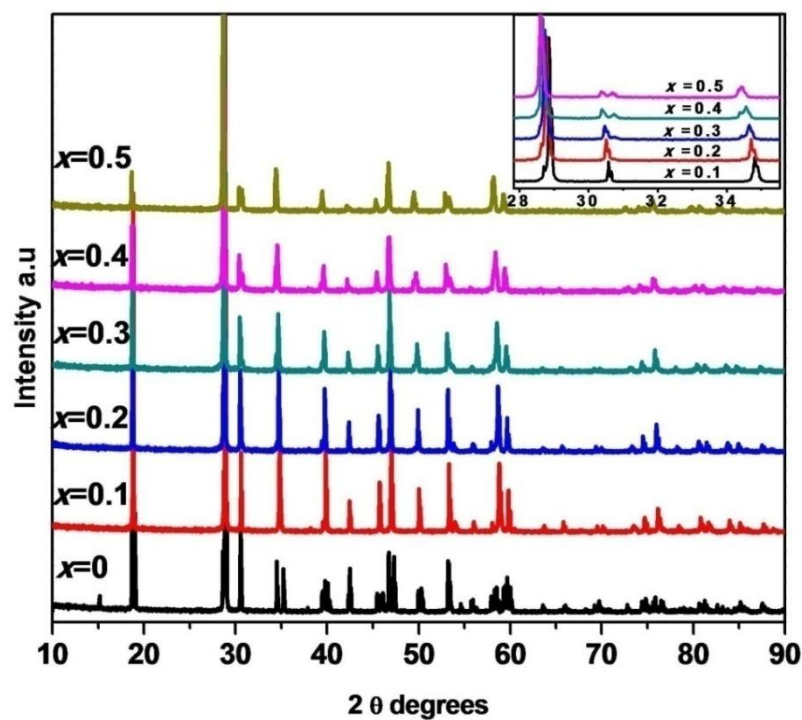


Fig. 3.1 Powder XRD patterns of $[(\text{Li}_{0.5}\text{La}_{0.5})_x\text{Bi}_{1-x}][\text{Mo}_x\text{V}_{1-x}]\text{O}_4$ ($x = 0.1, 0.2, 0.3, 0.4, 0.5$) pigments calcined at 800°C .

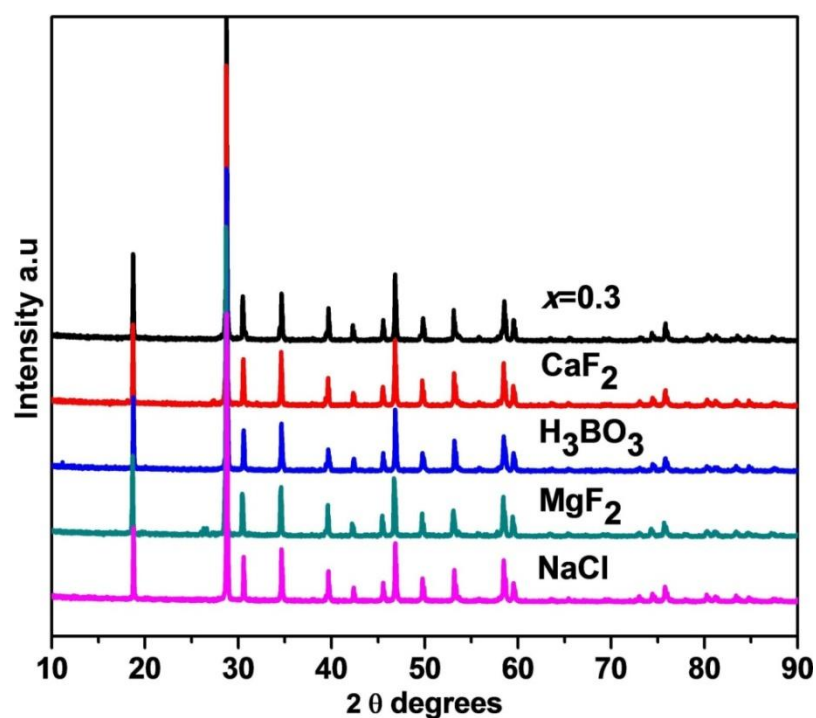


Fig. 3.2 Powder XRD patterns of $[(\text{Li}_{0.5}\text{La}_{0.5})_x\text{Bi}_{1-x}][\text{Mo}_x\text{V}_{1-x}]\text{O}_4$ ($x = 0.3$) pigments in the presence of different mineralizers calcined at 700°C .

The powder X-ray diffraction patterns of the samples $[(\text{Li}_{0.33}\text{Ca}_{0.33}\text{La}_{0.33})_x\text{Bi}_{1-x}][\text{Mo}_x\text{V}_{1-x}]\text{O}_4$ ($x = 0.05, 0.10, 0.15, 0.20$) calcined at 800°C are shown in Fig. 3.3. The solid solutions are successfully formed within this compositional range as indicated by the XRD patterns. Here, A site is shared by Li^+ , Ca^{2+} , La^{3+} and Bi^{3+} ions and is surrounded by eight oxygen atoms forming AO_8 polyhedra. Since the ionic radii of Ca^{2+} ($r = 1.12 \text{ \AA}$ when coordination number is 8) is similar to Bi^{3+} and La^{3+} , Ca^{2+} prefers to occupy A site. V^{5+} and Mo^{6+} ions share B sites and are four coordinated forming BO_4 tetrahedra. The peaks can be well indexed to the powder diffraction file 01-074-4892 of BiVO_4 with tetragonal scheelite phase (t-s). But $x = 0.05$ crystallize in the monoclinic scheelite phase (m-s) corresponding to powder diffraction file 01-083-1699. It is evidenced by the peak splitting around 35° shown in inset of Fig. 3.3.

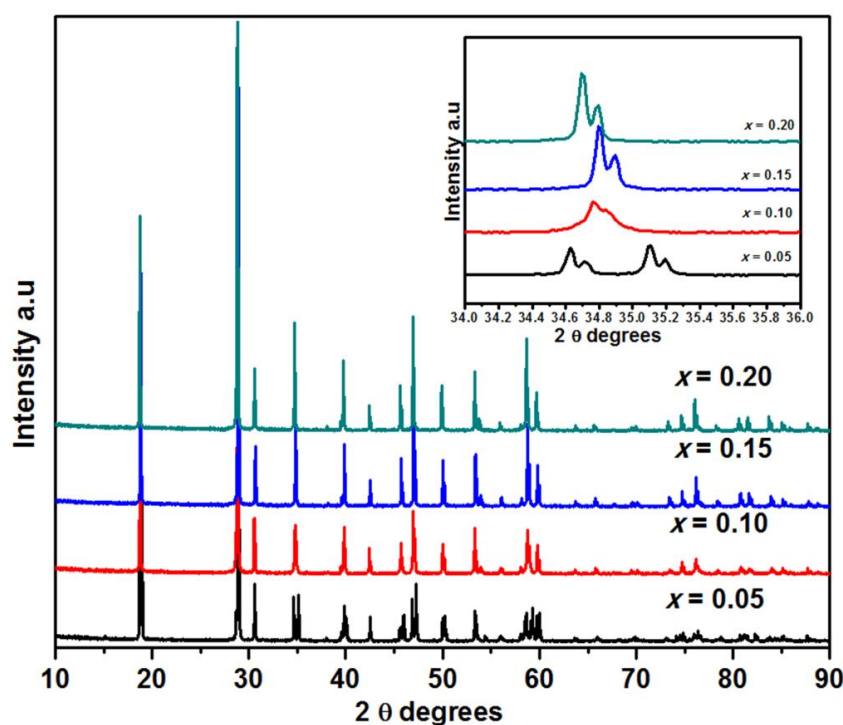


Fig. 3.3 Powder XRD patterns of $[(\text{Li}_{0.33}\text{Ca}_{0.33}\text{La}_{0.33})_x\text{Bi}_{1-x}][\text{Mo}_x\text{V}_{1-x}]\text{O}_4$ ($x = 0.05, 0.10, 0.15, 0.20$) pigments calcined at 800°C .

Structural refinement

Rietveld refinement of XRD data is the best method to validate the crystal system and the space group in which the compound belongs. The structural refinement of all the XRD patterns for $[(\text{Li}_{0.5}\text{La}_{0.5})_x\text{Bi}_{1-x}][\text{Mo}_x\text{V}_{1-x}]\text{O}_4$ ($x = 0.1, 0.2, 0.3, 0.4, 0.5$) pigments were performed by the Rietveld analysis using the X'pert plus program. The starting model for the refinement of the phases was taken from the

reported crystal structure of BiVO_4 . Here Bi/Li/La are at ($4b$: 0, 1/4, 5/8) sites, V and Mo at ($4a$: 0, 1/4, 1/8) sites and O at ($16f$: x , y , z), $Z = 4$ in the space group $I4_1/a$, no.88. The profile was fitted using the Pseudo Voigt profile function. The unit cell volume linearly increases with an increase of x due to the replacement of Bi^{3+} with the Li^+ and La^{3+} and V^{5+} with Mo^{6+} , almost following Vegard's law illustrated in Fig.3.4.

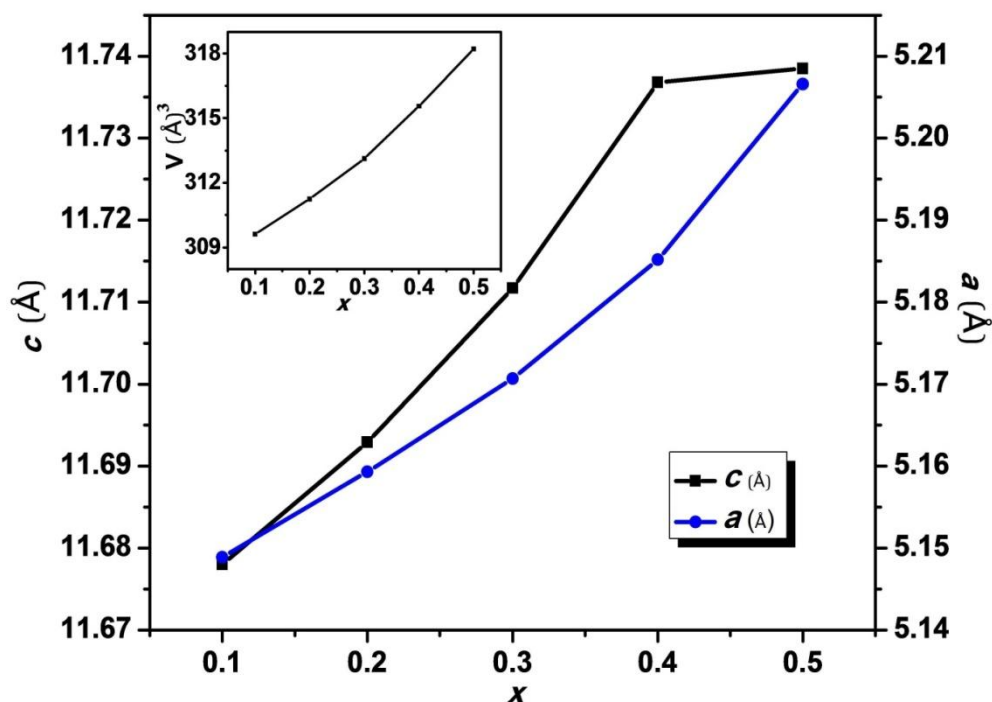


Fig. 3.4 Variation of lattice parameters with x in $[(\text{Li}_{0.5}\text{La}_{0.5})_x\text{Bi}_{1-x}][\text{Mo}_x\text{V}_{1-x}]\text{O}_4$ ($x = 0.1, 0.2, 0.3, 0.4, 0.5$) pigments.

Schematic representation of the crystal structure and the coordination polyhedra of $\text{Li}_{0.15}\text{La}_{0.15}\text{Bi}_{0.7}\text{Mo}_{0.3}\text{V}_{0.7}\text{O}_4$ pigment generated using the diamond software is given in the Fig.3.5. However compositions with the mineralizer added yielded a much better fit as compared to the base composition. The R factors, the refined oxygen coordinates, other parameters obtained from the Rietveld refinement of the powder diffraction data for the samples are given in Tables 3.1 and 3.2.

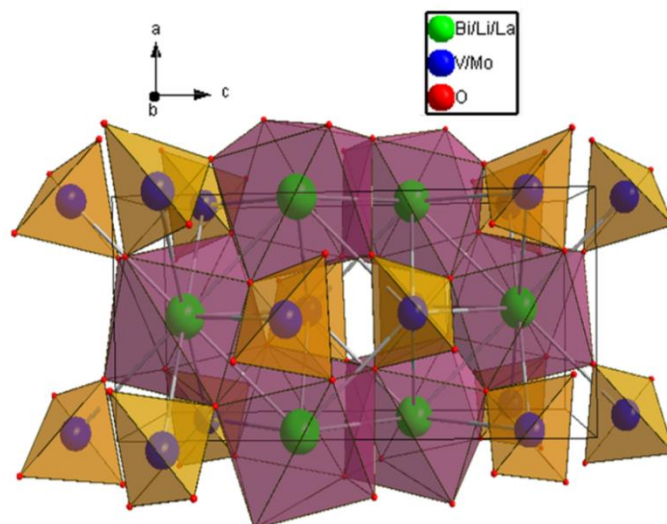


Fig. 3.5 Schematic representation of the crystal structure and the coordination polyhedras of $\text{Li}_{0.15}\text{La}_{0.15}\text{Bi}_{0.7}\text{Mo}_{0.3}\text{V}_{0.3}\text{O}_4$.

Table 3.1 Rietveld refined parameters of $[(\text{Li}_{0.5}\text{La}_{0.5})_x \text{Bi}_{1-x}][\text{Mo}_x\text{V}_{1-x}]\text{O}_4$ ($x = 0.1, 0.2, 0.3, 0.4, 0.5$) pigments

Composition	$x = 0.1$	$x = 0.2$	$x = 0.3$	$x = 0.4$	$x = 0.5$
Lattice parameters					
a (Å)	5.1489(8)	5.1593(1)	5.1707(1)	5.1852(2)	5.2066(3)
c (Å)	11.6780(2)	11.6929(3)	11.7117(4)	11.7368(6)	11.7385(8)
$V(\text{Å})^3$	309.61	311.25	313.12	315.56	318.22
Crystallite size(nm)	135	130	113	97	117
R-factors					
R_{exp} (%)	11.37	11.46	11.38	11.44	11.97
R_p (%)	13.83	12.43	12.07	14.60	15.23
R_{wp} (%)	18.36	16.11	16.15	19.56	20.67
R_{Bragg} (%)	8.97	4.72	5.20	9.06	11.93
χ^2	2.60	1.97	2.01	2.92	2.98
Oxygen position coordinates					
x	0.141(3)	0.148(2)	0.141(2)	0.139(3)	0.142(3)
y	0.080(2)	0.001(2)	0.004(2)	0.015(3)	0.073(3)
z	0.222(1)	0.206(9)	0.210(9)	0.216(1)	0.217(1)
No. of variables	18	18	18	18	18

Table 3.2 Rietveld refined parameters of $[(\text{Li}_{0.5}\text{La}_{0.5})_x\text{Bi}_{1-x}][\text{Mo}_x\text{V}_x]\text{O}_4$ ($x = 0.3$) pigments with different mineralizers

Mineralizer	H_3BO_3	MgF_2	CaF_2	NaCl
R-factors				
\mathbf{R}_p (%)	9.30	9.38	8.65	9.05
\mathbf{R}_{wp} (%)	12.40	12.73	11.86	12.03
\mathbf{R}_{Bragg} (%)	1.85	2.87	1.34	3.77
χ^2	1.15	1.23	1.09	1.07
Oxygen position coordinates				
x	0.141(2)	0.140(2)	0.141(2)	0.133(1)
y	-0.007(1)	-0.009(1)	-0.002(1)	-0.020(1)
z	0.206(7)	0.204(7)	0.206(7)	0.209(6)
No. of variables	18	18	18	18

The crystallite size was calculated from Debye Scherrer formula $D = 0.9\lambda/\beta\cos\theta$, where D is the crystallite size, λ is the wavelength of X-ray used, β and θ are the half width of X-ray diffraction lines and half diffraction angle of 2θ .^{24,25} While calculating, the instrumental broadening was corrected using a Si standard. The crystallite size was found to decrease with increase in concentration of $(\text{LiLa})_{1/2}\text{MoO}_4$ upto $x = 0.4$ and then increases for $x = 0.5$ which is shown in Table 3.1. The crystallite size on mineralizer addition to $[(\text{Li}_{0.5}\text{La}_{0.5})_x\text{Bi}_{1-x}][\text{Mo}_x\text{V}_{1-x}]\text{O}_4$ with $x = 0.3$, was found in the range 87-108 nm. For the samples $[(\text{Li}_{0.33}\text{Ca}_{0.33}\text{La}_{0.33})_x\text{Bi}_{1-x}][\text{Mo}_x\text{V}_{1-x}]\text{O}_4$ ($x = 0.05, 0.10, 0.15, 0.20$) the crystallite size was found in the range 164 -132 nm.

3.3.2 Morphological and Micro chemical Studies

The microstructure reveals the crystalline nature of particles. Thus addition of $(\text{LiLa})_{1/2}\text{MoO}_4$ causes reduction in the particle size of BiVO_4 (Fig.3.6).The particles are agglomerated to some extent. The particles are in the scale of 6–8 μm in average size. Scanning electron micrographs of the selected $\text{Li}_{0.15}\text{La}_{0.15}\text{Bi}_{0.7}\text{Mo}_{0.3}\text{V}_{0.7}\text{O}_4$ pigment and those of the pigments with different mineralizers on the pigment are

presented in Fig.3.7. A grain size of 1-2 μm is obtained in the mineralizer added pigments. Also a high degree of homogeneity is evident.

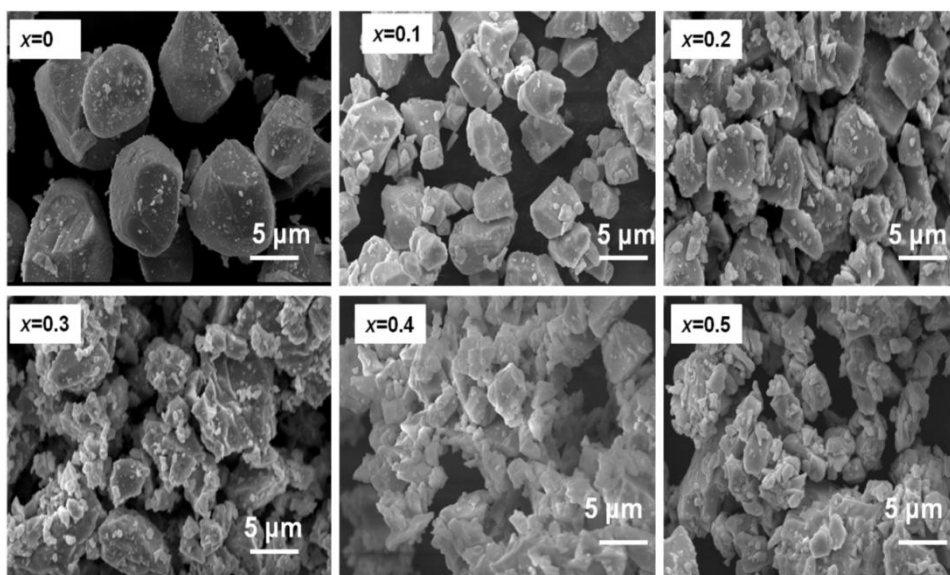


Fig. 3.6 SEM photographs of $[(\text{Li}_{0.5}\text{La}_{0.5})_x \text{Bi}_{1-x}][\text{Mo}_x \text{V}_{1-x}]\text{O}_4$ pigments.

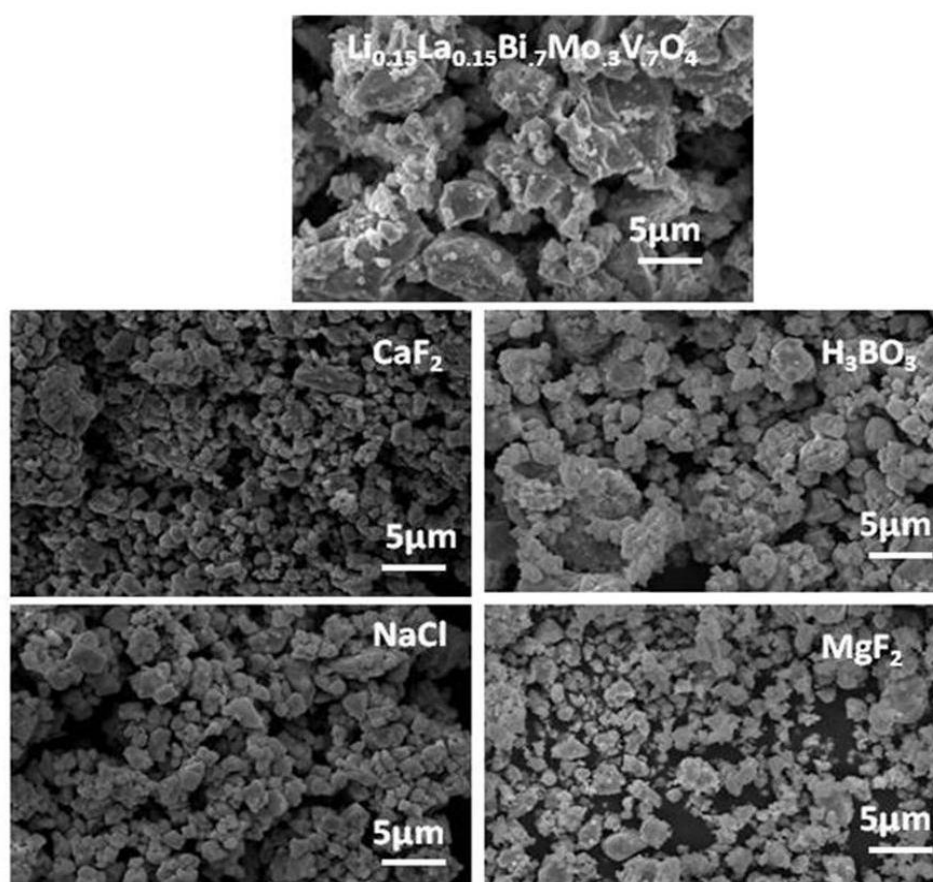


Fig. 3.7 SEM photographs of $\text{Li}_{0.15}\text{La}_{0.15}\text{Bi}_{0.7}\text{Mo}_{0.3}\text{V}_{0.3}\text{O}_4$ pigment with various mineralizers.

Similarly, addition of $(\text{LiCaLa})_{1/3}\text{MoO}_4$ causes reduction in the particle size of BiVO_4 (Fig.3.8). The particles are agglomerated to some extent. The particles are more or less the same size obtained by adding $(\text{LiLa})_{1/2}\text{MoO}_4$ to BiVO_4 about 6–8 μm in average size.

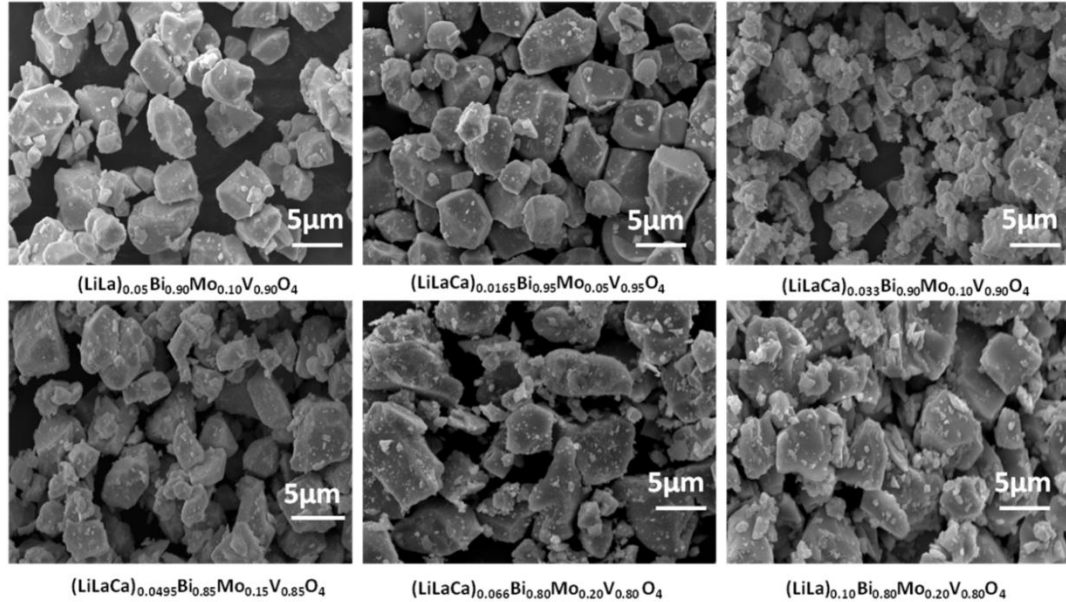


Fig. 3.8 SEM photographs of $[(\text{Li}_{0.33}\text{Ca}_{0.33}\text{La}_{0.33})_x\text{Bi}_{1-x}][\text{Mo}_x\text{V}_{1-x}]\text{O}_4$ ($x = 0.05, 0.10, 0.15, 0.20$) pigments. For the sake of comparison $[(\text{Li}_{0.5}\text{La}_{0.5})_x\text{Bi}_{1-x}][\text{Mo}_x\text{V}_{1-x}]\text{O}_4$ ($x = 0.10, 0.20$) too are shown.

The EDS was used to further determine the chemical composition of the as-obtained pigments. EDS spectra (Fig.3.9) of a typical $\text{Li}_{0.15}\text{La}_{0.15}\text{Bi}_{0.7}\text{Mo}_{0.3}\text{V}_{0.7}\text{O}_4$ sample shows the presence of Bi, V, La, Mo and O elements, with close approximation to the calculated value. The Li element is not detected due to going beyond the detection range of the instrument.

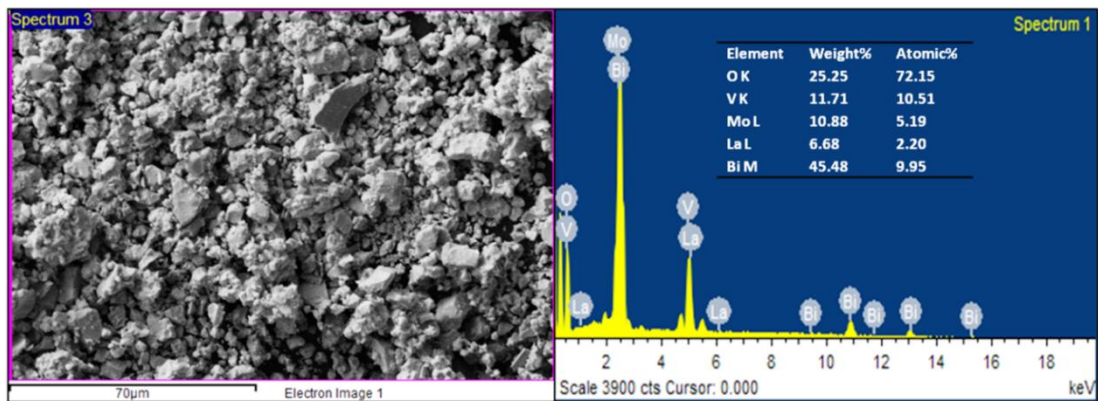


Fig. 3.9 EDS analysis of $\text{Li}_{0.15}\text{La}_{0.15}\text{Bi}_{0.7}\text{Mo}_{0.3}\text{V}_{0.7}\text{O}_4$ pigment.

EDS spectra (Fig.3.10) of a typical $(\text{LiLaCa})_{0.099}\text{Bi}_{0.9}\text{Mo}_{0.1}\text{V}_{0.9}\text{O}_4$ sample shows the presence of Bi, Ca, La, Mo, V and O elements, with close approximation to the calculated value. X- ray mapping analysis (Fig.3.11) also reveals that the elements are uniformly distributed within the matrix. SEM EDS analysis confirms the close agreement between the stoichiometric and the actual composition.

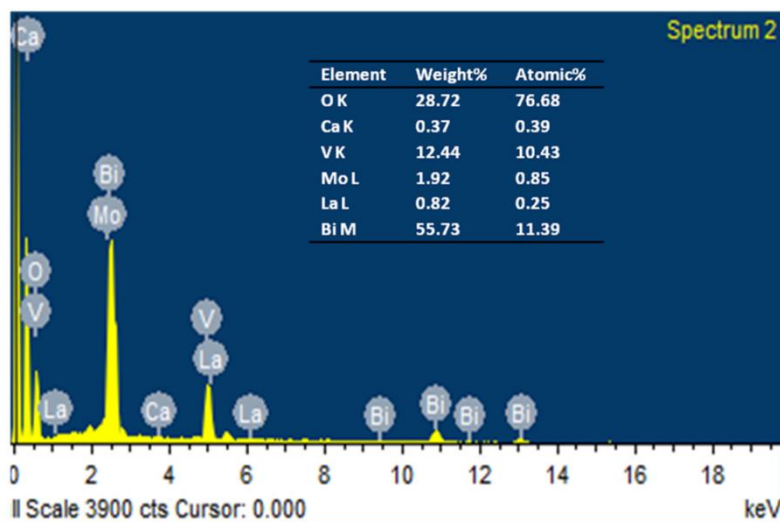


Fig.3.10 EDS spectra of $(\text{LiLaCa})_{0.099}\text{Bi}_{0.9}\text{Mo}_{0.1}\text{V}_{0.9}\text{O}_4$ pigment.

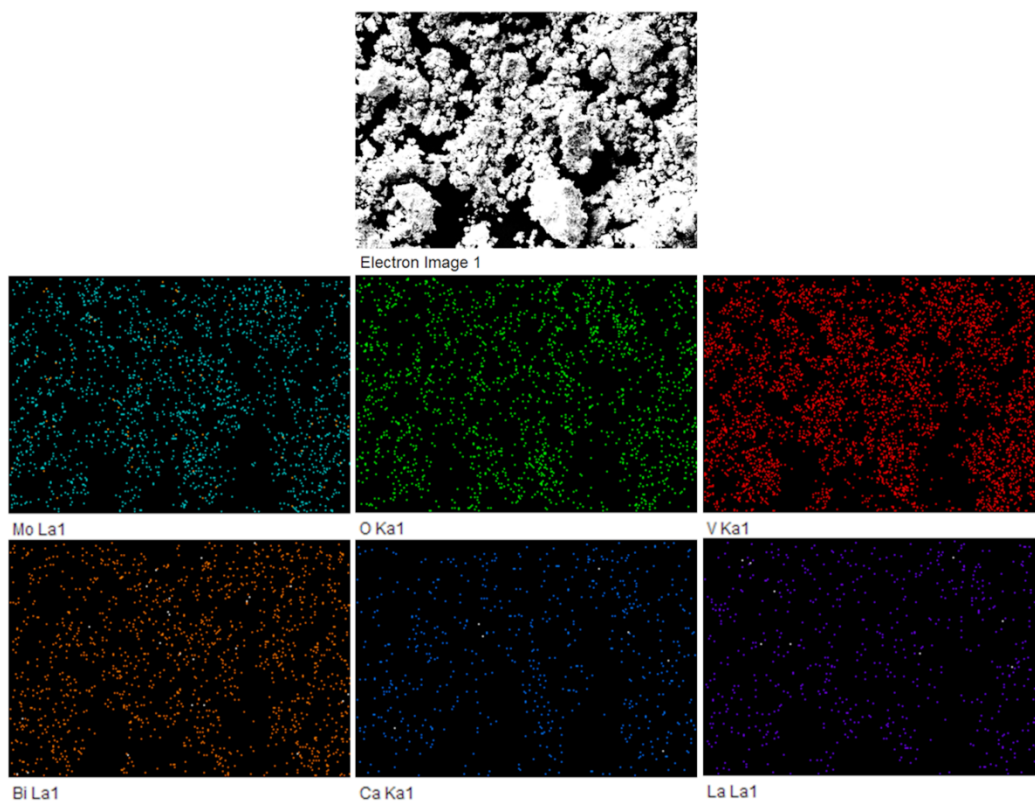


Fig.3.11 X-ray dot mapping of $(\text{LiLaCa})_{0.099}\text{Bi}_{0.9}\text{Mo}_{0.1}\text{V}_{0.9}\text{O}_4$ pigment.

3.3.3 Particle size analysis

The particle size distribution of the typical pigment, $\text{Li}_{0.15}\text{La}_{0.15}\text{Bi}_{0.7}\text{Mo}_{0.3}\text{V}_{0.7}\text{O}_4$ synthesized at 800°C reveals a mean diameter of $5.15\ \mu\text{m}$ (size of 90% particles $< 8.99\ \mu\text{m}$, 50% particles $< 5.06\ \mu\text{m}$ and 10% particles $< 1.19\ \mu\text{m}$). The 1% NaCl mineralizer added $\text{Li}_{0.15}\text{La}_{0.15}\text{Bi}_{0.7}\text{Mo}_{0.3}\text{V}_{0.7}\text{O}_4$ synthesized at 700°C has a mean diameter of $2.48\ \mu\text{m}$ (size of 90% particles $< 3.66\ \mu\text{m}$, 50% particles $< 2.61\ \mu\text{m}$ and 10% particles $< 0.80\ \mu\text{m}$), respectively. The particle size correlates well with the results obtained from SEM. The decrease in particle size has a marked influence on optical properties as discussed later.

3.3.4 UV-Visible Studies

The reflectance spectra of $[(\text{Li}_{0.5}\text{La}_{0.5})_x\text{Bi}_{1-x}][\text{Mo}_x\text{V}_{1-x}]\text{O}_4$ is shown in Fig.3.12 and the inset shows the corresponding Tauc plots. All the samples showed a steep band shape, which is a characteristic of band gap transition.²⁶ With the increase of the x value, the band gap absorption edge of $[(\text{Li}_{0.5}\text{La}_{0.5})_x\text{Bi}_{1-x}][\text{Mo}_x\text{V}_{1-x}]\text{O}_4$ samples is blue shifted.

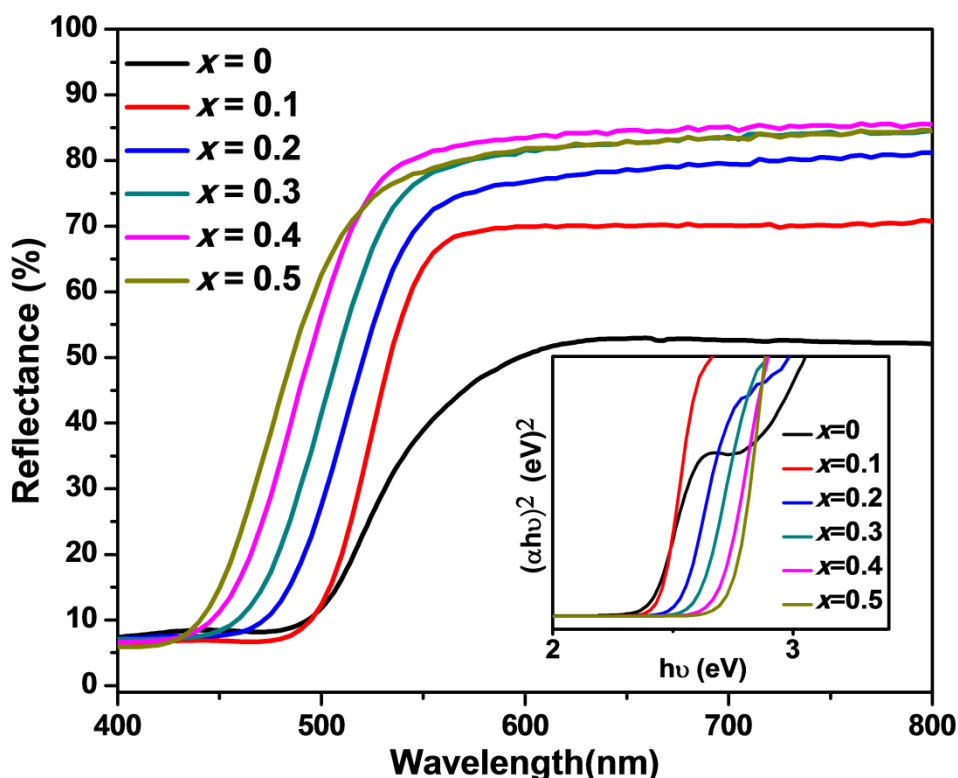


Fig. 3.12 Reflectance spectra of $[(\text{Li}_{0.5}\text{La}_{0.5})_x\text{Bi}_{1-x}][\text{Mo}_x\text{V}_{1-x}]\text{O}_4$ ($x = 0, 0.1, 0.2, 0.3, 0.4, 0.5$) pigments (Tauc plots in the inset).

As a crystalline semiconductor, the optical absorption near the band edge follows the formula $\alpha h\nu = A(h\nu - E_g)^{n/2}$, where α , ν , E_g and A are absorption coefficient, light frequency, band gap and a constant, respectively. Among them, n depends on the characteristics of the transition in a semiconductor, i.e. direct transition ($n = 1$) or indirect transition ($n = 4$). For BiVO_4 , the value of n is 1.²⁷ The band gap energy (E_g value) of the samples can be estimated from a plot $(\alpha h\nu)^2$ versus photon energy ($h\nu$). The intercept of the tangent to the X-axis will give a good approximation of the band gap energy for the samples. Plots of the $(\alpha h\nu)^2$ versus photon energy ($h\nu$) of samples are shown in inset of Fig.3.12. The band gap linearly increases with x as given in Table 3.3.

The absorption of BiVO_4 arises due to the charge-transfer of the hybrid orbital of Bi 6s and O 2p to V 3d orbitals. The pigments obtained are of tetragonal scheelite type. The distortions and symmetry constraints of monoclinic scheelite BiVO_4 are slightly different from those of tetragonal scheelite BiVO_4 , although they possess the same scheelite structure. Therefore, there is no lone-pair distortion around Bi^{3+} due to the balanced symmetry constraints.²⁸ The lesser the degree of distortion of the local structure, the less the Bi 6s and O 2p orbitals overlap. Also, the inclusion of Mo 4d and La 5d orbitals above the V 3d orbitals results in widening of the conduction band. This leads to reduced interaction between O 2p and V 3d orbitals. This in turn increases the band gap.

When mineralizers such as NaCl, CaF_2 , H_3BO_3 and MgF_2 were added to $\text{Li}_{0.15}\text{La}_{0.15}\text{Bi}_{0.7}\text{Mo}_{0.3}\text{V}_{0.7}\text{O}_4$, a slight change in the optical absorption edges is observed. The reflectance spectra of the mineralizer added samples of $\text{Li}_{0.15}\text{La}_{0.15}\text{Bi}_{0.7}\text{Mo}_{0.3}\text{V}_{0.7}\text{O}_4$ pigments are shown in Fig.3.13 with the corresponding Tauc plots inset. The obtained band gap values show a minor variation given in Table 3.4.

The absorption edge of $[(\text{Li}_{0.33}\text{Ca}_{0.33}\text{La}_{0.33})_x \text{Bi}_{1-x}][\text{Mo}_x \text{V}_{1-x}]\text{O}_4$ ($x = 0.05, 0.10, 0.15, 0.20$) pigments gets blue shifted (Fig.3.14). Thus it is evident that the absorption edge of BiVO_4 can be gently shifted by $(\text{LiLa})_{1/2}\text{MoO}_4$ addition. It can be further modified by $(\text{LiCaLa})_{1/3}\text{MoO}_4$ addition. Thus, a fine tuning of band gap is possible by suitable compositional adjustments.

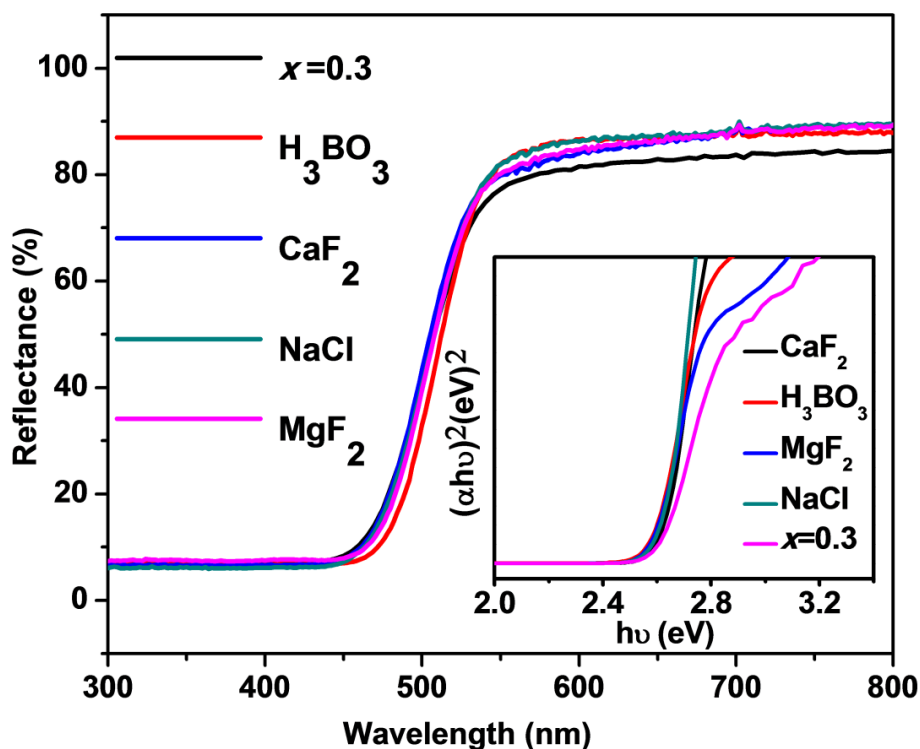


Fig. 3.13 Reflectance spectra of $\text{Li}_{0.15}\text{La}_{0.15}\text{Bi}_{0.7}\text{Mo}_{0.3}\text{V}_{0.3}\text{O}_4$ pigment with various mineralizers (Tauc plots in the inset).

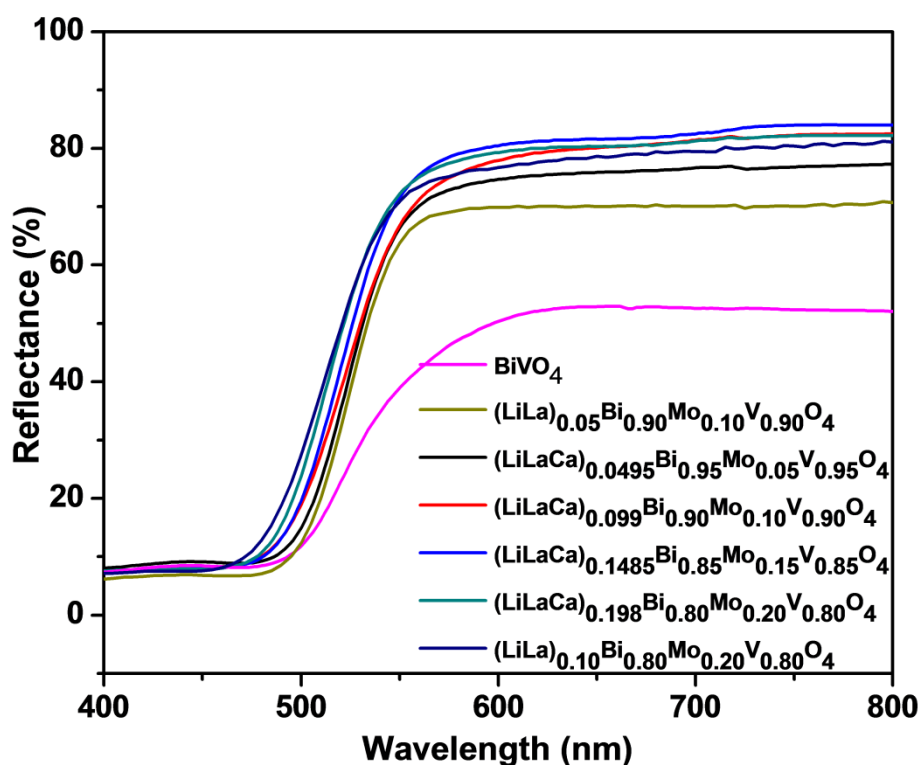


Fig. 3.14 Reflectance spectra of $[(\text{Li}_{0.33}\text{Ca}_{0.33}\text{La}_{0.33})_x \text{Bi}_{1-x}][\text{Mo}_x \text{V}_{1-x}]\text{O}_4$ ($x = 0.05, 0.10, 0.15, 0.20$) pigments. For the sake of comparison $[(\text{Li}_{0.5}\text{La}_{0.5})_x \text{Bi}_{1-x}][\text{Mo}_x \text{V}_{1-x}]\text{O}_4$ ($x = 0.10, 0.20$) too are shown.

3.3.5 Color Analysis

Table 3.3 summarizes the CIE 1976 color coordinates of the powdered $[(\text{Li}_{0.5}\text{La}_{0.5})_x\text{Bi}_{1-x}][\text{Mo}_x\text{V}_{1-x}]\text{O}_4$ ($x = 0, 0.1, 0.2, 0.3, 0.4, 0.5$) pigment samples. Addition of $(\text{LiLa})_{1/2}\text{MoO}_4$ into BiVO_4 (from $x = 0$ to 0.3) leads to a continuous increase in the yellow component (b^* from 52 to 76) and chroma (C^* from 54 to 76) values of the pigments. The hue angle (h^0) also increases considerably from 74.8 to 98.3. The hue angles (h^0) of the powdered $[(\text{Li}_{0.5}\text{La}_{0.5})_x\text{Bi}_{1-x}][\text{Mo}_x\text{V}_{1-x}]\text{O}_4$ ($x = 0.1, 0.2, 0.3, 0.4, 0.5$) pigment samples were found to be in the yellow region of the cylindrical color space ($h^0=70\text{-}105^0$ for yellow). Also, with the increase of x , a^* value gradually shifts from 14.29 to -8.97 indicating a greenish yellow hue characteristic of BiVO_4 pigments (Fig.3.15). When x reaches 0.5, L^* increases to 87.73 as well as a^* reaches -8.97, but the b^* values continue diminishing. On adding various mineralizers to $x=0.3$, there is a significant improvement in the yellow color characteristics (Fig.3.16). Except MgF_2 other mineralizers yield a greenish yellow hue. From Table 3.4, it is seen that by the addition of NaCl mineralizer to $x=0.3$ composition, the highest b^* value of 85.25 is obtained. The obtained b^* value is higher when compared to commercially available BiVO_4 marketed as Sicopal yellow L1100.²⁹

Table 3.3 CIE color coordinates and band gap of $[(\text{Li}_{0.5}\text{La}_{0.5})_x\text{Bi}_{1-x}][\text{Mo}_x\text{V}_{1-x}]\text{O}_4$ ($x = 0, 0.1, 0.2, 0.3, 0.4, 0.5$) pigments

Composition	L^*	a^*	b^*	C^*	h^0	E_g (eV)
$x = 0$	65.79	14.29	52.57	54.47	74.78	2.37
$x = 0.1$	77.26	10.60	72.95	73.72	81.72	2.42
$x = 0.2$	81.40	4.25	76.86	76.98	86.82	2.53
$x = 0.3$	85.27	-2.21	76.15	76.19	91.67	2.57
$x = 0.4$	87.97	-7.88	69.35	69.80	96.49	2.68
$x = 0.5$	87.73	-8.97	61.56	62.21	98.3	2.74
Sicopal yellow²⁹	94.4	-16.7	76.9	78.7	77.8	-

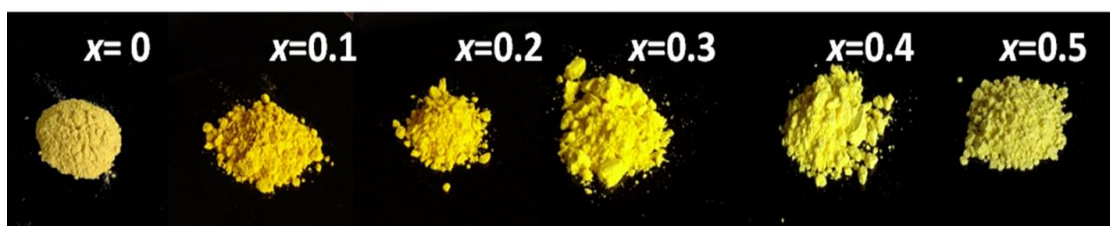


Fig. 3.15 Photographs of $[(\text{Li}_{0.5}\text{La}_{0.5})_x\text{Bi}_{1-x}][\text{Mo}_x\text{V}_{1-x}]\text{O}_4$ ($x = 0, 0.1, 0.2, 0.3, 0.4, 0.5$) pigments.

Table 3.4 CIE color coordinates and band gap of $\text{Li}_{0.15}\text{La}_{0.15}\text{Bi}_{0.7}\text{Mo}_{0.3}\text{V}_{0.7}\text{O}_4$ pigments in the presence of 1% mineralizers

$\text{Li}_{0.15}\text{La}_{0.15}\text{Bi}_{0.7}\text{Mo}_{0.3}\text{V}_{0.7}\text{O}_4$	L^*	a^*	b^*	C^*	h°	$E_g(\text{eV})$
No mineralizer	85.27	-2.21	76.15	76.19	91.67	2.57
CaF_2	87.01	-4.39	84.19	84.3	93	2.57
H_3BO_3	84.56	-2.4	84.15	84.18	91.64	2.54
MgF_2	83.31	3.75	84.28	84.36	87.44	2.58
NaCl	85.49	-4.78	85.25	85.38	93.22	2.58
Sicopal yellow ²⁹	94.4	-16.7	76.9	78.7	77.8	-

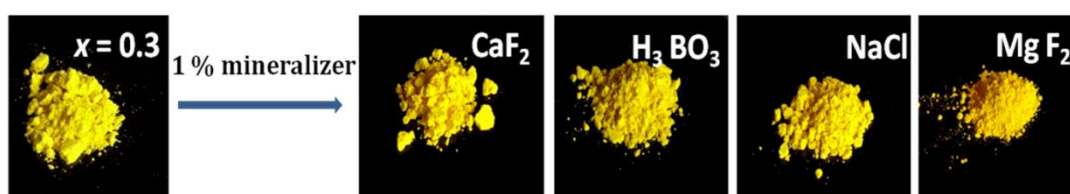


Fig. 3.16 Photographs of $\text{Li}_{0.15}\text{La}_{0.15}\text{Bi}_{0.7}\text{Mo}_{0.3}\text{V}_{0.7}\text{O}_4$ pigment in the presence of 1% mineralizers.

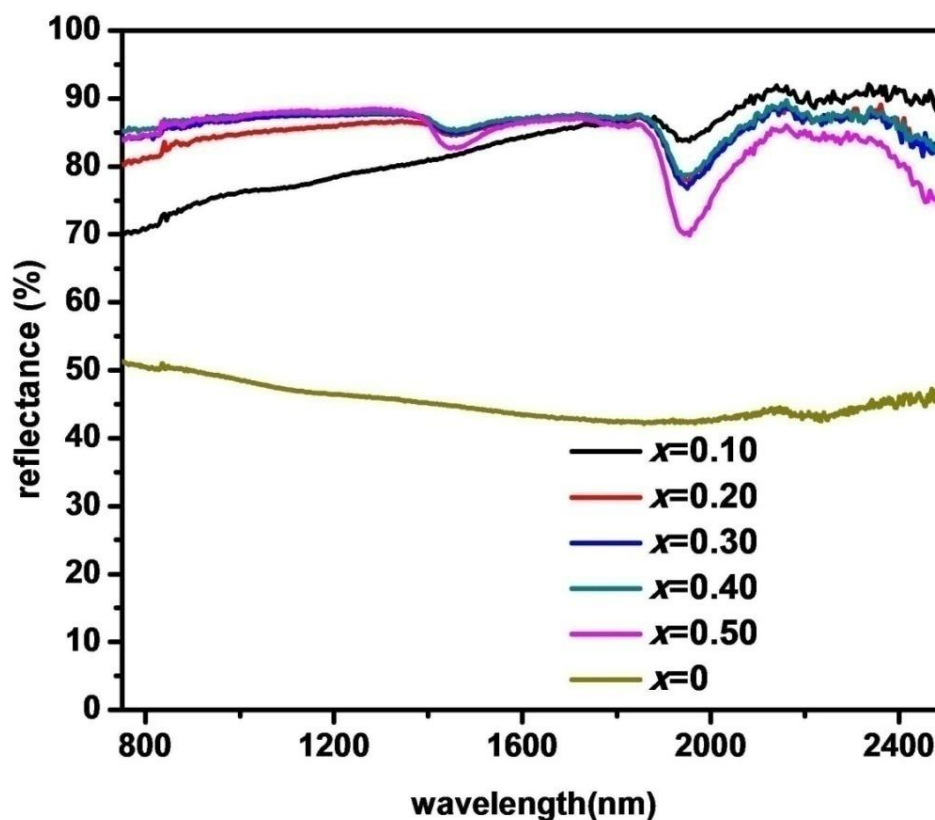
Addition of $(\text{LiCaLa})_{1/3}\text{MoO}_4$ into BiVO_4 (from $x = 0.05$ to 0.20) leads to a continuous increase in the yellow component (b^* from 52 to 78) of the pigments. The pigments obtained are of reddish yellow hue. The obtained b^* value is also higher when compared to commercially available Sicopal Yellow L1100. Table 3.5 summarizes the CIE 1976 color coordinates of the powdered $[(\text{Li}_{0.33}\text{Ca}_{0.33}\text{La}_{0.33})_x\text{Bi}_{1-x}][\text{Mo}_x\text{V}_{1-x}]\text{O}_4$ ($x = 0.05, 0.10, 0.15, 0.20$) pigments.

Table 3.5 CIE color coordinates and band gap of $[(\text{Li}_{0.33}\text{Ca}_{0.33}\text{La}_{0.33})_x\text{Bi}_{1-x}][\text{Mo}_x\text{V}_{1-x}]\text{O}_4$ ($x = 0.05, 0.10, 0.15, 0.20$) pigments

Composition	L^*	a^*	b^*	C^*	h^0	E_g (eV)
$x = 0.05$	78.8	12.14	71.83	72.85	80.4	2.43
$x = 0.10$	80.02	11.65	75.18	76.08	81.19	2.46
$x = 0.15$	81.72	9.85	77.96	78.58	82.79	2.48
$x = 0.20$	82.36	6.15	78.32	78.57	85.5	2.49
Sicopal yellow ²⁹	94.4	-16.7	76.9	78.7	77.8	-

3.3.6 IR Reflectance studies

A cool non white coating that absorbs in the visible range should be highly reflective in the near-infrared part of the electromagnetic spectrum in order to maintain a high solar reflectance. Fig. 3.17 illustrates the IR reflectance spectra of powdered $[(\text{Li}_{0.5}\text{La}_{0.5})_x\text{Bi}_{1-x}][\text{Mo}_x\text{V}_{1-x}]\text{O}_4$ ($x = 0, 0.1, 0.2, 0.3, 0.4, 0.5$) pigment samples.

**Fig. 3.17** IR reflectance spectra of $[(\text{Li}_{0.5}\text{La}_{0.5})_x\text{Bi}_{1-x}][\text{Mo}_x\text{V}_{1-x}]\text{O}_4$ ($x = 0, 0.1, 0.2, 0.3, 0.4, 0.5$) pigments.

It is seen that the NIR reflectance is enhanced by up to 88% in the 1100 nm range. Addition of mineralizers to $\text{Li}_{0.15}\text{La}_{0.15}\text{Bi}_{0.7}\text{Mo}_{0.3}\text{V}_{0.7}\text{O}_4$ pigment further increases the NIR reflectance, up to 94% when CaF_2 is added. Enhancement in IR reflectance may be due to the decrease in particle size.³⁰ The IR reflectance spectra of powdered $\text{Li}_{0.15}\text{La}_{0.15}\text{Bi}_{0.7}\text{Mo}_{0.3}\text{V}_{0.7}\text{O}_4$ pigments with various mineralizers are shown in Fig. 3.18. The IR solar reflectance spectra determined in accordance with ASTM Standard G173-03 of powdered $[(\text{Li}_{0.5}\text{La}_{0.5})_x\text{Bi}_{1-x}][\text{Mo}_x\text{V}_{1-x}]\text{O}_4$ ($x = 0, 0.1, 0.2, 0.3, 0.4, 0.5$) pigments are presented in Fig.3.19. Fig.3.20 illustrates the IR reflectance spectra of powdered $[(\text{Li}_{0.33}\text{Ca}_{0.33}\text{La}_{0.33})_x\text{Bi}_{1-x}][\text{Mo}_x\text{V}_{1-x}]\text{O}_4$ ($x = 0.05, 0.10, 0.15, 0.20$) pigment samples which exhibit NIR reflectance of 81, 85, 86, 84 % respectively. The results encourage the application of the developed pigments for cool roof applications to mitigate the urban island effect.³¹

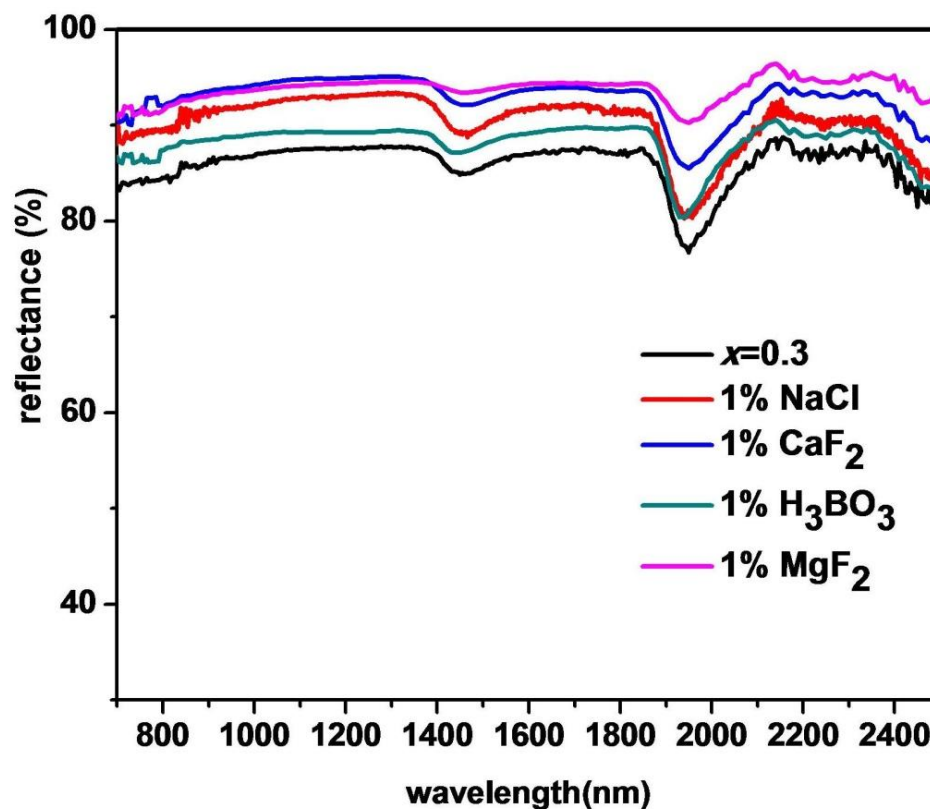


Fig. 3.18 IR reflectance spectra of $\text{Li}_{0.15}\text{La}_{0.15}\text{Bi}_{0.7}\text{Mo}_{0.3}\text{V}_{0.7}\text{O}_4$ pigments with different mineralizers.

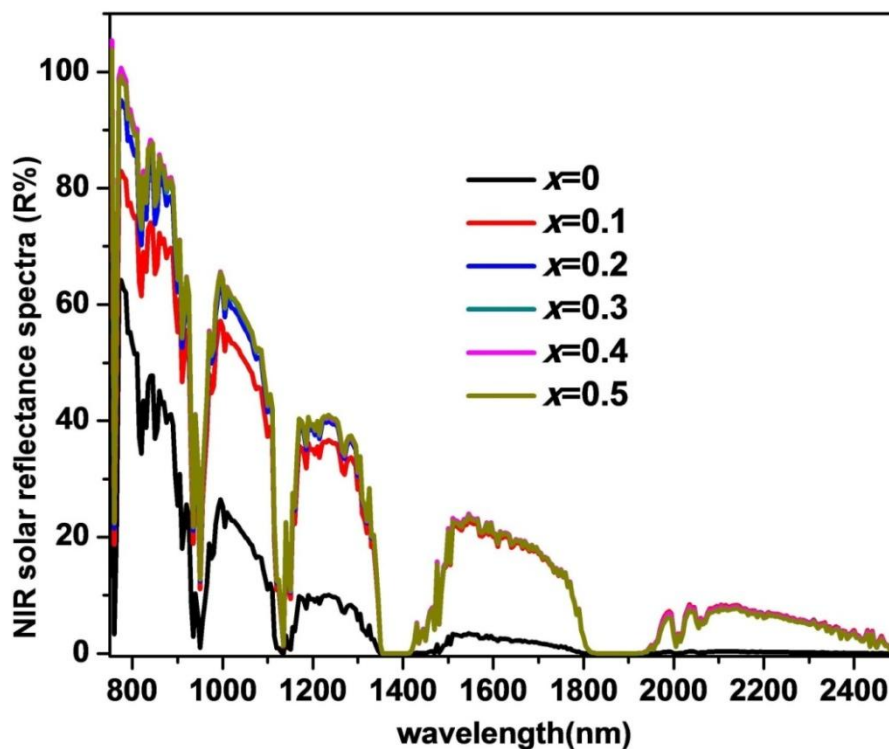


Fig. 3.19 IR solar reflectance spectra of $[(\text{Li}_{0.5}\text{La}_{0.5})_x \text{Bi}_{1-x}][\text{Mo}_x\text{V}_{1-x}]\text{O}_4$ ($x = 0, 0.1, 0.2, 0.3, 0.4, 0.5$) pigments.

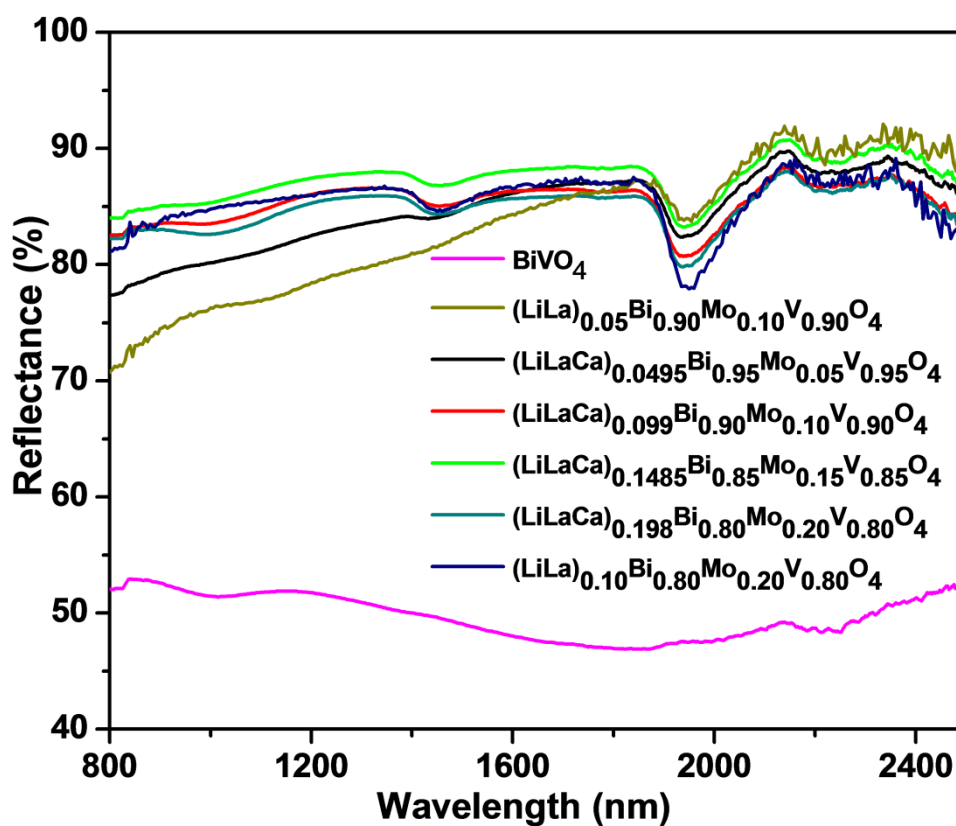


Fig. 3.20 IR reflectance spectra of $[(\text{Li}_{0.33}\text{Ca}_{0.33}\text{La}_{0.33})_x \text{Bi}_{1-x}][\text{Mo}_x\text{V}_{1-x}]\text{O}_4$ ($x = 0.05, 0.10, 0.15, 0.20$) pigments.

3.4 Conclusions

New yellow pigments have been successfully prepared via a solid state route by effective solid solution formation between BiVO_4 and $(\text{LiLa})_{1/2}\text{MoO}_4\text{/(LiCaLa)}_{1/3}\text{MoO}_4$. Optimization of coloristic properties has been successfully accomplished using various mineralizers. The developed pigments find use in formulating relatively less toxic pigments for paints and plastics. Also, the high IR reflectance characteristics may find application in “cool roof” construction.

3.5 References

1. Buxbaum, G.; Pfaff, G., Eds.; Introduction. In *Industrial Inorganic Pigments*. WILEY-VCH Verlag GmbH & Co KGaA, Weinheim, **2005**.
2. Roméro, S.; Mosset, A.; Macaudière, P.; Trombe, J.C., Effect of some dopant elements on the low temperature formation of $\gamma\text{-Ce}_2\text{S}_3$. *J. Alloys Compd.* **2000**, *302* (1–2), 118-127.
3. Jansen, M.; Letschert HP. Inorganic yellow-red pigments without toxic metals. *Nature*. **2000**, *404* (6781), 980-982.
4. Pailhé N, Gaudon M, Demourgues A. (Ca^{2+} , V^{5+}) co-doped $\text{Y}_2\text{Ti}_2\text{O}_7$ yellow pigment. *Mater. Res. Bull.* **2009**, *44* (8), 1771-1777.
5. Kumari, L. S.; Gayathri, T. H.; Sameera, S.; Rao, P. P., Y-doped Bi_2MoO_6 yellow pigments for the coloration of plastics. *J. Am. Ceram. Soc.* **2011**, *94* (2), 320-323.
6. Luňáková, P.; Trojan, M.; Luxová, J.; Trojan, J., $\text{BaSn}_{1-x}\text{Tb}_x\text{O}_3$: A new yellow pigment based on a perovskite structure. *Dyes Pigm.* **2013**, *96* (1), 264-268.
7. Furukawa, S.; Masui, T.; Imanaka, N., New environment-friendly yellow pigments based on $\text{CeO}_2\text{-ZrO}_2$ solid solutions. *J. Alloys Compd.* **2008**, *451*(1–2), 640-643.
8. Sleight, A. W.; Linn, W. J., Olefin oxidation over oxide catalysts with the scheelite structure. *Ann. NY Acad. Sci.* **1976**, *272* (1), 22-44.
9. Endriss, H., *High Performance Pigments*. In: Smith HM, editor. Bismuth Vanadates. New York: Wiley-VCH; **2002**.
10. Saimi, T.; Hideki, K.; Akihiko, K., Selective preparation of monoclinic and tetragonal BiVO_4 with scheelite structure and their photocatalytic properties. *Chem Mater.* **2001**, *13*, 4624-4628.
11. Hartmanova, M.; Le, M. T.; Jergel, M.; Šmatko, V.; Kundracik, F., Structure and electrical conductivity of multicomponent metal oxides having scheelite structure. *Russ J Electrochem.* **2009**, *45* (6), 621-629.
12. Jo, W. J.; Jang, J.-W.; Kong, K.-j.; Kang, H. J.; Kim, J. Y.; Jun, H.; Parmar, K. P. S.; Lee, J. S., Phosphate doping into monoclinic BiVO_4 for enhanced photoelectrochemical water oxidation activity. *Angew. Chem. Int. Ed.* **2012**, *51* (13), 3147-3151.

13. Bi, J.; Li, J.; Wu, L.; Zheng, H.; Su, W., Effects of aluminum substitution on photocatalytic property of BiVO_4 under visible light irradiation. *Mater. Res. Bull.* **2012**, *47* (3), 850-855.
14. Tücks, A.; Beck, H. P., The photochromic effect of bismuth vanadate pigments. Part I: Synthesis, characterization and lightfastness of pigment coatings. *J. Solid State Chem.* **2005**, *178*, 1145-1146.
15. Bhattacharya, A. K.; Mallick, K. K.; Hartridge, A., Phase transition in BiVO_4 . *Mater. Lett.* **1997**, *30* (1), 7-13.
16. Bierlein, J. D.; Sleight, A. W., Ferroelasticity in BiVO_4 . *Solid State Commun.* **1975**, *16* (1), 69-70.
17. de Moraes, J. R.; da Silva, F. R.; Gomes, L.; Mazzocchi, V. L.; Parente, C. B. R.; Baldochi, S. L., Growth and spectroscopic characterizations: properties of $\text{Nd:LiLa}(\text{MoO}_4)_2$ single crystal fibers. *Cryst. Engg. Comm.* **2013**, *15* (12), 2260-2268.
18. Wood, P.; Glasser, F. P., Preparation and properties of pigmentary grade BiVO_4 precipitated from aqueous solution. *Ceram. Int.* **2004**, *30* (6), 875-82.
19. Kumari, L. S.; Rao, P. P.; Radhakrishnan, A.N., James, V.; Sameera, S.; Koshy, P., Brilliant yellow color and enhanced NIR reflectance of monoclinic BiVO_4 through distortion in VO_4^{3-} tetrahedra. *Sol. Energy Mater. Sol. Cells.* **2013**, *112*, 134-143.
20. Russu, S.; Tromp, M.; Tsapatsaris, N.; Beesley, A. M.; Schroeder, S. L. M.; Weller, M. T.; Evans, J., High-throughput synthesis and characterization of BiMoVOX materials. *AIP Conf. Proc.* **2007**, *882* (1), 535-537.
21. Zhang, L.; Chen, D. P.; Jiao, X., Monoclinic structured BiVO_4 nanosheets: hydrothermal preparation, formation mechanism and coloristic and photocatalytic properties. *J. Phys. Chem. B.* **2006**, *110* (6), 2668-2673.
22. Standard tables for reference solar spectral irradiances: Direct normal and hemispherical on 37° tilted surface. ASTM International: West Conshohocken, PA, **2012**.
23. Shannon, R., Revised effective ionic radii and systematic studies of interatomic distances in halides and chalcogenides. *Acta Crystallogr. A.* **1976**, *32* (5), 751-67.

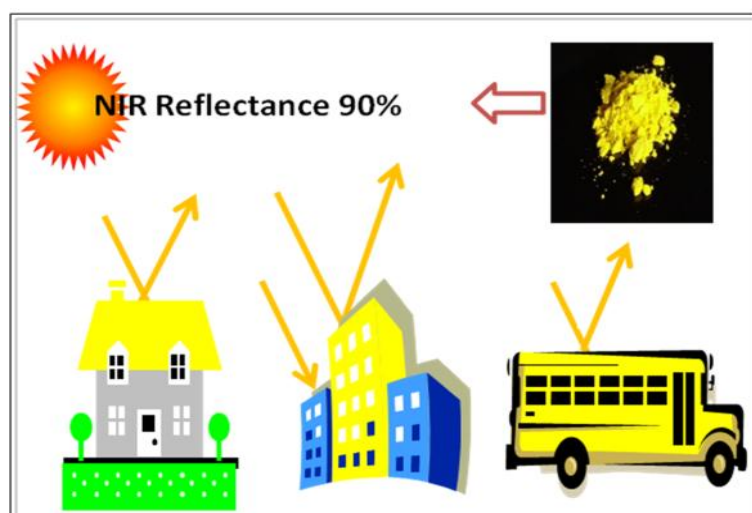
24. Scherrer, P., Bestimmung der Grösse und der inneren Struktur von Kolloidteilchen mittels Röntgenstrahlen. *Nachr. Ges. Wiss. Göttingen* **1918**, *2*, 98-100.
25. Langford, J. I.; Wilson, A. J. C., Scherrer after sixty years: A survey and some new results in the determination of crystallite size. *J. Appl. Crystallogr.* **1978**, *11* (2), 102-113.
26. Walsh, A.; Yan, Y.; Huda, M. N.; Al-Jassim, M. M.; Wei, S.-H., Band edge electronic structure of BiVO_4 : Elucidating the role of the Bi s and V d orbitals. *Chem Mater.* **2009**, *21* (3), 547-551.
27. Payne, D. J.; Robinson, M. D. M.; Egde, R. G.; Walsh, A.; McNulty, J.; Smith, K. E.; Piper, L. F. J., The nature of electron lone pairs in BiVO_4 . *Appl. Phys. Lett.* **2011**, *98* (21), 212110-212113.
28. Yu, J.; Kudo, A., Effects of structural variation on the photocatalytic performance of hydrothermally synthesized BiVO_4 . *Adv. Funct. Mater.* **2006**, *16* (16), 2163-2169.
29. Masui, T.; Honda, T.; Wondrusch, M.; Imanaka, N., Imanaka N. Novel and environmentally friendly $(\text{Bi,Ca,Zn})\text{VO}_4$ yellow pigments. *Dyes Pigm.* **2013**, *99* (3), 636-641.
30. Jeevanandam, P.; Mulukutla, R. S.; Phillips, M.; Chaudhuri, S.; Erickson, L. E.; Klabunde, K. J., Near infrared reflectance properties of metal oxide nanoparticles. *J. Phys. Chem. C.* **2007**, *111* (5), 1912-1918.
31. Akbari, H.; Pomerantz, M.; Taha, H., Cool surfaces and shade trees to reduce energy use and improve air quality in urban areas. *Sol. Energy.* **2001**, *70* (3), 295-310.

CHAPTER 4

YELLOW PIGMENTS IN $\text{BiVO}_4 - (\text{LiRE})_{1/2}\text{MoO}_4$ SYSTEM

Overview

Brilliant IR reflecting yellow colorants are developed in rare earth double molybdate substituted BiVO_4 solid solutions. The color characteristics are comparable to commercial BiVO_4 pigment. Incorporation of double rare earth molybdates of La, Gd, Tb, Y and Lu into BiVO_4 results in non toxic IR reflecting cool pigments. The NIR reflectance of these pigments range from 84 to 90 %.



4.1 Introduction

The urban heat island effect emerging in metropolitan cities produces elevated urban air temperatures. Solar radiation consists of about 5% ultraviolet radiation, 43% visible radiation and 52 % infrared radiation. A major contribution of heat comes from the IR radiation, which transfers heat to the underlying structure in buildings and automobiles causing thermal discomfort and health problems. A substantial amount of energy is consumed to cool buildings, thus increasing energy demand.¹ Cool paints absorb less solar energy, which keeps the surface at a lower temperature and decreases energy transfer by radiation. Passive cooling of buildings helps reduction in air pollution due to low energy usage and power plant emissions. Therefore, current interest in the pigment industry is focused on developing non toxic cool pigments that aid in energy savings.² Bright yellow shades are particularly challenging, with preferential reformulation away from cadmium pigments and lead chromates within the plastics and surface coating markets.³ There is an urgent need for developing IR reflecting non toxic yellows, which are limited in the current market.

Recently, BiVO_4 has attracted wide attention for its photocatalytic,⁴ ferroelastic,⁵ dielectric,⁶ ionic and electronic conductive properties,⁷ which makes it attractive for use in gas sensors,⁸ microwave resonator devices,⁶ wastewater treatment⁹ and water splitting.⁹ BiVO_4 has been identified as an ideal candidate for pigmentary applications.¹⁰ Recently, many researchers, including our group have reported BiVO_4 based pigments such as $(\text{Bi}, \text{La})\text{VO}_4$,¹¹ $(\text{Bi}, \text{Ca}, \text{Zn})\text{VO}_4$,¹² $(\text{Bi}, \text{Ca}, \text{Zn}, \text{La})\text{VO}_4$,¹³ $\text{Ta}^{5+}/\text{P}^{5+}$ substituted BiVO_4 ¹⁴ and SiO_2 coated BiVO_4 .¹⁵ So, development of nontoxic IR reflecting BiVO_4 based pigments can lead to cool surface coating formulations for buildings and automobile shells.

Double alkali rare earth molybdates and tungstates of the type $\text{ARE}(\text{XO}_4)_2$; $\text{X} = \text{Mo}, \text{W}$ ¹⁶ have a variety of applications in optoelectronics,¹⁷ catalysis and so on. Mostly depending on the relation between ionic radii of A and RE, they crystallize in diverse symmetries: tetragonal, orthorhombic, monoclinic and even triclinic.¹⁸ They crystallize in various structural forms according to the ratio of $R_{\text{RE}}/R_{\text{A}}$. Among the alkali metals, we have chosen lithium rare earth molybdates to form solid solutions with BiVO_4 to further ameliorate its color parameters. BiVO_4 has three main crystal forms: zircon structure with tetragonal system¹⁹ and scheelite structure with monoclinic²⁰ and tetragonal systems.⁷ BiVO_4 undergoes a reversible second order ferroelastic phase transition from monoclinic scheelite to tetragonal scheelite, which

can be induced by a high temperature of about 255°C or high pressure.²¹ This phase transition can also be achieved by incorporating larger ions than V⁵⁺ at the B-site, as discussed in the previous chapter. (LiLa)_{1/2}MoO₄ substitution on BiVO₄ leads to [(Li_{0.5}La_{0.5})_xBi_{1-x}][Mo_xV_{1-x}]O₄ based pigments. Among the developed pigments Li_{0.10}La_{0.10}Bi_{0.8}Mo_{0.2}V_{0.8}O₄ composition exhibited intense yellow color characterized by the highest *b** value.

Rare earths show interesting optical properties, as they have a partially filled f orbital. Rao *et al.* obtained colors ranging from pale yellow to orange red based on doping Ln³⁺ ions into the host lattice of Bi₂O₃.²² Thus, rare earth substitution allows further tuning of band gap of the material. In this regard, we made an attempt to substitute various rare earths in the selected composition to produce various colorants. Li_{0.10}RE_{0.10}Bi_{0.8}Mo_{0.2}V_{0.8}O₄; RE = La, Pr, Sm, Gd, Tb, Dy, Y, Yb and Lu pigments were prepared and analyzed for their crystalline structure, morphological, composition and optical characteristics. The relationship between observed band gap and the color characteristics of these materials has been emphasized.

4.2 Experimental Section

4.2.1 Materials and Methods

The pigments of the formula Li_{0.10}RE_{0.10}Bi_{0.8}Mo_{0.2}V_{0.8}O₄; RE = La, Pr, Sm, Gd, Tb, Dy, Y, Yb and Lu were prepared by the conventional solid state reaction route. Li₂CO₃ (99.9 % purity, Acros Organics), La₂O₃, Pr₆O₁₁, Sm₂O₃, Gd₂O₃, Tb₄O₇, Dy₂O₃, Y₂O₃, Yb₂O₃, Lu₂O₃, V₂O₅ (99.99 % purity, Sigma- Aldrich), Bi₂O₃ (99.999 % purity, Sigma-Aldrich) and MoO₃ (99.5 % purity, Sigma-Aldrich) were weighed in the required stoichiometric amount and then were wet mixed thoroughly in an agate mortar using acetone as the medium. For comparison BiVO₄ samples were also prepared. The mixed product was dried in an air oven at 100°C for 1 h. The process of mixing and drying was repeated three times to get a homogeneous mixture. The dried mixture was then calcined in a platinum crucible in an electrical furnace. The heating of the furnace was programmed increasing the temperature initially at 10°C per minute up to the temperature (400-500°C) and afterward, the heating rate was decreased to 5°C per minute up to the required temperature (800°C). The samples were soaked at the final temperature 800°C for 6 h. The calcined samples were ground thoroughly in an agate mortar into fine powder for further analysis.

4.2.2 Characterizations

The calcined powders were characterized by means of X-ray powder diffraction (XRD) using a Ni filtered Cu-K α radiation ($\lambda = 1.54056 \text{ \AA}$) with a PANalytical X'pert Pro diffractometer operated at 45kV and 30mA for its crystalline structure. Data were collected from 10 to 90° 2 θ range with a step size of 0.016°. The structural refinement of all the XRD patterns was performed by the Rietveld analysis using the X'pert plus program. Particle morphological analysis of the powder was performed by means of a scanning electron microscope with JEOL JSM-5600 LV SEM with an acceleration voltage of 15 kV. Energy dispersive analysis and elemental mapping of the samples was analyzed using Silicon Drift Detector–X-MaxN attached with a Carl Zeiss EVO SEM. EDS elemental mapping was conducted by AZtec Energy EDS Microanalysis software. The UV visible spectra of the samples was measured with a UV–vis–NIR spectrophotometer (Shimadzu, UV-3600) using BaSO₄ as a reference. Optical measurements were performed in the 220 to 800 nm wavelength range with a step size of 2 nm. The color of the pigments was evaluated according to The Commission Internationale del' Eclairage (CIE) through $L^*a^*b^*$ 1976 color scales (CIE-LAB 1976 color scales) as described in the previous sections. The infrared reflectance of the powdered pigment samples was measured with a UV–Vis–NIR spectrophotometer (Shimadzu, UV–3600 with an integrating sphere attachment) using poly–tetrafluoroethylene (PTFE) as a reference in the 700 to 2500 nm range with a step size of 5 nm.

4.3 Results and Discussion

4.3.1 X-Ray Diffraction Analysis

Fig. 4.1(a) shows the powder X-ray diffraction patterns of pigments calcined at 800°C. XRD analysis indicates that the pigments are highly crystalline in nature. All the reflections are indexed as per the monoclinic tetragonal (s-t) phase with a space group $I4_{1/a}$ and the reflections can be well indexed according to the powder diffraction file no. 01-074-4892. Fig. 1(b) shows the zoom-in part of the 2 θ range from 18–19.5°. The line in Fig. 4.1(b) indicates the inclination of the shift of the (101) peak toward the higher angle side as the decrease of ionic radius of rare earth. From

Tb onward, minor REVO_4 phase formation starts to occur with evidence of peaks around 24° and 33° trending toward higher angles with heavier rare earths.

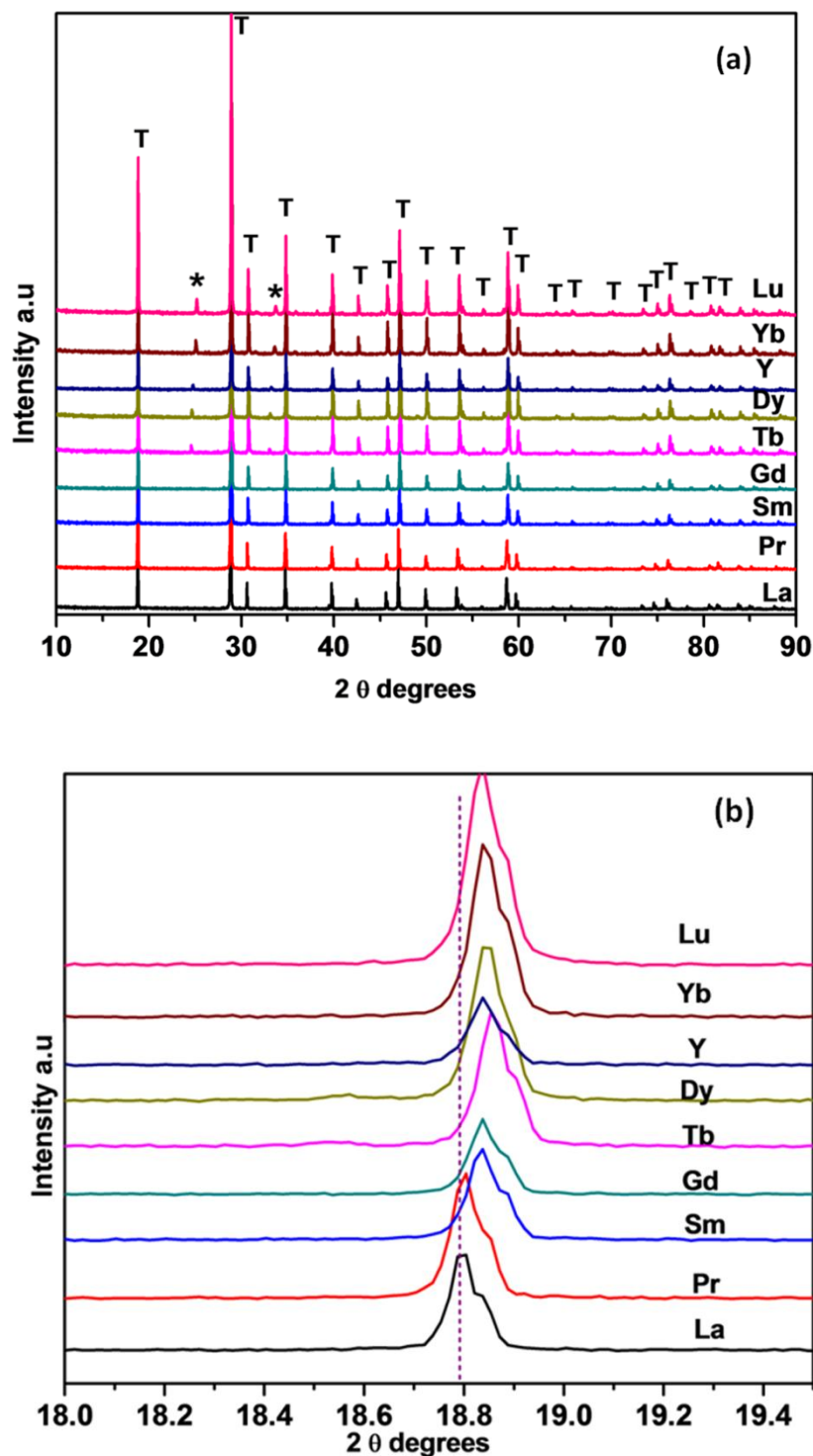


Fig. 4.1 (a) X-ray powder diffraction patterns of $\text{Li}_{0.10}\text{RE}_{0.10}\text{Bi}_{0.8}\text{Mo}_{0.2}\text{V}_{0.8}\text{O}_4$ pigments. (b) Zoomed view of peak position around 18.8° .

Structural refinement

The structural refinement of all the XRD patterns for rare earth doped $\text{Li}_{0.10}\text{RE}_{0.10}\text{Bi}_{0.8}\text{Mo}_{0.2}\text{V}_{0.8}\text{O}_4$ pigments were performed by the Rietveld analysis using the X'pert Plus program. The starting model for the refinement of the phases was taken from the reported crystal structure of BiVO_4 . Here Bi/Li/RE are at ($4b$: 0, 1/4, 5/8) sites, V and Mo at ($4a$: 0, 1/4, 1/8) sites and O at ($16f$: x, y, z), $Z = 4$ in the space group $I4_{1/a}$, no.88. The profile was fitted using a Pseudo Voigt profile function and Caglioti profile parameters were refined. Fig. 4.2 shows the typical best fit for sample $\text{Li}_{0.10}\text{Gd}_{0.10}\text{Bi}_{0.8}\text{Mo}_{0.2}\text{V}_{0.8}\text{O}_4$ with the observed, calculated, the difference powder diffraction profiles and the expected Bragg reflections. The refined lattice parameters obtained from the Rietveld analysis of the powder diffraction data for the samples are given in Table 4.1. As said earlier, space group $I4_{1/a}$ is observed for $R_{\text{RE}}/R_{\text{A}}$ over the range from 1.341 to 0.805 for alkali rare earth double molybdates. Here too the obtained solid solutions exhibit the values within this range.

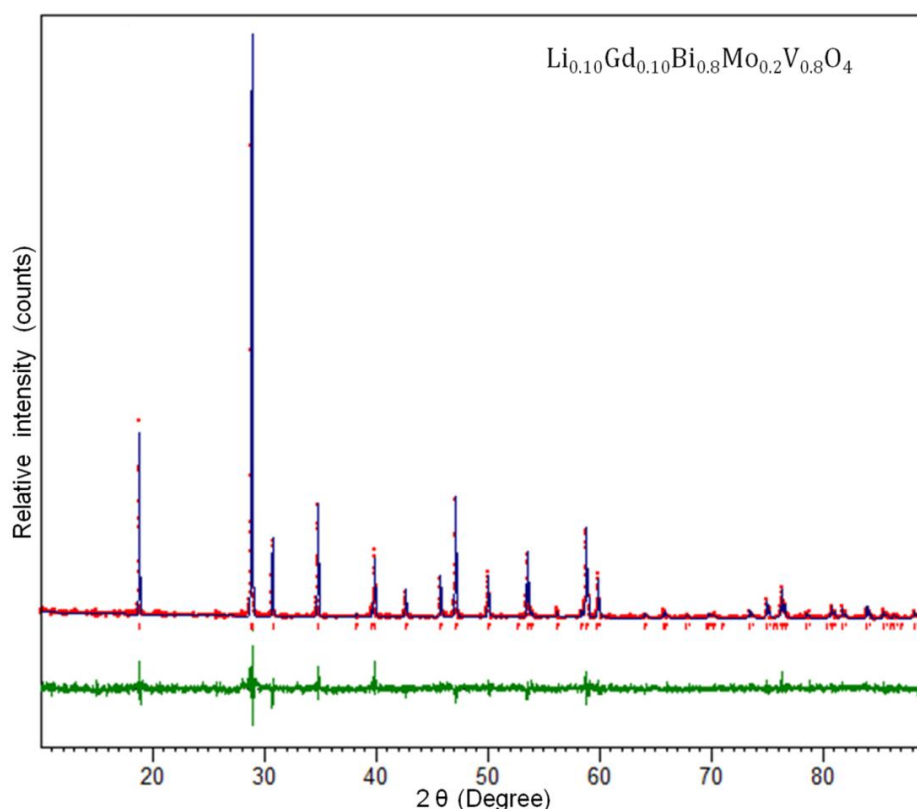


Fig. 4.2 Rietveld refinement for $\text{Li}_{0.10}\text{Gd}_{0.10}\text{Bi}_{0.8}\text{Mo}_{0.2}\text{V}_{0.8}\text{O}_4$ with observed (points), calculated (continuous line) and the difference $I_{\text{obs}} - I_{\text{calc}}$ (bottom line) data.

Table 4.1 Rietveld refined parameters of the Li_{0.10}RE_{0.10}Bi_{0.8}Mo_{0.2}V_{0.8}O₄ pigments

RE	La	Pr	Sm	Gd	Tb	Dy	Y	Yb	Lu
<i>a</i> (Å)	5.1626 (6)	5.1582 (8)	5.1526 (7)	5.1497 (7)	5.1497 (6)	5.1485 (6)	5.1501 (8)	5.1497 (7)	5.1505 (7)
<i>c</i> (Å)	11.6837 (1)	11.6564 (2)	11.6312 (2)	11.6170 (2)	11.6146 (2)	11.6092 (2)	11.6127 (2)	11.6128 (2)	11.6174 (2)
V(Å) ³	311.40	310.14	308.80	308.07	308.02	307.73	308.01	307.97	308.18
R-factors									
R _{exp} (%)	15.68	15.03	14.92	15.03	10.69	10.18	14.90	10.39	10.25
R _p (%)	12.78	13.43	12.09	11.02	9.37	9.41	12.63	10.72	11.14
R _{wp} (%)	16.94	17.67	16.07	14.87	12.61	12.65	17.18	15.04	15.49
R _{Bragg} (%)	5.93	7.95	4.95	3.76	3.97	4.41	5.48	5.70	6.45
χ ²	1.16	1.38	2.01	1.00	1.39	1.54	1.32	2.09	2.28
Oxygen position coordinates									
<i>x</i>	0.134 (2)	0.130 (2)	0.135 (2)	0.133 (2)	0.140 (2)	0.133 (2)	0.142 (2)	0.138 (2)	0.139 (2)
<i>y</i>	-0.034 (2)	-0.051 (2)	-0.020 (2)	-0.009 (2)	-0.005 (1)	-0.009 (2)	0.006 (2)	-0.016 (2)	-0.034 (2)
<i>z</i>	0.2111 (9)	0.217 (1)	0.2102 (9)	0.2102 (9)	0.2068 (7)	0.2114 (8)	0.2102 (9)	0.2110 (9)	0.2132 (9)

4.3.2 Morphological and Micro chemical Studies

The SEM micrographs obtained are shown in Fig.4.3. The particles are agglomerated, to some extent. SEM analysis shows that the morphology is irregular and the average size of samples are about 4-7 μm. Compared to BiVO₄, there is a marked difference in particle size. There is a slight variation in particle size upon rare earth variation.

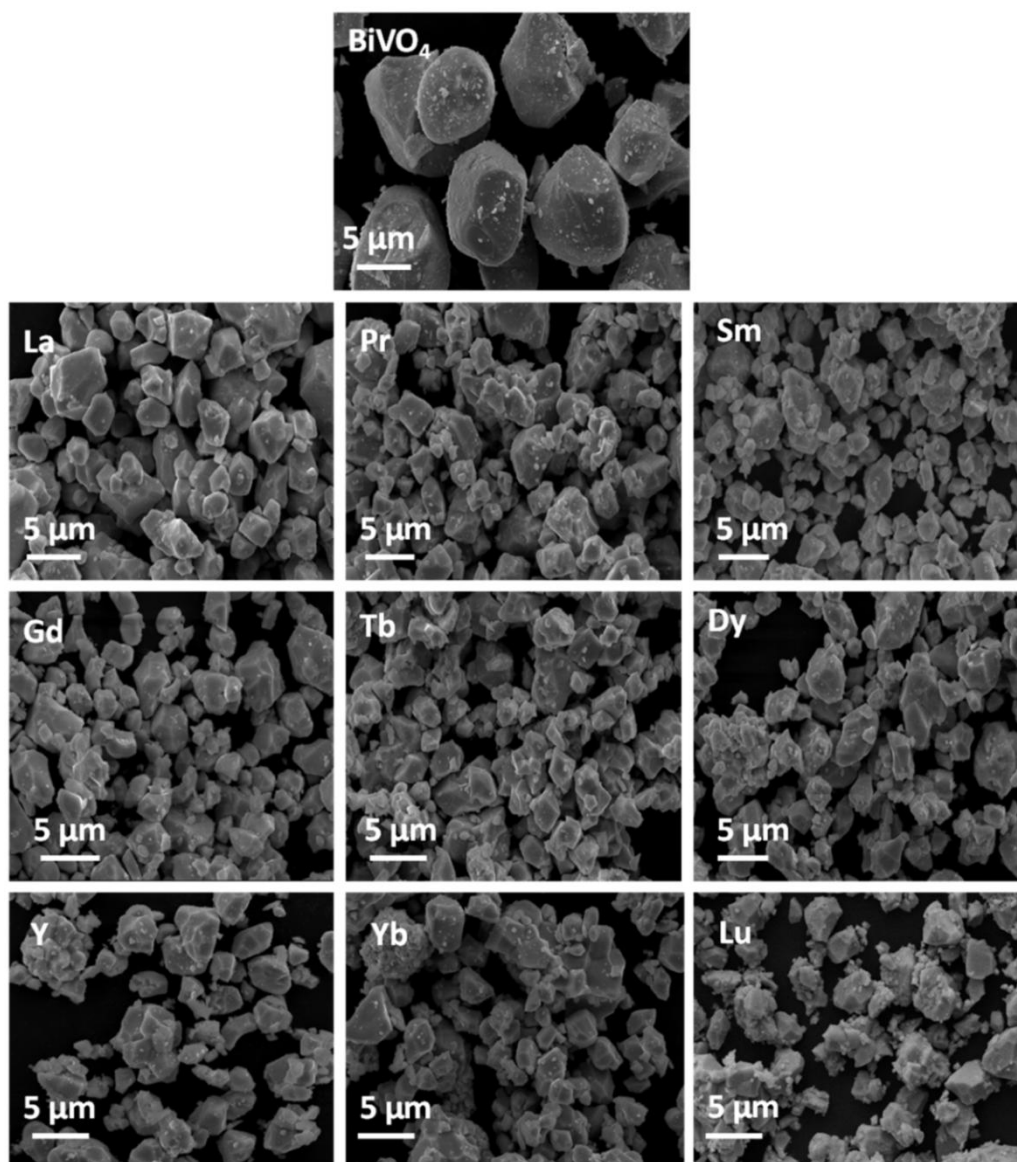


Fig.4.3 SEM micrographs of $\text{Li}_{0.10}\text{RE}_{0.10}\text{Bi}_{0.8}\text{Mo}_{0.2}\text{V}_{0.8}\text{O}_4$ pigments.

The EDS was used to determinate the chemical composition of the as-obtained pigments. The EDS spectrum (Fig.4.4) of the $\text{Li}_{0.10}\text{Gd}_{0.10}\text{Bi}_{0.8}\text{Mo}_{0.2}\text{V}_{0.8}\text{O}_4$ sample shows the presence of Bi, V, Gd, Mo and O elements, with close approximation to the calculated value. The Li element is not detected due to going beyond the detection range of the instrument. X- ray mapping analysis also reveals that the elements are uniformly distributed within the matrix. The results confirm solid solution formation between $(\text{LiRE})_{1/2}\text{MoO}_4$ and BiVO_4 , leading to a $\text{Li}_{0.10}\text{RE}_{0.10}\text{Bi}_{0.8}\text{Mo}_{0.2}\text{V}_{0.8}\text{O}_4$ pigment system, agreeing with the XRD analysis above. SEM EDS analysis confirms the close agreement between the stoichiometric and the actual composition.

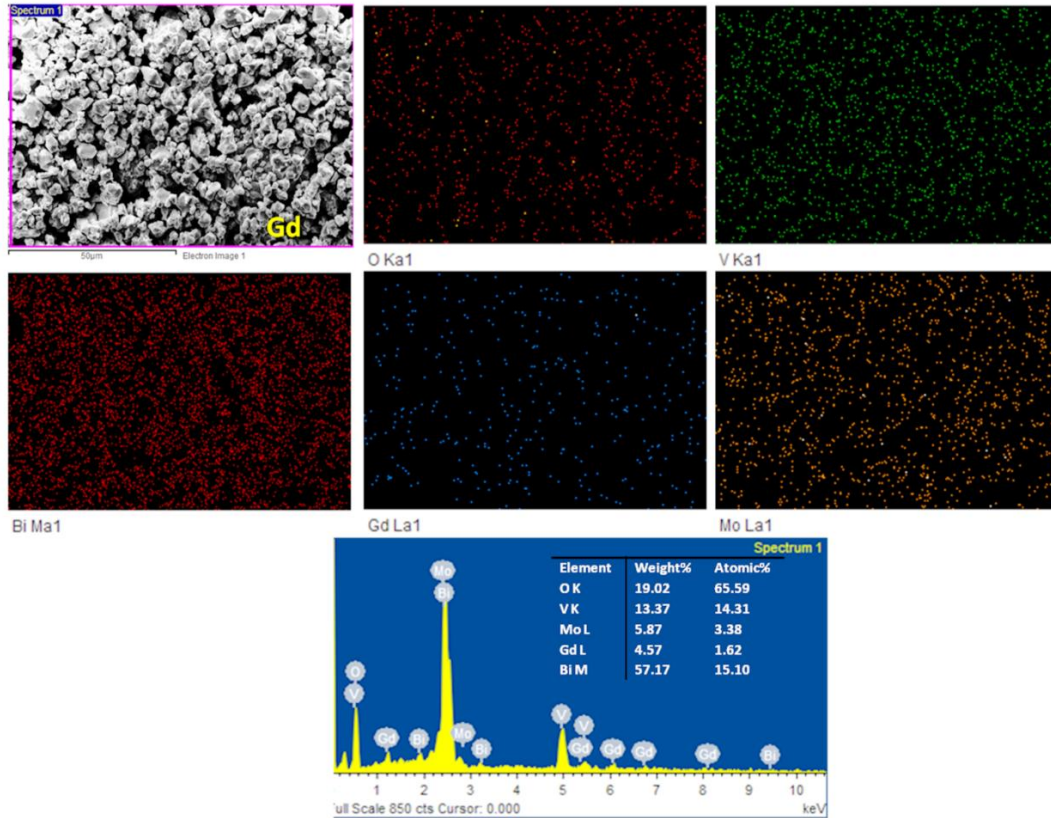


Fig.4.4 X-ray dot mapping and EDS analysis of $\text{Li}_{0.10}\text{Gd}_{0.10}\text{Bi}_{0.8}\text{Mo}_{0.2}\text{V}_{0.8}\text{O}_4$ pigment.

4.3.3 UV-Visible Studies

Fig.4.5 shows the reflectance spectra of $\text{Li}_{0.10}\text{RE}_{0.10}\text{Bi}_{0.8}\text{Mo}_{0.2}\text{V}_{0.8}\text{O}_4$ pigments. UV visible spectra exhibit shift in absorption edge with respect to different rare earths. Visible light absorption in BiVO_4 is due to the excitation of electrons from VB consisting of Bi 6s and O 2p to CB of V 3d orbitals of VO_4^{3-} . As a crystalline semiconductor, the optical absorption near the band edge observes the formula²³ $\alpha h\nu = A (h\nu - E_g)^{n/2}$ where α , ν , E_g and A are absorption coefficient, light frequency, band gap and a constant, respectively. Among them, n depends on the characteristics of the transition in a semiconductor, i.e. direct transition ($n = 1$) or indirect transition ($n = 4$). For BiVO_4 , the value of n is 1.²⁴ The band gap energy (E_g value) of BiVO_4 can thus be calculated from Tauc plot which is $(\alpha h\nu)^2$ versus photon energy ($h\nu$). The intercept of the tangent to the x-axis will give a good estimation of the band gap energy for the pigments. The band gap energy for the pigments is given in Table 4. 2. There is an increase of band gap compared to BiVO_4 . This means that the empty 3d orbital of V^{5+} in solid solution is incorporated by extra energy levels. With the incorporation of alkali rare earth double molybdates, there is a shift of spectra toward shorter wavelength.

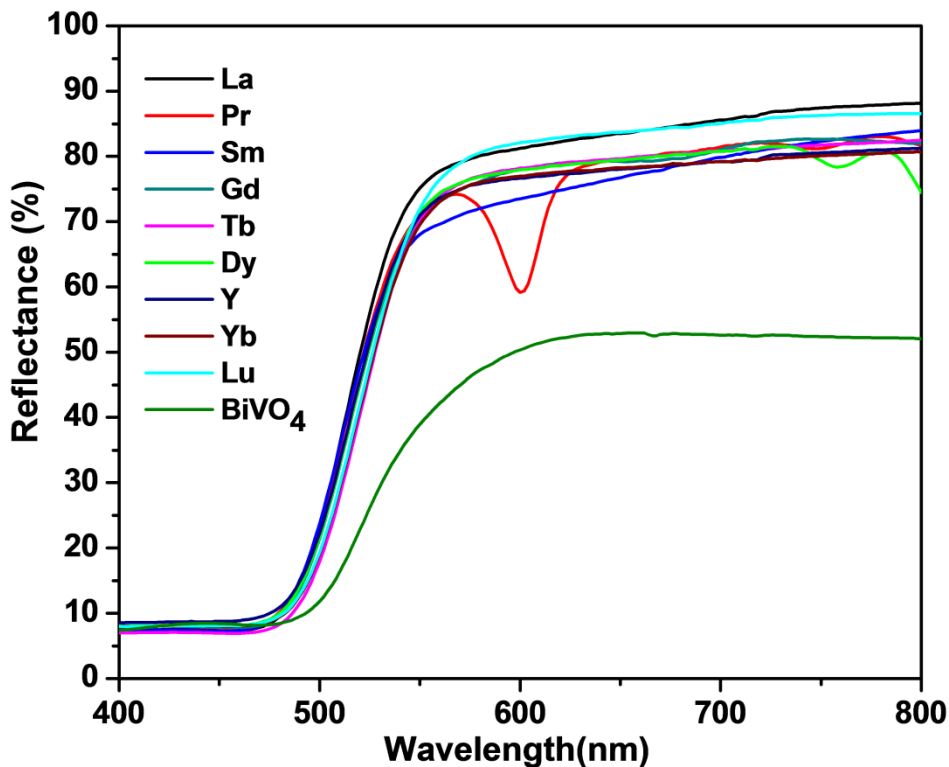


Fig.4.5 Reflectance spectra of $\text{Li}_{0.10}\text{RE}_{0.10}\text{Bi}_{0.8}\text{Mo}_{0.2}\text{V}_{0.8}\text{O}_4$ pigments.

4.3.4 Band gap Analysis

The optical band gap variation of rare earth sesquioxides has been studied by Prokofiev *et al.* who has stated that the occupied 4f band in rare earth sesquioxides lies above the O 2p level, and hence the 4f-d transition determines band gap.²⁵ In the case of La, there is absence of f electrons and the inclusion of Mo 4d and La 5d orbitals above the V 3d orbitals results in widening of conduction band. This leads to reduced interaction between O 2p and V 3d orbitals. It might be suggested that such partial occupation of V 3d orbital is originated from the hybridization between Mo 4d, La 5d and V 3d orbitals. This in turn increases the band gap to 2.51 eV. The variation of E_g can be explained by the energy of the RE 4f levels lowering in energy with an increasing occupation of 4f electrons. The occupied 4f band in Pr oxide lies above the O 2p band, and thus, 4f-5d transition may determine the band-gap energy. The 4f electronic level gradually becomes lowered with an increase of their atomic number, finally lying in the valence band, which results in an increase of band gap energy from Pr to Sm. The high stability of the half- and fully-filled 4f shells causes the position of the 4f orbital of Gd and Lu oxides to locate deep in the valence band causing the high band gap values. As soon as the f-band enters into the 2p band the E_g values

gradually increase. The presence of Y 4d level changes the band structure by modifying the conduction band with Mo 4d above the V 3d orbital and the band gap calculated is 2.44 eV.

Fig. 4.6 shows the schematic representation of the band structures of BiVO_4 and $\text{Li}_{0.10}\text{RE}_{0.10}\text{Bi}_{0.8}\text{Mo}_{0.2}\text{V}_{0.8}\text{O}_4$ pigments. Zhou *et al.* studied the role of rare earths in Bi_2RNbO_7 where the position of the 4f band of the rare earth ion in Bi_2RNbO_7 determined the band gap.²⁶ The importance of partially filled 4f shell in layered perovskite tantalates has been reported by Machida *et al.*²⁷ Considering the presence of zircon type rare earth vanadates, from Tb onwards a slight modification in band structure is expected. The zircon structure and tetragonal crystal structure consist of isolated VO_4 tetrahedra and AO_8 dodecahedra. A study by Panchal *et al.* reveals that most of the features of the band structure in scheelite are qualitatively similar to the ones in the zircon structure.²⁸ This difference in RE 4f levels and the corresponding difference in the band gaps lead to different colors.

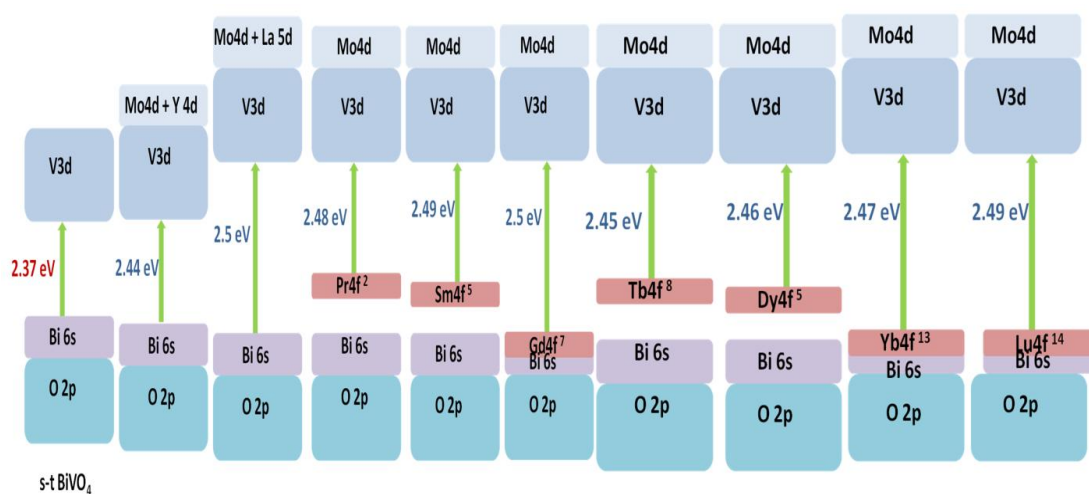


Fig. 4.6 Schematic band structure diagrams of BiVO_4 and $\text{Li}_{0.10}\text{RE}_{0.10}\text{Bi}_{0.8}\text{Mo}_{0.2}\text{V}_{0.8}\text{O}_4$ pigments.

4.3.5 Color Analysis

Table 4.2 displays the CIE 1976 color coordinates of the $\text{Li}_{0.10}\text{RE}_{0.10}\text{Bi}_{0.8}\text{Mo}_{0.2}\text{V}_{0.8}\text{O}_4$ pigments. Incorporation of various alkali rare earth double molybdates into BiVO_4 enhances the yellow component (b^* from 52.57 to 81.86). The chroma (C^*) range from 75.53 to 82.08 and hue angle (h°) values from 82.18 to 92.33. The hue angles (h°) of the samples imply the intense yellow color of

the developed pigments ($h^\circ=70-105^\circ$ for yellow). Fig.4.7 presents the comparison of color coordinates (C^*) and (h°) of samples indicating the enhancement in yellow hue comparable to commercial sicopal yellow L1100¹³ as well as molybdenum doped cerium gadolinium oxide.²⁹

The absorption edge varies with various RE accompanying with the changes of the width or the position of the valence bands and conduction bands, which may be one of the reasons for the widening of the optical gap. As a result, the chromaticity of the pigments depends on the identity of the rare earth element (Fig.4.8). La incorporation gives the highest b^* value of 81.86.

Table 4.2 CIE color coordinates and band gap of $\text{Li}_{0.10}\text{RE}_{0.10}\text{Bi}_{0.8}\text{Mo}_{0.2}\text{V}_{0.8}\text{O}_4$ pigments

RE	L^*	a^*	b^*	C^*	h°	Eg (eV)
La	83.30	6.04	81.86	82.08	85.77	2.50
Pr	80.39	2.08	75.50	75.53	88.41	2.48
Sm	80.47	4.63	77.06	77.19	86.55	2.45
Gd	81.44	5.51	79.94	80.13	86.05	2.43
Tb	80.70	9.99	80.35	80.97	82.90	2.46
Dy	81.33	-3.15	77.88	77.95	92.33	2.45
Y	81.57	7.26	77.34	77.68	84.63	2.44
Yb	80.59	9.13	76.49	77.04	83.18	2.45
Lu	82.05	10.8	78.72	79.46	82.18	2.46
BiVO₄	65.79	14.29	52.57	54.47	74.78	2.37
Sicopal yellow¹²	94.4	-16.7	76.9	78.7	77.8	2.51

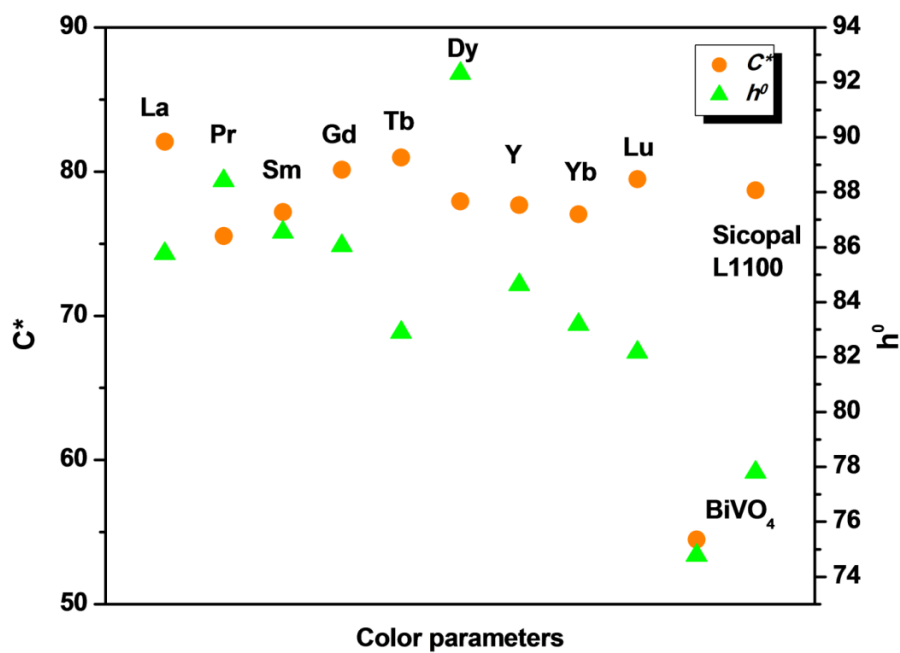


Fig. 4.7 Variation of color coordinates (C^*) and (h°) of $\text{Li}_{0.10}\text{RE}_{0.10}\text{Bi}_{0.8}\text{Mo}_{0.2}\text{V}_{0.8}\text{O}_4$ pigments with different rare earths.

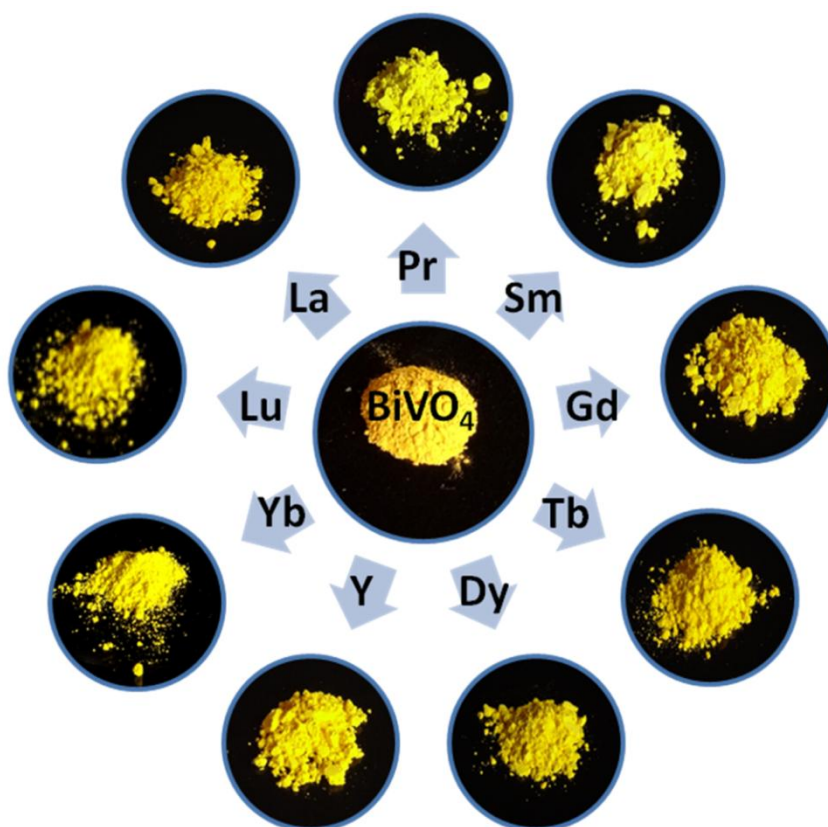


Fig. 4.8 Photographs of $\text{Li}_{0.10}\text{RE}_{0.10}\text{Bi}_{0.8}\text{Mo}_{0.2}\text{V}_{0.8}\text{O}_4$ pigments with different rare earths.

4.3.6 IR Reflectance Studies

The IR reflectance spectra of selected pigments are displayed in Fig. 4.9. NIR reflectance follows the order $\text{La} > \text{Lu} > \text{Gd} > \text{Pr} > \text{Tb} > \text{Y} > \text{Yb} > \text{Sm} > \text{Dy}$ in the 1100 nm range. Certain transitions in NIR region is observed for Pr, Sm, Dy and Yb. Therefore, these rare earths are not favorable for use as IR reflecting colorants. NIR reflectance obtained for RE = La, Lu, Gd, Tb and Y are 90, 88, 87, 86 and 84 % respectively. The highest NIR reflectance of 90 % was observed for La based pigment.

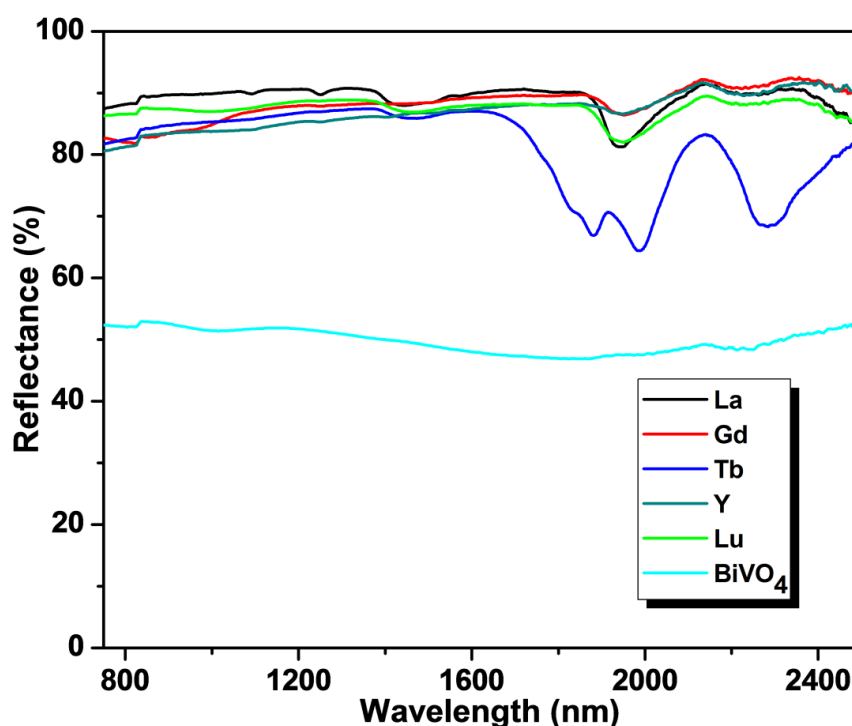


Fig. 4.9 IR reflectance spectra of $\text{Li}_{0.10}\text{RE}_{0.10}\text{Bi}_{0.8}\text{Mo}_{0.2}\text{V}_{0.8}\text{O}_4$ pigments with selected rare earths; RE = La, Gd, Tb, Y and Lu.

4.4 Conclusions

New ecological yellow pigments have been successfully prepared via a solid-state route by effective solid solution formation between BiVO_4 and various rare earths; (RE = La, Pr, Sm, Gd, Tb, Dy, Y, Yb and Lu) in $(\text{LiRE})_{1/2}\text{MoO}_4$, leading to $\text{Li}_{0.10}\text{RE}_{0.10}\text{Bi}_{0.8}\text{Mo}_{0.2}\text{V}_{0.8}\text{O}_4$ pigments. Interesting hues of yellow shades were obtained using different rare earths. Remarkable IR reflectance was observed for La, Lu, Gd, Tb and Y in $\text{Li}_{0.10}\text{RE}_{0.10}\text{Bi}_{0.8}\text{Mo}_{0.2}\text{V}_{0.8}\text{O}_4$ pigments. These pigments, as cool coatings, can lead to sustainability of roofs. Also, their use in automobiles will lead to energy saving coatings.

4.5 References

1. Santamouris, M.; Synnefa, A.; Karlessi, T., Using advanced cool materials in the urban built environment to mitigate heat islands and improve thermal comfort conditions. *Sol. Energy* **2011**, *85* (12), 3085-3102.
2. Levinson, R.; Berdahl, P.; Akbari, H., Solar spectral optical properties of pigments—Part II: survey of common colorants. *Sol. Energy Mater. Sol. Cells* **2005**, *89* (4), 351-389.
3. Buxbaum, G.; Pfaff, G., Eds.; Introduction. In *Industrial Inorganic Pigments*. WILEY-VCH Verlag GmbH & Co KGaA, Weinheim, **2005**.
4. Kudo, A.; Ueda, K.; Kato, H.; Mikami, I., Photocatalytic O₂ evolution under visible light irradiation on BiVO₄ in aqueous AgNO₃ solution. *Catal. Lett.* **1998**, *53* (3-4), 229-230.
5. Manolikas, C.; Amelinckx, S., Ferroelastic domains in BiVO₄. *Phys. Status Solidi A* **1980**, *60* (1), 167-172.
6. Valant, M.; Suvorov, D., Chemical compatibility between silver electrodes and low-firing binary-oxide compounds: Conceptual study. *J. Am. Ceram. Soc.* **2000**, *83* (11), 2721-2729.
7. Hoffart, L.; Heider, U.; Huggins, R. A.; Witschel, W.; Jooss, R.; Lentz, A., Crystal growth and conductivity investigations on BiVO₄ single crystals. *Ionics* **1996**, *2* (1), 34-38.
8. Sun, Y.; Wu, C.; Long, R.; Cui, Y.; Zhang, S.; Xie, Y., Synthetic loosely packed monoclinic BiVO₄ nanoellipsoids with novel multiresponses to visible light, trace gas and temperature. *Chem. Commun.* **2009**, (30), 4542-4544.
9. Xi, G.; Ye, J., Synthesis of bismuth vanadate nanoplates with exposed {001} facets and enhanced visible-light photocatalytic properties. *Chem. Commun.* **2010**, *46* (11), 1893-1895.
10. Endriss, H., Bismuth Vanadates. In *High Performance Pigments*, Wiley-VCH Verlag GmbH & Co. KGaA: **2009**.
11. Wendusu; Ikawa, K.-i.; Masui, T.; Imanaka, N., Novel environment-friendly yellow pigments based on (Bi, La)VO₄. *Chem. Lett.* **2011**, *40* (8), 792-794.
12. Masui, T.; Honda, T.; Wendusu; Imanaka, N., Novel and environmentally friendly (Bi,Ca,Zn)VO₄ yellow pigments. *Dyes Pigm.* **2013**, *99* (3), 636-641.

13. Wendusu; Honda, T.; Masui, T.; Imanaka, N., Novel environmentally friendly (Bi, Ca, Zn, La)VO₄ inorganic yellow pigments. *RSC Adv.* **2013**, *3* (47), 24941-24945.
14. Sandhya Kumari, L.; Prabhakar Rao, P.; Narayana Pillai Radhakrishnan, A.; James, V.; Sameera, S.; Koshy, P., Brilliant yellow color and enhanced NIR reflectance of monoclinic BiVO₄ through distortion in VO₄³⁻ tetrahedra. *Sol. Energy Mater. Sol. Cells.* **2013**, *112*, 134-143.
15. Strobel, R.; Metz, H. J.; Pratsinis, S. E., Brilliant yellow, transparent pure, and SiO₂-coated BiVO₄ nanoparticles made in flames. *Chem. Mater.* **2008**, *20* (20), 6346-6351.
16. Maier, A. A.; Provotorov, M. V.; Balashov, V. A., Double molybdates and tungstates of the rare earth and alkali metals. *Russ. Chem. Rev.* **1973**, *42* (10), 822.
17. Kato, A.; Oishi, S.; Shishido, T.; Yamazaki, M.; Iida, S., Evaluation of stoichiometric rare-earth molybdate and tungstate compounds as laser materials. *J. Phys. Chem. Solids* **2005**, *66* (11), 2079-2081.
18. Chimitova, O. D.; Atuchin, V. V.; Bazarov, B. G.; Molokeevev, M. S.; Bazarova, Z. G. In The formation and structural parameters of new double molybdates RbLn(MoO₄)₂ (Ln = Pr, Nd, Sm, Eu), *Proc. SPIE.* 8771, Metamaterials VIII, 87711A, May 6, **2013**; 87711A-87711A-9.
19. Bhattacharya, A. K.; Mallick, K. K.; Hartridge, A., Phase transition in BiVO₄. *Mater. Lett.* **1997**, *30* (1), 7-13.
20. Liu, J.; Wang, H.; Wang, S.; Yan, H., Hydrothermal preparation of BiVO₄ powders. *Mater. Sci. Eng., B* **2003**, *104* (1-2), 36-39.
21. Bierlein, J. D.; Sleight, A. W., Ferroelasticity in BiVO₄. *Solid State Commun.* **1975**, *16* (1), 69-70.
22. Prabhakar Rao, P.; Reddy, M. L. P., Synthesis and characterisation of (BiRE)₂O₃ (RE: Y, Ce) pigments. *Dyes Pigm.* **2004**, *63* (2), 169-174.
23. Butler, M. A., Photoelectrolysis and physical properties of the semiconducting electrode WO₂. *J. Appl. Phys.* **1977**, *48* (5), 1914-1920.
24. Zhou, L.; Wang, W.; Liu, S.; Zhang, L.; Xu, H.; Zhu, W., A sonochemical route to visible-light-driven high-activity BiVO₄ photocatalyst. *J. Mol. Catal. A: Chem.* **2006**, *252* (1-2), 120-124.

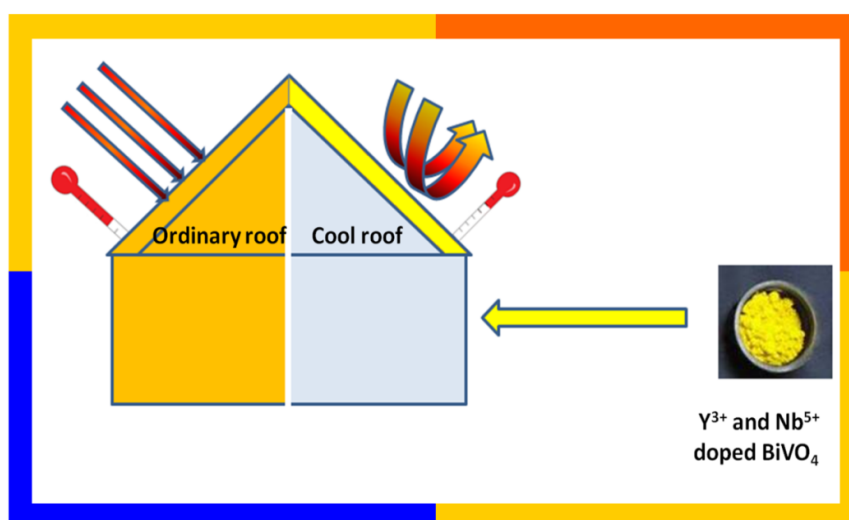
25. Prokofiev, A. V.; Shelykh, A. I.; Golubkov, A. V.; Smirnov, I. A., Crystal growth and optical properties of rare earth sesquiselenides and sesquisulphides - new magneto-optic materials. *J. Alloy Compd.* **1995**, *219* (1–2), 172-175.
26. Zou, Z.; Ye, J.; Arakawa, H., Role of R in Bi_2RNbO_7 (R = Y, Rare Earth): Effect on band structure and photocatalytic properties. *J. Phys. Chem. B* **2001**, *106* (3), 517-520.
27. Machida, M.; Yabunaka, J.-i.; Kijima, T., Efficient photocatalytic decomposition of water with the novel layered tantalate $\text{RbNdTa}_2\text{O}_7$. *Chem. Commun.* **1999**, (19), 1939-1940.
28. Panchal, V.; Errandonea, D.; Segura, A.; Rodríguez-Hernandez, P.; Muñoz, A.; Lopez-Moreno, S.; Bettinelli, M., The electronic structure of zircon-type orthovanadates: Effects of high-pressure and cation substitution. *J. Appl. Phys.* **2011**, *110* (4), 043723.
29. Radhika, S. P.; Sreeram, K. J.; Unni Nair, B., Mo-doped cerium gadolinium oxide as environmentally sustainable yellow pigments. *ACS Sustainable Chem. Eng.* **2014**, *2* (5), 1251-1256.

CHAPTER 5A

YELLOW PIGMENTS IN BiVO_4 - YNbO_4 SYSTEM

Overview

New yellow inorganic pigments, $(\text{BiV})_{1-x}(\text{YNb})_x\text{O}_4$ ($x = 0, 0.02, 0.04, 0.06, 0.08, 0.10$) exhibit brilliant yellow colors ($L^* = 80.34$, $a^* = 14.28$, $b^* = 75.46$) with significant enhancement of NIR reflectance to 91% when compared to undoped BiVO_4 at 1100 nm range.



5A.1 Introduction

Current research activities in the field of color industry is the search for new pigment systems with yellow hues that may substitute for those commercially available, which in most cases do not meet the environmental requirements currently. BiVO₄ pigments extend the familiar range of yellow inorganic pigments, e.g. iron yellow, chrome yellow, cadmium yellow, nickel titanium yellow, and chromium titanium yellow. So work has been focused on BiVO₄ which has attracted current attention as a non-toxic yellow pigment.¹ There are three crystalline phases reported for synthetic BiVO₄, zircon structure with tetragonal system (z-t) and scheelite structure with monoclinic (s-m) and tetragonal (s-t) systems.² However, BiVO₄ (s-m) is more distorted by a 6s² lone pair of Bi³⁺ and shows vivid yellow over that of BiVO₄ (s-t) exhibiting murky yellow.

In general, colors of solids appear brilliant and pure when the corresponding mechanism for a selective absorption of light is related to an electronic interband transition, leading to a steep absorption edge in the visible spectrum. The width of the band gap is determined by the extent of overlap of the valence orbitals, and by the difference between the electronegativities of the cations and anions involved.³ To raise the valence band level and hence reduce the band gap of metal oxides, three options remain open firstly anion substitution with less electronegative species producing lower binding energy anion p states and inclusion of nd⁰ and ns²/nd¹⁰ cations.⁴ The energies of valence and conduction band edges are often manipulated by making solid solutions between end members. Thus various color hues maybe produced by fine tuning of band gaps.⁵

Transition or rare earth metal doping of BiVO₄ has been investigated with respect to metal loading as in the case of Cu-BiVO₄⁶, Eu/BiVO₄⁷, or Y-substitution of BiVO₄ which leads to stabilization of the tetragonal phase in Bi_{1-x}Y_xVO₄ catalysts for glucose reforming.⁸ Substitution of Ta/P into V site in BiVO₄ led to enhanced NIR reflectance and color.⁹ Thus, the extension of the color palette with NIR reflectance functionality of BiVO₄ is a factor that will increase the commercial competitiveness of this pigment. However, the studies about the pigmentary properties of BiVO₄ are still inadequate, since most of the research concerning this system is focused on photocatalytic properties. Hence developing yellow colored high IR reflective inorganic pigments become an important issue. Thus further studies are still needed to

optimize the IR reflectance and color properties of BiVO₄ based yellow pigments, which could be an interesting alternative to the existing heavy metal based pigments. The effect of isovalent doping of Y³⁺ and Nb⁵⁺ on the BiVO₄ system to yield IR reflective yellow pigments is investigated in this part of the chapter. The crystal phase, microstructure and optical absorption property of (BiV)_{1-x}(YNb)_xO₄ based pigments is discussed here.

5A.2 Experimental Section

5A.2.1 Materials and Methods

Compositions based on the formula (BiV)_{1-x}(YNb)_xO₄ ($x = 0, 0.02, 0.04, 0.06, 0.08, 0.1$) were prepared by the traditional solid state reaction technique using Bi₂O₃, V₂O₅, Y₂O₃, Nb₂O₅ all 99.99% purity (Sigma-Aldrich). Stoichiometric mixtures of the starting materials were ground and mixed thoroughly in an agate mortar using acetone as the wetting medium. The powder was then dried in an air oven at 100°C. The well-mixed powders were calcined at 800 °C for 6 h. The calcination process was repeated three times with intermittent grinding to ensure the completion of the reaction and to improve the color properties.

5A.2.2 Characterizations

The crystal structure of the prepared samples were determined by the X-ray diffraction pattern in the 10 to 80° 2θ range using a Ni-filtered Cu Kα radiation ($\lambda = 1.54060 \text{ \AA}$) with a powder X-ray diffractometer (XRD) (Philips X'pert Pro). Morphological analysis of the powders was performed by means of a scanning electron microscope (SEM) (JEOL, JSM- 5600LV). Transmission electron microscopy (TEM) images of the samples were taken using a FEI Tecnai 30G² S-Twin microscope operated at 300kV. A small amount of finely powdered sample was dispersed in acetone medium by ultrasonication, drop cast on carbon-coated copper grids, and dried the excess acetone naturally. The particle size analysis of the samples was analysed in water medium with calgon as the dispersing agent using the Laser Scattering Particle Size Analyzer (CILAS 930 Liquid). The optical properties of the samples were examined on a UV–vis Spectrometer (Shimadzu UV–2450 Kyoto, Japan) in the 200–780 nm range using BaSO₄ as a reference. The band gap values were calculated from the corresponding absorbance spectra by straight forward

extrapolation method using the formula $E_g(\text{eV}) = hc/\lambda$ (where λ represents the wavelength in nm). The color properties of the samples were estimated in terms of CIE $L^*a^*b^*$ system as discussed in the previous chapters. The near-infrared reflectance of the samples was measured with a UV–vis–NIR spectrophotometer (Shimadzu, UV-3600) using poly-tetrafluoroethylene (PTFE) as a reference. Optical measurements were performed in the 700 to 2500 nm range.

5A.3 Results and Discussion

5A.3.1 X-Ray Diffraction Analysis

Powder XRD patterns of the samples are shown in Fig. 5A.1. Compositions with $x = 0.02$ and 0.04 crystallize in the monoclinic scheelite (s-m) phase with space group $I_{2/b}$ and the reflections can be well indexed according to the powder diffraction file 01-074-4893. For $x = 0.06$ onwards the compositions crystallize in the tetragonal scheelite (s-t) phase with space group $I4_{1/a}$ and the reflections can be indexed according to the powder diffraction file 01-074-4892. The difference in the XRD patterns between BiVO₄ (s-m) and BiVO₄ (s-t) can be judged by the existence of a peak at 15° and splitting of peaks at 18.5° , 35° , and 46° of 2θ .²

The basic structural unit of BiVO₄ is constructed by VO₄ tetrahedron and BiO₈ dodecahedron. The V site is surrounded by four oxygen atoms forming a VO₄ tetrahedron. The Bi site is surrounded by eight oxygen atoms forming a BiO₈ dodecahedron.¹⁰ The structural difference between the monoclinic and tetragonal scheelite forms lies in the arrangement of the transition metal tetrahedra. The tetragonal scheelite form consists of interlinked transition metal tetrahedra while they are isolated in the monoclinic form.¹¹

After the monophasic phase formation upto $x = 0.06$, Bi₄V₂O₁₁ minor phase appears. The ionic radii of Bi³⁺ in eight fold coordination is 0.117 nm and V⁵⁺ in four fold coordination is 0.035 nm and doping Y³⁺ (0.101 nm) into Bi³⁺ and Nb⁵⁺ (0.048 nm)¹² into V⁵⁺ will cause slight distortion in the VO₄ tetrahedron and BiO₈ dodecahedron of the lattice as obvious by difference in ionic radius. The lattice parameters of the (BiV)_{1-x}(YNb)_xO₄ samples are summarized in Table 5A1. The lattice volume of $x = 0.06$ crystallizing in tetragonal scheelite form is smaller than that of monoclinic BiVO₄ ($x = 0$) as seen in Table 5A.1. This indicates that some strain has been induced in the lattice leading to lattice distortion. It is observed that the slight

distortion of crystal structure in BiVO₄ enhances the optical properties as discussed in the later part of the section.¹⁰

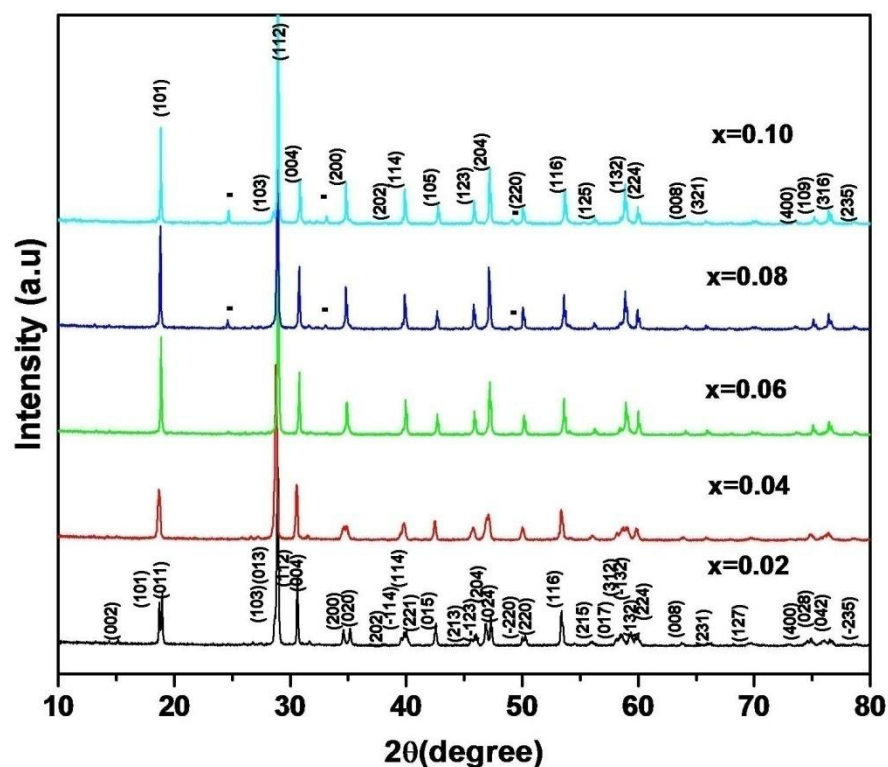


Fig. 5A.1 Powder X ray diffraction patterns of (BiV)_{1-x}(YNb)_xO₄ samples ($x = 0.02, 0.04, 0.06, 0.08, 0.10$).

Table 5A.1 Lattice parameters of (BiV)_{1-x}(YNb)_xO₄ samples ($x = 0, 0.02, 0.04, 0.06, 0.08, 0.10$)

Sample	a / (Å)	b / (Å)	c / (Å)	V / (Å) ³	Space group
$x = 0$	5.1980	5.1138	11.6877	310.67	I _{2/b}
$x = 0.02$	5.1951	5.1028	11.7000	310.16	I _{2/b}
$x = 0.04$	5.1811	5.1377	11.6561	310.27	I4 _{1/a}
$x = 0.06$	5.1582	-	11.6164	309.08	I4 _{1/a}
$x = 0.08$	5.1517	-	11.6112	308.16	I4 _{1/a}
$x = 0.10$	5.1432	-	11.6202	307.38	I4 _{1/a}

5A.3.2 Morphological and Micro chemical Studies

The SEM photographs show reduction in particle size with increase of substitution in Fig. 5A.2. The particle size decreases from 6-10 μm for undoped to 1-4 μm for $x = 0.10$. The particle size analysis also revealed a reduction in particle size from $x = 0$ with a mean diameter of 5.47 μm (size of 90% particles < 16.54 μm , 50% particles < 3.65 μm and 10% particles < 0.64 μm) to $x = 0.10$ with a mean diameter of 3.52 μm (size of 90% particles < 7.52 μm , 50% particles < 4.06 μm and 10% particles < 0.45 μm).

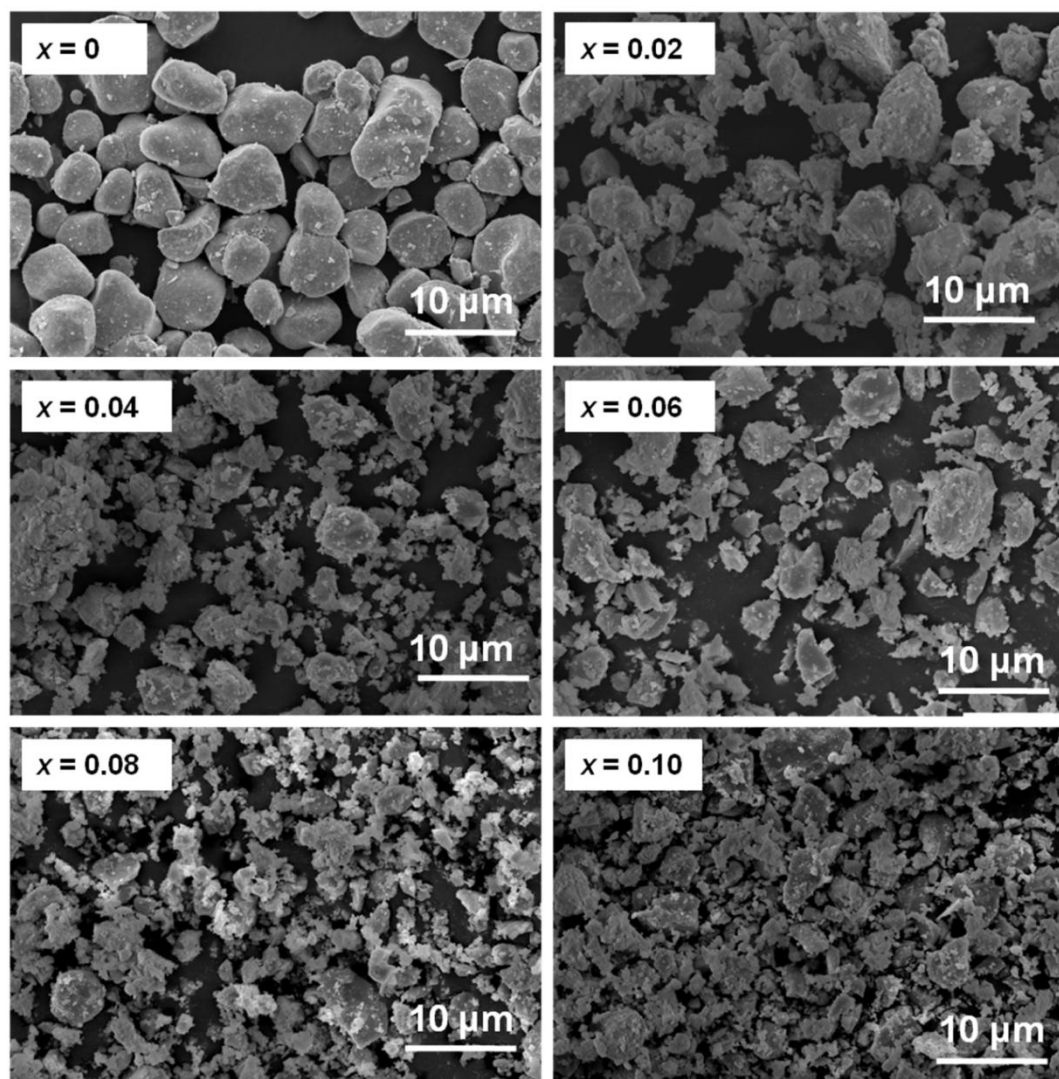


Fig. 5A.2 Typical SEM photographs of $(\text{BiV})_{1-x}(\text{YNb})_x\text{O}_4$ samples ($x = 0, 0.02, 0.04, 0.06, 0.08, 0.10$).

The elemental composition of (BiV)_{1-x}(YNb)_xO₄ samples ($x = 0.02, 0.04, 0.06, 0.08, 0.10$) pigments were checked by energy dispersive spectroscopy (EDS) analysis attached with TEM. Fig. 5A.3 show EDS analysis of selected sample (BiV)_{0.94}(YNb)_{0.06}O₄ pigment and identifies the presence of bismuth, niobium, yttrium, vanadium and oxygen in a ratio close to theoretical composition. The presence of copper and carbon impurities in the EDS spectrum is contributed by the TEM grid.

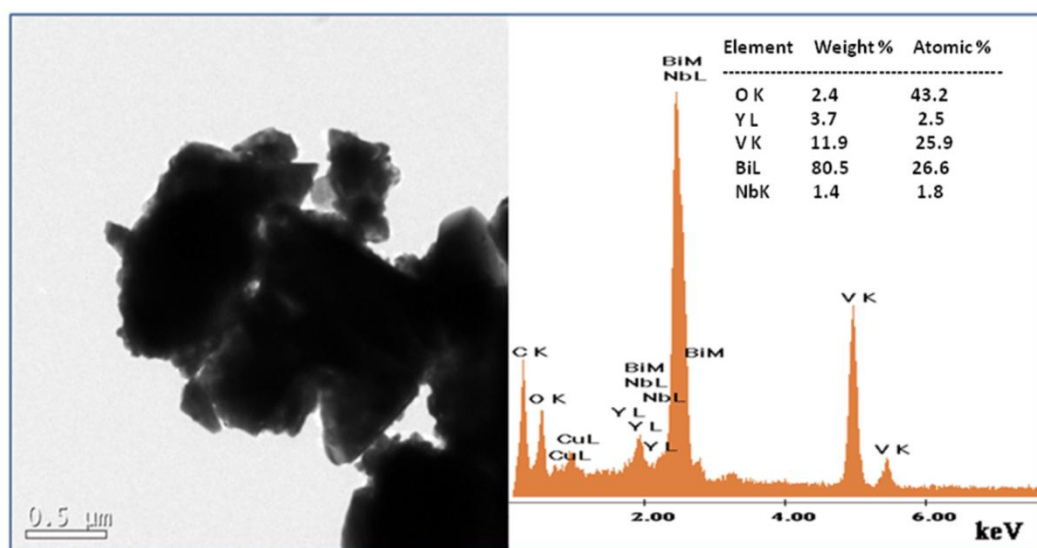


Fig. 5A.3 EDS analysis of (BiV)_{0.94}(YNb)_{0.06}O₄ pigment.

5A.3.3 UV visible Studies

The absorption spectra in UV-vis-NIR region of the samples are shown in Fig. 5A.4 and reflection spectra is shown in the inset. The samples absorb in the blue region and hence the complementary color yellow is observed. The absorption edge is seen to be very steep, indicating the electron transition from valence band to conduction band. The absorption edge of pure BiVO₄ prepared by solid state reaction gets blue shifted and the band gap changes from 2.29 to 2.36 eV on substitution of Y³⁺ and Nb⁵⁺. The band gap values were obtained by a straight forward extrapolation method and are given in Table 5A.2. The slight band gap differences observed between the samples may also be attributed to their differences in particle size. Generally the semiconductor with smaller particle size is expected to have a larger energy band gap.¹³

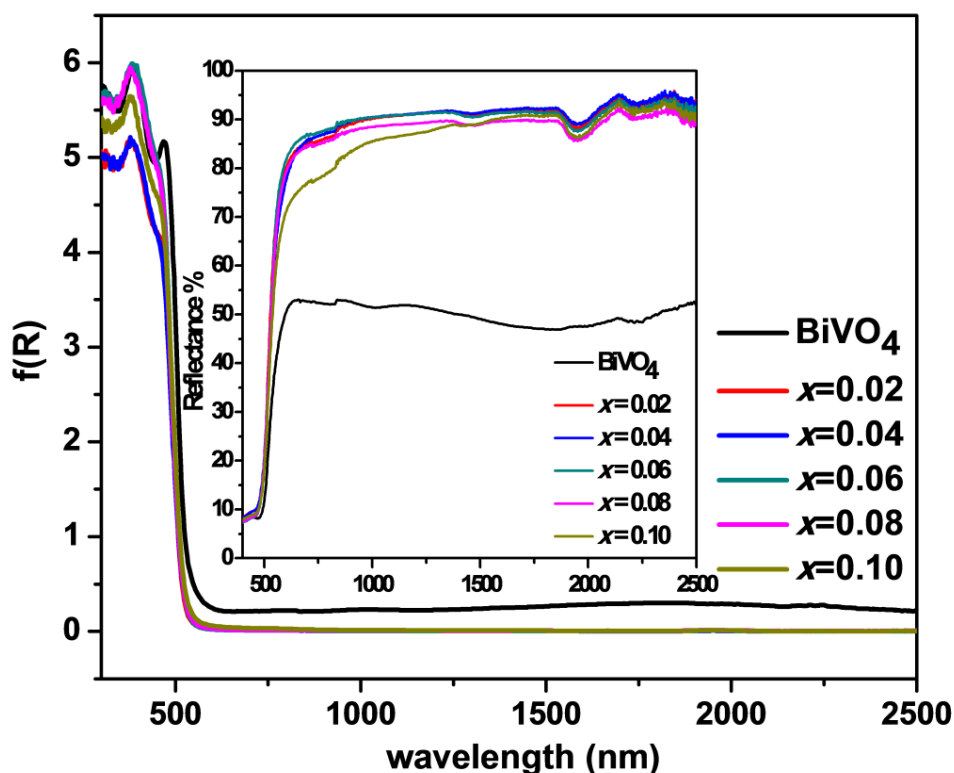


Fig. 5A.4 Absorption spectra of (BiV)_{1-x}(YNb)_xO₄ pigment powders ($x = 0, 0.02, 0.04, 0.06, 0.08, 0.10$) (reflection spectra shown in inset).

5A.3.4 Color Analysis

Among the prepared samples the most attractive color was obtained for $x = 0.06$ which is of pure tetragonal scheelite phase. The b^* value decreases on higher substitutions due to secondary phase. The observed hue angles of the developed pigments are found to be in the yellow region of the cylindrical color space ($h^\circ = 70\text{--}105$ for yellow).¹⁴

Table 5A.2 CIE L^* a^* b^* values and band gap of (BiV)_{1-x}(YNb)_xO₄ samples

Composition	L^*	a^*	b^*	C^*	h°	E_g (eV)
$x = 0$	65.79	14.29	52.57	54.47	74.78	2.29
$x = 0.02$	78.25	13.80	69.61	70.96	78.79	2.33
$x = 0.04$	79.86	12.66	73.09	74.18	80.17	2.34
$x = 0.06$	80.34	14.28	75.46	76.80	79.28	2.35
$x = 0.08$	79.34	13.92	73.36	74.67	79.26	2.36
$x = 0.10$	76.32	13.25	67.18	67.47	78.84	2.33

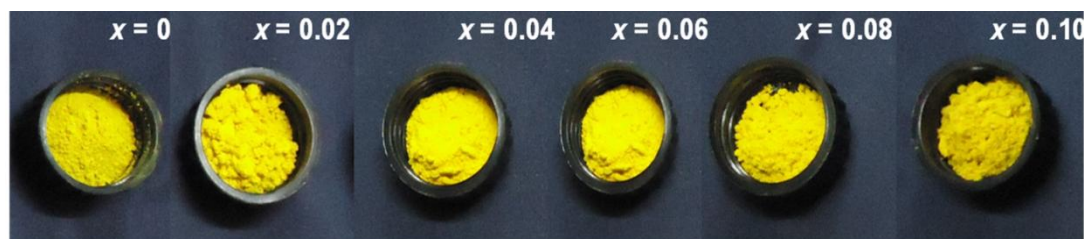


Fig. 5A.5 Photographs of (BiV)_{1-x}(YNb)_xO₄ pigment powders.

The photographs of the pigments are shown in Fig. 5A.5. The coloring mechanism of monoclinic BiVO₄ results from the charge transfer transition from the valence band of a hybrid orbital of Bi 6s and O 2p to the conduction band of V3d.¹⁵ By doping, the 4d levels of Y³⁺ and Nb⁵⁺ mix up with Bi 6p and V 3d. The addition of 4d levels may broaden the conduction band and a V3d interaction with O2p level is reduced. The inclusions of bigger 4d levels of Y³⁺ and Nb⁵⁺ have slightly increased the band gap. The increased band gap suggests the increase in width of conduction band made of positioning Nb 4d orbitals at a higher energy level than V 3d orbitals. The schematic band structure of bismuth vanadate and Y³⁺, Nb⁵⁺ substituted BiVO₄ is shown in Fig. 5A.6.

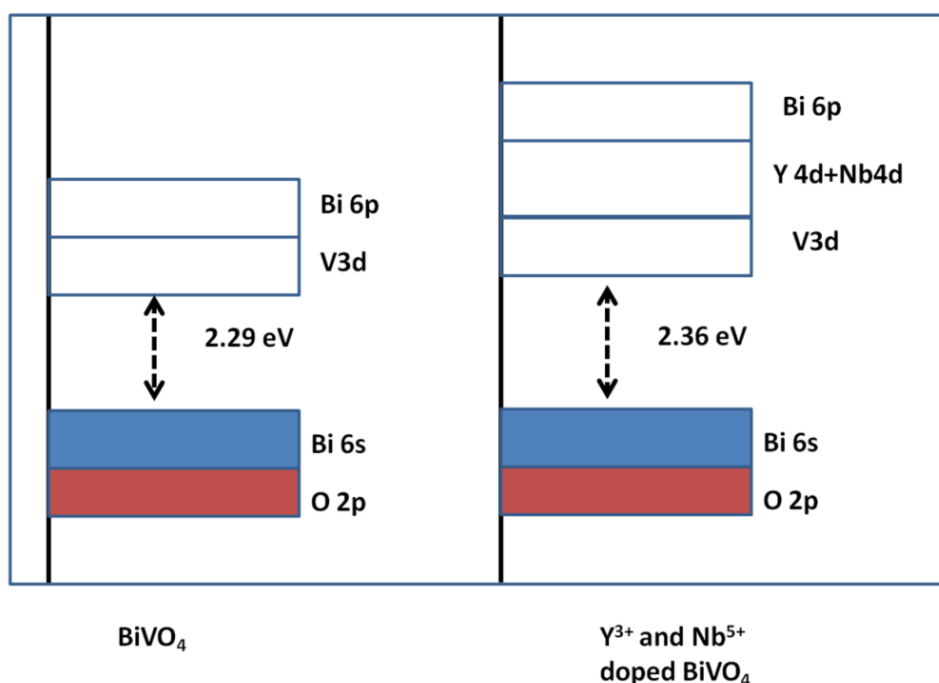


Fig. 5A.6 Schematic band structure of BiVO₄ and Y³⁺, Nb⁵⁺ substituted BiVO₄.

5A.3.5 IR Reflectance Studies

Doping of Y³⁺ and Nb⁵⁺ into BiVO₄ drastically enhances the NIR reflectance to 91%. For x greater than 0.06 a slight decrease in values up to 86 % is observed. The IR solar reflectance spectra determined in accordance with ASTM Standard E891-87 as described elsewhere¹⁶ of the yttrium and niobium doped BiVO₄ samples are given in Fig. 5A.7. The enhancement of the optical properties of BiVO₄ is mainly ascribed to the reduction in particle size and structural distortion in the lattice. In addition, the defects free formation in the substituted ones (absence of shallow absorption band in Fig. 5A.4) might have also contributed to the enhancement of the IR reflectance. The high IR reflectance displayed by all the newly obtained yellow-colored samples makes them interesting candidates for use as cool colorants.

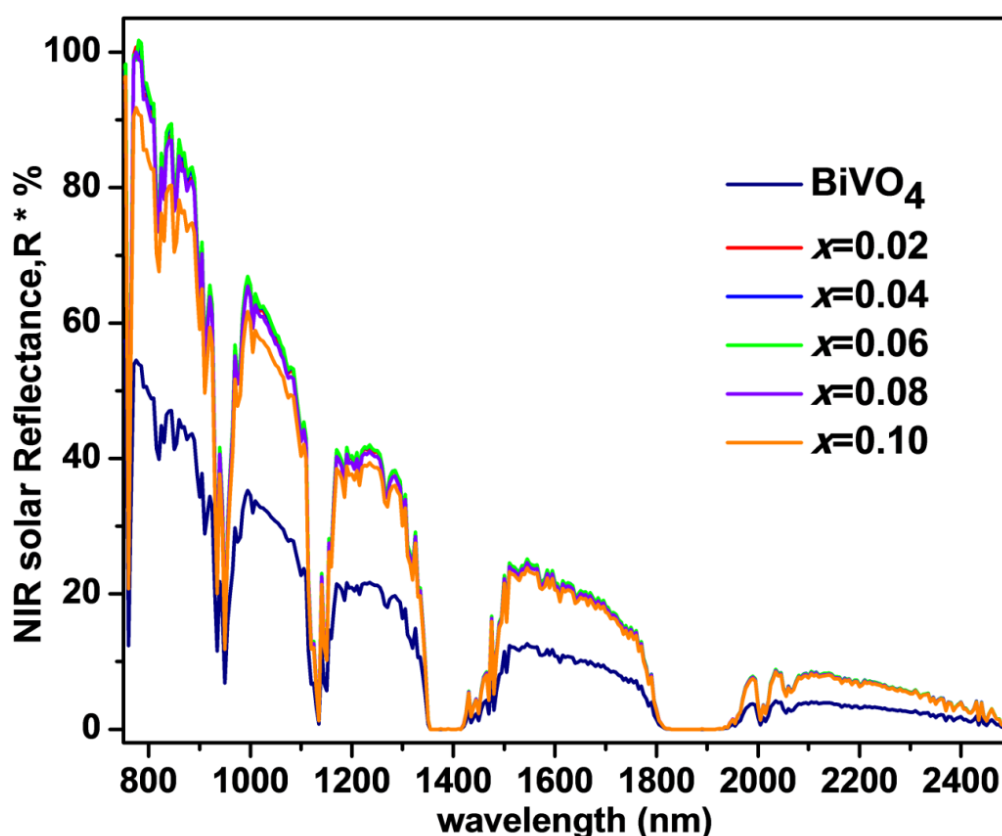


Fig. 5A.7 IR solar reflectance spectra of (BiV)_{1-x}(YNb)_xO₄ samples ($x = 0, 0.02, 0.04, 0.06, 0.08, 0.1$).

5A.4 Conclusions

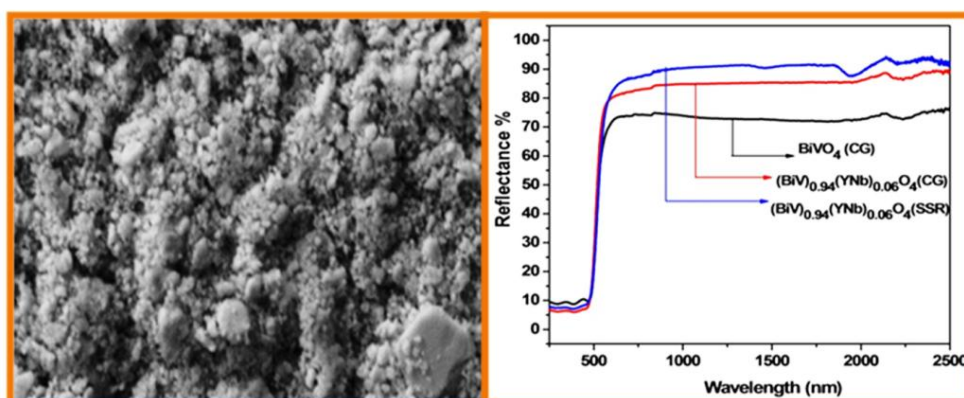
The incorporation of IR reflecting properties in pigments can lead to the cool roofing paint formulations. The results of solid solutions in the $(\text{BiV})_{1-x}(\text{YNb})_x\text{O}_4$ system demonstrate that the developed yellow pigments are interesting candidates as cool roof pigments. Tailoring these pigments for IR reflectance provides an easy passive energy-saving opportunity for exterior residential surfaces and automobiles.

CHAPTER 5B

YELLOW PIGMENT IN BiVO_4 - YNbO_4 SYSTEM BY CITRATE GEL METHOD

Overview

A nano yellow inorganic pigment, with high NIR reflectance of 85% is developed in $(\text{BiV})_{0.94}(\text{YNb})_{0.06}\text{O}_4$ solid solution.



5B.1 Introduction

The important physical–optical properties of pigments are their light absorption and scattering properties, which depend on the wavelength, particle size, particle shape and refractive index.¹⁷ While considering color performance, physical properties of a pigment such as morphology, particle size and shape, homogeneity etc are very important.¹⁸ The conventional solid state reaction route (SSR) uses powdered raw materials as the starting materials. This approach usually requires high temperatures and the aggregation and inhomogeneous shape are also unavoidable. Therefore, a simple and economical method for making high quality inorganic pigments is desirable. Doping, which forms the basis of most pigment applications can be readily achieved through soft chemical process and can tune the properties of particles as well as the size distribution.¹⁹ To achieve such better kind of physical properties and pigmentary properties the synthesis methods play a key role. Methods such as sol-gel, chemical co-precipitation, hydrothermal and colloid emulsion technique are some of the important chemical methods which usually do not require normal mixing, calcinations and grinding process. Among these wet chemical techniques, alkoxide sol-gel, hydrothermal and colloid emulsions are time consuming and involve the use of highly unstable alkoxides and difficult to maintain reaction conditions. The citrate gel process can avoid complex steps such as refluxing of alkoxides, resulting in less time consumption compared to other techniques.²⁰ Citrate gel (CG) method is one of the most important techniques for the synthesis of various functional materials because it offers many advantages over conventional solid state method in the synthesis of fine powders with higher uniformity in particle size distribution. This process involves complexation of metal ions by poly functional carboxyl acids, such as citric acid or tartaric acid having one hydroxyl group. On heating this mixture, the solvent (water) evaporates resulting in increased viscosity. On complete removal of water, the mixture is a polymeric gel and its constituents mixed at atomic level. This resin on heating at higher temperature produces the respective oxides.²¹ BiVO₄ is reported to have prepared by a citrate gel method with improved light absorption and photocatalytic properties.²²

In the present section, the preparation (BiV)_{0.94}(YNb)_{0.06}O₄ by a citric acid complexation process, is discussed. The aforementioned composition is selected as it displayed the best pigmentary properties among the solid state prepared samples seen

in the first section of the chapter. It can be found that a pigment with fine particles and homogeneity can be synthesized by citrate gel method.

5B.2 Experimental Section

5B.2.1 Materials and Methods

Typical compositions BiVO₄ and (BiV)_{0.94}(YNb)_{0.06}O₄ were synthesized by the citrate gel method (CG). Bi(NO₃)₃.5H₂O, NH₄VO₃, Y(NO₃)₃.6H₂O, NbCl₅ (Sigma-Aldrich, 99.9% purity) were used as starting materials. Distilled water and citric acid (Sigma-Aldrich, 99.9% purity) were used as solvent and chelating agent for the process. The citrate solution was prepared by dissolving appropriate amount of citric acid in distilled water. After complete homogenization of citrate solution, all the cationic solutions were dissolved in the citrate solution (1:2). The solution was kept for constant stirring for 1 h for homogenous mixing and concentrated by keeping it in the water bath (maintained at 100°C) for 12 h and the solution became viscous gel. The gel was dried to form a black product and then powdered by grinding in an agate mortar, which is the precursor. Then heat treatment of the precursor was carried out at 600°C for 4 h. The yellow powders obtained were used for further characterizations as described in first section of this chapter.

5B.2.2 Characterizations

The crystal structure of the prepared samples were determined by the X-ray diffraction pattern in the 10 to 80° 2θ range using a Ni-filtered Cu Kα radiation ($\lambda = 1.54060 \text{ \AA}$) with a powder X-ray diffractometer (XRD) (Philips X'pert Pro). Morphological analysis of the powders was performed by means of a scanning electron microscope (SEM) (JEOL, JSM- 5600LV). The quantitative microanalysis and elemental mapping of the samples was carried out by silicon drift detector X-MaxN attached with a Carl Zeiss EVO SEM apparatus. The particle size analysis of the samples was analysed in water medium with calgon as the dispersing agent using the Laser Scattering Particle Size Analyzer (CILAS 930 Liquid). The optical properties of the samples were examined on a UV-vis-NIR Spectrometer (Shimadzu, UV-3600) using BaSO₄ as a reference. The band gap values were calculated from the corresponding absorbance spectra by straight forward extrapolation method using the formula $E(\text{eV}) = hc/\lambda$ (where λ represents the wavelength in nm). The color properties

of the samples were estimated in terms of CIE $L^*a^*b^*$ system. The near-infrared reflectance of the samples was measured with a UV–vis–NIR spectrophotometer (Shimadzu, UV-3600) using poly-tetrafluoroethylene (PTFE) as a reference. Optical measurements were performed in the 700 to 2500 nm range.

5B.3 Results and Discussion

5B.3.1 X-Ray Diffraction Analysis

Powder XRD patterns of the samples are shown in Fig. 5B.1. Sharp peaks in the X-ray diffraction pattern indicate the crystalline nature of the samples prepared by CG route. There are no traces of extra peaks from impurities in the pattern. The reflections can be well indexed according to the powder diffraction file 01-074-4893. It is observed that phase formation of samples takes place at 600°C, which is a lower calcination temperature compared to that of the samples prepared by SSR route. The diffraction peaks of the sample prepared by CG method are broader than that prepared by SSR route, which hints the reduction of average crystallite size of the pigments.

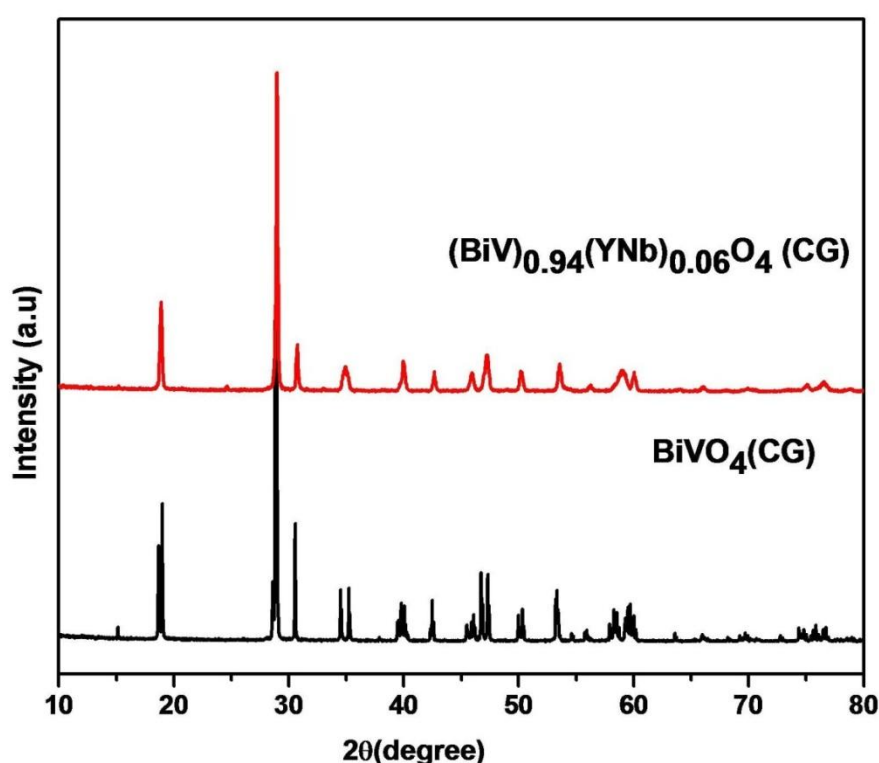


Fig. 5B.1 Powder X ray diffraction patterns of $(\text{BiV})_{1-x}(\text{YNb})_x\text{O}_4$ samples ($x = 0, 0.06$) prepared by CG route.

The lattice volumes of samples prepared by citrate gel route are smaller than those prepared by solid state route. Replacing some of the Bi and V cations with other cations imposes lattice strain or distortion in the lattice, which affects the color of the BiVO₄ as seen in later part of the section. Here in (BiV)_{0.94}(YNb)_{0.06}O₄ crystallizing in tetragonal scheelite form, the lattice volume is smaller than that of monoclinic BiVO₄ ($x = 0$) as seen in Table 5B.1. It indicates that some strain has been induced in the lattice leading to lattice distortion.

Table 5B.1 Lattice parameters of (BiV)_{1-x}(YNb)_xO₄ samples ($x = 0, 0.06$)

Sample	a / (Å)	b / (Å)	c / (Å)	V / (Å) ³	Space group
$x = 0$	5.1917	5.0899	11.6991	309.14	I _{2/b}
$x = 0.06$	5.1457	-	11.6232	307.76	I4 _{1/a}

5B.3.2 Morphological and Micro chemical Studies

The scanning electron micrographs of BiVO₄ and (BiV)_{0.94}(YNb)_{0.06}O₄ synthesized via CG route is presented in Fig. 5B.2. For both samples, particles are less agglomerated and the particle size is reduced compared to solid state route (SSR). Particles have uniform size and shape compared to the morphology of SSR samples. Moreover the particles are relatively spherically shaped and have smooth edges.

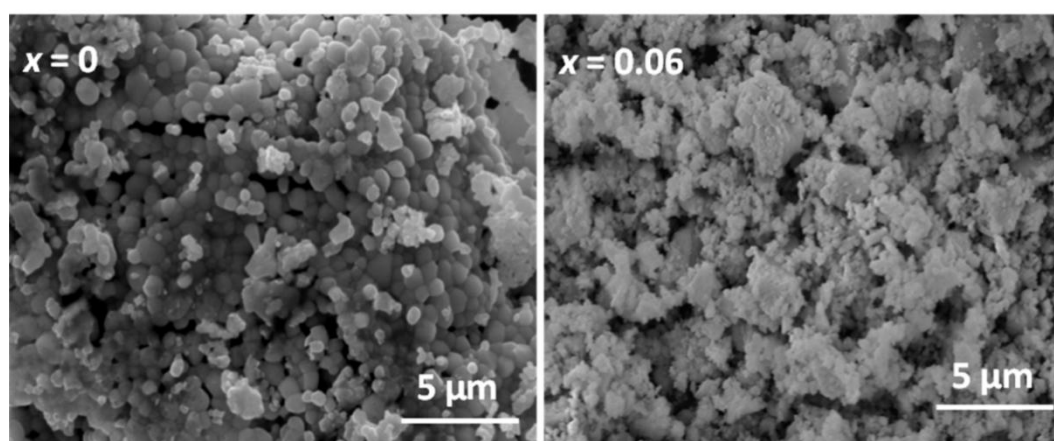
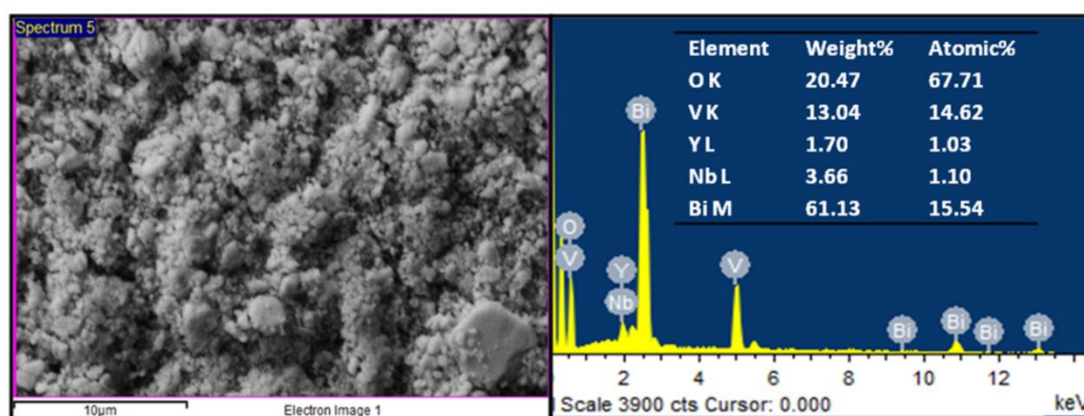


Fig. 5B.2 Typical SEM photographs of (BiV)_{1-x}(YNb)_xO₄ samples ($x = 0, 0.06$) prepared by CG route

The particle size analysis also revealed a reduction in particle size from $x = 0$ with a mean diameter of $2.20 \mu\text{m}$ (size of 90% particles $< 2.90 \mu\text{m}$, 50% particles $< 2.27 \mu\text{m}$ and 10% particles $< 1.53 \mu\text{m}$) to $x = 0.06$ with a mean diameter of $0.88 \mu\text{m}$ (size of 90% particles $< 1.51 \mu\text{m}$, 50% particles $< 1.09 \mu\text{m}$ and 10% particles $< 0.15 \mu\text{m}$).

EDS analysis of samples confirm that the samples are composed of Bi, V, Y, Nb and O in the appropriate ratio (Fig. 5B.3).

Fig. 5B.3 EDS analysis of $(\text{BiV})_{0.94}(\text{YNb})_{0.06}\text{O}_4$ ($x = 0.2, 0.8$).



5B.3.3 UV Visible studies

For a comparison reflectance spectra of typical samples BiVO_4 and $(\text{BiV})_{0.94}(\text{YNb})_{0.06}\text{O}_4$ prepared by CG route and SSR route is shown in Fig. 5B.4. The band gap values were obtained by a straight forward extrapolation method. From Fig. 5B.5, it is seen that the absorbance of $(\text{BiV})_{0.94}(\text{YNb})_{0.06}\text{O}_4$ prepared by CG route gets blue shifted and band gap gets increased from 2.33 to 2.42.

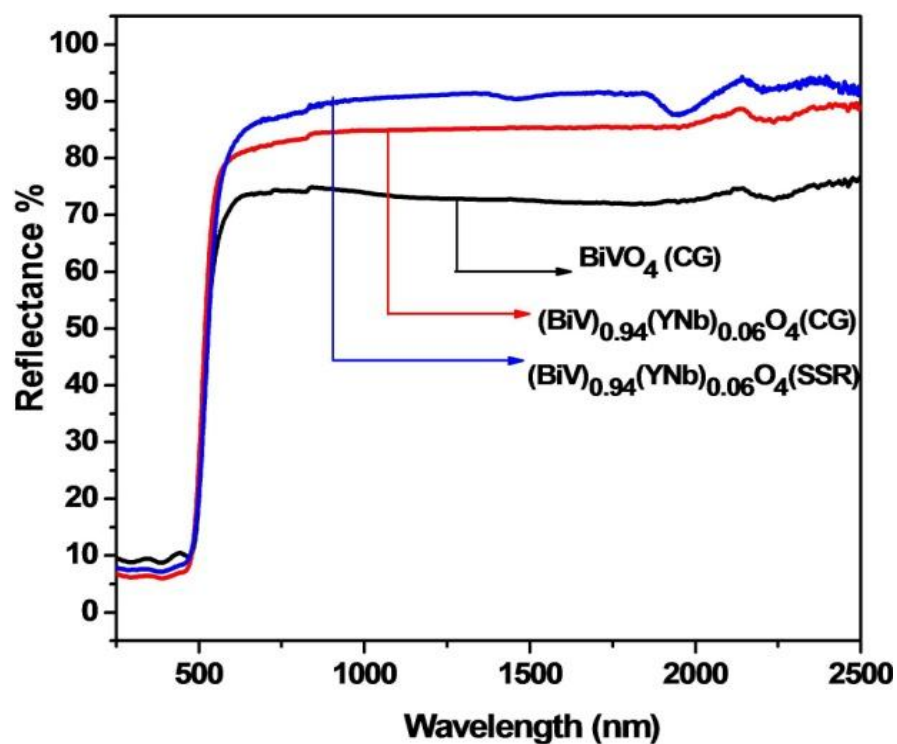


Fig. 5B.4 Reflectance spectra of BiVO_4 (CG), $(\text{BiV})_{0.94}(\text{YNb})_{0.06}\text{O}_4$ (CG,SSR)

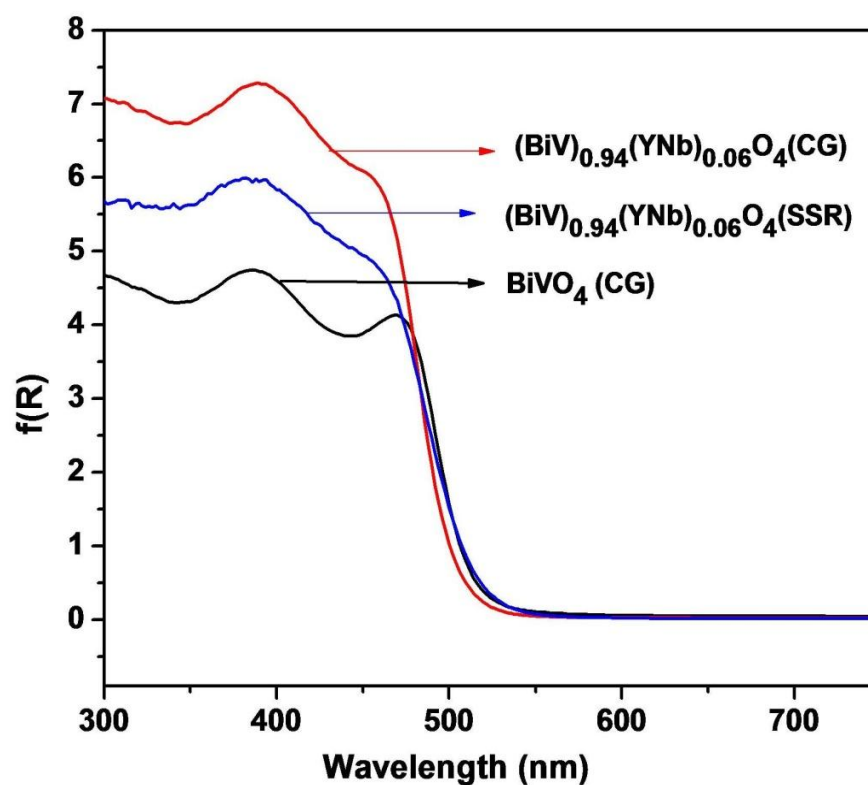


Fig. 5B.5 Absorbance spectra of BiVO_4 (CG), $(\text{BiV})_{0.94}(\text{YNb})_{0.06}\text{O}_4$ (CG,SSR)

5B.3.4 Color Analysis

Table 5B.2 lists the $L^*a^*b^*$ color coordinate data and band gap energies of the pigment compared with SSR prepared one as well as the commercial pigments. It can be seen that the b^* , chroma and hue value increases considerably for (BiV)_{0.94}(YNb)_{0.06}O₄ prepared by CG route. The pigments obtained are reddish yellow in hue while the commercial BiVO₄ marketed as Sicopal Yellow L1100 and praseodymium yellow are greenish yellow in hue. The b^* value of the obtained pigment is higher than the aforementioned samples. This suggests that bright yellow pigments can be synthesized by doping other cations into BiVO₄ as well as employing chemical methods.

Table 5B.2 CIE $L^* a^* b^*$ values and band gap of (BiV)_{1-x}(YNb)_xO₄ samples (CG route)

Composition	L^*	a^*	b^*	C^*	h^0	Eg (eV)
$x = 0$	65.79	14.29	52.57	54.47	74.78	2.29
$x = 0.06$	80.34	14.28	75.46	76.80	79.28	2.35
$x = 0$ (CG)	78.68	8.09	67.34	67.82	83.14	2.33
$x = 0.06$ (CG)	83.15	4.36	81.71	81.82	86.93	2.42
Pr yellow ²³	83.5	-3.28	70.3	-	-	2.43
Sicopal yellow ²⁴	94.40	-16.7	76.9	78.7	77.8	2.51

5B.3.5 IR Reflectance Studies

The NIR reflectance of citrate gel prepared samples is lower (85%) than that of solid state prepared samples (91%) as seen in Fig.5B.4. This may be due to low reflectivity of the of CG route samples due to the smooth texture of the samples. Still, the IR reflectance is high enough to be considered for cool colorants.

5B.4 Conclusions

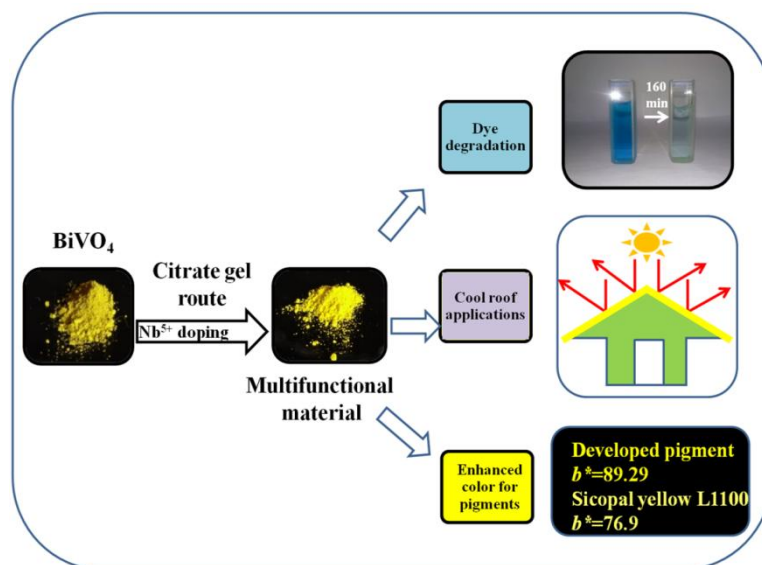
A (BiV)_{0.94}(YNb)_{0.06}O₄ pigment with tetragonal scheelite structure was synthesized by citrate gel technique, which displays bright yellow color with high IR reflectance. The designed cool pigment may find usage in surface coating applications.

CHAPTER 5C

YELLOW PIGMENTS IN $\text{BiV}_{1-x}\text{Nb}_x\text{O}_4$ SYSTEM BY CITRATE GEL METHOD

Overview

Multifunctional materials are developed in $\text{BiV}_{1-x}\text{Nb}_x\text{O}_4$ solid solutions via structural variation by employing citrate gel route.



5C.1 Introduction

Visible light response of vanadate based colored compounds have attracted for a wide variety of applications.²⁵ Particularly bismuth vanadate (BiVO_4) has attracted wide attention because of its excellent physical and chemical properties, such as ionic conductivity,²⁶ ferroelasticity,²⁷ photochromicity,²⁸ gas sensing ability²⁹ etc. BiVO_4 is widely explored for its photocatalytic activity since it has response in visible region unless the widely known TiO_2 which has a major defect of being active in UV region only and thus reducing its performance in sunlight. BiVO_4 as a visible light driven photocatalyst has been studied extensively for the splitting of water,³⁰ the reduction of carbon dioxide into ethanol in water³¹ and the elimination of organic pollutants such as methylene blue (MB),³² methyl orange,³³ rhodamine,³⁴ etc under visible light irradiation. Since discharge of toxic dyestuff from the industries poses a serious threat to environment and health, sunlight driven degradation of these contaminants by photo responsive materials provides a green technique for the elimination of toxic contaminants from the environment by its efficiency and broad pertinence. The band gap of BiVO_4 (2.4 eV)¹⁵ allows favorable separation of e-h pairs which enhance its photoactivity. Also the non toxic behavior of BiVO_4 has made it a hot candidate especially for lead free paint applications.³⁵ However, BiVO_4 is very sensitive to factors such as synthesis techniques, resultant crystal structure and defect contents. So difficulty arises in controlling the photophysical properties of BiVO_4 .

BiVO_4 exists in three crystal forms: monoclinic³⁶ (distorted scheelite structure, fergusonite structure), tetragonal³⁷ (scheelite structure) and tetragonal³⁸ (zircon type structure). The investigation results indicate that the visible light response of BiVO_4 strongly depends on its crystal form and morphology.² The properties, phase formation and morphology of BiVO_4 are related to the synthetic method, raw materials and reaction conditions.³⁹ Monoclinic BiVO_4 , when synthesized by high temperature route leads to irregular shape and large crystal size due to its rapid crystal growth feature. Therefore, the tendency to form a large number of defects, which are unfavorable for the photocatalytic performance, will be found in the products due to the volatilization of ions. Other methods include hydrothermal,⁴⁰ sol-gel,⁴¹ coprecipitation,⁴² metallo organic deposition,⁴³ ultrasonic spray pyrolysis,⁴⁴ etc which results in nano sized particles. Also the aid of surfactants and other inorganic

materials are utilized in these preparation procedures which are costly and limits its industrial applicability. Thus various efforts have been made to improve its properties by changing the synthesis conditions. BiVO_4 has been modified by noble metal loading,⁴⁵ cation⁴⁶ or anion⁴⁷ substitution or by combination with other oxide materials to form composites.⁴⁸ Structural substitution and solid solution formation⁴⁹ can improve band structure, efficient e-h separation and the morphological properties of the respective material, such as particle size or shape. In the present work, citrate gel route has been employed to synthesize Nb^{5+} doped BiVO_4 because it offers many advantages over conventional solid state method in the synthesis of fine powders, such as higher uniformity in particle size distribution, non agglomeration etc.

Transition metal cation doping may change the e-h behavior leading to changes in the electronic structure of the material.⁵⁰ The effect of various transition metals on BiVO_4 have been studied by DFT calculations.⁵¹ According to this report, the solubility of Nb^{5+} is the highest in BiVO_4 host. Improvement in coloristic and NIR reflectance properties were observed by P^{5+} / Ta^{5+} substitutions on BiVO_4 .⁹ High NIR reflective pigments are now in great demand for the construction of cool roofs. A cool roof reflects radiations in the infrared region and results in less heat build-up thereby reducing cooling costs.⁵² In this section, the multifunctional capability of BiVO_4 surpassing the color performance of commercial BiVO_4 pigment, Sicopal Yellow L1100 by a citric acid complexation process is detailed. It can be found that materials with good stoichiometry and particle size can be synthesized. The as-obtained Nb^{5+} doped BiVO_4 materials exhibit enhanced photocatalytic dye degradation under sunlight irradiation thus possessing the potential for environmental and energy saving applications.

5C.2 Experimental Section

5C.2.1 Materials and Methods

Samples BiVO_4 , $\text{BiV}_{0.975}\text{Nb}_{0.025}\text{O}_4$, $\text{BiV}_{0.95}\text{Nb}_{0.05}\text{O}_4$, and $\text{BiV}_{0.925}\text{Nb}_{0.075}\text{O}_4$ were synthesized by the citrate gel method (CG). $\text{Bi}(\text{NO}_3)_3 \cdot 5\text{H}_2\text{O}$, NH_4VO_3 , NbCl_5 (Sigma Aldrich, 99.9% purity) were used as starting materials. Distilled water and citric acid (Sigma Aldrich, 99.9% purity) were used as solvent and chelating agent for the process. The citrate solution was prepared by dissolving appropriate amount of citric acid in distilled water. After complete homogenization of citrate solution, all the

cationic solutions were dissolved in the citrate solution (1:2). The solution was kept for constant stirring for 1 h for homogenous mixing and concentrated by keeping it in the water bath (maintained at 100°C) for 12 h and the solution became viscous gel. The gel was dried to form a black product and then powdered by grinding in an agate mortar, which is the precursor. Then heat treatment of the precursor was carried out separately at various temperatures 300, 400 and 500°C for two hours respectively.

5C.2.2 Characterizations

The calcined powders were characterized by means of X-ray powder diffraction (XRD) using a Ni filtered Cu-K α radiation ($\lambda = 1.54060 \text{ \AA}$) with a PANalytical X'pert Pro diffractometer operated at 45kV and 30mA for its crystalline structure. Data were collected from 10 to 70° 2 θ range with a step size of 0.016°. The Raman spectra of the powder samples were acquired using an integrated micro-Infrared micro-Raman system using a 513 nm helium-neon laser operating at 10mW with a spatial resolution of 2 μm . Particle morphological analysis of the powder was performed by means of a scanning electron microscope with JEOL JSM-5600 LV SEM with an acceleration voltage of 15 kV. The TEM images and selected area electron diffraction (SAED) pattern of the samples were carried out on a FEI Tecnai 30G² S-Twin transmission electron microscope (TEM) operating at 300 kV. Energy dispersive analysis and elemental mapping of the samples was analyzed using Silicon Drift Detector–X-MaxN attached with a Carl Zeiss EVO SEM. EDS elemental mapping was conducted by AZtecEnergy EDS Microanalysis software. The UV visible spectra of the samples was measured with a UV–Vis–NIR spectrophotometer (Shimadzu, UV-3600) using BaSO₄ as a reference. Optical measurements were performed in the 220 to 800 nm wavelength range. The color properties and NIR reflectance of the samples were estimated in as discussed in the previous chapters. The Brunauer-Emmet-Teller (BET) surface area of the materials were analysed by nitrogen adsorption – desorption measurement using Micrometrics Tristar Surface Area Analyser.

Photocatalytic study

The photocatalytic activity of samples, processed via citrate gel route, was studied by monitoring the degradation of methylene blue dye in an aqueous suspension containing the samples under continuous solar-radiation exposure and

magnetic stirring. All photocatalytic experiments were carried out under similar conditions in the city of Thiruvananthapuram (latitude: 8.460 N; longitude: 76.980 E), (India). All the solar experiments were performed on an average light intensity of 8×10^4 lux in order to avail maximum sunlight. A 75 mL of aqueous suspension was prepared by mixing 1×10^{-5} M dispersing 0.02 g of the samples in the de-ionized water. The resulting suspension was equilibrated by stirring in dark for 20 min to stabilize the adsorption of MB dye on the surface of samples. The stable aqueous suspension was then exposed to natural sunlight. Following sunlight exposure, 8 mL of aqueous suspension was taken out of suspension after each 20 min interval for total 160 min of sunlight exposure for obtaining the absorption spectra. The degraded solution of MB was analyzed by a UV-visible spectrophotometer (Hitachi 3900H) and the absorption peak at 664 nm was monitored.

The organic intermediates obtained at various intervals were analyzed by the high-pressure liquid chromatography and gas chromatography mass spectrometry (HPLC and GC–MS) method. The degradation products were characterized by a GCMS-QP2010 (SHIMADZU Corporation, Japan). The organic intermediates produced during degradation, were extracted with equal volumes of ethyl acetate and directly used for further study. GC conditions included split injection mode with carrier gas Helium and MS conditions included an ion source temperature of 200°C.

5C.3 Results and Discussion

5C.3.1 X-Ray Diffraction Analysis

From the powder XRD patterns analysis of BiVO_4 , $\text{BiV}_{0.975}\text{Nb}_{0.025}\text{O}_4$, $\text{BiV}_{0.95}\text{Nb}_{0.05}\text{O}_4$ and $\text{BiV}_{0.925}\text{Nb}_{0.075}\text{O}_4$ calcined at 300, 400 and 500°C, it is seen that the samples calcined at 500°C are the most crystalline in nature. Fig. 5C.1 (a) shows the powder X-ray diffraction patterns of samples calcined at 500°C. All the reflections are indexed as per the monoclinic scheelite (s-m) phase with a space group $I_{2/b}$ and the reflections can be well indexed according to the powder diffraction file no. 01-083-1699. As said earlier, BiVO_4 has three main crystal forms: zircon- structure with tetragonal system and scheelite structure with monoclinic and tetragonal systems. The crystal structure of monoclinic scheelite BiVO_4 is much similar to that of tetragonal scheelite, except for the distortion.⁵³ The Bi–O polyhedron in the former is more

distorted than that of tetragonal scheelite BiVO_4 due to the presence of a $6s^2$ lone pair of Bi^{3+} . The difference in the XRD patterns between BiVO_4 (s-m) and BiVO_4 (s-t) can be judged by the existence of a peak at 15° and splitting of peaks at 18.5° , 35° , and 46° of 2θ .² It is, therefore convenient to distinguish monoclinic and tetragonal scheelite BiVO_4 from XRD patterns. It is observed that on progressive doping with Nb^{5+} , the splitting of peaks at 18.5° , 35° , and 46° of 2θ are decreasing. A typical zoomed prominent peak position around 2θ 18° is shown in Fig.5C.1 (b) and also provided a graph showing the variation of the peak split width upon Nb^{5+} doping shown in inset. This graph reveals a linear decreasing trend of the peak split width upon Nb^{5+} doping. These results suggest that the progressive doping of Nb^{5+} induces a structural variation from monoclinic scheelite to tetragonal scheelite type.

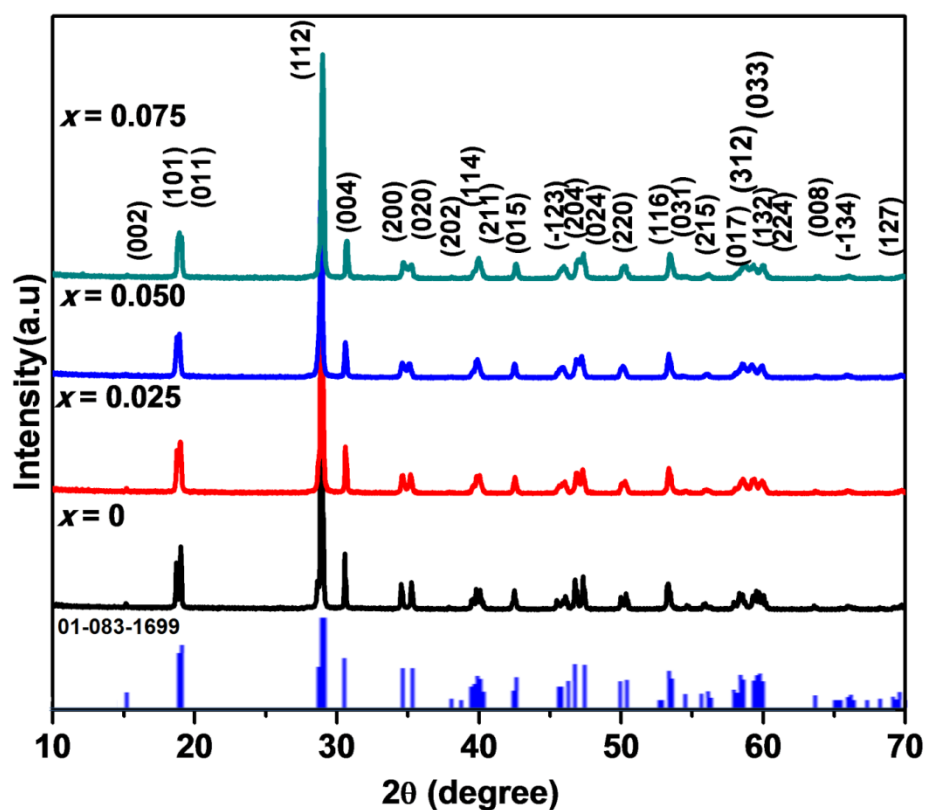


Fig. 5C.1 (a) Powder XRD patterns of $\text{BiV}_{1-x}\text{Nb}_x\text{O}_4$; $x = 0, 0.025, 0.05, 0.075$ synthesized at 500°C and the reference pattern.

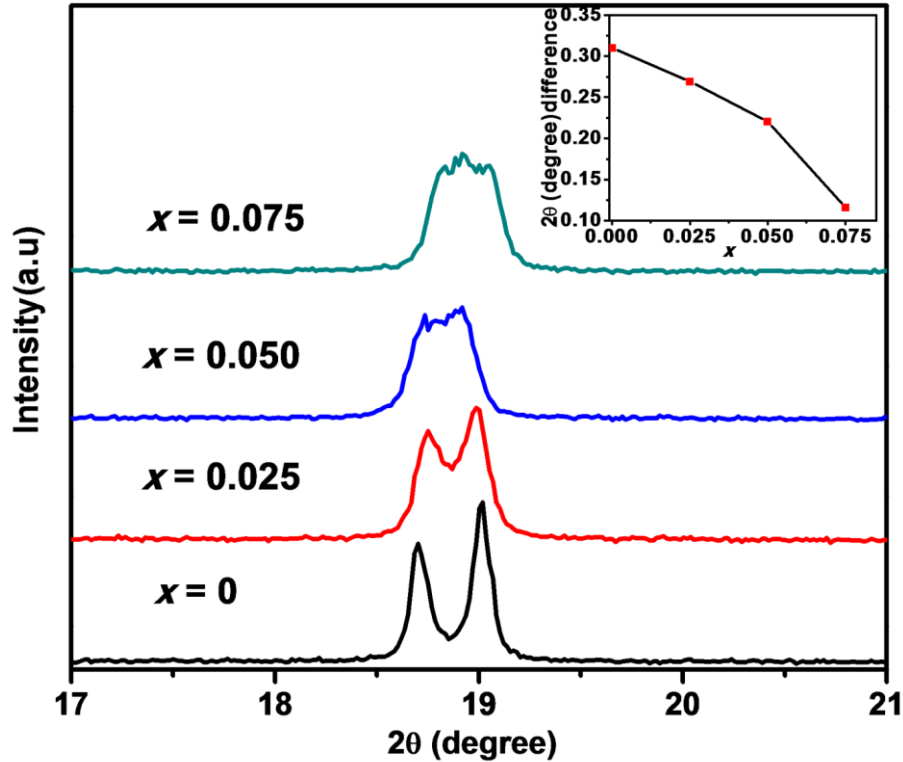


Fig. 5C.1 (b) Zoomed peak position of the characteristic monoclinic peak around 2θ 18° for the XRD patterns of $\text{BiV}_{1-x}\text{Nb}_x\text{O}_4$; $x = 0, 0.025, 0.05, 0.075$ synthesized at 500°C . (Inset shows variation of the peak split width with Nb^{5+} substitution.)

The crystalline nature of the phases is evident from powder diffraction patterns which suggest that all the samples on Nb^{5+} doping form solid solutions in BiVO_4 . The structure is constructed by VO_4 tetrahedron and BiO_8 dodecahedron structural units. The V site is bordered by four oxygen atoms forming a VO_4 tetrahedron and the Bi site too by eight oxygen atoms making a BiO_8 dodecahedron. The slightly distorted feature comes from the fact that there are four types of Bi-O bonds and two types of V-O bonds.⁵⁴ The ionic radii of Bi^{3+} in eight fold coordination is 0.117 nm and V^{5+} in four fold coordination is 0.035 nm and doping Nb^{5+} (0.048 nm)⁵⁵ into V^{5+} will cause slight distortion in the VO_4 tetrahedron and BiO_8 dodecahedron of the lattice as obvious by difference in ionic radius. The crystallite size is calculated from the Debye Scherrer formula⁵⁶

$$D = 0.9\lambda/\beta\cos\theta, \quad (5.1)$$

where D is the crystallite size, λ is the wavelength of X-ray used, β and θ are the half width of the X-ray diffraction lines and half diffraction angle 2θ . The instrumental broadening was rectified using silicon as the external standard. The crystallite size of BiVO_4 is found to be in the range 74-123 nm at various temperatures (300-500°C). On doping with Nb^{5+} , a reduction in crystallite size is observed. The crystallite size obtained at various temperatures is given in Table 5C.1.

The strain induced in the lattice is estimated using Williamson-Hall (W-H) method where both size-induced and strain-induced broadening are deconvoluted by considering the peak width as a function of 2θ . According to W-H method, the width of individual reflections can be expressed as follows:⁵⁷

$$\beta \cos \theta = \frac{K\lambda}{D} + 4\varepsilon \sin \theta \quad (5.2)$$

where β is the width of peaks, D is the crystallite size, λ is the wavelength of Cu $K\alpha$ radiation and ε is the crystal strain effect. A plot is drawn with $4\sin\theta$ along the x-axis and $\beta_{\text{hkl}} \cos\theta$ along the y-axis. From the linear fit to the plot, the strain ε was determined from the slope of the fit. The lattice strain induced in $\text{BiV}_{0.975}\text{Nb}_{0.025}\text{O}_4$ sample synthesized at 500°C is 0.31 % whereas in BiVO_4 it is about 0.18% (Fig. 5C.2). It is observed that on doping, as crystallite size decreases lattice strain increases (Table 5C.1). It is obvious from W-H plot that on Nb^{5+} doping, atomic shifts might have induced some strain in BiVO_4 lattice which may be responsible for the enhancement of color as discussed in the latter part of the section.

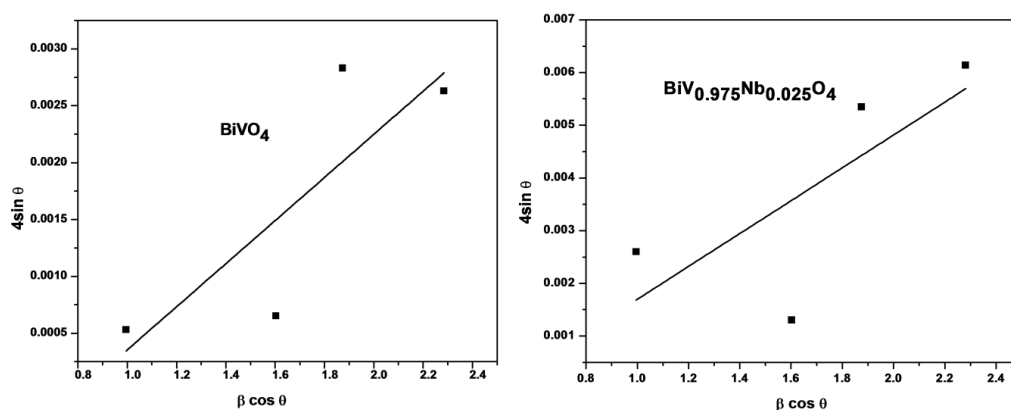


Fig. 5C.2 W-H plots of $\text{BiV}_{1-x}\text{Nb}_x\text{O}_4$; $x = 0, 0.025$ synthesized at 500°C.

Table 5C.1 Crystallite size and lattice strain of BiV_{1-x}Nb_xO₄ (x = 0, 0.025, 0.05, 0.075) synthesized at different temperatures.

Sample	Crystallite size (nm)			Lattice strain (%)		
	300°C	400°C	500°C	300°C	400°C	500°C
BiVO₄	74	77	123	0.14	0.17	0.19
BiV_{0.975}Nb_{0.025}O₄	49	53	91	0.37	0.33	0.35
BiV_{0.95}Nb_{0.05}O₄	46	51	87	0.26	0.34	0.30
BiV_{0.925}Nb_{0.075}O₄	40	57	77	0.22	0.29	0.29

5C.3.2 Raman Spectra Analysis

Raman scattering spectra of the samples calcined at 500°C, was performed to understand its local structure shown in Fig. 5C.3 (a). To identify more accurately the peak positions, we fitted the Raman spectra using Lorentz function. Typical Lorentz fits are presented in Fig. 5C.3 (b). The Raman spectra shows characteristic bands of monoclinic scheelite structure in agreement with the literature.⁵⁸ In this regard, the 218 cm⁻¹ band was the external mode of BiVO₄, which gave little structural information. The Raman bands at 337 (B_g anti-symmetry) and 372 cm⁻¹ (A_g symmetry) were assigned to the asymmetric and symmetric deformation modes of the VO₄³⁻ tetrahedron, respectively. Meanwhile, the most intense Raman band at about 813 cm⁻¹ (A_g symmetry) was assigned to the symmetric V-O stretching mode. The shifts of Raman band at 813 cm⁻¹ (V-O stretching vibration) to lower frequency indicate increasing V-O bond distance corresponding to the shorter bond length. This increase of shorter bond length improves the symmetry of VO₄ tetrahedra and further evidences a state of structural variation of monoclinic to tetragonal phase. The V-O bond lengths are affected by position of bismuth ions and correlates with the variations occurring in the unit cell.⁵⁹ A functional relationship exists between the Raman stretching frequency ν and the metal-oxygen bond length R in the local structure.⁶⁰

$$\nu \text{ cm}^{-1} = 21349 \exp(-1.9176 R \text{ \AA}) \quad (5.3)$$

The FWHM obtained from Lorentzian peak fitting for $x = 0, 0.025, 0.050, 0.075$ are 69.7, 83.1, 81.7, 75.6 respectively. This indicates that there is heterogeneity with respect to the local strain induced in doped samples and the highest variation is seen for $x = 0.025$ which may be the reason for the enhancement of color in samples. A continuous shift of this Raman band to lower wave numbers, from 813 to 811 cm^{-1} reveals that the average short-range symmetry of the VO_4 tetrahedra becomes more regular. The shifting of the corresponding symmetric V-O stretching mode in Nb^{5+} doped BiVO_4 (m-s) towards lower wave number leads to increase in bond length from 1.7044 (\AA) to 1.7052 (\AA). The variations induced in BiVO_4 unit cell are evident from Raman analysis. Thus it is evident that slight change in the V-O bond length may be responsible for the enhanced photoresponse of the samples.

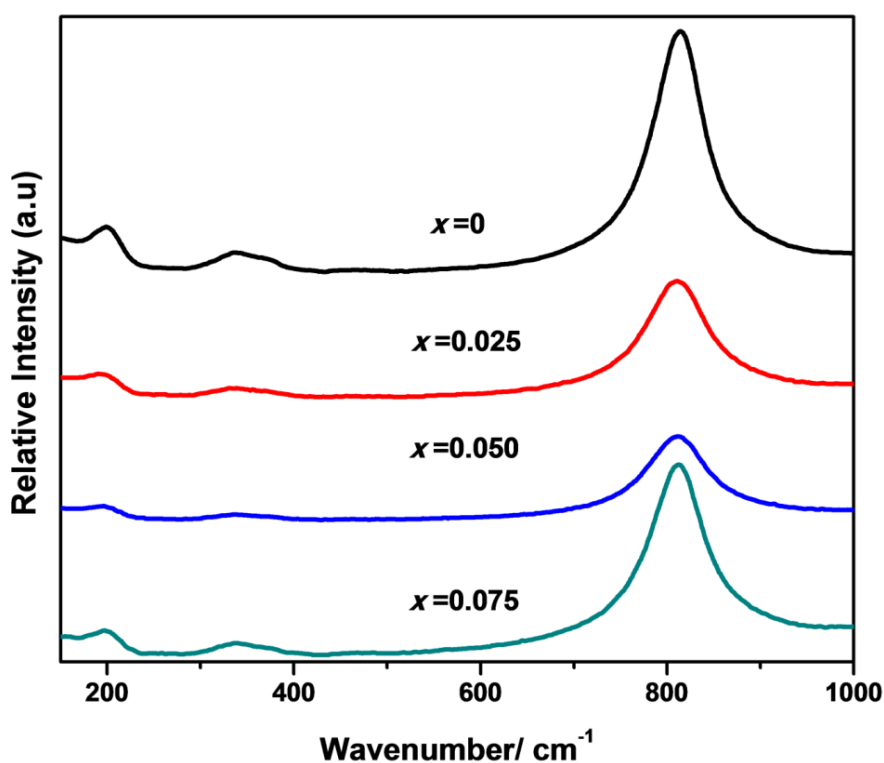


Fig. 5C.3 (a). Raman spectra of $\text{BiV}_{1-x}\text{Nb}_x\text{O}_4$; $x = 0, 0.025, 0.05, 0.075$ synthesized at 500°C .

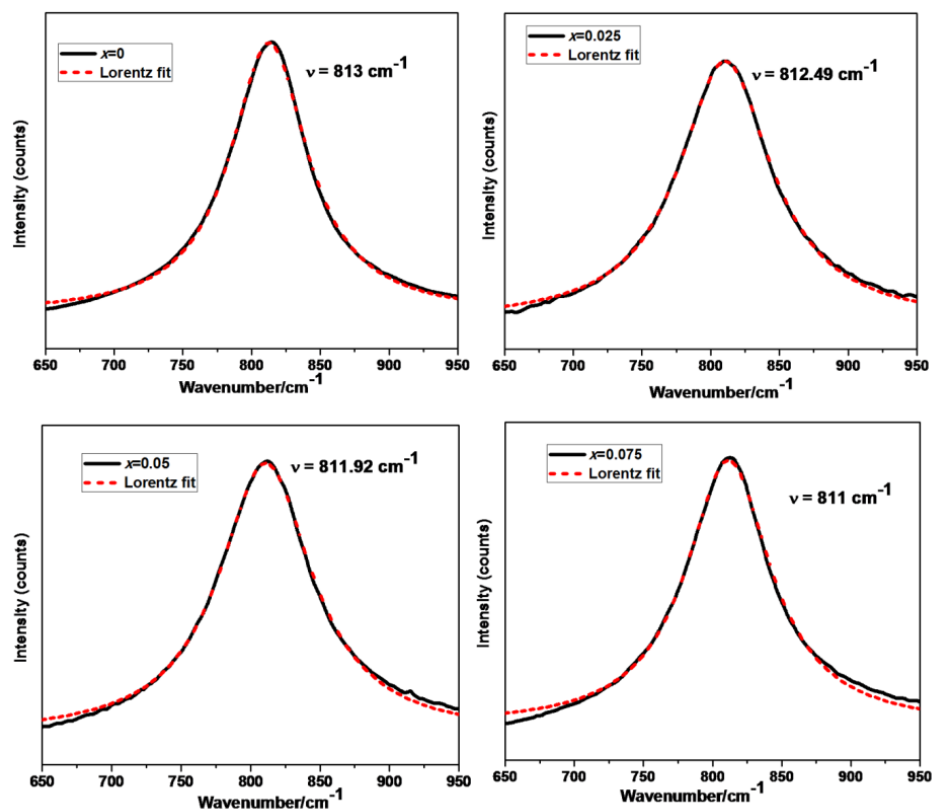


Fig. 5C.3 (b). Lorentz fits Raman mode around 812 cm^{-1} of $\text{BiV}_{1-x}\text{Nb}_x\text{O}_4$; $x = 0, 0.025, 0.05, 0.075$ calcined at 500°C .

5C3.3 Morphological and Micro chemical Studies

The homogeneous and crystalline nature of the samples can also be observed in the SEM photographs (Fig. 5C.4). The samples have a particle size of about 100 nm when synthesized at 300°C and the particle size is increased to about 400 nm at 500°C . There is a slight increase in particle size upon Nb^{5+} doping. From the micrographs it is clear that the particles texture is smooth and somewhat spherical in nature and they are distributed uniformly.

EDS analysis of samples confirm that the samples are composed of Bi, V, Nb and O in the appropriate ratio. Elemental X-ray dot mapping analysis of typical $\text{BiV}_{0.975}\text{Nb}_{0.025}\text{O}_4$ pigment calcined at 500°C confirms that niobium ions are uniformly distributed in BiVO_4 lattice (Fig. 5C.5).

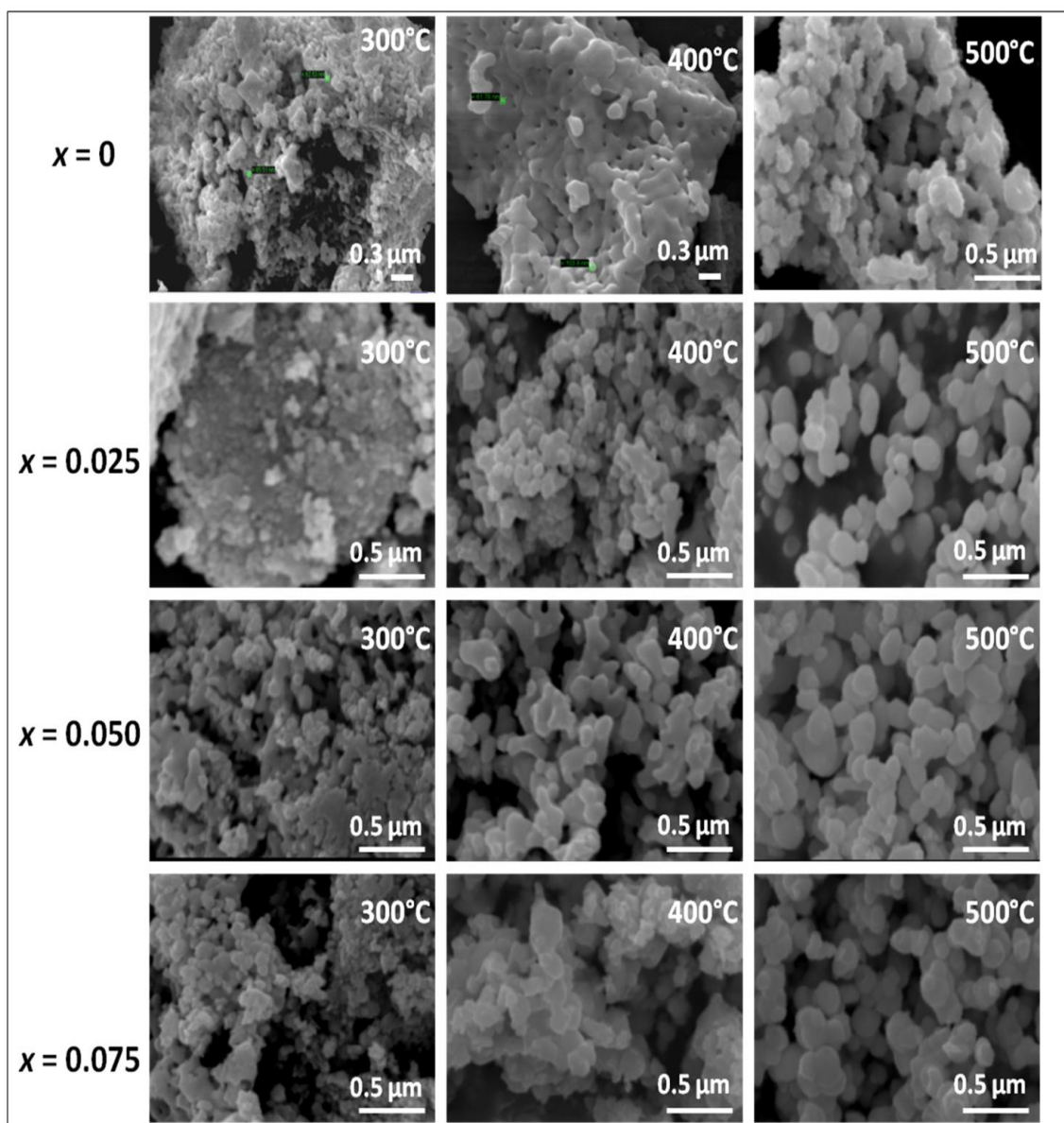


Fig. 5C.4 SEM micrographs of $\text{BiV}_{1-x}\text{Nb}_x\text{O}_4$; $x = 0, 0.025, 0.05, 0.075$ synthesized at various temperatures

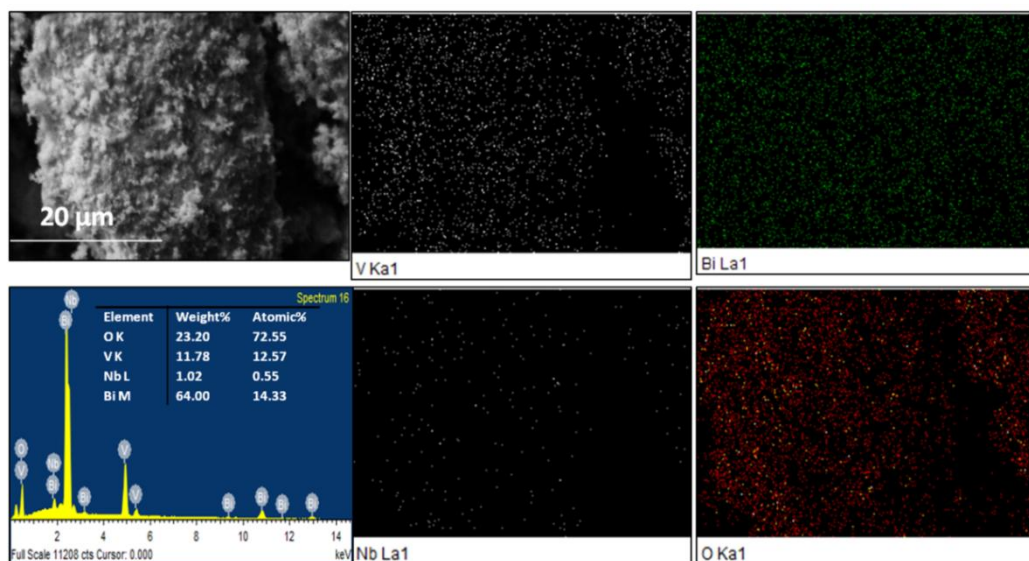


Fig. 5C.5 EDS spectra and elemental mapping data of (a) Bi, (b) V, (c) Nb, (O) in $\text{BiV}_{0.975}\text{Nb}_{0.025}\text{O}_4$ sample synthesized at 500°C .

TEM images of the samples calcined at 500°C reveals that particles are a bit aggregated (Fig. 5C.6). TEM investigation confirms the particle diameter in the size range of 100–300 nm and the SAED patterns indicate that they are polycrystalline. TEM confirms that particle size is slightly affected by niobium doping.

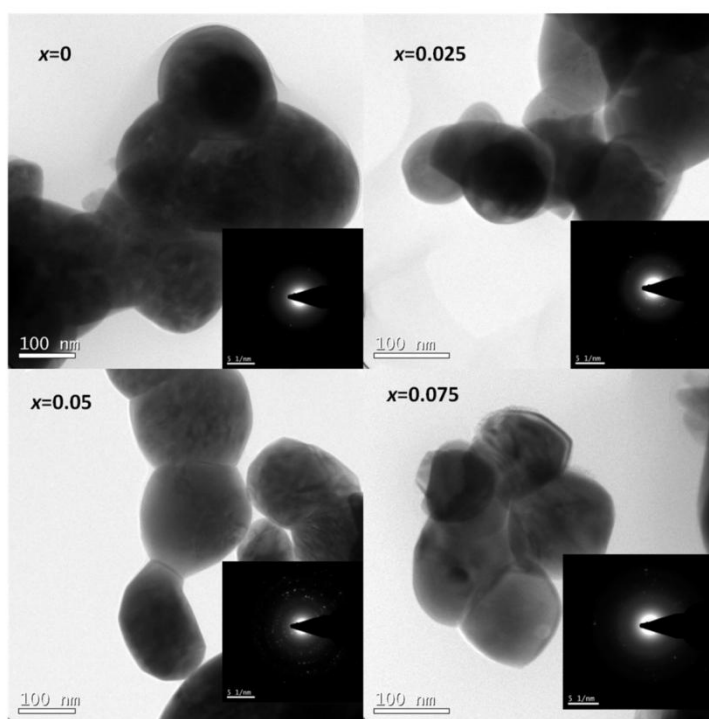


Fig. 5C.6 TEM micrographs of $\text{BiV}_{1-x}\text{Nb}_x\text{O}_4$; $x = 0, 0.025, 0.05, 0.075$ pigments (SAED patterns inset).

5C.3.4 UV Visible studies

The absorption spectra of the BiVO₄, BiV_{0.975}Nb_{0.025}O₄, BiV_{0.95}Nb_{0.05}O₄, BiV_{0.925}Nb_{0.075}O₄ samples synthesized at 500°C, represented with Kubelka-Munk absorption function, $f(R) = (1-R)^2/2R$, where R is the reflectance (Fig. 5C.7). The colors of the samples are bright yellow and possess steep absorption edge in the visible light region. The steep absorption edge means that the visible light absorption is due to the band-gap transition.⁴ It is well known that the band-gap transition of BiVO₄ is formed by charge-transfer from the hybrid orbitals of Bi 6s and O 2p to V 3d orbitals. As a crystalline semiconductor, the optical absorption near the band edge follows the formula:⁶¹

$$\alpha h\nu = A(h\nu - E_g)^{n/2} \quad (5.4)$$

where α , ν , E_g and A are absorption coefficient, light frequency, band gap and a constant, respectively. Among them, n depends on the characteristics of the transition in a semiconductor, i.e. direct transition ($n = 1$) or indirect transition ($n = 4$). For BiVO₄, the value of n is 1.⁶² The band gap energy (E_g value) of BiVO₄ can thus be estimated from a plot $(\alpha h\nu)^2$ versus photon energy ($h\nu$). The intercept of the tangent to the x-axis will give a good approximation of the band gap energy for the samples. Tauc plots of the $(\alpha h\nu)^2$ versus photon energy ($h\nu$) of samples at 500°C are shown in Fig.5C.8. The addition of Nb⁵⁺ resulted in slight variations in band gap. The band gap energy of BiVO₄ can be calculated as 2.44 to 2.51 eV from Tauc plots, which means they have suitable band gaps for photocatalytic decomposition of organic contaminants under sunlight irradiation. The band gap energies of each sample were found to decrease with increasing synthesis temperature. For samples synthesized at 300-500°C, on increase of dopant content it is seen that the band gap increases for $x = 0.025$ and then gets slightly decreased again. The estimated band gap energies of the samples are given in Table 5C.2.

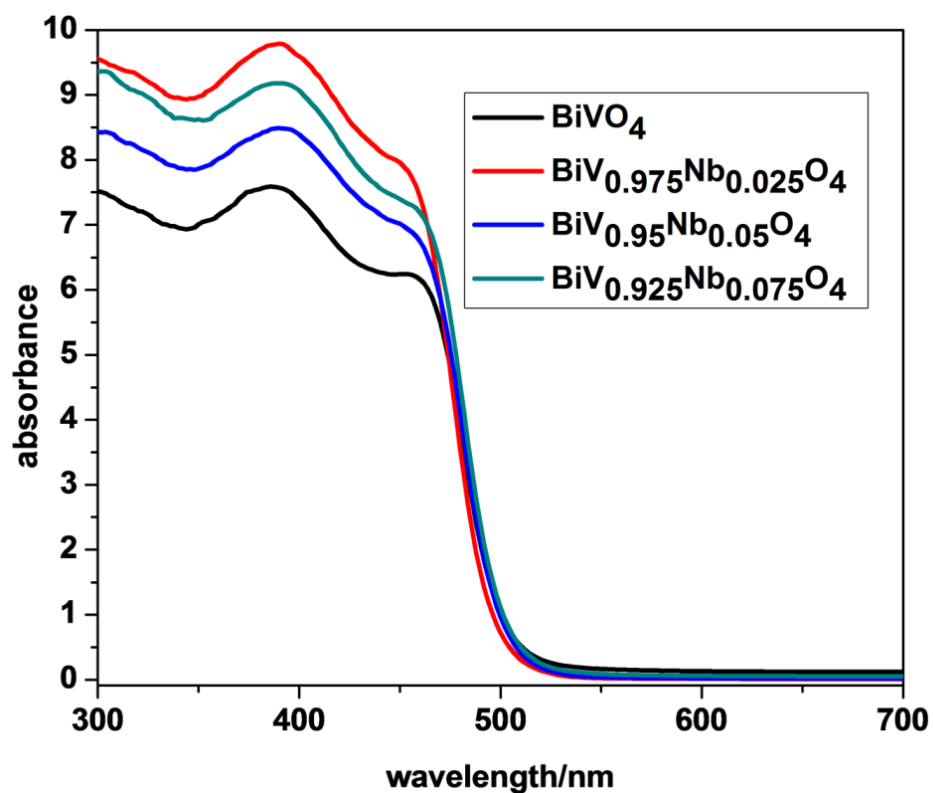


Fig. 5C.7 Absorption spectra of $\text{BiV}_{1-x}\text{Nb}_x\text{O}_4$; $x = 0, 0.025, 0.05, 0.075$ synthesized at 500°C .

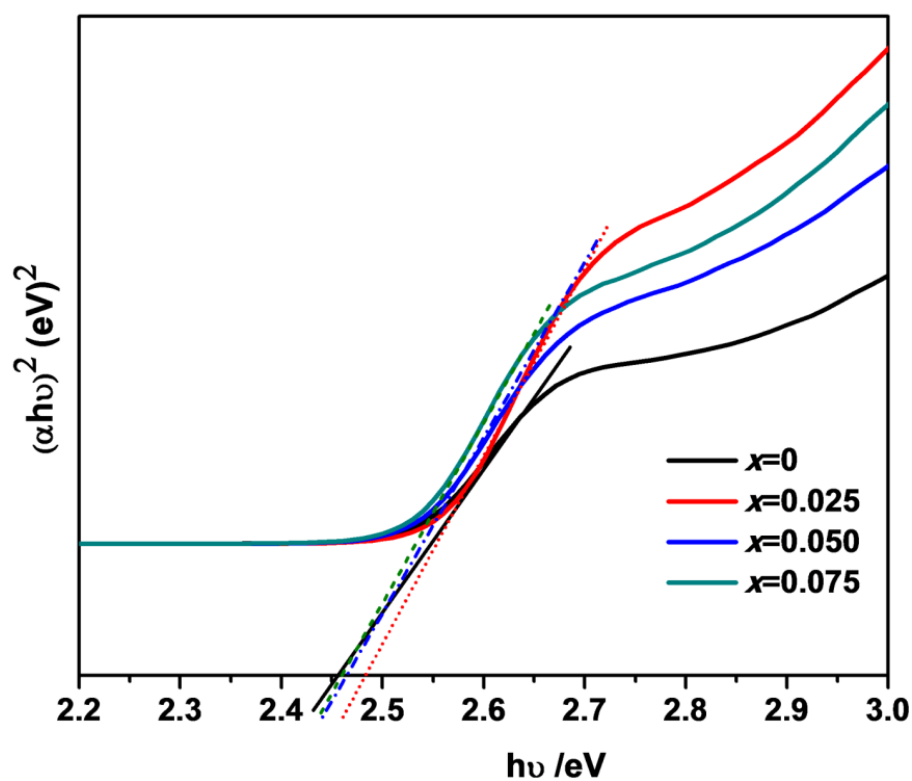


Fig. 5C.8 Tauc plots of $\text{BiV}_{1-x}\text{Nb}_x\text{O}_4$; $x = 0, 0.025, 0.05, 0.075$ calcined at 500°C .

Thus there is a slight variation observed in the electronic structure of the samples when Nb⁵⁺ is doped into BiVO₄, thereby the distortion of the VO₄³⁻ tetrahedron occurs. This distortion is due to the lone pair electron of Bi³⁺ in the local structure of the BiVO₄. There may be a change in the extent of overlapping of Bi 6s and O 2p with the inclusion of Nb 4d orbitals. This overlapping is directly proportional to the degree of distortion which in turn helps in the mobility of photogenerated holes.

5C.3.5 Color Analysis

The color coordinates of the BiV_{1-x}Nb_xO₄ ($x = 0, 0.025, 0.05, 0.075$) pigments are given in Table 5C.2. All the samples are yellow as the hue falls in the yellow region of the color space. The b^* value increases with each doping concentrations with increase in synthesis temperature. On increase of calcination temperature, the shades shift from greenish yellow to reddish yellow. The samples calcined at 500°C are reddish yellow while the lower temperatures yield greenish yellow. The samples calcined at 500°C shows an increment in b^* value from 71 to 89 upon Nb⁵⁺ doping (0.025). Further doping results in a slight decrease in b^* value up to 80. The enhancement in color may be due to the increased lattice strain imposed on BiVO₄ through Nb⁵⁺ doping. Thus the samples calcined at 500°C exhibit better yellow colors. The b^* value obtained for $x = 0.025$ is higher than commercial BiVO₄ (Sicopal Yellow L1100).²⁴ This implies the potential utility of the developed pigments for coloring applications.

5C.3.6 IR Reflectance Studies

The IR reflectance spectra of BiV_{1-x}Nb_xO₄ ($x = 0, 0.025, 0.05, 0.075$) samples synthesized at 500°C are given in Fig. 5C.9. It is seen that the pigments calcined at 500°C shows the highest NIR reflectivity compared to lower synthesis temperatures. BiVO₄ synthesized by citrate gel route possesses an NIR reflectance of 61% in the 1100 nm range. Doping of Nb⁵⁺ into BiVO₄ enhances the NIR reflectance to 86 % for $x = 0.025$. For x greater than 0.025 a slight decrease in values up to 68% is observed. The IR solar reflectance spectra determined in accordance with ASTM Standard G173-03⁶³ of powdered samples are presented in Fig. 5C.10. The enhancement of the optical properties of BiVO₄ is mainly ascribed to the reduction in crystallite size and

structural variation in the lattice. The high IR reflectance displayed by all the newly obtained yellow colored samples makes them interesting candidates for use as cool colorants.

Table 5C.2 Color coordinates and band gap energies of $\text{BiV}_{1-x}\text{Nb}_x\text{O}_4$ ($x = 0, 0.025, 0.05, 0.075$) synthesized at different temperatures.

Calcination	Composition	L^*	a^*	b^*	C^*	h^θ	E_g (eV)
300°C	$x = 0$	71.52	-3.6	65.21	65.31	93.17	2.49
	$x = 0.025$	65.58	-5.07	58.02	58.25	95.0	2.51
	$x = 0.050$	62.56	-3.75	54.42	54.55	93.96	2.48
	$x = 0.075$	48.37	-3.88	35.59	35.8	96.26	2.48
400°C	$x = 0$	77.23	-2.79	72.0	72.06	92.23	2.46
	$x = 0.025$	82.49	-3.0	82.33	82.39	92.10	2.49
	$x = 0.050$	71.97	-3.88	65.37	65.49	93.41	2.46
	$x = 0.075$	70.27	-3.36	63.56	63.65	93.04	2.44
500°C	$x = 0$	77.18	-0.53	71.19	71.19	90.44	2.45
	$x = 0.025$	85.99	0.93	89.29	89.29	89.40	2.48
	$x = 0.050$	83.99	2.49	85.54	85.54	8.32	2.46
	$x = 0.075$	79.72	1.64	80.13	80.13	88.82	2.44
	Sicopal yellow ²⁴	94.4	-16.7	76.9	78.7	77.8	2.51

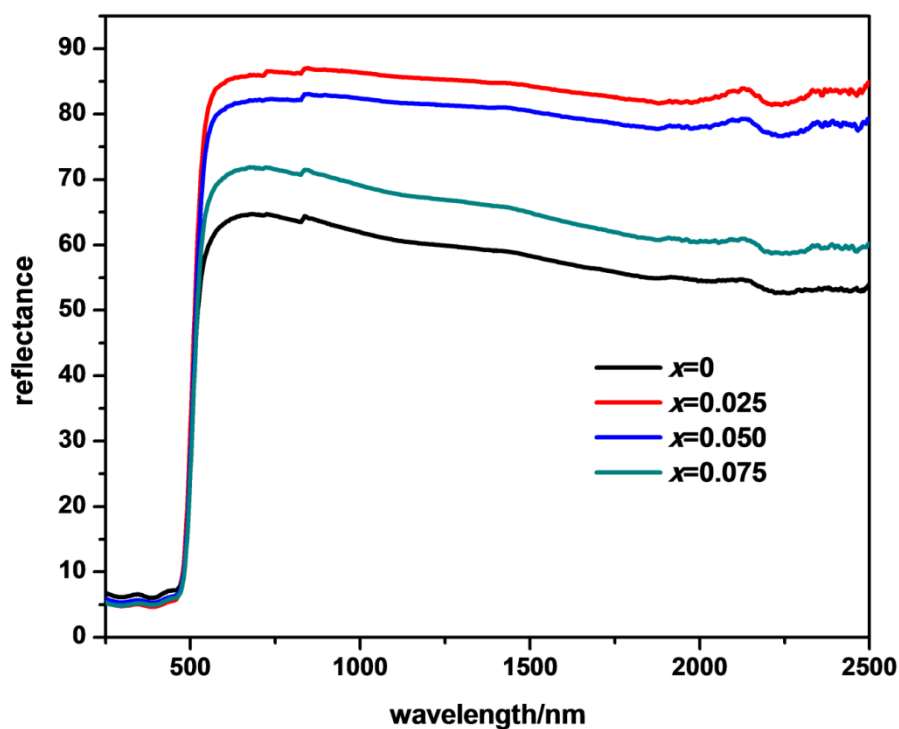


Fig. 5C.9 UV vis NIR reflectance spectra of $\text{BiV}_{1-x}\text{Nb}_x\text{O}_4$; $x = 0, 0.025, 0.05, 0.075$.

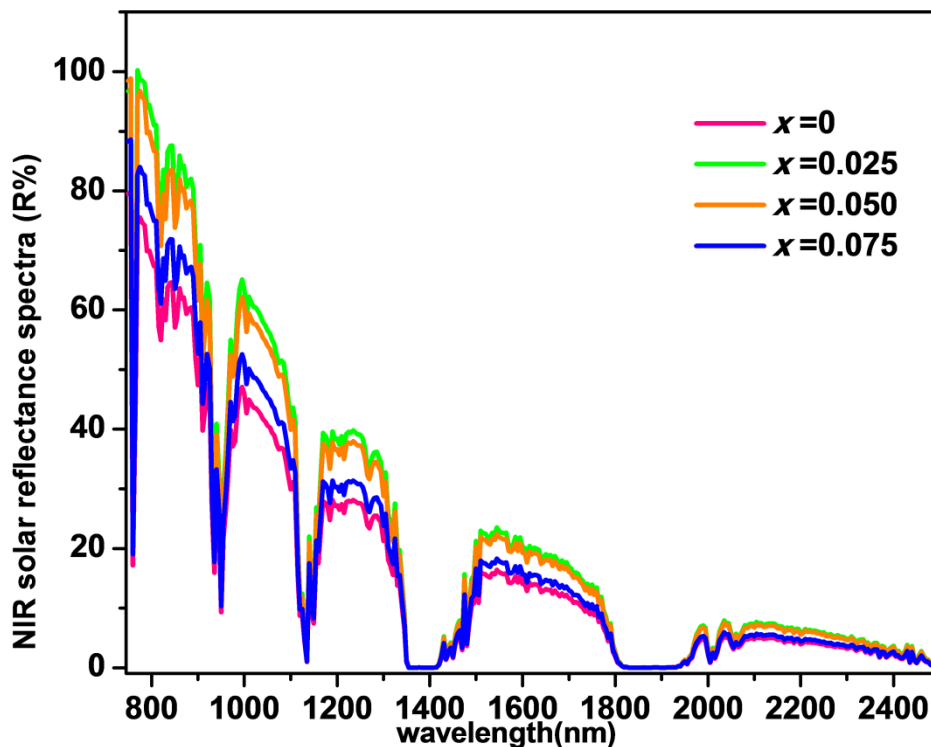


Fig. 5C.10 IR solar reflectance spectra of BiV_{1-x}Nb_xO₄; $x = 0, 0.025, 0.05, 0.075$.

5C.3.7 Photocatalytic studies

Temporal changes in the concentration of MB were monitored by examining the variations in maximal absorbance in UV–Vis spectra at 664 nm. In the presence of the photocatalyst and visible light irradiation, the degradation of MB obviously increased. It can be found that the doping of Nb⁵⁺ affects the photocatalytic activity of BiVO₄. Fig. 5C.11 shows the temporal absorption spectral patterns of MB during the photo degradation process in typical BiV_{0.95}Nb_{0.05}O₄ sample synthesized at 500°C. The typical sample shows the highest degradation activity. Photocatalytic efficiency (C) of samples was calculated by the following equation,

$$C = (A_0 - A) / A_0 \times 100\%, \quad (5.5)$$

where A_0 is the absorbance of its maximum absorbance wavelength, A is the absorbance at the same wavelength of extracted solution. For $x = 0$, C was found to be 81, for $x = 0.050$ it was 88. The absorption peak gradually shifted from 664 nm to 616 nm with a decrease in absorption during the process of photocatalytic degradation. Such a blue-shift is characteristic process of N-demethylation derivatives of MB. With the photocatalytic degradation of MB, the absorption peak at 664 nm

disappeared due to the formation of a mixture of N-demethylated analogs (Azure B, Azure A, Azure C and Thionine) of MB.⁶⁴ This result suggested that demethylation process was likely to be a major step in the photocatalytic oxidation of MB.

As a direct electron transition semiconductor, the monoclinic BiVO_4 is excited by the incident photons with energy equal to or greater than their band energy level. Electrons and holes that migrate to the surface of the semiconductor without recombination can respectively reduce or oxidize the reactants adsorbed by the semiconductor. In the process of migration to the surface of the semiconductor, the mobility of the photo-generated charge carriers is a key factor. In general, charge separation and transfer of photogenerated electrons and holes are strongly affected by the crystal structural features of the materials, namely, crystallinity, defects, and any crystal structure distortion. Additionally, surface properties such as particle size, surface area, surface structure, and active reaction sites, which are mainly related to the morphology of the materials, are also important.

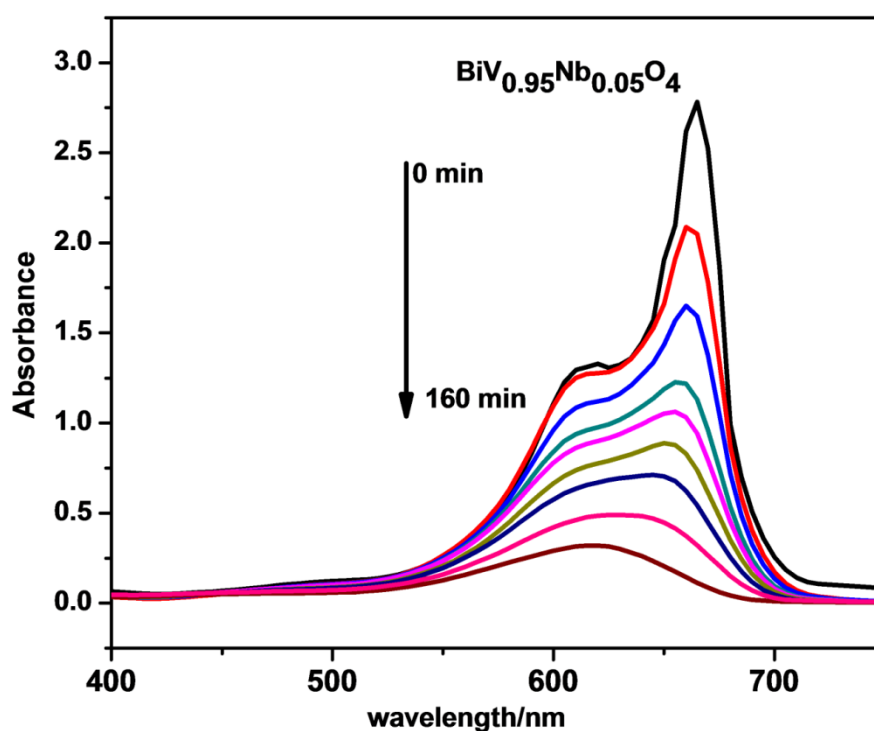


Fig. 5C.11 UV visible spectral changes of MB as a function of irradiation time for $\text{BiV}_{0.95}\text{Nb}_{0.05}\text{O}_4$ sample under sunlight.

With the increase of the doping concentration ($x = 0.075$), the activity decreases as the tendency of structural variation to tetragonal scheelite as obvious from the X-ray diffraction patterns as seen earlier. The dopant addition may cause variations in VO_4 tetrahedron which is favorable for the separation of photo-excited e-h pairs. Also, change in the electronic structures varies the degree of delocalization of photogenerated e-h pairs and leads to change in photocatalytic activity. The results show that up to $x = 0.05$ doping of Nb^{5+} shows enhanced photocatalytic activity than the undoped sample. When the doping percentage is increased, photocatalytic property decreases, due to the tendency to shift the structure from monoclinic to tetragonal. The surface area also gets increased from $1.08 \text{ m}^2/\text{g}$ for undoped to $2.72 \text{ m}^2/\text{g}$ for $x = 0.05$ doping of Nb^{5+} . This implies that increase in surface area too might have contributed to an increased photocatalytic activity.

Fig. 5C.12 shows a MS chromatogram obtained after MB degradation after 160 min of irradiation using $\text{BiV}_{0.95}\text{Nb}_{0.05}\text{O}_4$ photocatalyst. The direct ESI mass spectrum is shown in Fig.5C.13 which shows main two peaks at retention time of 3.95 and 14.96 for MB. The two products identified in GC-MS spectra are at 256 m/z and 135 m/z . These can be assigned to the chemical structures Azure A⁶⁵ and thiophene.⁶⁶ Also many peaks with different intensities were observed in addition to MB dye suggesting that new products are formed in the course of degradation. This shows the complexity of the photocatalytic process.

Further HPLC analysis was also conducted to identify more organic intermediates using a ThermoScientific Q-Exactive ESI-HPLC MS instrument. The degraded MB samples collected at various intervals were dissolved in equal amounts of HPLC grade methanol and used for analysis. The formation of Azure C ($\text{m/z}=242.2$) was confirmed by HPLC analysis. Also phenothiazin could be detected at $\text{m/z}=200$ from thionin deamination.⁶⁵ Thus GCMS and HPLC analysis confirmed the photodegradation of MB by forming various organic intermediates.

Total organic carbon (TOC) was analyzed with a Liqui TOC II analyzer (elementar, Germany). Prior to injection into the TOC analyzer, the samples were centrifuged to remove any catalyst particles. The results showed that 65 % and 70% of TOC could be removed within 160 min of sunlight irradiation when BiVO_4 and

$\text{BiV}_{0.95}\text{Nb}_{0.05}\text{O}_4$ were used as photocatalyst. Total inorganic carbon (TIC) remained constant throughout the reaction indicating no formation of any harmful substances in the photodegradation process.

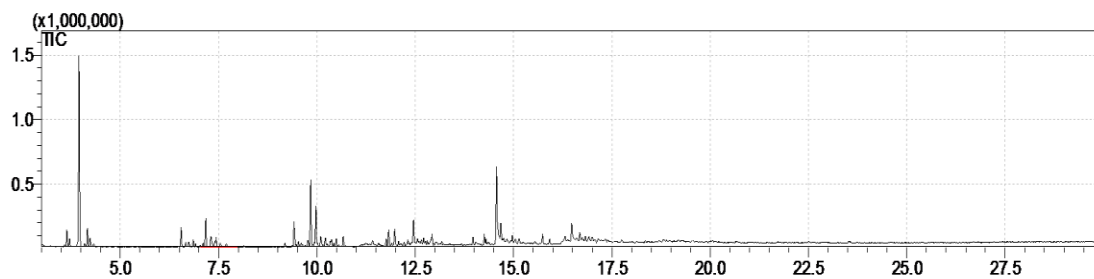


Fig. 5C.12 GC MS chromatogram of MB degradation after 160 min sunlight irradiation.

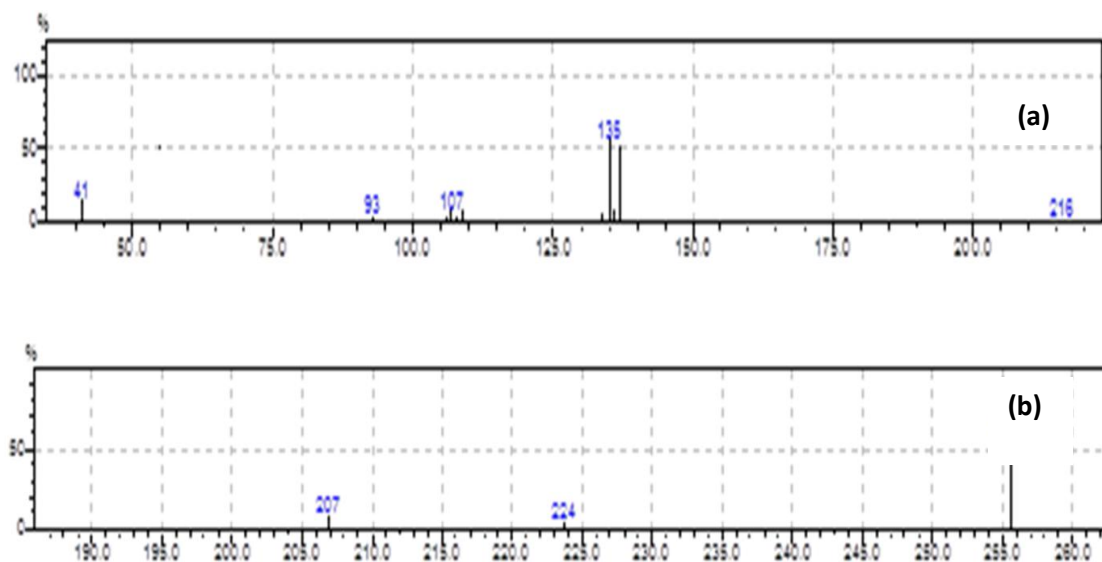


Fig. 5C.13 GC MS spectra of MB and its intermediate degradation products at retention time (a) 3.45 min and (b) 14.56 min.

5C.4 Conclusions

Multifunctional novel non-toxic materials in $\text{BiV}_{1-x}\text{Nb}_x\text{O}_4$ system are reported for the first time. The fine particles are prepared by citrate complexation route. The pigments exhibit excellent color characteristics comparable to commercial BiVO_4 . Also the high IR reflectance of these pigments indicates their potential for cool roof applications. The high photon absorption capability of these materials is seen by considerable methylene blue dye degradation property.

5.5 References

1. (a) Neves, M. C.; Lehocky, M.; Soares, R.; Lapick Jr., L.; Trindade, T., Chemical bath deposition of cerium doped BiVO₄. *Dyes Pigm.* **2003**, *59* (2), 181-184; (b) Gotić, M.; Musić, S.; Ivanda, M.; Šoufek, M.; Popović, S., Synthesis and characterisation of bismuth(III) vanadate. *J. Mol. Struct.* **2005**, *744–747*, 535-540.
2. Saimi, T.; Hideki, K.; Akihiko, K., Selective preparation of monoclinic and tetragonal BiVO₄ with scheelite structure and their photocatalytic properties. *Chem. Mater.* **2001**, *13*, 4624-4628.
3. Jansen, M.; Letschert, H. P., Inorganic yellow-red pigments without toxic metals. *Nature* **2000**, *404* (6781), 980-982.
4. Walsh, A.; Yan, Y.; Huda, M. N.; Al-Jassim, M. M.; Wei, S.-H., Band edge electronic structure of BiVO₄: Elucidating the role of the Bi s and V d orbitals. *Chem. Mater.* **2009**, *21* (3), 547-551.
5. Dolgos, M. R.; Paraskos, A. M.; Stoltzfus, M. W.; Yarnell, S. C.; Woodward, P. M., The electronic structures of vanadate salts: Cation substitution as a tool for band gap manipulation. *J. Solid State Chem.* **2009**, *182* (7), 1964-1971.
6. Xu, H.; Li, H.; Wu, C.; Chu, J.; Yan, Y.; Shu, H.; Gu, Z., Preparation, characterization and photocatalytic properties of Cu-loaded BiVO₄. *J. Hazard. Mater.* **2008**, *153* (1–2), 877-884.
7. Zhang, A.; Zhang, J., Effects of europium doping on the photocatalytic behavior of BiVO₄. *J. Hazard. Mater.* **2010**, *173* (1-3), 265–272.
8. Jing, D.; Liu, M.; Shi, J.; Tang, W.; Guo, L., Hydrogen production under visible light by photocatalytic reforming of glucose over an oxide solid solution photocatalyst. *Catal. Commun.* **2010**, *12* (4), 264-267.
9. Kumari, L. S.; Rao, P. P.; Radhakrishnan, A.N., James, V.; Sameera, S.; Koshy, P., Brilliant yellow color and enhanced NIR reflectance of monoclinic BiVO₄ through distortion in VO₄³⁻ tetrahedra. *Sol. Energy Mater. Sol. Cells* **2013**, *112*, 134-143.
10. Zhao, Z.; Li, Z.; Zou, Z., Electronic structure and optical properties of monoclinic clinobisvanite BiVO₄. *Phys. Chem. Chem. Phys.* **2011**, *13* (10), 4746-4753.

11. Muktha, B.; Guru, T. N. G., Effect of substitution in the scheelite-like series, $A_x\text{Ba}_{1-x}\text{Bi}_2\text{Mo}_4\text{O}_{16}$ ($A = \text{Ca}, \text{Sr}, \text{Pb}$). *Mater. Res. Bull.* **2007**, *42*, 2150–2155.
12. Shannon, R. D., Revised effective ionic radii and systematic studies of interatomic distances in halides and chalcogenides. *Acta Crystallogr., Sect. A: Cryst. Phys., Diffr., Theor. Gen. Crystallogr.* **1976**, *32*, 751–757.
13. Wang, S. F.; Yang, H.; Xian, T.; Liu, X. Q., Size-controlled synthesis and photocatalytic properties of YMnO_3 nanoparticles. *Catal. Commun.* **2011**, *12*, 625–628.
14. Sulcová, P.; M. Trojan, M., Thermal analysis of pigments based on Bi_2O_3 . *J. Therm. Anal. Calorim.* **2006**, *84* (3), 737–740.
15. Kudo, A.; Omori, K.; Kato, H., A novel aqueous process for preparation of crystal form-controlled and highly crystalline BiVO_4 powder from layered vanadates at room temperature and its photocatalytic and photophysical properties. *J. Am. Chem. Soc.* **1999**, *121* (49), 11459–11467.
16. Ronnen Levinson, R.; Hashem Akbari, H.; Berdahl, P., Measuring solar reflectance—Part II: Review of practical methods. *Sol. Energy* **2010**, *84*, 1745–1759.
17. Fernández-Osorio, A.; Pineda-Villanueva, E.; Chávez-Fernández, J., Synthesis of nanosized $(\text{Zn}_{1-x}\text{Co}_x)\text{Al}_2\text{O}_4$ spinels: New pink ceramic pigments. *Mater. Res. Bull.* **2012**, *47* (2), 445–452.
18. (a) Kiomarsipour, N.; Shoja Razavi, R.; Ghani, K.; Kioumarsipour, M., Evaluation of shape and size effects on optical properties of ZnO pigment. *Appl. Surf. Sci.* **2013**, *270*, 33–38; (b) van der Linden, E. G.; Malta, L. F. B.; Medeiros, M. E., Evaluation of synthetic routes to pigmentary grade bismuth vanadate. *Dyes Pigm.* **2011**, *90* (1), 36–40; (c) Fernandez-Gonzalez, R.; Julian-Lopez, B.; Cordoncillo, E.; Escribano, P., New insights on the structural and optical properties of Ce-Ti mixed oxide nanoparticles doped with praseodymium. *J. Mater. Chem.* **2011**, *21* (2), 497–504.
19. Sumaletha, N.; Rajesh, K.; Mukundan, P.; Warriar, K. G. K., Environmentally benign sol-gel derived nanocrystalline rod shaped calcium doped cerium phosphate yellow-green pigment. *J. Sol-Gel Sci. Technol.* **2009**, *52* (2), 242–250.

20. Murugan, A. V.; Gaikwad, A. B.; Ravi, V., Preparation of nanocrystalline $\text{Mg}_4\text{Nb}_2\text{O}_9$ by citrate gel method. *Bull. Mater. Sci.* **2006**, *29* (1), 7-9.
21. Anilkumar, M.; Pasrichab, R.; Ravi, V., Synthesis of bismuth oxide nanoparticles by citrate gel method. *Ceram. Int.* **2005**, *31*, 889–891.
22. Lu, W.; Yu, J.; Zhang, Y.; Yu, D.; Zhou, X., Synthesis and photocatalytic properties of BiVO_4 by a citric acid complexation process. *Rare Metals* **2011**, *30* (1), 203-207.
23. Imanaka, N.; Masui, T.; Furukawa, S., Novel nontoxic and environment-friendly inorganic yellow pigments. *Chem. Lett.* **2008**, *37* (1), 104-105.
24. Masui, T.; Honda, T.; Wendusu; Imanaka, N., Novel and environmentally friendly (Bi,Ca,Zn) VO_4 yellow pigments. *Dyes Pigm.* **2013**, *99* (3), 636-641.
25. Xie, H.; Tsuboi, T.; Huang, W.; Huang, Y.; Qin, L.; Seo, H. J., Luminescence and quantum efficiencies of Eu^{3+} -doped vanadate garnets. *J. Am. Ceram. Soc.* **2014**, *97* (5), 1434-1441.
26. Vinke, I. C.; Diepgrond, J.; Boukamp, B. A.; de Vries, K. J.; Burggraaf, A. J., Bulk and electrochemical properties of BiVO_4 . *Solid State Ion.*, **1992**, *57* (1–2), 83-89.
27. Bierlein, J. D.; Sleight, A. W., Ferroelasticity in BiVO_4 . *Solid State Commun.* **1975**, *16* (1), 69-70.
28. Tücks, A.; Beck, H. P., The photochromic effect of bismuth vanadate pigments: Investigations on the photochromic mechanism. *Dyes Pigm.* **2007**, *72* (2), 163-177.
29. Zhao, Y.; Xie, Y.; Zhu, X.; Yan, S.; Wang, S., Surfactant-free synthesis of hyperbranched monoclinic bismuth vanadate and its applications in photocatalysis, gas sensing, and lithium-ion batteries. *Chem. Eur. J.* **2008**, *14* (5), 1601-1606.
30. Iwase, A.; Kudo, A., Photoelectrochemical water splitting using visible-light-responsive BiVO_4 fine particles prepared in an aqueous acetic acid solution. *J. Mater. Chem.* **2010**, *20* (35), 7536-7542.
31. Liu, Y.; Huang, B.; Dai, Y.; Zhang, X.; Qin, X.; Jiang, M.; Whangbo, M.-H., Selective ethanol formation from photocatalytic reduction of carbon dioxide in water with BiVO_4 photocatalyst. *Catal. Commun.* **2009**, *11* (3), 210-213.

32. Nagabhushana, G. P.; Nagaraju, G.; Chandrappa, G. T., Synthesis of bismuth vanadate: its application in H₂ evolution and sunlight-driven photodegradation. *J. Mater. Chem.A.* **2013**, *1* (2), 388-394.
33. Li, H.; Liu, G.; Duan, X., Monoclinic BiVO₄ with regular morphologies: Hydrothermal synthesis, characterization and photocatalytic properties. *Mater. Chem. Phys.* **2009**, *115* (1), 9-13.
34. Zhang, Y.; Li, G.; Yang, X.; Yang, H.; Lu, Z.; Chen, R., Monoclinic BiVO₄ micro-/nanostructures: Microwave and ultrasonic wave combined synthesis and their visible-light photocatalytic activities. *J. Alloys Compd.* **2013**, *551*, 544-550.
35. Endriss, H., Bismuth Vanadates. In *High Performance Pigments*, Wiley-VCH Verlag GmbH & Co. KGaA: **2009**.
36. Liu, J.; Wang, H.; Wang, S.; Yan, H., Hydrothermal preparation of BiVO₄ powders. *Mater. Sci. Eng. B.* **2003**, *104* (1-2), 36-39.
37. Hoffart, L.; Heider, U.; Huggins, R. A.; Witschel, W.; Jooss, R.; Lentz, A., Crystal growth and conductivity investigations on BiVO₄ single crystals. *Ionics* **1996**, *2* (1), 34-38.
38. Bhattacharya, A. K.; Mallick, K. K.; Hartridge, A., Phase transition in BiVO₄. *Mater. Lett.* **1997**, *30* (1), 7-13.
39. Wood, P.; Glasser, F. P., Preparation and properties of pigmentary grade BiVO₄ precipitated from aqueous solution. *Ceram. Int.* **2004**, *30* (6), 875-882.
40. Fan, H.; Wang, D.; Wang, L.; Li, H.; Wang, P.; Jiang, T.; Xie, T., Hydrothermal synthesis and photoelectric properties of BiVO₄ with different morphologies: An efficient visible-light photocatalyst. *Appl. Surf. Sci.* **2011**, *257* (17), 7758-7762.
41. Wang, M.; Liu, Q.; Che, Y.; Zhang, L.; Zhang, D., Characterization and photocatalytic properties of N-doped BiVO₄ synthesized via a sol-gel method. *J. Alloys Compd.* **2013**, *548*, 70-76.
42. García-Pérez, U. M.; Sepúlveda-Guzmán, S.; Martínez-de la Cruz, A., Nanostructured BiVO₄ photocatalysts synthesized via a polymer-assisted coprecipitation method and their photocatalytic properties under visible-light irradiation. *Solid State Sci.* **2012**, *14* (3), 293-298.

43. Galembeck, A.; Alves, O. L., Bismuth vanadate synthesis by metallo-organic decomposition: thermal decomposition study and particle size control. *J. Mater. Sci.* **2002**, *37* (10), 1923-1927.
44. Dunkle, S. S.; Helmich, R. J.; Suslick, K. S., BiVO₄ as a visible-light photocatalyst prepared by ultrasonic spray pyrolysis. *J. Phys. Chem. C.* **2009**, *113* (28), 11980-11983.
45. Chatchai, P.; Kishioka, S.-y.; Murakami, Y.; Nosaka, A. Y.; Nosaka, Y., Enhanced photoelectrocatalytic activity of FTO/WO₃/BiVO₄ electrode modified with gold nanoparticles for water oxidation under visible light irradiation. *Electrochim. Acta.* **2010**, *55* (3), 592-596.
46. Luo, W.; Wang, J.; Zhao, X.; Zhao, Z.; Li, Z.; Zou, Z., Formation energy and photoelectrochemical properties of BiVO₄ after doping at Bi³⁺ or V⁵⁺ sites with higher valence metal ions. *Phys.Chem.Chem.Phys.* **2013**, *15* (3), 1006-1013.
47. Jiang, H.; Dai, H.; Deng, J.; Liu, Y.; Zhang, L.; Ji, K., Porous F-doped BiVO₄: Synthesis and enhanced photocatalytic performance for the degradation of phenol under visible-light illumination. *Solid State Sci.* **2013**, *17*, 21-27.
48. Zhang, L.; Tan, G.; Wei, S.; Ren, H.; Xia, A.; Luo, Y., Microwave hydrothermal synthesis and photocatalytic properties of TiO₂/BiVO₄ composite photocatalysts. *Ceram. Int.* **2013**, *39* (8), 8597-8604.
49. Dragomir, M.; Arčon, I.; Gardonio, S.; Valant, M., Phase relations and optoelectronic characteristics in the NdVO₄-BiVO₄ system. *Acta Mater.* **2013**, *61* (4), 1126-1135.
50. Park, H. S.; Kweon, K. E.; Ye, H.; Paek, E.; Hwang, G. S.; Bard, A. J., Factors in the metal doping of BiVO₄ for improved photoelectrocatalytic activity as studied by scanning electrochemical microscopy and first-principles density-functional calculation. *J. Phys. Chem. C.* **2011**, *115* (36), 17870-17879.
51. Zhao, Z.; Luo, W.; Li, Z.; Zou, Z., Density functional theory study of doping effects in monoclinic clinobisvanite BiVO₄. *Phys. Lett. A.* **2010**, *374* (48), 4919-4927.
52. Akbari, H.; Pomerantz, M.; Taha, H., Cool surfaces and shade trees to reduce energy use and improve air quality in urban areas. *Sol. Energy.* **2001**, *70* (3), 295-310.

53. David, W. I. F.; Glazer, A. M.; Hewat, A. W., The structure and ferroelastic phase transition of BiVO₄. *Phase Transit.* **1979**, *1* (2), 155-169.
54. Zhao, Z.; Li, Z.; Zou, Z., Electronic structure and optical properties of monoclinic clinobisvanite BiVO₄. *Phys.Chem.Chem.Phys.* **2011**, *13* (10), 4746-4753.
55. Shannon, R., Revised effective ionic radii and systematic studies of interatomic distances in halides and chalcogenides. *Acta Crystallogr. Sect. A* **1976**, *32* (5), 751-767.
56. Langford, J. I.; Wilson, A. J. C., Scherrer after sixty years: A survey and some new results in the determination of crystallite size. *J. Appl. Crystallogr.* **1978**, *11* (2), 102-113.
57. Khorsand Zak, A.; Abd. Majid, W. H.; Abrishami, M. E.; Yousefi, R., X-ray analysis of ZnO nanoparticles by Williamson–Hall and size–strain plot methods. *Solid State Sci.* **2011**, *13* (1), 251-256.
58. Frost, R. L.; Henry, D. A.; Weier, M. L.; Martens, W., Raman spectroscopy of three polymorphs of BiVO₄: clinobisvanite, dreyerite and pucherite, with comparisons to (VO₄)³⁻ bearing minerals: namibite, pottsite and schumacherite. *J. Raman Spectrosc.* **2006**, *37* (7), 722-732.
59. Yu, J.; Kudo, A., Effects of structural variation on the photocatalytic performance of hydrothermally synthesized BiVO₄. *Adv. Funct. Mater.* **2006**, *16* (16), 2163-2169.
60. Hardcastle, F. D.; Wachs, I. E., Determination of vanadium-oxygen bond distances and bond orders by Raman spectroscopy. *J. Phys. Chem.* **1991**, *95* (13), 5031-5041.
61. Butler, M. A., Photoelectrolysis and physical properties of the semiconducting electrode WO₂. *J. Appl. Phys.* **1977**, *48* (5), 1914-1920.
62. Zhou, L.; Wang, W.; Liu, S.; Zhang, L.; Xu, H.; Zhu, W., A sonochemical route to visible-light-driven high-activity BiVO₄ photocatalyst. *J. Mol. Catal. A: Chem.* **2006**, *252* (1–2), 120-124.
63. Standard tables for reference solar spectral irradiances: Direct normal and hemispherical on 37° tilted surface. ASTM International: West Conshohocken, PA, **2012**.

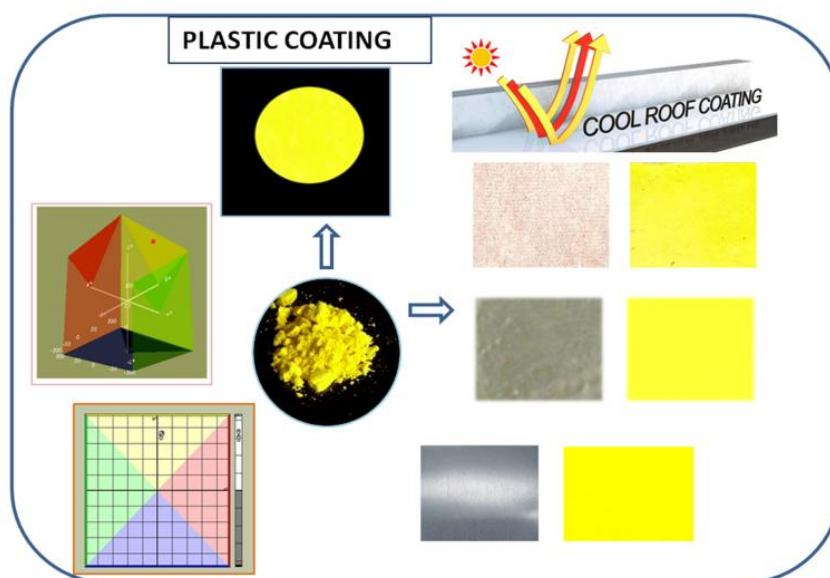
64. (a) Zhang, T.; Oyama, T.; Aoshima, A.; Hidaka, H.; Zhao, J.; Serpone, N., Photooxidative N-demethylation of methylene blue in aqueous TiO₂ dispersions under UV irradiation. *J. Photochem. Photobiol A.* **2001**, *140* (2), 163-172 (b) Zhang, T.; Oyama, T. k.; Horikoshi, S.; Hidaka, H.; Zhao, J.; Serpone, N., Photocatalyzed N-demethylation and degradation of methylene blue in titania dispersions exposed to concentrated sunlight. *Sol. Energy Mater. Sol. Cells.* **2002**, *73* (3), 287-303.
65. Rauf, M.A.;Meetani, M.A.;Khaleel ,A.;Ahmed.A.; Photocatalytic degradation of methylene blue using a mixed catalyst and product analysis by LC/MS. *Chem.Eng. J.* **2010**, *157*(2-3), 373-378.
66. Huang, F.; Chen, L.; Wang H.; Yan, Z.; Analysis of the degradation mechanism of methylene blue by atmospheric pressure dielectric barrier discharge plasma. *Chem. Eng. J.* **2010**, *162*, 250–256.

CHAPTER 6

APPLICATION STUDY OF POTENTIAL YELLOW PIGMENTS

Overview

Various less-toxic inorganic pigments were synthesized with a viewpoint of alternatives to the existing toxic inorganic pigments in the market. Among them, selected pigments having superior coloristic properties demonstrate their coloristic performance on certain substrates. These pigments exhibit good light resistance and chemical stability for various applications.



6.1 Introduction

High-quality pigments are needed by the paint industry almost exclusively. When choosing a pigment for a particular application, several points have to be considered.

1. Coloring properties: color, tinting strength or lightening power, hiding power.
2. General chemical and physical properties: chemical composition, moisture and salt content, content of water-soluble and acid-soluble matter, particle size, density, and hardness.
3. Stability properties: resistance toward light, weather, heat, and chemicals, anticorrosive properties, retention of gloss.
4. Behavior in binders: interaction with the binder properties, dispersibility, special properties in certain binders, compatibility, and solidifying effect.

When a photon enters a pigmented film, it may be absorbed or scattered by a pigment particle or simply pass through the film (the binder being assumed to be nonabsorbent) shown in Fig. 6.1. The important physical-optical properties of pigments are therefore their light absorption and light-scattering properties. If absorption is very small compared with scattering, the pigment is a white pigment. If absorption is much higher than scattering over the entire visible region, the pigment is a black pigment. In a colored pigment, absorption (and usually scattering) is selective (i.e., dependent on wavelength).¹

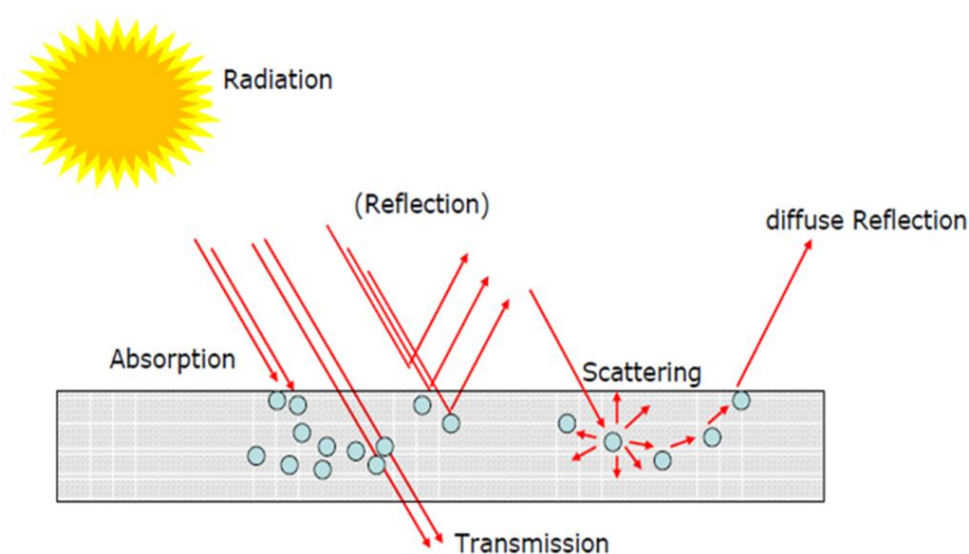


Fig. 6.1 Interaction of pigmented surface with sun-radiation.

Inorganic pigments are highly appreciated in coatings because of their:

1. High opacity
2. Easy-dispersion
3. Excellent light and weather fastness
4. Excellent organic solvent resistance
5. Good heat fastness (when required)

Infrared reflective pigments are the pigments of choice when colored coatings are required that minimize the heat retained in the protective coating. A cool coating reflects a high percentage of incident infrared radiation, while transmitting high levels in the visible spectra. This will reduce the amount of solar energy entering buildings which results on a cool surface when exposed to the sun. In hot summer time, cool coatings will help to keep the roof temperature down, minimizing the energy required to keep homes and buildings maintained at a comfortable temperature.

In automotive applications, for example, continuous exposure to direct sun could result in degradation of appearance and a reduced lifespan for convertible rooftops, paints, dashboards, leather and vinyl seats, steering wheels, and interior and exterior door handles. Overheated roof surfaces can drive higher energy costs due to increased cooling requirements, and they can have a potential negative environmental impact by contributing to the urban heat island effect.

The solar-opaque white surface is the coolest type of roofing surface.² The reflectance of nonwhite surfaces in the IR spectrum can be maximized by coloring the top coat with IR reflective inorganic pigments that strongly reflect the wavelengths in infrared region in addition to reflecting some visible light selectively. A large number of field studies have established the effects of the large-scale use of cool coatings on the reduction of energy use for cooling.³ The cooling energy savings due to the application of cool coatings is found to be between 12% and 25% for residential buildings, between 5% and 18% for office buildings and between 7% and 17% for commercial buildings.⁴

As mentioned in introductory chapter some of the benefits of infrared reflective coatings are

General:

- (i) Longer life-cycle due to less polymer degradation and thermal expansion due to lower temperature.
- (ii) Aesthetically pleasing colors.
- (iii) Cooler to touch for better handling
- (iv) Improved system durability and less thermal degradation.

Roofing:

- (i) Less heat to transfer into buildings.
- (ii) Reduced 'Urban heat island effect'.
- (iii) Low energy demand for air conditioning, particularly in equatorial regions.
- (iv) Help to reduce the production of air pollutants from electricity generation.⁵

In this chapter, selected pigments with best coloristic properties demonstrate their coloring as well as IR reflecting property on various substrates. The light fastness and chemical resistance of these pigments have been evaluated.

6.2 Methods

The color coordinates of coatings were determined using a portable spectrophotometer Miniscan EZ 4000S (Hunter Lab USA). The thickness of the paint films was estimated using Bruker's DektakXT stylus profiler. IR reflectance of the coated and uncoated specimens was measured according to "ASTM E903-12: standard test method for solar absorption, reflectance, and transmittance of materials using integrating spheres"⁶, using a spectrophotometer (Shimadzu, model UV 3600) equipped with an integrating sphere. The standard reference material was polytetrafluoroethylene (PTFE) in the 700 to 2500 nm range with a step size of 5 nm. The IR solar reflectance in the wavelength range from 700 to 2500 nm was calculated in accordance with the ASTM standard number G173-03.⁷ The NIR solar reflectance is expressed as the integral of the percent reflectance times the solar irradiance divided by the integral of the solar irradiance when integrated over the 700-2500 nm range as shown in the formula,

$$R = \frac{\int_{700}^{2500} r(\lambda)i(\lambda)d\lambda}{\int_{700}^{2500} i(\lambda)d\lambda} \quad (6.1)$$

where $r(\lambda)$ is the spectral reflectance obtained from the experiment and $i(\lambda)$ is the standard solar spectrum ($\text{Wm}^{-2} \text{nm}^{-1}$) obtained from the standard.

Evaluation of the IR reflectance of the pigmented coatings

Non white cool coatings that absorb less IR radiation can provide coatings similar in colour to that of conventional roofing materials, but with high solar reflectance. Brady and Wake presented the basic method for creating a coating with high IR reflectance⁸: color an otherwise transparent topcoat with pigments that weakly absorb and (optionally) strongly backscatter IR radiation, adding an IR-reflective basecoat (e.g., titanium dioxide rutile white) if both the topcoat and the substrate weakly reflect IR radiation (Fig. 6.2).

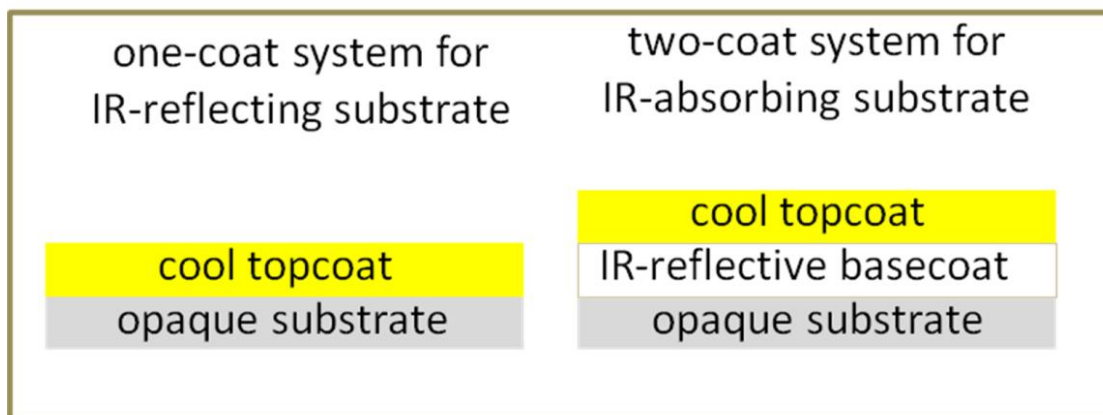


Fig. 6.2 Schematics of one-coat and two-coat systems.

6.3 Application study of $\text{Li}_{0.15}\text{RE}_{0.15}\text{Bi}_{0.7}\text{Mo}_{0.3}\text{V}_{0.7}\text{O}_4$ pigment (RE = La, Gd)

To study the potential of the above pigments as colorants for various applications, the color characteristics on plastics and IR reflectance study on asbestos cement roofing sheet, concrete cement and aluminium metal panel are evaluated.

6.3.1 Coloration of plastics

For the coloration of plastics, polymethyl methacrylate (PMMA) was used as the polymer matrix for making the pigmented compact. Polymethyl methacrylate (PMMA) is a versatile acrylic polymer which is transparent to visible light. Acrylic plastics have strong weather resistance that is well suited for automotive rear light assemblies, lenses, aircraft cockpits, dentures and windshields.⁹

Firstly, the color conferring ability of the pigment having the best color with 1% NaCl mineralizer added composition $\text{Li}_{0.15}\text{La}_{0.15}\text{Bi}_{0.7}\text{Mo}_{0.3}\text{V}_{0.7}\text{O}_4$ ($L^* = 85.49$, $a^* = -4.78$, $b^* = 85.25$) was selected. The pigment was ultrasonicated in an alcohol-water (1:4) mixture for 10 minutes to ensure complete dispersion of the pigment particles. A viscous solution of PMMA (90 wt%) was made using a conventional electric coil heater and 10 wt% of the pigment was slowly added with stirring and converted to a thick paste. The paste was then transferred in a mould and compressed into a cylindrical disc shown in Fig. 6.3. The color coordinates measured at different parts of the disc revealed uniform color values indicating uniform dispersion of pigment in PMMA.

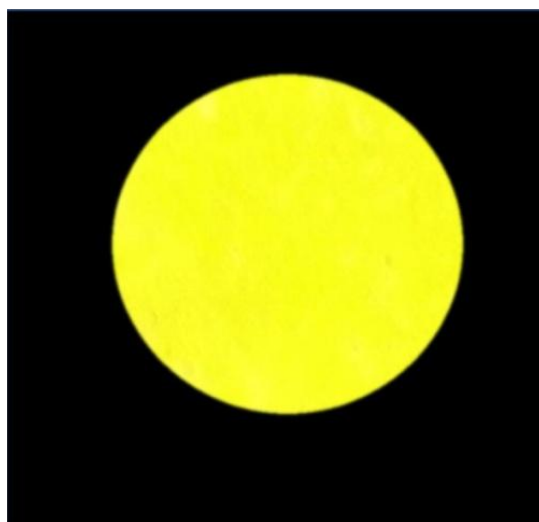


Fig. 6.3 Photograph of 10 wt% $\text{Li}_{0.15}\text{La}_{0.15}\text{Bi}_{0.7}\text{Mo}_{0.3}\text{V}_{0.7}\text{O}_4$ + PMMA.

Light resistance studies

The light resistance of the typical pigmented polymers was tested by exposing it to natural sunlight (12 h exposure, 45° angle facing the sun, 25 days) at the interval of one day and measured the color coordinates. The $L^*a^*b^*$ values of pigmented compact were found to be nearly same as that of the unexposed sample which indicates that the pigmented polymer is resistant to light.

Table 6.1 Color coordinates of 10 wt% $\text{Li}_{0.15}\text{La}_{0.15}\text{Bi}_{0.7}\text{Mo}_{0.3}\text{V}_{0.7}\text{O}_4$ pigment in PMMA on exposure to sunlight

Time duration	L^*	a^*	b^*	C^*	h^0
0	82.46	-2.36	78.61	78.64	91.73
Day 5	82.34	-2.31	78.55	76.89	87.55
Day 10	82.13	-2.11	77.84	77.87	88.45
Day 15	81.74	-1.89	77.23	77.25	88.60
Day 20	81.68	-2.01	77.67	77.70	80.23
Day 25	81.29	-1.76	77.45	77.47	88.70

6.3.2 IR reflectance study on an asbestos cement roofing sheet

In order to assess the performance of the pigments as cool colorants for reducing the heat built-up, the IR reflectance of the designed pigments by coating on to a roofing material like asbestos cement sheet (made up of small amounts of asbestos fibers locked in cement slurry) was evaluated. The use of cement-based materials in roofs and walls is common in tropical climates as they are highly resistant to severe weather. However, unprotected cement-based materials manifest undesirable thermal properties after a short time of use.¹⁰ Asbestos cement roofing is widely used in developing, tropical countries. This material is common in low-cost housing, industrial and farm buildings. The relevance of its use has served as motivation for the study of the IR reflectance of cool colored coatings, composed of infrared reflective pigments.

The IR reflectance of 1% CaF_2 added $\text{Li}_{0.15}\text{La}_{0.15}\text{Bi}_{0.7}\text{Mo}_{0.3}\text{V}_{0.7}\text{O}_4$ pigment is 94%. The particular pigment was selected to prepare IR reflecting coatings on a

building roofing material like asbestos cement sheet. The coating was undertaken in a two-step process. In the first step, a small strip of asbestos is pre-coated with TiO_2 , an inexpensive white pigment possessing high IR reflectance. In the second step, the designed typical pigment is applied to the pre-coated substrate material. The pigment samples were ground and was ultrasonicated (Vibronics, 250W, India) for 10 min to ensure the complete dispersion of the pigment particles in acrylic acid using polyurethane as a binder. The resulted viscous solution was coated on the asbestos cement sheet surface and was allowed to dry in an oven at 150°C . The thickness of the films was in 50–65 μm range.

The IR reflectance of the typical pigment sample coated directly over the roofing material and coated over a base coat of TiO_2 on the roofing material is shown in Fig. 6.4. The corresponding IR solar reflectance spectrum is shown in Fig. 6.5. The photographs of the resultant coating samples are depicted in Fig. 6.6. The results clearly indicate that bare asbestos possesses a low IR reflectance of 44%. The yellow pigment coated over bare asbestos possesses a IR reflectance of 85% whereas the yellow pigment over a TiO_2 base coat exhibited a IR reflectance of 97%.

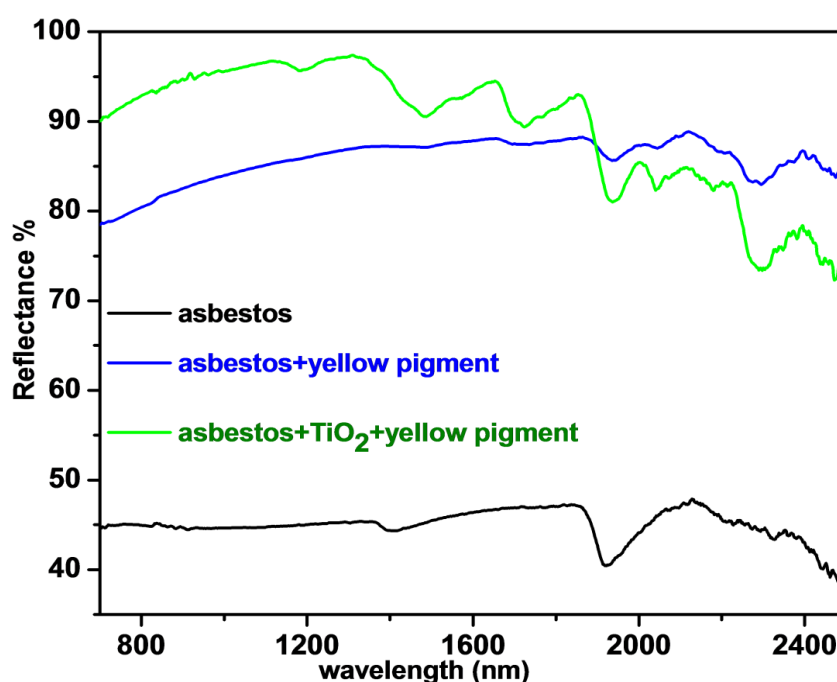


Fig. 6.4 IR reflectance spectra of pigment coated asbestos cement sheets with and without TiO_2 base coat.

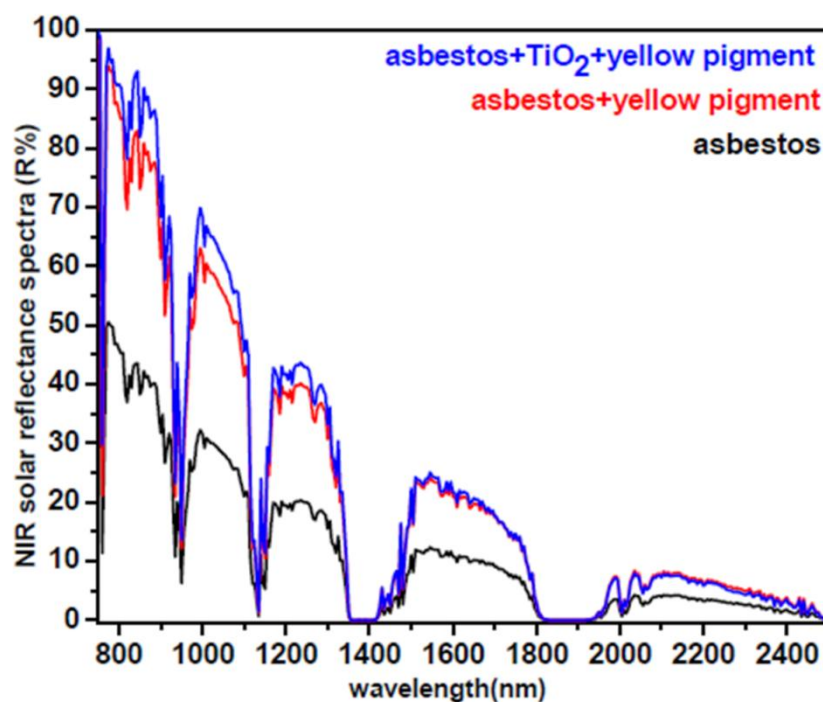


Fig. 6.5 IR solar reflectance spectra of pigment coated asbestos cement sheets with and without TiO_2 base coat.

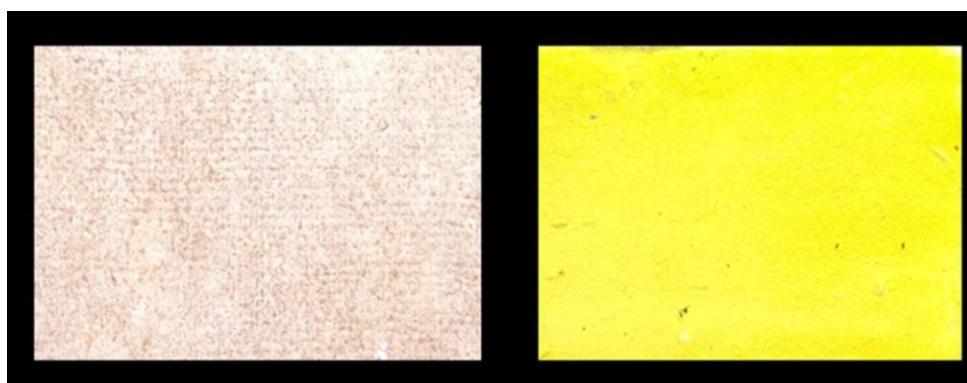


Fig. 6.6 Photographs of bare asbestos and pigment coated asbestos.

Light resistance studies

The light resistance of the typical pigmented coating over asbestos was tested by exposing it to natural sunlight (12 h exposure, 45° angle facing the sun, 25 days) at the interval of five days and measured the color coordinates. The $L^*a^*b^*$ values of pigmented coating were found to be nearly same as that of the unexposed sample which indicates its resistance to light (Table 6.2).

Table 6.2 Color coordinates of $\text{Li}_{0.15}\text{La}_{0.15}\text{Bi}_{0.7}\text{Mo}_{0.3}\text{V}_{0.7}\text{O}_4$ pigment in asbestos cement sheet on exposure to sunlight.

Time duration	L^*	a^*	b^*	ΔE^*_{ab}
0	84.71	-2.65	69.47	-
Day 5	84.33	-2.51	69.41	0.41
Day 10	84.21	-2.54	69.38	0.52
Day 15	84.25	-2.48	69.29	0.52
Day 20	84.19	-2.41	69.22	0.62
Day 25	84.03	-2.39	69.21	0.77

6.3.3 IR reflectance study on concrete cement

The particular pigments $\text{Li}_{0.10}\text{La}_{0.10}\text{Bi}_{0.8}\text{Mo}_{0.2}\text{V}_{0.8}\text{O}_4$ and $\text{Li}_{0.10}\text{Gd}_{0.10}\text{Bi}_{0.8}\text{Mo}_{0.2}\text{V}_{0.8}\text{O}_4$ were selected to prepare IR reflecting coatings. Their performance was tested on a building roofing material, concrete cement. The coating was done in a two-step process. In the first step, the concrete cement block is precoated with TiO_2 , an inexpensive white pigment possessing high IR reflectance. In the second step, the designed typical pigment is applied to the precoated substrate material. The pigment samples were ground and was ultrasonicated (Vibronics, 250W, India) for 10 min to ensure the complete dispersion of the pigment particles in acrylic acid using polyurethane as a binder. The resulted viscous solution was coated on the concrete sheet surface and was allowed to dry in an oven at 150 °C. The thickness of the films was in 40–45 μm range.

The IR reflectance spectrum of the pigments coated over bare concrete cement surface is shown in Fig. 6.7. The IR solar reflectance spectra determined in accordance with ASTM standard G173-0323 is shown in Fig. 6.8, and the photographs of the resultant coating samples are shown in the inset. The results clearly indicate that a bare concrete surface possesses a low IR reflectance of 27% and IR solar reflectance of 25%. The results point out that these coatings can enhance the IR solar reflectance (Table 6.3). These nonwhite coatings can reduce the surface temperature of the roof and lead to energy savings.

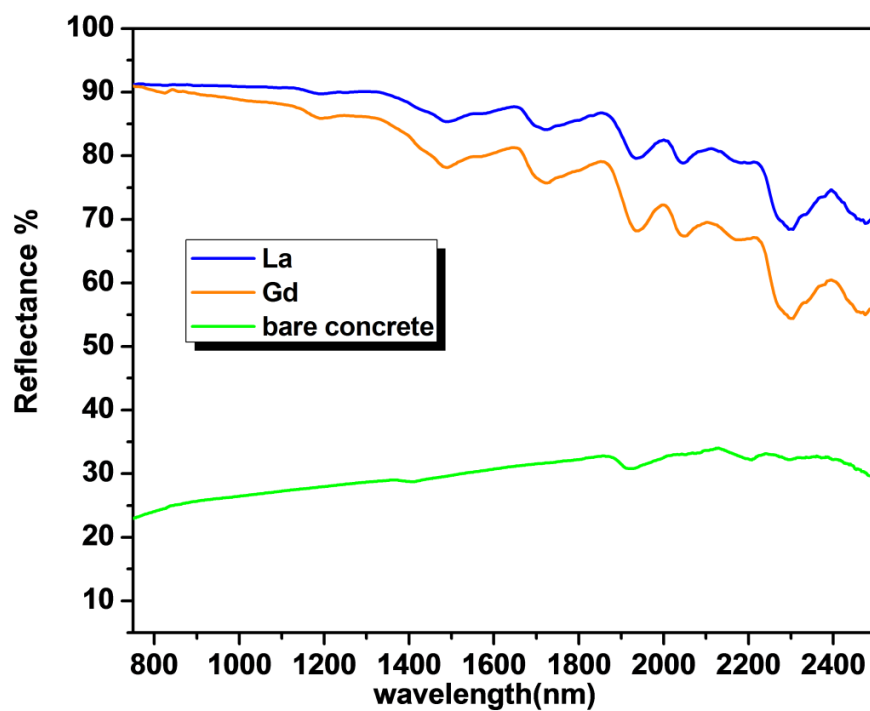


Fig. 6.7 IR reflectance spectra of $\text{Li}_{0.10}\text{RE}_{0.10}\text{Bi}_{0.8}\text{Mo}_{0.2}\text{V}_{0.8}\text{O}_4$; RE = La, Gd pigments coated over concrete cement surface.

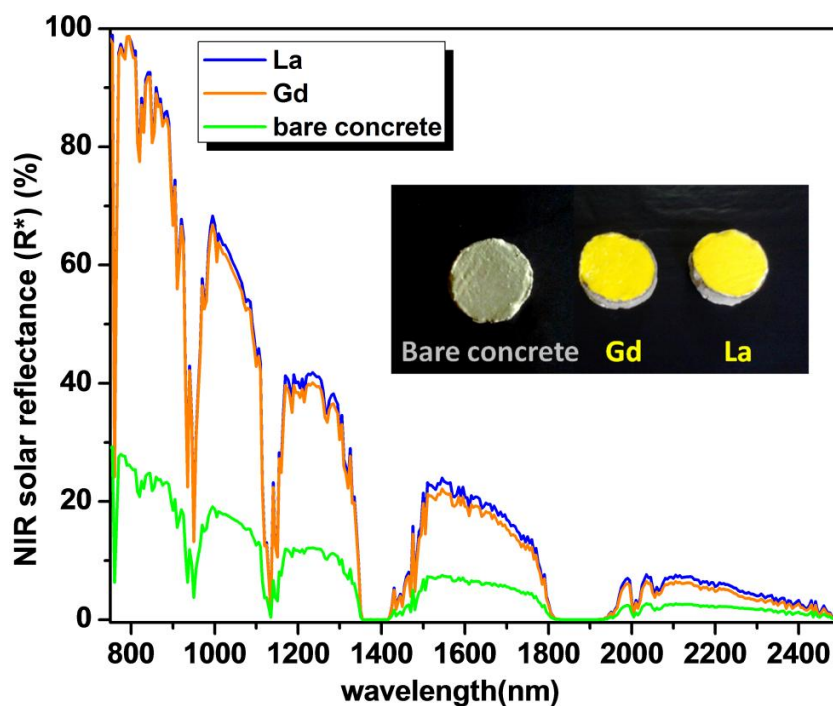


Fig. 6.8 IR solar reflectance spectra of $\text{Li}_{0.10}\text{RE}_{0.10}\text{Bi}_{0.8}\text{Mo}_{0.2}\text{V}_{0.8}\text{O}_4$; RE = La, Gd pigments coated over concrete cement surface (inset: photographs of samples).

Table 6.3 IR solar reflectance and color coordinates of $\text{Li}_{0.10}\text{RE}_{0.10}\text{Bi}_{0.8}\text{Mo}_{0.2}\text{V}_{0.8}\text{O}_4$ pigments; RE = La, Gd coated over concrete cement surface

Parameter	La(concrete)	Gd(concrete)
<i>L</i>	86.24	87.73
<i>a</i> *	3.22	3.79
<i>b</i> *	90.98	86.87
<i>C</i> *	91.04	86.95
<i>h</i> ⁰	87.98	87.50
IR R (%)	90	87
IR R*(%)	89	86

Light resistance studies

The light resistance of the typical pigmented $\text{Li}_{0.15}\text{La}_{0.15}\text{Bi}_{0.7}\text{Mo}_{0.3}\text{V}_{0.7}\text{O}_4$ coating over concrete cement surface was tested by exposing it to natural sunlight (12 h exposure, 45° angle facing the sun, 25 days) at the interval of five days and measured the color coordinates. The ΔE^*_{ab} values of pigmented coating were found to be negligible which indicates it is resistant to light (Table 6.4).

Table 6.4 Color coordinates of $\text{Li}_{0.15}\text{La}_{0.15}\text{Bi}_{0.7}\text{Mo}_{0.3}\text{V}_{0.7}\text{O}_4$ pigment in concrete cement sheet on exposure to sunlight

Time duration	<i>L</i> *	<i>a</i> *	<i>b</i> *	ΔE^*_{ab}
0	86.24	3.22	90.98	-
Day 5	86.79	3.30	90.86	0.56
Day 10	86.48	3.27	90.56	0.47
Day 15	86.60	3.30	90.49	0.61
Day 20	86.48	3.11	90.37	0.66
Day 25	86.51	3.39	90.31	0.74

6.3.4 IR reflectance study on aluminium metal panel

Conventional colored coatings used in automobiles increase the interior temperatures. This leads to increased air conditioning usage, which affects the fuel consumption of the vehicle. The performance of particular pigments $\text{Li}_{0.10}\text{La}_{0.10}\text{Bi}_{0.8}\text{Mo}_{0.2}\text{V}_{0.8}\text{O}_4$ and $\text{Li}_{0.10}\text{Gd}_{0.10}\text{Bi}_{0.8}\text{Mo}_{0.2}\text{V}_{0.8}\text{O}_4$ was tested on an aluminum metal sheet to evaluate their applicability in automobiles. The coating procedure was done in a single step procedure where TiO_2 was not used as base coat.

The IR solar reflectance values obtained for $\text{Li}_{0.10}\text{La}_{0.10}\text{Bi}_{0.8}\text{Mo}_{0.2}\text{V}_{0.8}\text{O}_4$ and $\text{Li}_{0.10}\text{Gd}_{0.10}\text{Bi}_{0.8}\text{Mo}_{0.2}\text{V}_{0.8}\text{O}_4$ were 71 and 67, respectively. The IR reflectance of the coatings over metal sheets is illustrated in Fig. 6.9. The IR solar reflectance spectra determined in accordance with ASTM standard G173-03 of the same is shown in Fig.6.10, and the photographs of the resultant coating samples are shown in the inset. The results point out that these coatings can enhance the IR solar reflectance. The color coordinates of these coatings are shown in Table 6.5. The color values indicate enhanced coloration to the concrete and metal substrate. These cool light colored coatings can thus reduce the energy consumption required for cooling the interior of automobiles and buildings.

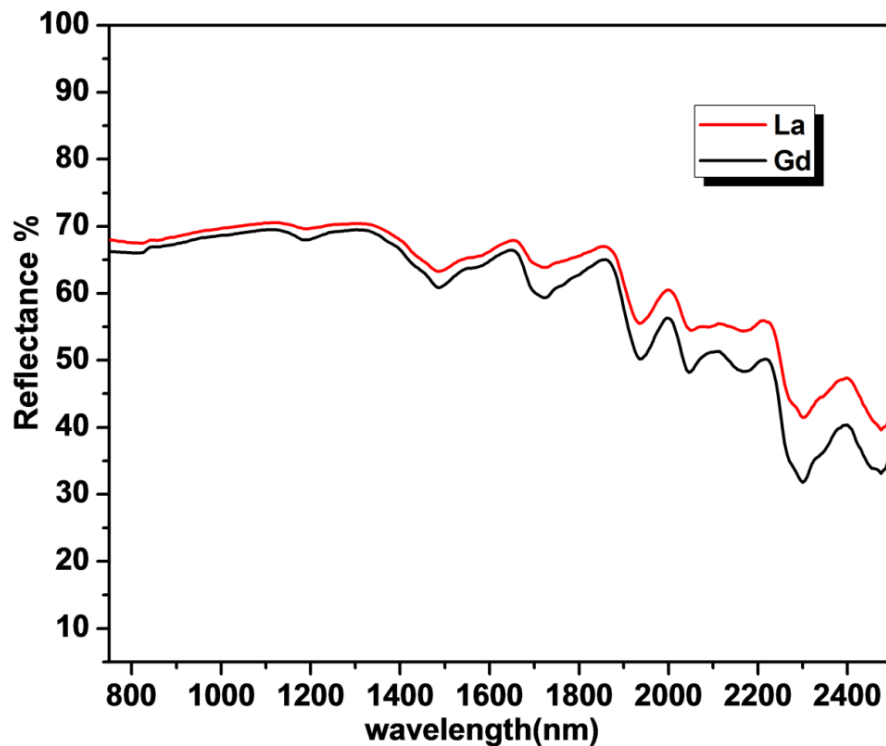


Fig. 6.9 IR reflectance spectra of $\text{Li}_{0.10}\text{RE}_{0.10}\text{Bi}_{0.8}\text{Mo}_{0.2}\text{V}_{0.8}\text{O}_4$; RE = La, Gd pigments coated over a metal panel.

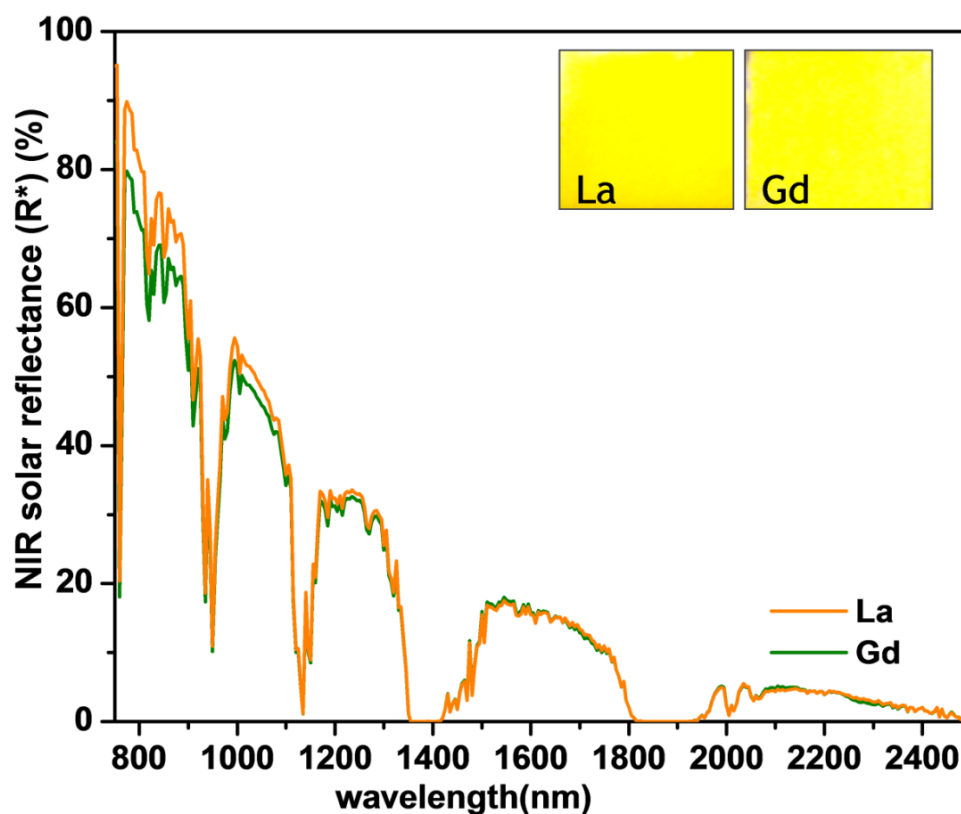


Fig. 6.10 IR solar reflectance spectra of $\text{Li}_{0.10}\text{RE}_{0.10}\text{Bi}_{0.8}\text{Mo}_{0.2}\text{V}_{0.8}\text{O}_4$ pigments; RE = La, Gd coated over a metal panel (inset: photographs of samples).

Table 6.5 IR solar reflectance and color coordinates of $\text{Li}_{0.10}\text{RE}_{0.10}\text{Bi}_{0.8}\text{Mo}_{0.2}\text{V}_{0.8}\text{O}_4$ pigments; RE = La, Gd coated over metal panel

Parameter	La(metal)	Gd(metal)
L	79.63	79.37
a^*	-2.33	-1.98
b^*	83.71	76.28
C^*	83.75	76.30
h^0	91.61	91.49
IR R (%)	70	69
IR R*(%)	71	67

6.4 Chemical resistance tests of $\text{Li}_{0.15}\text{RE}_{0.15}\text{Bi}_{0.7}\text{Mo}_{0.3}\text{V}_{0.7}\text{O}_4$ pigment (RE = La, Gd)

The acid/alkali/water resistance of the typical $\text{Li}_{0.10}\text{La}_{0.10}\text{Bi}_{0.8}\text{Mo}_{0.2}\text{V}_{0.8}\text{O}_4$ and $\text{Li}_{0.10}\text{Gd}_{0.10}\text{Bi}_{0.8}\text{Mo}_{0.2}\text{V}_{0.8}\text{O}_4$ pigment was carried out in 10% HCl, NaOH or H_2O . A pre-weighed amount of the pigment was treated with acid/alkali or water and soaked for half an hour with constant stirring using a magnetic stirrer. The pigment powder was then filtered, washed with water, dried and weighed. Negligible weight loss of pigment was noticed for the acid, alkali and water tested. The color coordinates of the resultant tested sample was measured and compared with the untreated sample. The total color difference was calculated and is summarized in Table 6.6. The negligible values of reveal that the pigments are chemically stable towards the acid/alkali/ H_2O tested. The industrially acceptable limits of are as follows: when $\Delta E_{ab}^* \leq 1$ unit indicate that the color change is almost indistinguishable from the original color, whereas, $\Delta E_{ab}^* \leq 5$ units are considered to be very good.

Table 6.6 Color coordinates of $\text{Li}_{0.10}\text{RE}_{0.10}\text{Bi}_{0.8}\text{Mo}_{0.2}\text{V}_{0.8}\text{O}_4$; (RE = La, Gd) pigment after acid/alkali resistance tests

RE	Acid/Alkali	ΔL^*	Δa^*	Δb^*	ΔE_{ab}^*
La	HCl	0.5	0.7	0.4	0.95
La	NaOH	0.4	0.5	0.3	0.71
La	H_2O	0.2	0.4	0.1	0.45
Gd	HCl	0.6	0.7	0.5	1.04
Gd	NaOH	0.7	0.3	0.4	0.86
Gd	H_2O	0.3	0.1	0.2	0.37

$$\Delta E_{ab}^* = \sqrt{(\Delta L^*)^2 + (\Delta a^*)^2 + (\Delta b^*)^2} \quad (6.2)$$

6.5 Application study of $(\text{BiV})_{0.975}\text{Nb}_{0.025}\text{O}_4$ pigment over concrete cement

The particular pigment $(\text{BiV})_{0.975}\text{Nb}_{0.025}\text{O}_4$ calcined at 500°C was selected for application studies on a roofing material, concrete cement to evaluate the IR reflective properties. The coating procedure is same as described in the earlier part. The thickness of the films was in 55–65 μm range.

The IR reflectance spectrum of the pigment $(\text{BiV})_{0.975}\text{Nb}_{0.025}\text{O}_4$ coated over bare concrete cement surface is shown in Fig. 6.11. The IR solar reflectance spectra determined in accordance with ASTM standard G173-03 is shown in Fig.6.12 and the photographs of the resultant coating sample is shown in Fig. 6.13. A bare concrete surface possesses a low IR reflectance of 27% and IR solar reflectance of 25% while the $(\text{BiV})_{0.975}\text{Nb}_{0.025}\text{O}_4$ pigment coated over TiO_2 base coat provides a IR reflectance of 81 % and IR solar reflectance of 79%. The pigment also imparts its color well to the substrate under study as revealed by the color coordinates shown in Table 6.7.

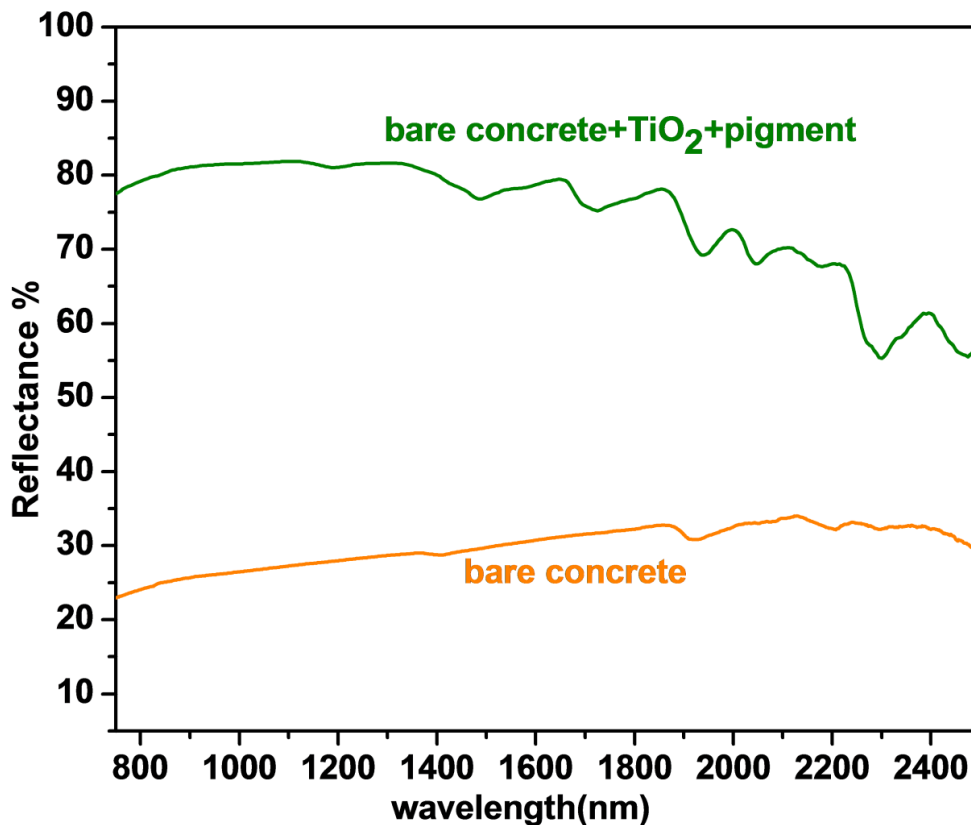


Fig. 6.11 IR reflectance spectra of $(\text{BiV})_{0.975}\text{Nb}_{0.025}\text{O}_4$ pigment coated over concrete cement surface.

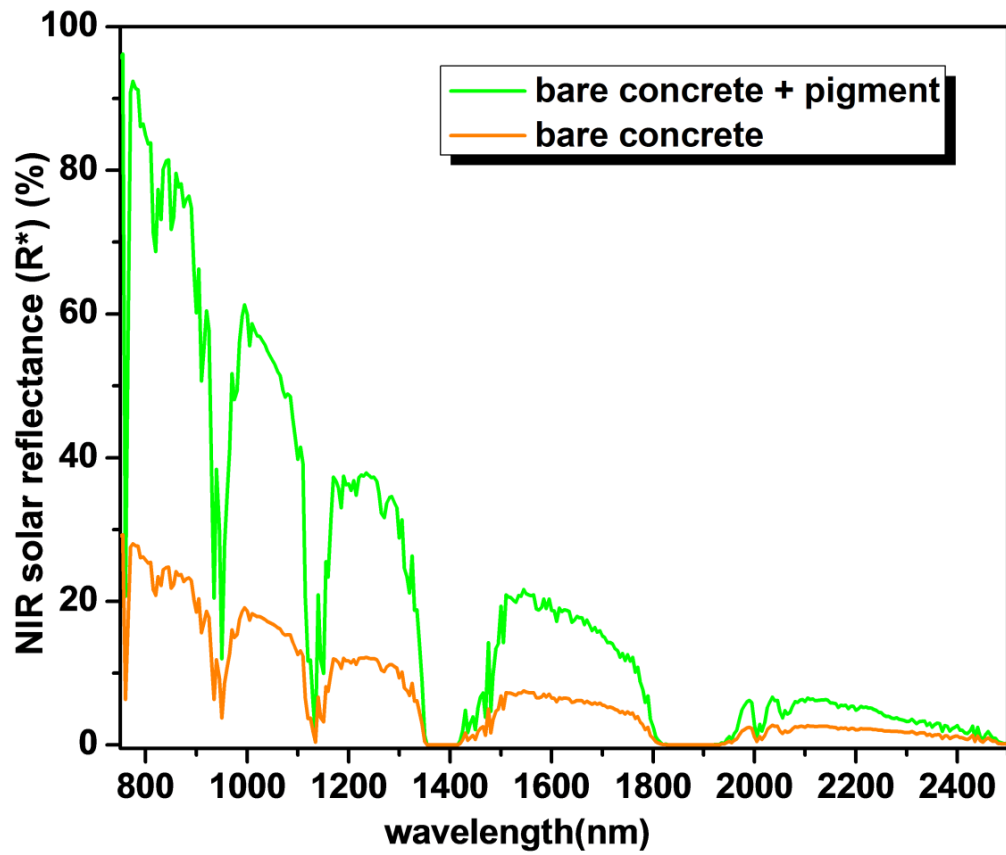


Fig. 6.12 IR solar reflectance spectra of $(\text{BiV})_{0.975}\text{Nb}_{0.025}\text{O}_4$ pigment coated over concrete cement surface.

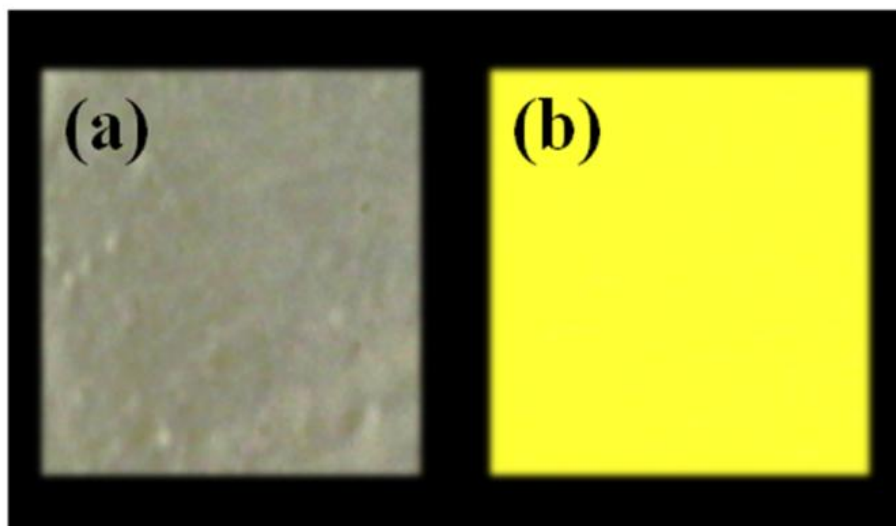


Fig. 6.13 Photographs of bare concrete and pigment coated concrete.

Table 6.7 IR solar reflectance and color coordinates of $(\text{BiV})_{0.975}\text{Nb}_{0.025}\text{O}_4$ pigments coated over concrete cement surface

Parameter	$(\text{BiV})_{0.975}\text{Nb}_{0.025}\text{O}_4$
L	77.75
a^*	4.21
b^*	81.43
C^*	81.54
h^θ	87.04
IR R (%)	81
IR R*(%)	79

A three dimensional color plot using EasyMatch QC software coupled to Miniscan EZ 4000S spectrophotometer of the $(\text{BiV})_{0.975}\text{Nb}_{0.025}\text{O}_4$ pigment coated over concrete cement surface is illustrated in Fig. 6.13.

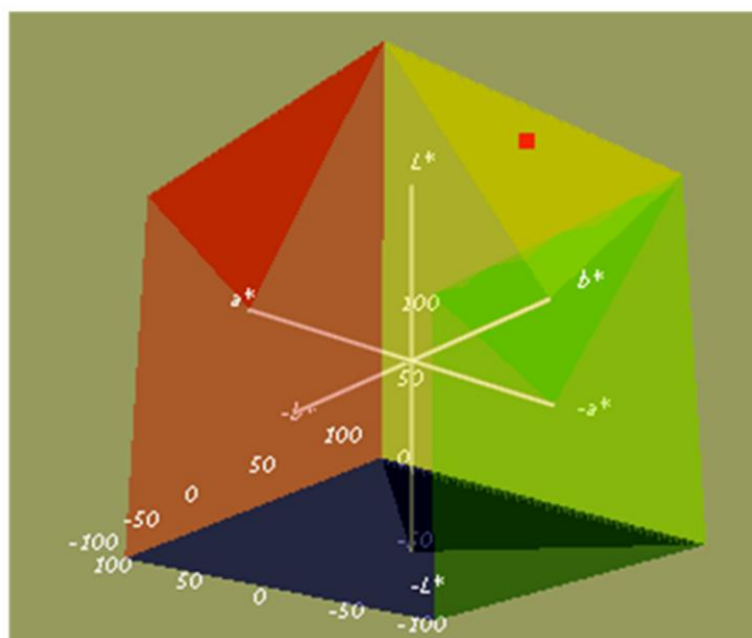


Fig. 6.14 Three dimensional color plot of $(\text{BiV})_{0.975}\text{Nb}_{0.025}\text{O}_4$ pigment.

Light resistance studies

The light resistance of the typical $(\text{BiV})_{0.975}\text{Nb}_{0.025}\text{O}_4$ pigment over concrete cement surface was conducted as described in the earlier part of this chapter. The ΔE_{ab}^* values of pigmented coating were found to be negligible which indicates its resistance to light (Table 6.8).

Table 6.8 Color coordinates of $(\text{BiV})_{0.975}\text{Nb}_{0.025}\text{O}_4$ pigment in concrete cement sheet on exposure to sunlight.

Time duration	L^*	a^*	b^*	ΔE_{ab}^*
0	77.75	4.21	81.43	-
Day 5	77.68	4.19	81.29	0.15
Day 10	77.63	4.18	81.31	0.17
Day 15	77.71	4.12	81.30	0.16
Day 20	77.59	4.09	81.18	0.32
Day 25	77.55	4.03	81.01	0.49

6.6 Chemical resistance tests of $(\text{BiV})_{0.975}\text{Nb}_{0.025}\text{O}_4$ pigment

The acid/alkali resistance of the typical $(\text{BiV})_{0.975}\text{Nb}_{0.025}\text{O}_4$ pigment was carried out in 10% HCl, NaOH or water as described earlier in this chapter. The total color difference calculated is summarized in Table 6.9. The negligible values reveal that the pigments are chemically stable towards the acid/alkali tested.

Table 6.9 Color coordinates of $(\text{BiV})_{0.975}\text{Nb}_{0.025}\text{O}_4$ pigment after acid/alkali resistance tests

Acid/Alkali	ΔL^*	Δa^*	Δb^*	ΔE_{ab}^*
HCl	0.3	0.9	0.5	1.07
NaOH	0.2	0.4	0.8	0.92
H ₂ O	0.2	0.3	0.4	0.53

6.7 Conclusions

The developed pigments could confer their color as well as IR reflecting properties to the substrate under study. These pigments as cool coatings can lead to sustainability of roofs. These cool colored coatings can thus reduce the energy consumption required for cooling the interior of automobiles and buildings. These cool colored coatings can also be used to manufacture other cool colored building and paving materials. The properties of these yellow inorganic pigments suggest a passive solution that combines energy efficiency and the aesthetic appeal of the products.

6.8 References

1. Buxbaum, G.; Pfaff, G., Eds.; Introduction. In *Industrial Inorganic Pigments*. WILEY-VCH Verlag GmbH & Co KGaA, Weinheim, **2005**.
2. Seneca, A.; Santamouris, A.; Miller, W.; Livada, A. In A comparative study of the thermal performance of reflective coatings for the urban environment, *Proceedings of the International Conference “Passive and Low Energy Cooling for the Built Environment”* Greece, **2005**.
3. (a) Rosenfeld, J.; Romm, J.; Akbari, H.; Pomerantz, M., Cool communities: strategies for heat islands mitigation and smog reduction. *Energy Build.* **1998**, *28*, 51–62; (b) Taha, H.; Konopacki, S.; Gabersek, S., Impacts of large-scale surface modifications on meteorological conditions and energy use: a 10-region modeling study. *Theor. Appl. Climatol.* **1999**, *62*, 175–185; (c) Akbari, H.; Taha, H., The impact of trees and white surfaces on residential heating and cooling energy use in four Canadian cities. *Energy* **1992**, *17*(2), 141–149.
4. Akbari, H.; Konopacki, S., Calculating energy saving potentials from heat island reduction strategies. *Energy Policy* **2005**, *33*, 751–756.
5. Bendiganavale, A. K.; Malshe, V. C., Infrared Reflective Inorganic Pigments. *Recent Patents on Chemical Engineering* **2008**, *1*, 67-69.
6. ASTM E903-12 :Standard Test Method for Solar Absorptance, Reflectance, and Transmittance of Materials Using Integrating Spheres ASTM International: West Conshohocken, PA, **2012**.
7. ASTM G 173-03: Standard tables for reference solar spectral irradiances: Direct normal and hemispherical on 37° tilted surface. ASTM International: West Conshohocken, PA, **2012**.
8. Brady, R. F.; Wake, L. V., Principles and formulations for organic coatings with tailored infrared properties. *Prog. Org. Coat.* **1992**, *20* (1), 1-25.
9. Harper, C. A.; Petrie, E. M., A. In *Plastics Materials and Processes : A Concise Encyclopedia*, John Wiley & Sons, Inc.: **2003**; 1-48.
10. Alvarado, J. L.; Martinez, E., Passive cooling of cement-based roofs in tropical climates. *Energy Build.* **2008**, *40* (3), 358–364.

CHAPTER 7

CONCLUSIONS AND FUTURE SCOPE OF THE WORK

Overview

Significant conclusions derived from the work based on development of eco-friendly yellow inorganic pigments for coloring applications are presented in this concluding chapter. Future scope of this work is also presented here.

7.1 Conclusions

The development of eco-friendly inorganic pigments has become a matter of prime focus as industry has realized the potential of pigments for various applications. The relevant conclusions derived from the current work focused on developing environmentally friendly yellow inorganic pigments is presented here.

- Bismuth vanadate (BiVO_4) is a yellow pigment widely used in ceramics and polymeric systems. However, it has been proven difficult to control the pigmentary colors of BiVO_4 . The extension of the color pallet of BiVO_4 is a factor that will increase the commercial competitiveness of this pigment. A crucial way to improve the properties of materials is through compositional design in the form of solid solutions.
- Band structure engineering by making solid solutions between two compounds with different band gap can be regarded as one of the efficient methods for producing various shades of the colorants. In view of this, a range of yellow inorganic pigments based on BiVO_4 were synthesized as alternatives to the currently used toxic ceramic pigments.
- Scheelite solid solutions in $(\text{BiV})_x(\text{CaW})_{1-x}\text{O}_4$ ($x = 0.2, 0.4, 0.6, 0.8$) enhanced the $L^*a^*b^*$ values than that of BiVO_4 and are also comparable to praseodymium yellow. Among the pigments, $(\text{BiV})_{0.6}(\text{CaW})_{0.4}\text{O}_4$ exhibited hue angle close to 90° . CaWO_4 tailored with BiVO_4 allows fine tuning of the band gap resulting in various shades of yellow. The developed pigments may find potential application in the coloring of various plastic materials due to their high color quality.
- Powellite solid solutions in $(\text{BiV})_x(\text{CaMo})_{1-x}\text{O}_4$ ($x = 0.2, 0.4, 0.6, 0.8$) ameliorate the $L^*a^*b^*$ values than that of BiVO_4 and $(\text{BiV})_x(\text{CaW})_{1-x}\text{O}_4$. The synthesized pigments were found to have high IR reflectance. Typical pigment $(\text{BiV})_{0.2}(\text{CaMo})_{0.8}\text{O}_4$ exhibit IR reflectance as high as 91 % in the 1100 nm range. Particle size has a marked influence on IR reflectance. The

developed pigments appear as good candidates in the formulation of cool pigments.

- An attempt has been made to improve and tune the color characteristics of BiVO_4 through solid solution formation with $(\text{LiLa})_{1/2}\text{MoO}_4$ as well as $(\text{LiCaLa})_{1/3}\text{MoO}_4$. Various shades of toxic metal free pigments were obtained ranging from reddish to greenish yellow as a result of a blue shift of the absorption edge with substitution. Addition of various mineralizers significantly enhanced the yellow hue ($L^* = 85.5$, $a^* = -4.8$, $b^* = 85.3$) making it better than a commercially available BiVO_4 pigment ($L^* = 94.4$, $a^* = -16.7$, $b^* = 76.9$). The IR reflectance of BiVO_4 is enhanced with substitution and addition of a mineralizer upto 94%. Mineralizers improve the greenish yellow hue characteristic of BiVO_4 pigment. They also improve morphology as well as crystallinity and help in the formation of the host lattice structure at a lower calcination temperature.
- Brilliant IR reflecting yellow colorants are developed in rare earth double molybdate substituted BiVO_4 solid solutions. $\text{Li}_{0.10}\text{RE}_{0.10}\text{Bi}_{0.8}\text{Mo}_{0.2}\text{V}_{0.8}\text{O}_4$ (RE = La, Pr, Sm, Gd, Tb, Dy, Y, Yb and Lu) pigments have a strong optical absorption in the UV-blue light wavelength region. CIE LAB color analysis shows that different hues of yellow shades are obtained in these solid solutions. Rare earth substitution allows further tuning of band gap of the material. The color characteristics are comparable to commercial BiVO_4 pigment. La substitution exhibited intense yellow color characterized by the highest b^* (color) value among the developed pigments. Incorporation of double rare earth molybdates of La, Gd, Tb, Y and Lu into BiVO_4 results in non toxic IR reflecting cool pigments. High IR reflectance is obtained by incorporation of La, Gd, Tb, Y and Lu. The IR reflectance of these pigments range from 84 to 90 %.
- Isovalent dopants namely Y^{3+} and Nb^{5+} on BiVO_4 yielded yellow inorganic pigments, $(\text{BiV})_{1-x}(\text{YNb})_x\text{O}_4$ with brilliant yellow colors ($L^* = 80.34$, $a^* = 14.28$, $b^* = 75.46$) and significant enhancement of IR reflectance to 91% when compared to undoped BiVO_4 at 1100 nm range. Further, the solid solutions allow fine tuning of the band gap displaying various yellow colors.

The lattice distortion and reduction in particle size are responsible for the enhancement of the pigment characteristics.

- Nano yellow inorganic pigment, with high IR reflectance is developed in $(\text{BiV})_{0.94}(\text{YNb})_{0.06}\text{O}_4$ solid solutions. Citrate gel route has been employed to synthesize these materials followed by calcination at lower temperature leading to fine particles. The synthesized material via citrate gel route offers significant improvement in the IR reflectance and color coordinates.
- Multifunctional materials are developed in $\text{BiV}_{1-x}\text{Nb}_x\text{O}_4$ solid solutions via structural variation. Citrate gel route has been employed to synthesize these materials followed by calcination at various temperatures leading to fine particles. Nb^{5+} doped BiVO_4 pigments exhibit better multifunctional properties like good coloristic properties, impressive IR reflectance and notable methylene blue dye degradation property than BiVO_4 .
- Potential yellow pigments were tested for their suitability for coloring applications. Typical $\text{Li}_{0.10}\text{La}/\text{Gd}_{0.10}\text{Bi}_{0.8}\text{Mo}_{0.2}\text{V}_{0.8}\text{O}_4$ pigments impart their color as well as IR reflectance to various substrates like PMMA, asbestos cement, concrete cement and metal panel. Typical $(\text{BiV})_{0.975}\text{Nb}_{0.025}\text{O}_4$ pigment demonstrate color and IR reflecting property on concrete cement block. The pigments are found to exhibit good light fastness and chemical stability. The results imply the usage of these pigments for energy saving coatings for buildings and automotives.

Thus, the synthesized pigments are found to be interesting alternatives to existing toxic yellow pigments for various coloring applications.

7.2 Future scope

This kind of study is of current interest in preparing visible responsive compounds for potential applications in solar cells, photocatalysts and colored pigments.

Visible light response of the materials makes them possible candidates for dye degradation under visible light.

The possibility of these compounds for hydrogen production through the photo electrolysis of water and as photo catalyst for water purification can be explored.

Since BiVO_4 exhibit photochromic behaviour, the photochromic study of the developed pigments can be conducted.

Study the energy savings of developed pigments for cool roof applications.

LIST OF PUBLICATIONS

1. Brilliant IR Reflecting Yellow Colorants in Rare Earth Double Molybdate Substituted BiVO₄ Solid Solutions for Energy Saving Applications.
Sameera, S.; Rao, P. P.; Divya, S.; Raj, A. K. V., *ACS Sustain. Chem. Eng.* **2015**, 3 (6), 1227-1233.
2. Probing Structural Variation and Multifunctionality in Niobium Doped Bismuth Vanadate Materials.
Sameera, S.; Rao, P. P.; James, V.; Raj, A. K. V.; Chitradevi, G. R.; Kumari, L. S., *Dalton Trans.* **2014**, 43, 15851-15860.
3. Influence of (LiLa)_{1/2}MoO₄ Substitution on the Pigmentary Properties of BiVO₄.
Sameera, S.; Rao, P. P.; James, V.; Divya, S.; Raj, A. K. V., *Dyes Pigm.* **2014**, 104, 41-47.
4. Potential NIR Reflecting Yellow Pigments in (BiV)_{1-x}(YNb)_xO₄ Solid Solutions.
Sameera, S.; Rao, P. P.; Kumari, L. S.; James, V.; Divya, S., *Chem. Lett.* **2013**, 42 (5), 521-523.
5. New Scheelite-Based Environmentally Friendly Yellow Pigments: (BiV)_x(CaW)_{1-x}O₄.
Sameera, S.; Rao, P. P.; Kumari, L. S.; Koshy, P., *Chem. Lett.* **2009**, 38 (11), 1088-1089.

Publications out of the thesis

6. Pigments Based on Terbium-Doped Yttrium Cerate with High NIR Reflectance for Cool Roof and Surface Coating Applications.
Raj, A. K. V.; Rao, P. P.; **Sameera, S.**; Divya, S., *Dyes Pigm.* **2015**, 122, 116-125.

7. Effects of Rare Earth Substitution on the Optical Properties of Bi₂MoO₆ for Coloring Applications.
Kumari, L. S.; Rao, P. P.; **Sameera, S.**; James, V.; Koshy, P., *Mater. Res. Bull.* **2015**, *70*, 93-98.
8. A Blue Chromophore Based on Mn³⁺ in Triagonal Bipyramidal Coordination with Longer Apical Bond Lengths.
Divya, S.; Rao, P. P.; **Sameera, S.**; James, V.; Raj, A. K. V., Monoclinic LaGa_{1-x}M_xGe₂O₇; *RSc Adv.* **2015**, (5), 27278-27281.
9. Remarkable Changes in the Photoluminescent Properties of Y₂Ce₂O₇:Eu³⁺ Red Phosphors Through Modification of the Cerium Oxidation States and Oxygen Vacancy Ordering.
Raj, A. K. V.; Rao, P. P.; Sreena, T. S.; **Sameera, S.**; James, V.; Renju, U. A., *Phys. Chem. Chem. Phys.* **2014**, *16* (43), 23699-23710.
10. Synthesis of Novel Nontoxic Yellow Pigments: Sr₂Ce_{1-x}Tb_xO₄.
Raj, A. K. V.; Rao, P. P.; **Sameera, S.**; James, V.; Divya, S., *Chem. Lett.* **2014**, *43* (7), 982-984.
11. Multiferroic Based Reddish Brown Pigments: Bi_{1-x}M_xFeO₃ (M = Y and La) for Coloring Applications.
James, V.; Rao, P. P.; **Sameera, S.**; Divya, S., *Ceram. Int.* **2014**, *40* (1, Part B), 2229-2235.
12. Brilliant Yellow Color and Enhanced NIR Reflectance of Monoclinic BiVO₄ Through Distortion in VO₄³⁻ Tetrahedra.
Kumari, L. S.; Rao, P. P.; Radhakrishnan, A.N., James, V.; **Sameera, S.**; Koshy, P., *Sol. Energy Mater. Sol. Cells.* **2013**, *112*, 134-143.
13. Synthesis and Optical Properties of Ce_{0.95}Pr_{0.05-x}M_xO₂ (M = Mn, Si) as Potential Ecological Red Pigments for Coloration of Plastics.

Kumari, L. S.; Rao, P. P.; **Sameera, S.**; Koshy, P., *Ceram. Int.* **2012**, 38 (5), 4009-4016.

14. Structure and Dielectric Properties of a New Series of Pyrochlores in the Ca–Sm–Ti–M–O (M = Nb and Ta) System.

Sameera, S.; Rao, P. P.; Chandran, M. R., *J. Mater. Sci.- Mater. Electron.* **2011**, 22 (11), 1631-1636.

15. Y-Doped Bi₂MoO₆ Yellow Pigments for the Coloration of Plastics.

Kumari, L. S.; Gayathri, T. H.; **Sameera, S.**; Rao, P. P., *J. Am. Ceram. Soc.* **2011**, 94 (2), 320-323.

16. New Powellite Type oxides in Ca–R–Nb–Mo–O System (R = Y, La, Nd, Sm or Bi) -Their Synthesis, Structure and Dielectric properties.

Ravindran Nair, K.; Rao, P. P.; **Sameera, S.**; Mohan, V. S.; Chandran, M. R.; Koshy, P., *Mat. Lett.* **2008**, 62 (17–18), 2868-2871.

PAPERS PRESENTED AT CONFERENCES

1. **Sameera, S.;** Rao, P. P.; Divya, S.; Raj, A. K. V., Methods for improving BiVO₄ based pigments for NIR reflecting colorants. International Conference on Science, Technology and Application of Rare Earths (*ICSTAR 2015*), Kovalam, Kerala, India, April **2015**. (Poster presentation)
2. **Sameera, S.;** Rao, P. P.; James, V.; Raj, A. K. V.; Divya, S., Ecological IR reflecting pigments in (BiV)_x(CaMo)_{1-x}O₄ for cool roof applications. National Conference on Advanced Technologies for Materials Processing and Diagnostics 2014, Kochi, Kerala, India, September **2014**. (Best poster award)
3. **Sameera, S.;** Rao, P. P.; James, V.; Raj, A. K. V.; Divya, S., Yellow pigments based on (LiRE)_{1/2}MoO₄ - BiVO₄ solid solutions for cool roof applications. International Conference on Advanced Functional Materials (*ICAFM 2014*), Thiruvananthapuram, Kerala, India, February **2014**. (Poster presentation)
4. **Sameera, S.;** Rao, P. P.; James, V.; Raj, A. K. V.; Divya, S., Enhanced NIR reflecting yellow pigments: (BiV)_{1-x}(ReP)_xO₄ (Re =Y, Gd) for cool roof applications. 25th Kerala Science Congress, 2013, Technopark, Thiruvananthapuram, Kerala, India, February **2013**. (Oral presentation)
5. James, V.; Rao, P. P.; **Sameera, S.;** Divya, S., Synthesis and optical properties of La doped BiFeO₃ thin films for window coating applications. National Symposium on Polymers and Coatings (*NSPC-2012*), Indian Institute of Chemical Technology (IICT), Hyderabad, India, September **2012**. (Poster presentation)
6. **Sameera, S.;** Rao, P. P.; Kumari, L. S.; Chandran, M.R., Synthesis and characterization of new eco-Friendly pigments in (BiV)_{1-x}(YNb)_xO₄. Indian Analytical Science Congress (*IASC-2012*), Kanyakumari, Tamil Nadu, India, January **2012**. (Poster presentation)

7. **Sameera, S.;** Rao, P. P.; Kumari, L. S., Synthesis and characterization of new eco-friendly pigments in Bi_2RNbO_7 system: (R = Y, La, Pr, Sm, Gd, Yb). 23rd Kerala Science Congress 2011, Centre for Earth Science Studies (CESS), Thiruvananthapuram, Kerala, India, January **2011**. (Poster presentation)